# Energy and Water Exchange Processes in Boreal Permafrost Ecosystems

Dissertation

zur Erlangung des akademischen Grades

Dr. rer. nat.

im Fach Geographie

eingereicht an der

Mathematisch-Naturwissenschaftlichen Fakultät
der Humboldt-Universität zu Berlin

von

Simone Maria Stünzi (M. Sc.)

Präsidentin der Humboldt-Universität zu Berlin
Prof. Dr.-Ing. Dr. Sabine Kunst

Dekan der Mathematisch-Naturwissenschaftlichen Fakultät
Prof. Dr. Elmar Kulke

---

| | |
|---|---|
| Gutachterinnen: | Prof. Dr. Julia Boike |
| | PD Dr. Kirsten Thonicke |
| | Associate Prof. Dr. Jennifer Baltzer |
| Tag der mündlichen Prüfung: | 6. Dezember 2021 |

# Thesis Summary

Boreal forests in permafrost regions make up around one-third of the global forest cover and control the regional and global climate. Boreal forests are known to efficiently protect underlying permafrost from thawing giving rise to a highly sensitive interplay between vegetation, climate, and the hydrothermal regime of the ground. So far, only a small fraction of the mechanisms controlling this interplay have been investigated and understood. It can be expected that the future development of the boreal forests under climate warming excerpts a critical impact on permafrost stability. The direct influence of climatic changes on the forest and the indirect effect through a change in permafrost or forest disturbance dynamics can lead to extensive ecosystem shifts such as a change in forest composition or density, which will, in turn, affect permafrost persistence. Changes to this tightly coupled ecosystem will potentially destabilize ecosystem functions such as the carbon stored within the vegetation and permafrost. This dissertation aims to understand how complex interactions of heat and water fluxes between vegetation, ground, and atmosphere control the sensitivity of boreal permafrost ecosystems.

Within this dissertation, I have adapted a one-dimensional, numerical land surface model (CryoGrid), which can be used to simulate the physical processes in permafrost regions, for the application in vegetated areas by coupling a detailed multilayer canopy model (CLM-ml v0), and a dynamic larch stand model. In three closely related studies, I have successfully reproduced the energy transfer and thermal regime of typical boreal permafrost ecosystems at different study sites in eastern Siberia. An intensive validation of the model allows precise quantification of the different heat- and water fluxes controlling the stability of permafrost under boreal forest covers.

The numerical simulations revealed that the forests exert a strong control on the thermal and hydrological state of permafrost through changing the radiation

balance and snow cover phenology. The forest cover has a net stabilizing effect on the permafrost ground below. Canopy shading below the canopy is the main controlling mechanism, along with enhanced longwave radiation due to low turbulent fluxes, higher or lower groundwater content, and a higher snowpack. The detailed physical model has enabled me to study the variation in the insulation effect of different forest types and forest densities as well as the feedback mechanisms occurring after forest disturbances such as fires or logging. Forest cover changes, such as densification or a shift in dominant plant functional type are found to significantly alter the ground hydrothermal conditions leading to both soil drying and wetting with increased active layer thicknesses. Such changes in permafrost conditions can all have a favoring effect on either evergreen needleleaf or deciduous hardwood expansion, lead to the complete loss of forest cover or a shift in the forest density. Finally, I have found first indicators for the existence of tipping behavior in larch forests after disturbances such as fires and logging causing irreversible forest dieback triggered by changing soil water conditions. My results reveal the high sensitivity of this unique ecosystem and contribute to a better understanding of the impact of forest disturbances and climatic changes.

In summary, my results suggest that local, detailed, and specific land surface models are required to fully comprehend the complex dynamics in boreal permafrost ecosystems. The research revealed that climatic changes and associated feedbacks between permafrost, climate, boreal forest, and forest disturbances will destabilize tightly coupled ecosystem functions such as its role as a carbon sink. The induced changes will likely affect key forest and permafrost characteristics triggering and enhancing feedback mechanisms such as swamping, droughts, fires, or forest loss.

# Kurzfassung

Boreale Wälder umfassen etwa ein Drittel der weltweiten Waldfläche und regulieren das regionale und globale Klima. Boreale Wälder schützen den darunter liegenden Permafrost wirksam vor dem Auftauen. Dies führt zu hochsensiblen Wechselwirkungen zwischen Vegetation, Klima und dem hydrothermalen Regime des Bodens. Bislang wurde nur ein kleiner Teil der Mechanismen, die dieses Zusammenspiel steuern, genauer untersucht und verstanden. Unter dem Einfluss der Klimaerwärmung ist es zu erwarten, dass die zukünftige Entwicklung der borealen Wälder kritische Auswirkungen auf die Permafroststabilität haben wird. Der direkte Einfluss von Klimaveränderungen auf den Wald und die indirekten Auswirkungen durch eine Veränderung des Permafrosts oder sich wandelnde Störungsregime, wie bspw. häufiger auftretende Waldbrände, können zu weitreichenden Veränderungen im Ökosystem führen. So kann beispielsweise eine Änderung der Walddichte oder -zusammensetzung sich wiederum auf die Persistenz des Permafrosts auswirken und Ökosystemfunktionen wie die Speicherung von Kohlenstoff in der Vegetation und im Permafrost destabilisieren. Ziel dieser Dissertation ist es zu verstehen, wie die komplexen Wechselwirkungen der Wärme- und Wasserflüsse zwischen Vegetation, Boden und Atmosphäre die Empfindlichkeit der borealen Permafrostökosysteme steuern.

Im Rahmen dieser Dissertation habe ich ein eindimensionales, numerisches Landoberflächenmodell (CryoGrid), welches zur Simulation der physikalischen Prozesse in Permafrostgebieten verwendet werden kann, für die Anwendung in bewaldetem Gebieten angepasst. Dazu habe ich ein detailliertes mehrschichtiges Kronendachmodell und ein dynamisches Lärchenbestandsmodell daran gekoppelt. In drei eng miteinander verbundenen Studien habe ich den Energietransfer und das Wärmeregime typischer borealer Permafrostökosysteme an verschiedenen Untersuchungsstandorten in Ostsibirien erfolgreich reproduziert. Eine intensive Va-

lidierung des Modells ermöglicht eine genaue Quantifizierung der verschiedenen Wärme- und Wasserflüsse, welche die Stabilität des Permafrosts unter borealen Wäldern steuern. Die numerischen Simulationen ergaben, dass die Wälder den thermischen und hydrologischen Zustand des Permafrosts stark beeinflussen, indem sie die Strahlungsbilanz und die Phänologie der Schneedecke verändern. Die Waldbedeckung hat eine stabilisierende Wirkung auf den darunter liegenden Permafrostboden. Die Beschattung durch das Kronendach ist dabei der wichtigste Steuerungsmechanismus, dazu kommen geringe turbulente Flüsse was die langwellige Strahlung unter dem Blätterdach verstärkt, einen höheren oder niedrigeren Grundwassergehalt und eine höhere Schneedecke. Anhand des physikalischen Modells konnte ich die unterschiedliche Isolierwirkung verschiedener Walddichten und -typen sowie die Rückkopplungsmechanismen nach Waldstörungen wie Bränden oder Abholzung untersuchen. Veränderungen der Waldbedeckung, wie z.B. eine Verdichtung oder Verschiebung der vorherrschenden Baumarten, führen zu einer erheblichen Veränderung der hydrothermalen Bedingungen des Bodens und resultieren in tieferen Auftauschichten und trockneren oder feuchteren Böden. Solche Änderungen der Permafrostbedingungen können die Ausbreitung von immergrünen Nadel- oder Laubhölzern begünstigen, zum vollständigen Verlust der Waldbedeckung oder zu einer Verschiebung der Walddichte führen. Schlussendlich habe ich erste Anzeichen für das Vorhandensein von Kippverhalten in Lärchenwäldern nach Störungen wie Bränden und Holzschlag gefunden, die zu irreversiblem Waldsterben führen, ausgelöst durch veränderte Bodenwasserverhältnisse. Meine Ergebnisse zeigen die hohe Empfindlichkeit dieses einzigartigen Ökosystems und tragen zu einem besseren Verständnis der Auswirkungen von Waldstörungen und klimatischen Veränderungen bei.

Zusammenfassend deuten die Ergebnisse darauf hin, dass lokale, detaillierte und spezifische Landoberflächenmodelle erforderlich sind, um die komplexe Dynamik der borealen Permafrostökosysteme vollständig zu erfassen. Meine Forschung hat gezeigt, dass klimatische Veränderungen und damit verbundenen Rückkopplungen zwischen Permafrost, Klima, borealem Wald und Waldstörungen die eng gekoppelten Ökosystemfunktionen, wie z.B. die Rolle als Kohlenstoffsenke, destabilisieren können. Die induzierten Veränderungen werden sich wahrscheinlich auf wichtige Wald- und Permafrostmerkmale auswirken und Rückkopplungsmechanismen wie Überschwemmungen, Dürreperioden, Brände und Waldverlust auslösen.

# Acknowledgments

Throughout the past three years, I have received a great deal of support and encouragement from many colleagues and friends. I want to start by thanking my main supervisor, Moritz Langer. Thank you for your continuous trust, patience, and invaluable guidance that quickly became indispensable for me. I would also like to thank Julia Boike for her support, encouragement, and mentoring over the years, as well as for agreeing to examine this dissertation. I would also like to thank Ulrike Herzschuh and Stefan Kruse for their supervision and collaboration throughout my Ph.D.

I especially want to thank my collaborators at NEFU in Yakutsk. Thank you, Luidmila Pestryakova, Alexey Nikolajewitsch Pestryakov, Evgeniy Zakharov, Levina Sardana Nikolaevna, and Lena Ushnizkaya. You didn't only make the extensive fieldwork plans with all of its logistical difficulties possible but have also left me with incredible memories and friendships. I furthermore want to thank all my expedition buddies, especially Luise Schulte, Frederic Brieger, Stuart Vyse, Stefan Kruse, and Elisabeth Dietze. I want to thank everyone that has helped me before and after the two field campaigns, including the AWI logistics team, Stephan Jacobi, Alexander Oehme, Niko Borneman, and Peter Schreiber. Special thanks goes to Bill Cable who managed to successfully teach me how to prepare, set up, and troubleshoot complete AWSs within the first couple of weeks of my Ph.D.

I am deeply grateful for the support from the entire PermaRisk team, Soraya, Becca, Alex, Stephan, Thomas, Rui, Erik, Jan, Tina, and Lisa, the Sparc research group, the entire A6, all of my fellow Ph.D. students, and the entire Permafrost and ENVI sections at AWI Potsdam. I am especially grateful for the discussions and suggestions for this thesis provided by Frederieke Miesner, Moritz Langer, Rebecca Rolph, Thomas Schneider von Deimling, and Erik Chan as well as by Rahel Felder, Sebastian-Felix Ernst, and Anna Stünzi.

At HU Berlin, I would like to thank Prof. Dr. Dörthe Tetzlaff and Prof. Dr. Christoph Schneider for their support at a distance. Additionally, I would like to express my gratitude to Kirsten Thonicke and Jenn Baltzer for agreeing to examine my dissertation. I would furthermore like to thank Anne Gädeke from PIK for the fruitful collaboration and scientific discussions during my Ph.D.

I am thankful to the POLMAR graduate school at AWI, the Geo.X Young Academy and all of its members, the WiNS program at the HU Berlin, and APECS for providing a supportive framework for my Ph.D. project.

Last but not least, I am forever thankful for my parents, my sister, and my brother, as well as for my friends for all the support, love, and happy distractions. Finally, I want to express my deepest gratitude to my partner, Sebastian, for his never-ending encouragement and love.

# Selbständigkeitserklärung

Ich erkläre, dass ich die Dissertation selbstständig und nur unter Verwendung der von mir gemäß §7 Abs. 3 der Promotionsordnung der Mathematisch-Naturwissenschaftlichen Fakultät, veröffentlicht im Amtlichen Mitteilungsblatt der Humboldt-Universität zu Berlin, Nr. 42/2018 am 11.07.2018 angegebenen Hilfsmittel angefertigt habe.

Berlin, 16. September 2021 Simone M. Stünzi

# Contents

# List of Figures

# List of Tables

# Part I

# Background and synthesis

# Chapter 1

# Introduction

## 1.1 Boreal forests and permafrost

Boreal forests contain about 30% of the global forest area and are the largest terrestrial ecosystem (*Gauthier et al.*, 2015). Due to the sheer size, boreal forests store over 30% of terrestrial carbon (*Kasischke*, 2000), twice as much as tropical forests. Boreal forests are additionally an essential component of regional and global climate patterns, exerting a strong control on numerous climate feedback mechanisms (*Achard et al.*, 2006; *Zhang et al.*, 2018; *Bonan et al.*, 2018).

Located in high latitudes between 45° to 70° North, 80% of boreal forests are underlain by permafrost (*Helbig et al.*, 2016). Permafrost, which is defined as ground material that has been at a temperature below 0 °C for at least two consecutive years (*Van Everdingen*, 1998), is estimated to cover about 14 million square kilometers or 15% of the land surface in the Northern Hemisphere. As an important component of the Earth's cryosphere and the global carbon cycle, permafrost contains about 1'300 Gt of carbon, twice as much as the atmosphere (*Hugelius et al.*, 2014). Carbon in boreal forest regions has been estimated to store 652 Gt of soil carbon and 78 Gt of plant biomass carbon (*Kasischke*, 2000).

The distribution and condition of permafrost are directly linked to the snow and vegetation cover, topography, water bodies, the geothermal heat flux, and the air temperature. Therefore, predicting permafrost sensitivity to a warming climate is highly complex, with many uncertainties (*Boike et al.*, 2013). Permafrost is often found to be in disequilibrium with climatic conditions due to the thermal inertia of the ground. This imbalance can be intensified by the insulating effect of an organic soil layer, a litter layer, or vegetation cover (*Yershov*, 2004). About 55%

of permafrost area is covered by boreal forest. Boreal forests exert a strong control on permafrost stability (*Gruber*, 2012; *Helbig et al.*, 2016). Although boreal forests underlain by permafrost are highly adapted to extreme temperature conditions, they are sensitive to climatic changes (*IPCC*, 2019, 2021), and prone to vegetation shifts.

Over the last century, the surface temperature in the Arctic has on average increased at a rate 50% greater than in the Northern Hemisphere as a whole (*Meyer et al.*, 2015; *IPCC*, 2021). Boreal forest regions are expected to warm by 4 to 11 ° C by 2100, which is double the global average warming rate, accompanied by a modest precipitation increase (*Scheffer et al.*, 2012; *IPCC*, 2021). During 2007-2016, continuous zone permafrost temperatures have already increased by 0.39 (±0.15) ° C (*Biskaborn et al.*, 2019) and for Central Yakutia, permafrost temperature rises by 1 - 1.5 ° C over the past three decades have been reported (*Gorokhov and Fedorov*, 2018).

The induced climatological changes can promote an increasing active layer thickness or trigger the partial disappearance of the near-surface permafrost. This leads to changing hydrological conditions and vegetation patterns, which could trigger thermokarst development and other erosion processes. Moreover, climate change has a direct impact on the water, heat, and nutrient budget of boreal ecosystems (*Pearson et al.*, 2013). Boreal forests are expected to increase in density, change in species composition, and expand northwards under warming climatic conditions (*Holtmeier and Broll*, 2005; *Mamet et al.*, 2019). Extensive ecosystem shifts such as changes in composition, density, and distribution of Arctic vegetation are already reported all over the Arctic and sub-Arctic (*Pearson et al.*, 2013).

Vegetation changes and transitions trigger multiple feedback mechanisms of different magnitudes between the permafrost, the forest cover, and the atmosphere (*Chapin et al.*, 2005; *Pearson et al.*, 2013). As such, a shift in the forest cover changes the below-canopy surface energy balance and the thermal and hydrological regime of the permafrost, which in turn leads to additional forest cover changes, both impacting the atmosphere through e.g. albedo change, changes in surface roughness, and resistances. The numerous interactions and interdependencies of the atmosphere, boreal vegetation, and permafrost are poorly understood and make predictions and interpretations of the current and future state of boreal permafrost ecosystems highly challenging. For example, globally, boreal forests currently act

as a carbon sink ($-29$ to $-46\,\mathrm{gCm^{-2}yr^{-1}}$) (*Schaphoff et al.*, 2016; *Hiyama et al.*, 2021; *Virkkala et al.*, 2021), but could eventually turn into a large carbon source, which has recently been reported in certain regions of boreal forests (*Zhao et al.*, 2021). To further our understanding of the current and future state of boreal permafrost ecosystems, this thesis aims to understand and quantify the complex feedback mechanisms.

Wide areas of the northeastern Eurasian continent are dominated by the deciduous needleleaf tree genus *Larix* Mill., while most other boreal forests are dominated by more typical evergreen needleleaf taxa (Figure 1.1). These larch-dominated ecosystems function as tightly coupled systems, fostering unique interactions between the permafrost, fires, and climate. In larch-dominated forest stands, the invasion of evergreen taxa is inhibited even though evergreen taxa are thought to represent the late-successional, stable forest stage and would therefore become dominant at some point (*Kharuk et al.*, 2007). It is assumed that the establishment of stable larch forests is controlled by complex vegetation-permafrost-climate interactions which remain poorly understood. A shallow active-layer depth (*Kajimoto*, 2010), a high fire frequency (*Rogers et al.*, 2015), and a certain regulation of the seasonal permafrost thawing conditions (*Tanaka et al.*, 2008; *Zhang et al.*, 2011; *Peng et al.*, 2020) are shown to be the main hindrances to the establishment of evergreen taxa (*Herzschuh*, 2019).

Warmer temperatures in the past 30 years have, nevertheless, had an impact on the growth of evergreen and deciduous taxa in Siberia. There have been measurable increases in growth increments, stand density, and regeneration propagation into tundra ecosystems (*Kharuk et al.*, 2005; *Esper et al.*, 2010; *Kharuk et al.*, 2015). Furthermore, recent studies have found that warming temperatures will likely lead to increased density of the vast Siberian larch forests, and in some regions, lead to an increase in evergreen conifer-dominated forests (mostly *Pinus spp.*), with an increase in birch wherever sufficient precipitation is available (*Shuman et al.*, 2011; *Kharuk et al.*, 2019). A warmer and drier climate in the future may favor the transition into a steppe, which would mean an irreversible loss of the larch forests (*Herzschuh et al.*, 2016). Additionally, changes in the natural fire cycles and upsurge of other disturbances (*Kharuk et al.*, 2021) could influence and hasten the transition of larch-dominated forests towards steppe or grasslands (*Gauthier et al.*, 2015). These shifts will modify the insulation capacity of the vegetation and

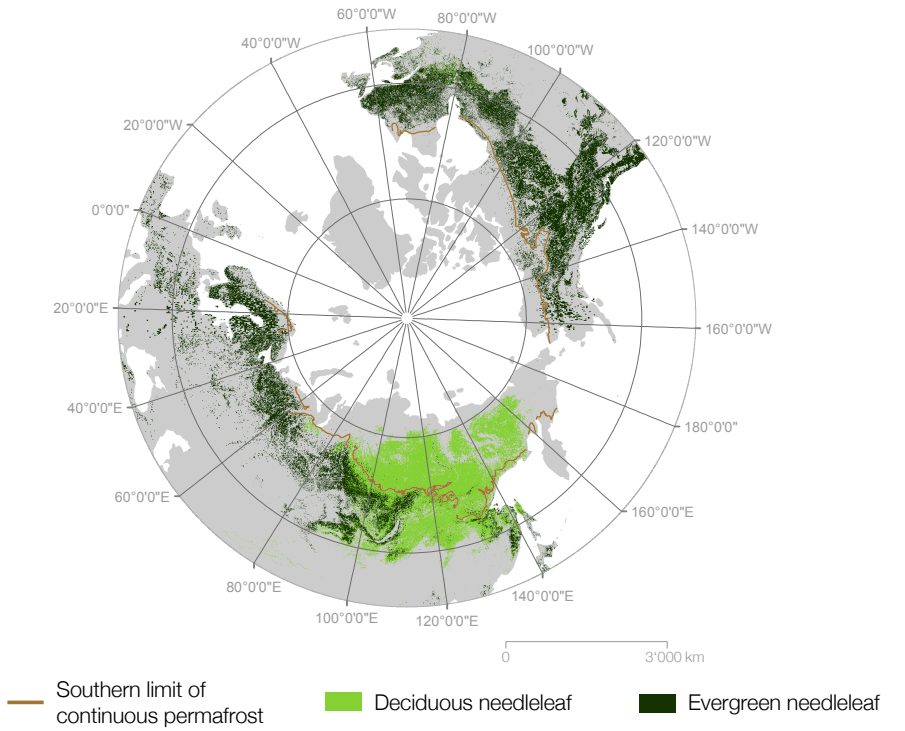


*Figure 1.1: Global evergreen needleleaf (dark green) and summergreen needleleaf (light green) boreal forest distribution and the boundary line between the discontinuous and continuous permafrost extent in brown. Data: ESA CCI Land Cover classes. ESA. Land Cover CCI Product User Guide Version 2. Tech. Rep. (2017) (after Herzschuh (2019)), permafrost extent from Land Resources of Russia - Maps of permafrost and Ground Ice (after Kotlyakov and Khromova (2002)).*

have a large impact on permafrost persistence, and the global carbon cycle. Therefore, there is a need to further understand the high variability in the influence of vegetation cover on permafrost persistence and to incorporate the local, heterogeneous and complex feedback mechanisms, caused by the various vegetation types and their relationship with permafrost (*Tchebakova et al.*, 2009; *Schuur and Mack*, 2018).

In the following section, I will provide a review of existing knowledge on ecosystem-protected permafrost and the feedbacks and interactions within this complex ecosystem.

## 1.2 Energy and water exchange in boreal forests underlain by permafrost

Forest density exerts a strong control on permafrost stability (*Yi et al.*, 2007; *Chasmer et al.*, 2011; *Fisher et al.*, 2016), and a direct feedback mechanism is expected to control the temporal ecosystem evolution (*Bonan et al.*, 1992; *Baltzer et al.*, 2014; *Carpino et al.*, 2018). Nevertheless, the exact magnitude of this feedback mechanism (Figure 1.2) is not fully understood and broad-scale vulnerability studies do not yet exist. Forests act as insulators, conductors, and storage units for heat and water. This is controlled by different factors such as the radiative heat transfer (shading, re-emission, and absorption), near-surface turbulence (including within- and below-canopy wind conditions), water- and snow interception, and soil properties (litter and organic layers, freezing characteristics, ground ice, and soil water retention). The canopy shades the forest floor below by reflecting and absorbing most downward solar radiation and by suppressing the majority of turbulent heat fluxes in the below-canopy space (*Chang et al.*, 2015). Furthermore, the canopy controls the surface albedo, which is much lower than in grasslands, especially during snow-covered periods (*Bonan and Shugart*, 1989; *Stuenzi and Schaepman-Strub*, 2020). The canopy decreases soil moisture and leads to a reduced thermal conductivity through precipitation interception (*Thomas and Rowntree*, 1992) and higher evapotranspiration (*Vitt et al.*, 2000). Additionally, the canopy slows snow melting in spring and reduces snow compaction because of the suppressed turbulent fluxes, which leads to higher snowpacks under denser canopies. Finally, the vegetation cover promotes the accumulation of an organic surface layer (*Bonan and Shugart*, 1989; *Yi et al.*, 2007), which further insulates the topsoil from the atmosphere.

A change in the forest density modifies the within- and below-canopy energy and water fluxes (*Chasmer et al.*, 2011). The forest composition also has an impact on the ground surface energy and water balance. The needle-shedding of deciduous taxa additionally impacts the within- and below-canopy fluxes (*Tanaka et al.*, 2008; *Zhang et al.*, 2011; *Peng et al.*, 2020), the litter and organic surface layers (*Bonan and Shugart*, 1989) and the fire regime (*Rogers et al.*, 2015). Since both, evergreen and deciduous taxa, can become established under similar climate conditions (*Esper and Schweingruber*, 2004; *Kharuk et al.*, 2007), the successful spread

of evergreen taxa into currently larch dominated areas and vice-versa mainly depends on the frequency of disturbance events, which have increased over the past decades (*Shuman et al.*, 2011; *Mekonnen et al.*, 2019; *Meredith et al.*, 2019).

Climatic changes have (1) a direct impact on permafrost thaw dynamics, while (2) leading to a change in forest structure and composition. Climate-induced changes in permafrost dynamics affect thaw depth, permafrost persistence, and water availability, and trigger structural changes in the vegetation cover. A change in forest canopy structure modifies through-canopy radiative heat transfer, snow and water interception and through-fall, near-surface turbulent fluxes, topsoil properties, and the fire regime – all of which trigger further changes in the energy and water fluxes of the underlying permafrost. Ultimately, all of these mechanisms and related interactions lead to a number of interrelated effects which result in positive or negative feedbacks on climate change (Figure 1.2).

In summary, I have identified the following uncertainties which make it difficult to accurately project boreal permafrost dynamics: (1) complex interactions and feedbacks between the ecosystem components of boreal forest, permafrost, disturbances (such as fires) and climate, (2) vegetation shifts causing large differences in forest density and composition, and (3) an increase in disturbances and unknown ecosystem resilience towards those disturbances.

Having identified these major challenges for ecosystem-protected permafrost modeling, I pose the following research question central to this thesis:

> How can the complex interactions and feedbacks between boreal forests and permafrost be modeled to successfully make predictions on the future development of this ecosystem and its role under changing climate conditions?

In the following, I will briefly explain the existing modeling schemes, and identify the need for a novel modeling approach to realistically assess these complex ecosystem dynamics.

## 1.3 Modeling of permafrost-boreal forest ecosystems

The vegetation–permafrost dynamics of the entire boreal regime and in eastern Siberia specifically have been studied in exploratory and descriptive field stud-

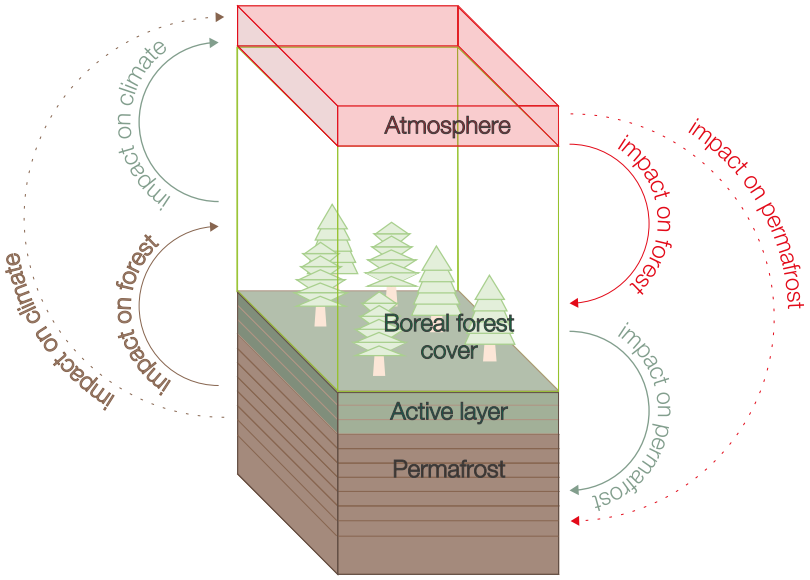


*Figure 1.2: Interactions between the atmosphere, boreal forest cover, and permafrost. The arrows display all the directions of impacts of change from the atmosphere on the boreal forest cover and the permafrost (red), from the permafrost on the boreal forest cover and the atmosphere (brown), and from the boreal forest cover on the atmosphere and the permafrost. Climatic change leads to a change in the forest density and structure, which leads to changes in all feedback processes between forest and permafrost. Additionally, climatic change leads to permafrost thawing and a change in the water availability, which also leads to forest density and structure changes.*

ies showing an insulation effect of forests on soil temperatures (e.g. *Chang et al.* (2015)). The biogeophysical processes controlling the evolution of the ecosystem have also been described by different conceptual models (*Beer et al.*, 2007; *Zhang et al.*, 2011; *Sato et al.*, 2016). Modeling schemes such as NEST (Northern Ecosystem Soil Temperature; *Zhang et al.* (2003)), SiBCliM (Siberian BioClimatic Model; *Tchebakova et al.* (2009)), Lund–Potsdam–Jena (LPJ DGVM – Dynamic Global Vegetation Model; *Beer et al.* (2007)), JULES (Joint UK Land Environment Simulator; *Chadburn et al.* (2015)) or ORCHIDEE–CAN (Organising Carbon and Hydrology In Dynamic Ecosystems – CANopy; *Chen et al.* (2016b)) have added a vegetation or canopy module, with defined exchange coefficients for the fluxes of mass and energy, to their soil modules. This is feasible to varying complexity

and the setups have successfully been used to address different mechanisms within permafrost underlain boreal forest systems. Such studies include research on the evolution of the vegetation carbon density under diverse warming scenarios (*Beer et al.*, 2007), the role of fire disturbances and fire return intervals (*Thonicke et al.*, 2001), unfrozen versus frozen ground and fire disturbances (*Zhang et al.*, 2011), or forest establishment and mortality (*Sato et al.*, 2016). All of these studies have improved knowledge on the essential processes in boreal permafrost areas. Nevertheless, it has often been pointed out that it is important to further understand how forest structure and canopy development (e.g. *Loranty et al.* (2018a)) or changes in the frequency and extent of wildfires (e.g. *Holloway et al.* (2020)) affect the thermal state and the snow regime of the ground, especially amid ongoing shifts in forest composition. The described model setups are often unable to capture important aspects such as either the vertical canopy structure or the leaf physiological properties which strongly control the energy transfer between the top-of-the-canopy atmosphere and the ground or the permafrost dynamics. To my knowledge, none of the existing models can reproduce the vertical tree structure and fluxes within the canopy in combination with a physically-based, highly-advanced permafrost model. Furthermore, most studies focus on well-researched boreal forest sites in Alaska and Canada, while the dynamics in eastern Siberia are considerably different in terms of dominant vegetation types and permafrost conditions.

The advanced multilayer canopy model which was coupled to CryoGrid within this dissertation introduces turbulent energy fluxes and a robust radiative transfer scheme through the canopy for a detailed analysis of the impact vegetation has on the hydrothermal regime of the permafrost ground below. This allows us to quantify the surface energy balance below a complex forest canopy and its direct impact on the hydrothermal regime of the permafrost ground. Within this dissertation, I have developed a tailored version of a one-dimensional land surface model (CryoGrid – CG, *Westermann et al.* (2016)) which has, so far, not included a vegetation scheme. Previously, the permafrost model has been used to successfully describe atmosphere–ground energy transfer and the ground thermal regime in barren and grass-covered permafrost areas (*Langer et al.*, 2016; *Westermann et al.*, 2016; *Nitzbon et al.*, 2019). I have adapted a state-of-the-art multilayer vegetation model (CLM-ml v0, originally developed for the Community Land Model – CLM – by *Bonan et al.* (2018)). By developing interfaces to couple the two models, I

have created a highly-detailed land surface model to reproduce the energy transfer and surface energy balance in ecosystem-protected permafrost regions. Furthermore, I have coupled a dynamic larch vegetation simulator (Lavesi) (*Kruse et al.*, 2016) to the novel model in order to simulate the future development of boreal forest-covered permafrost under warming climate scenarios. Combining these particular model components allows for the detailed study of the complex interactions between the different ecosystem components.

## 1.4 Research objectives

The climate-vegetation-soil interactions in the vast permafrost-dominated boreal forests are studied over a large transect in eastern Siberia. The underlying hypothesis is that common land surface models cannot capture the diverse feedback mechanisms between boreal vegetation and the underlying permafrost, and in particular, cannot capture the thermal insulation and the soil moisture that the forest affects. In three closely related research articles, the capacity of a novel model setup to simulate these exchanges is explored. The developed permafrost-multilayer canopy model is intended for use in permafrost-affected boreal forests. The overarching goal of this dissertation is to provide answers concerning the future development of the coupled permafrost-boreal forest ecosystems. In summary, I have identified the following main research objectives:

1. To improve the understanding of physical processes and feedbacks in permafrost-affected boreal forests, with a specific focus on boreal ecosystems in eastern Siberia.
2. To understand projected forest cover trajectories under a warming climate and constrain the relevance of forest cover changes for permafrost thaw and conditions.
3. To further the understanding of feedback processes and possible tipping behavior between permafrost, boreal forest, atmosphere, and disturbances.

Each of the three articles in this cumulative thesis contributes to the research objectives posed above. The full articles are provided in Part II. Chapter 2 gives an overview of the methodology used, namely the study sites and the observational data, as well as the different models this research is based upon. The contents of the articles are summarized in Chapter 3. Chapter 4 provides a synthesis, summarizing the main conclusions of this research and providing an outlook for further research.

# Chapter 2

# Methodology

In the first Chapter of this thesis, I have elaborated on the importance of boreal forests and their interactions with permafrost. Based on the large impact of the vast boreal permafrost regions on regional and global climate patterns and the inadequate modeling schemes currently available for this complex ecosystem, I have identified the research objectives of this thesis. In this Chapter, I provide an overview of the methodologies built upon to answer the posed research questions. Firstly, I introduce the suitable study areas and the gathered field data for model validation and parameterization that I have collected during two field campaigns to eastern Siberia in 2018 and 2019 (section 2.1). In a second step, I introduce the different models on which the detailed boreal forest-permafrost model is based (section 2.2).

## 2.1 Study area and observational data

### 2.1.1 Study area

The treeline of Northern Siberia is dominated by the deciduous needleleaf tree genus *Larix* Mill. up to N 75.5°, *Larix sibirica* Ledeb. from E $60-90°$, *Larix gmelinii* Rupr. between E $90-120°$, and *Larix cajanderi* Mayr. from E $120-160°$. Deciduous larch further grows in mixed stands with evergreen conifers (Siberian pine (*Pinus sibirica, Pinus sylvestris*), spruce (*Picea obovata Ledeb.*), and fir (*Abies sibirica*)), and hardwood (*Betula pendula Roth., B. pubescence Ehrh., Populus tremula L.*) (*Kharuk et al.*, 2019) (Figure 2.1). Evergreen conifers and hardwood prefer deeper active layers and a higher soil moisture availability but they can coexist

with deciduous larch (*Furyaev et al.*, 2001; *Ohta et al.*, 2001; *Rogers et al.*, 2015). All of these species are exceptionally well adapted to the harsh climatic conditions with short 60-90 days summers and cold winters with temperatures down to $-57\,^{\circ}\mathrm{C}$ (*Boike et al.*, 2016). The region experiences an extreme continental climate with long, cold winters and moderately warm summers. The temperature amplitude range is over $80\,^{\circ}\mathrm{C}$. Additionally, large areas are snow-covered from late September until the beginning of May and the climate is generally semi-arid to moist throughout the year (*Boike et al.*, 2016). The ecotone, called taiga, is further characterized by very low ground temperatures resulting in continuous permafrost. Permafrost thickness ranges from 200 to 600 m (*Yershov et al.*, 1991). The development of soil is hindered, resulting in podzolized, young, and very nutrient-poor soils. The landscape is composed of thermokarst lakes, alases, grassland, and forests (*Boike et al.*, 2016). The ground vegetation in forests is dominated by mosses and lichens that form carpets. Larch has shallow roots and grows on clay permafrost soils with an active layer of around 0.7 m and maximum wetness of 20-40% (*Ohta et al.*, 2001; *Rogers et al.*, 2015).

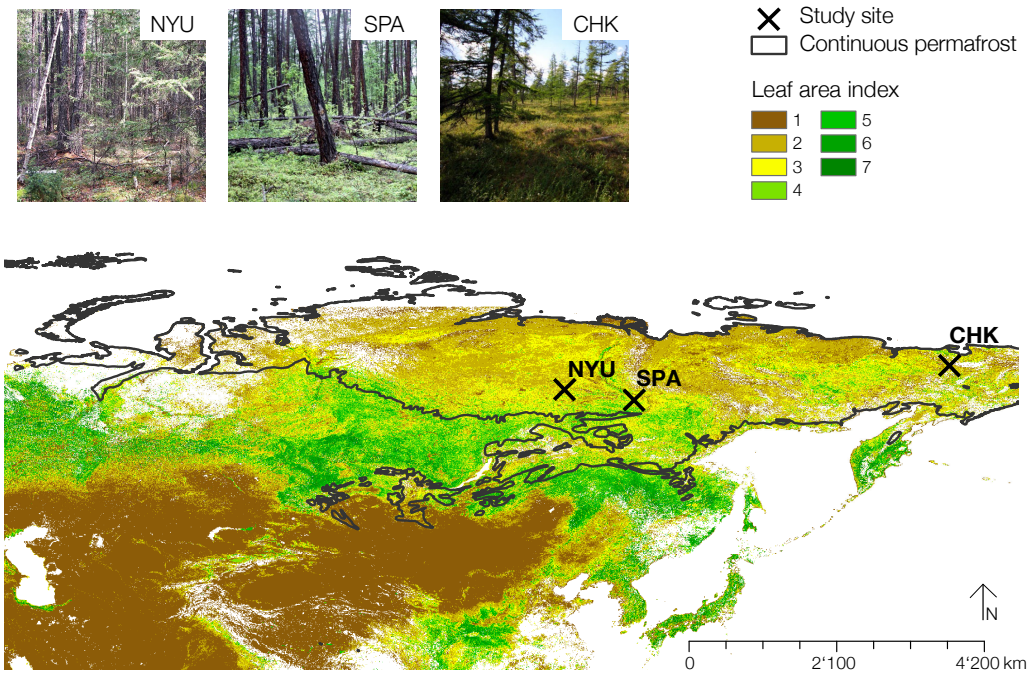


*Figure 2.1: Leaf area index ($m^2m^{-2}$) from satellite imagery (brown-green) and permafrost extent (black line) in north-eastern Siberia. The three study sites are marked with black crosses (Nyurba (NYU), Spasskaya Pad (SPA), and Chukotka (CHK)). Top left: Photographs showing the typical forest covers at the three study sites.*

*Data: ESA CCI Land Cover classes. ESA. Land Cover CCI Product User Guide Version 2. Tech. Rep. (2017) (after Herzschuh (2019)), permafrost extent from Land Resources of Russia - Maps of permafrost and Ground Ice (after Kotlyakov and Khromova (2002)), and Copernicus Global Land Service, Leaf Area Index (LAI) (after Copernicus Global Land Operations (2021)).*

Along a transect between the North-Eastern region of Chukotka and Southern Yakutia the two main locations of interest within this dissertation (Figure 2.1) were chosen to set up automatic weather stations (AWS, Campbell Scientific, detailed list of sensors see Table 2.2). Additionally, 100 iButtons and 6 Hobo Loggers (both stand-alone soil temperature sensors) were distributed at several locations. Additionally, a third study site, with an existing and available longer time series of measurement data was chosen for additional model validation and simulations. In the scope of this dissertation, I have run different simulation experiments at these three sites across this east-west transect through north-eastern Siberia. The transect covers a wide range of spatial differences, such as different climate condi-

tions (Figure 2.2), a variety in dominant plant functional types, and differing soil conditions (Table 2.1). In the following, I will provide an overview of the three study sites and their main characteristics, including the climate conditions (Figure 2.2). I will then provide a detailed explanation of the measurement set-up (section 2.1.2).

The most northern study area is located at Lake Ilirney in Chukotka at N 67.40°, E 168.37° and 603 masl. At the Chukotka site (CHK) the treeline is dominated by deciduous larch and underlain by continuous permafrost. The soil is clay dominated with a litter layer of undecomposed *Betula* roots, dead moss and dense rooting (0.01 m). The average measured tree height is 11 m. The organic horizon consists of organic black hummus with highly decomposed organic material, moss remains and good rooting (0.18 m). The thawed mineral sediment layer had a thickness of 0.37 m in August 2019 with little roots, dark grey clay matrix (40%) and clasts (60%). This site has been used as a study site in Article 2.

The central study site is near the well-described forest research station in Spasskaya Pad at N 62.14°, E 129.37°, and 237 masl (*Ohta et al.*, 2001; *Maximov*, 2015). Spasskaya Pad (SPA) is located in a continuous permafrost region. The main tree species is Dahurian larch (*Larix gmelinii*) with a stand density of 840 trees/ha. Understory vegetation (*Vaccinium*) is dense and 0.05 m high. The measured average tree height is 12 m. This site has been used as an external validation site in Article 1 and as one of the main study sites in Article 2 and 3 of this dissertation.

The most western study site is located south east of Nyurba at N 63.08°, E 117.99° and 117 masl, in a continuous permafrost boreal forest zone intermixed with some grassland and shallow lakes. The forest at Nyurba (NYU) is rather dense and mixed, with evergreen spruce (*Picea obovata* Ledeb.) and deciduous larch (*Larix gmelinii* Rupr.). The average tree height is 8 m (6 m for spruce and 12 m for larch). The forested soil at the NYU site has a litter layer of 0.08 m and an organic rich A-horizon reaching a depth of 0.16 m. It is rich in organic and undecomposed material and sandy. Mineral soil is podsolized and the rooting depth is 0.20 m. The average active layer thickness between spatially distributed point measurements was 0.75 m in mid-August 2018 and 0.73 m in early-August 2019. This site has been used as the main validation site in Article 1 and 2.

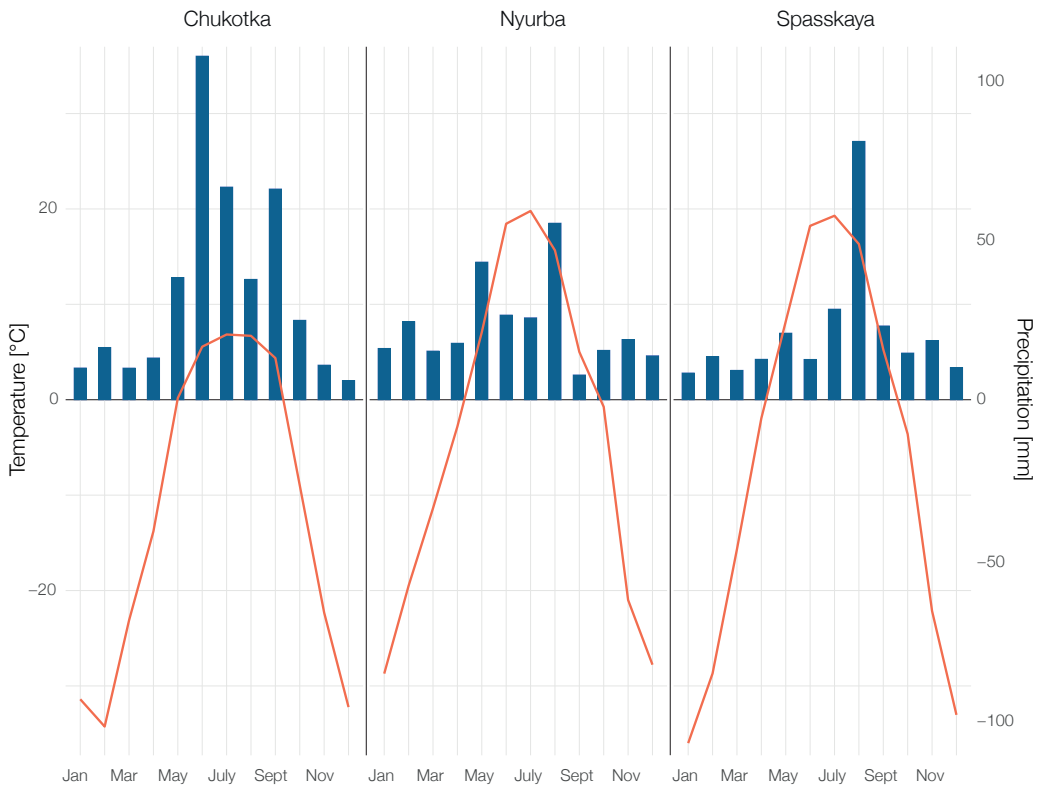


*Figure 2.2: Monthly average temperature (red) and total monthly solid and liquid precipitation (blue) for the three study sites (based on ERA-Interim ECMWF Reanalysis data for the study site coordinates).*

### 2.1.2 Meteorological and soil physical measurements

In the course of this dissertation, two automatic weather stations (AWS, Campbell Scientific, detailed list of sensors see Table 2.2, and Figure 2.3) were installed at the NYU and CHK sites. The AWS at NYU was fully functioning from August 2018 until August 2019, the AWS at CHK from July 2018 until September 2018. The AWS recorded air temperature and relative humidity at two heights (1.1 m and 2.5 m) above the ground. Wind speed and direction were measured at 3.2 m above ground. In addition, the stations measured liquid precipitation, snow depth, incoming and outgoing short- and longwave radiation and were equipped as Bowen Ratio stations. All meteorological variables were recorded at 10 min resolution and stored as 30 min averages. In order to install soil temperature and moisture sensors in the ground, soil pits were excavated in immediate vicinity (2.5 m) of the AWSs. In this soil pit, soil temperature and moisture measurement profiles were installed

*Table 2.1: Description of different study sites.*

| Study site | Nyurba (NYU) | Spasskaya Pad (SPA) | Chukotka (CHK) |
|---|---|---|---|
| Lat | N 63.08° | N 62.14° | N 67.40° |
| Lon | E 117.99° | E 129.37° | E 168.37° |
| Elevation [m asl] | 117 | 237 | 603 |
| Mean annual air temperature [°C] | -3.69 | -5.97 | -11.69 |
| Mean snow-covered air temperature [°C] | -9.6 | -12.7 | -17.7 |
| Mean snow-free air temperature[°C] | 13.6 | 13.7 | 6.0 |
| Solid precipitation [mm] | 101 | 84 | 116 |
| Liquid precipitation [mm] | 180 | 170 | 292 |
| Dominant plant functional type | Evergreen | Deciduous | Deciduous |
| Tree height [m] | 8 | 12 | 11 |
| Leaf area index [$m^2m^{-2}$] | 3 | 3 | 1 |

from the top to the bottom of the active layer consisting of 8 temperature sensors (0.07 m, 0.26 m, 0.88 m, 1.33 m, 1.28 m, 1.58 m, 1.98 m, 2.28 m) and 4 moisture probes (0.07 m, 0.26 m, 0.88 m, 1.33 m). In addition the conductive ground heat flux in the topsoil layer was measured with a heat flux plate installed at 0.02 m depth.

Furthermore, I recorded the near surface ground temperature with 100 stand-alone temperature loggers (iButtons, Table 2.2) with a measurement interval of 3 hours. These were installed in the upper 0.03 m of the organic soil at sampled forest sites. Additional soil temperature data were collected with 3 stand-alone soil temperature sensors (Hobo Loggers) at CHK and NYU.

Furthermore, at NYU, as one component of an extensive vegetation survey, the tree height of every tree within a 2 m distance was estimated along a 150 m transect from the grassland into the forest (*Kruse et al.*, 2020). Trees $< 2$ m were measured with measuring tape, while trees $> 2$ m were measured with a clinometer or visually estimated after repeated comparisons with clinometer measurements.

Together, the instrumentation with a variety of different loggers (*Langer et al.*, 2020; *Stuenzi et al.*, 2020), recorded the spatial and temporal variances across the different sites which are representative for a large area of the deciduous-dominated and mixed boreal forest domain in eastern Siberia.

As previously mentioned, the third study site, SPA, is a well-described study site

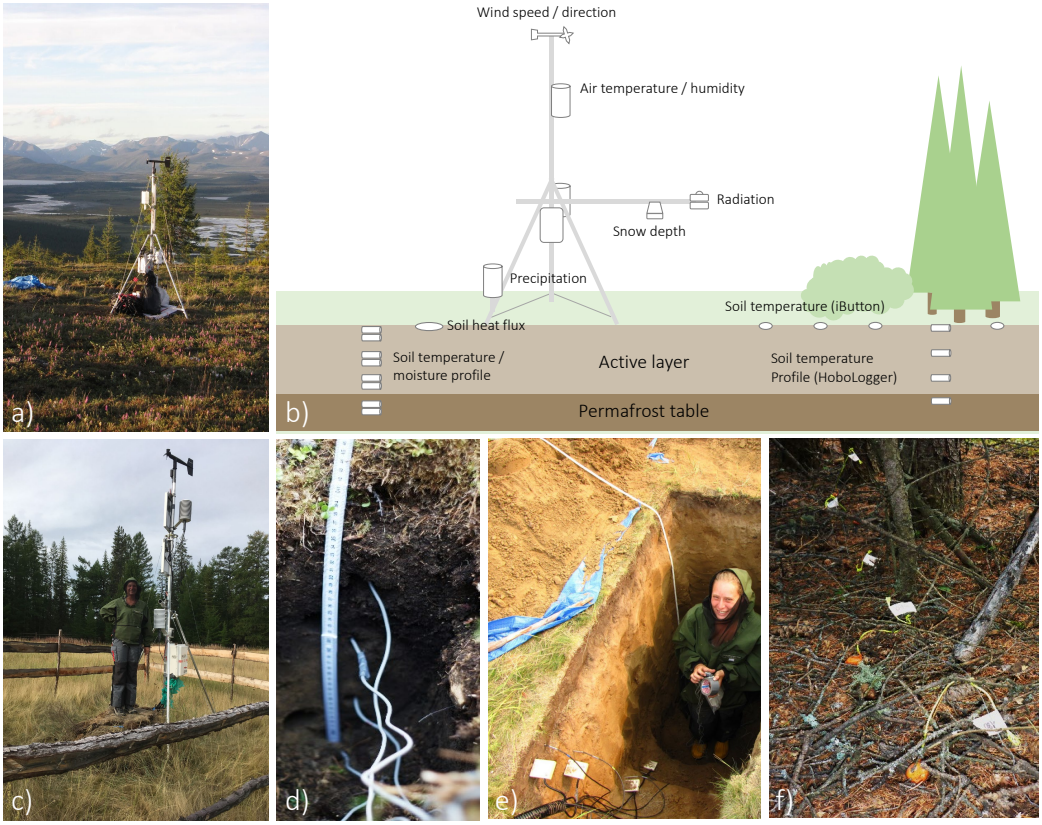


*Figure 2.3: a) Photograph of the automatic weatherstation deployed in CHK (July 2018). b) Schematic of the measurement set-up at the NYU site. c) Photograph of the automatic weatherstation in NYU before data collection and dismantling (August 2019, photo credit: Elisabeth Dietze). d) Photograph of a soil temperature profile using a HoboLogger at a forest site in CHK. e) Installation of the soil temperature profile in the vicinity of the NYU automatic weatherstation (August 2018, photo credit: Luise Schulte). f) Installation of stand-alone soil temperature sensors (iButtons) at a forest site near NYU (August 2018).*

in eastern Siberia with a unique and extensive measurement record of radiation and temperature data from below and above the forest canopy. This data set allows for a comprehensive model validation. In 1996, a 32 m observation tower was installed in the larch-dominated forest (*Ohta et al.*, 2001). Through the Arctic Data Archive system (ADS, http://ads.nipr.ac.jp/ (*Maximov et al.*, 2019), I have been provided with the latest available meteorological and radiation data from beneath and above the larch-dominated forest canopy for the time-period 2017-2018 (*Maximov et al.*, 2019). Each variable used was measured at 5-min intervals, except radiation (1-min). Ventilated shelters cover air temperature and humidity sensors. Net all-wave

*Table 2.2: Sensors used for field measurements.*

| Sensor | Brand | Measurement | Accuracy |
|---|---|---|---|
| Temperature and relative humidity probe (HMP155A) | Vaisala | Air temp. / rel. Humidity | ±1% (15 − 25 °C) |
| Alpine wind monitor (05103-45) | R. M. Young C. | Wind speed / direction | 1% of reading |
| Sonic ranging sensor (SR50A) | Campbell | Snow depth | 0.4% of height |
| Barometric sensor (CS100) | Setra | Barometric pressure | ±0.5 mb (20 °C) |
| 4-Component Net Radiometer (NR01) | Hukseflux | S/L in and out | 10% daily totals |
| Thermistor probe (107) | Campbell | Soil temperature | 0.2 °C |
| Heat flux sensor (HFP01) | Hukseflux | Ground heat flux | ±3% |
| Raingauge tipping bucket unheated (52203) | R. M. Young C. | Precip. (liquid) | 2% up to 25 mm $hr^{-1}$ |
| Water Content Reflectometer (CS616) | Campbell | Soil moisture | ±2.5% VWC |
| Hobo 4 Channel Data Logger + Temperaturesensor | Onset | Soil temperature | ±2 mV ±2.5% abs. reading |
| iButton (DS1922L) | Maxim Integrated | Soil temperature | ±0.5 °C (-10 − 65 °C) |

radiation and the four components of radiation are measured every minute, and the data loggers record average, maximum and minimum values. Upward and downward longwave radiation is corrected using the sensed temperature at domes and sensor bodies. Ground temperature is measured at seven depths, and soil moisture at five depths. A more detailed description of the sensors can be found in Table 1 in *Ohta et al.* (2001).

## 2.2 Coupled permafrost-multilayer vegetation model

### 2.2.1 CryoGrid permafrost model

As a basis of this thesis, I have made use of CryoGrid, a one-dimensional, numerical land surface model used to simulate the physical processes in permafrost regions. The numerical model simulates the below-ground temperature field based on temporally changing conditions at the ground-surface boundary. The model has been developed in order to simulate different permafrost landscape processes such as subsidence, thermokarst, or ice-wedge degradation (*Nitzbon et al.*, 2019). The model version is originally described in *Westermann et al.* (2016) and has since been extended with different functionalities such as lake heat transfer (*Langer et al.*, 2016), multi-tiling (*Nitzbon et al.*, 2019, 2020), and an extensive snow scheme based on CROCUS (*Vionnet et al.*, 2012; *Zweigel et al.*, 2021). To simulate the thermohy-

drological regime of the ground the one-dimensional heat equation is numerically solved including groundwater phase change. In Article 1, groundwater flow is simulated with an explicit instantaneous infiltration scheme (*Nitzbon et al.*, 2019). For the second and third articles, I have used an updated model for the phase partitioning between liquid water, ice, and water vapor (*Stuenzi et al.*, 2021a). This paramterization is based on *Painter and Karra* (2014). By smoothing the thermodynamically derived relationship and eliminating jump discontinuity at freezing the new relationship for phase partitioning of water in frozen soil shows improved performance for unsaturated ground conditions. The flow in freezing soil is solved by a modified nonisothermal Richards equation. This constitutive relationship is more applicable for dry soils or soils with high gas content. This leads to improved model performance for the dry ground conditions at the study sites studied within this dissertation.

The surface energy balance scheme is based on atmospheric stability functions and calculated as the upper boundary condition. The surface energy balance is comprised of the exchange of sensible and latent heat, radiation, evaporation, and condensation at the ground surface. Furthermore, the model simulates the evolution of the snow cover based on the extensive Crocus-based snowpack scheme explained in the following section 2.2.3. The model is forced by standard meteorological variables, which can be obtained from AWSs, reanalysis products, or climate models. The required forcing data include air temperature, precipitation (solid and liquid), wind speed, incoming short- and longwave radiation, humidity, and air pressure (*Westermann et al.*, 2016). The change of internal energy in the subsurface domain over time is composed of fluxes across the upper and lower boundaries and can be written as

$$\frac{\delta E}{\delta t} = S_{\mathrm{in}} + S_{\mathrm{out}} + L_{\mathrm{in}} + L_{\mathrm{out}} + Q_{\mathrm{h}} + Q_{\mathrm{e}} + Q_{\mathrm{s}}, \tag{2.1}$$

where the input to the uppermost grid cell is derived from the fluxes of shortwave ($S_{\mathrm{in}}$, $S_{\mathrm{out}}$) and longwave ($L_{\mathrm{in}}$, $L_{\mathrm{out}}$) radiation, as well as the latent ($Q_{\mathrm{e}}$), sensible ($Q_{\mathrm{h}}$), and the storage heat flux ($Q_{\mathrm{s}}$) between the atmosphere and the ground surface (*Westermann et al.*, 2016). Fluxes are noted as negative if the point away from the ground surface towards the atmosphere, and as positive, if they point towards the surface. Without a vegetation scheme, the incoming short- and longwave radiation ($S_{\mathrm{in}}$, $L_{\mathrm{in}}$) are provided directly by the forcing data. The outgoing

shortwave radiation equals the incoming shortwave radiation multiplied with the surface albedo ($\alpha$), which depends on ground covers such as snow, water or ice:

$$S_{\text{out}} = S_{\text{in}}(-\alpha), \tag{2.2}$$

Following the laws of Kirchoff and Stefan-Boltzmann, the outgoing longwave radiation is the sum of the reflected incoming longwave radiation and the surface emission of the ground:

$$L_{\text{out}} = -(1-\epsilon)L_{\text{in}} - \epsilon\sigma T_{\text{surf}}^4, \tag{2.3}$$

with $\epsilon$ being the ground surface emissivity, $\sigma$ the Stefan-Boltzmann constant and $T_{\text{surf}}$ the surface ground temperature in Kelvin [K]. The turbulent heat fluxes ($Q_{\text{h}}$ and $Q_{\text{e}}$) are calculated based on the Monin-Obukhov similarity theory (*Monin and Obukhov*, 1954), and explained in detail in *Westermann et al.* (2016):

$$Q_{\text{h}} = \frac{\rho_{\text{a}} c_{\text{p}}}{r_{\text{a}}^{H}}(T_{\text{air}}(h) - T_{\text{surf}}) \text{ and} \tag{2.4}$$

$$Q_{\text{e}} = \frac{\rho_{\text{a}} L_{\text{1g}}}{r_{\text{a}}^{\text{E}} + r_{\text{s}}}(q(h) - q_{\text{surf}}). \tag{2.5}$$

The air temperature ($T_{\text{air}}(h)$) and specific humidity ($q(h)$) are the air temperature and specific humidity at height $h$ and are provided by the meteorological forcing data. Parameters are the density of air ($\rho_{\text{a}}$), specific latent heat of water vaporization ($L_{\text{1g}}$), and specific heat capacity of air ($c_{\text{p}}$). The surface's resistance against evaporation ($r_{\text{s}}$) is a parameter set dependent on the surface condition (i.e. snow, soil, water, etc.). The aerodynamic resistances ($r_{\text{a}}^{\text{H}}$, $r_{\text{a}}^{\text{E}}$) of the lower atmosphere to turbulent heat transfer are calculated depending on the atmospheric stability. Finally, the specific humidity above the surface ($q_{\text{surf}}$) results from the surface temperature and the atmospheric pressure.

In terms of CryoGrid there has previously been much uncertainty in the model formulation concerning the insulation effect of surface vegetation and the litter layer. As detailed in the Introduction, they are both important factors for the topsoil temperature, and nevertheless, they are often neglected in common land

surface models (*Ekici et al.*, 2015). In previous CroyGrid versions, the vegetation has not been incorporated yet. The goal in this dissertation was to further develop CryoGrid for use in permafrost underlain boreal forest. Within this thesis, the surface energy balance of CryoGrid has been replaced by the multilayer canopy module described in the following section 2.2.2.

### 2.2.2 Multilayer canopy model

#### Canopy module

The biosphere is an essential part of common Land Surface Models (LSMs) used in Earth-System Models. The biosphere's key contribution to atmospheric greenhouse gas concentrations and carbon cycle feedbacks are often at the focus for the development of LSMs. Because of this focus, the coupling of plants and the atmosphere is frequently described in a rather simplistic way. Additionally, the representation of interactions in complex systems, such as boreal permafrost ecosystems, is generally overlooked in current LSMs (*Blyth et al.*, 2021). Furthermore, while there has been recent progress (e.g. *Chadburn et al.* (2015)), LSMs oftentimes lack the capability of accurately representing detailed permafrost dynamics.

Commonly used forest canopy representations (e.g. *Dickinson et al.* (1993); *Sellers et al.* (1996); *Harman and Finnigan* (2008)) ignore the vertical structure of the canopy and describe the canopy as a one- or two-leaf (also called big leaf) representation. Two-leaf representations include leaf physiological processes over nitrogen and light profiles and a sunlit and a shaded fraction of the canopy, while one-leaf representations consider a homogeneous single layer of phytomass. Such canopy representations ignore the roughness sublayer and parameterize the within-canopy turbulence in an ad-hoc, averaged manner. In a recent review, *Bonan et al.* (2021) have concluded that while the big-leaf canopy representations are simpler, more computationally efficient, and of greater utility for the coupling to the atmosphere, they are incorrect in their physics. In order to understand the processes controlling surface fluxes, the vertical structure of the canopy is crucial and the ad-hoc parameterizations used in simple one- and two-leaf representations of canopies are no longer valid. Especially because the focus here lies on the energy- and water fluxes between the canopy and the permafrost, a detailed representation of the within- and below-canopy fluxes is crucial. The multilayer canopy model used within this thesis is a state-of-the-art multilayer vegetation model (CLM-ml v0,

originally developed for the Community Land Model CLM by *Bonan et al.* (2018)). The detailed modeling scheme follows a similar concept as the multilayer approach in ORCHIDEE-CAN (*Chen et al.*, 2016b; *Ryder et al.*, 2016). The model provides a comprehensive parameterization of fluxes from the ground, through the multilayered canopy, up to the roughness sublayer. The implementation of this roughness sublayer allows the representation of different canopy structures and their impact on the vertical heat and moisture transfer. Photosynthesis, leaf-water potential, stomatal conductance, leaf temperature, and leaf fluxes are calculated in an iterative manner. This improves model performance in terms of capturing the stomatal conductance and canopy physiology, nighttime friction velocity, the diurnal radiative temperature cycle, and sensible heat flux (*Bonan et al.*, 2014, 2018). The within-canopy wind profile is calculated using above- and within-canopy coupling with a roughness sublayer parameterization (see *Bonan et al.* (2018) for further detail). This canopy model was developed for use with CLM soil properties. I have developed a CLM-independent multilayer canopy module which I have coupled to CryoGrid by integrating novel interactions and an improved snow cover parameterization. To set necessary parameters in the canopy module, the model makes use of CLM-defined plant functional type values for evergreen and deciduous needleleaf forests.

### 2.2.3 Coupled permafrost-forest model

In the context of this thesis, I have extended the described CryoGrid permafrost model (*Westermann et al.*, 2016) by a multilayer canopy module (*Bonan et al.*, 2014, 2018) described above, to simulate the energy- and water processes in boreal permafrost. The canopy model is coupled to CryoGrid by replacing its standard surface energy balance scheme while soil state variables are passed back to the forest module (Figure 2.4).

CryoGrid has, so far, not included a vegetation scheme but has been used to successfully describe atmosphere-ground energy transfer and the ground thermal regime in barren and grass-covered areas (*Langer et al.*, 2016; *Westermann et al.*, 2016; *Nitzbon et al.*, 2019). Within this thesis, I have tailored and implemented the multilayer vegetation scheme to simulate the turnover of heat, water, and snow between atmosphere, forest canopy and ground.

The top of the canopy surface energy balance is calculated based on atmospheric

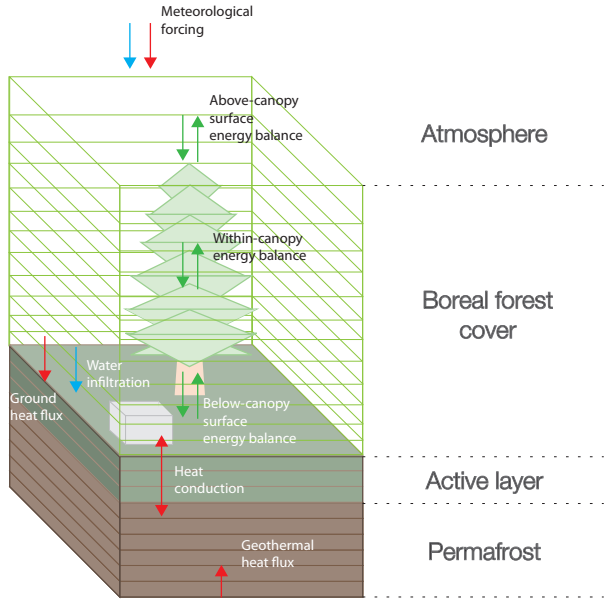


*Figure 2.4: Overview of the physical processes represented in the coupled permafrost-multilayer canopy model. Included are the above-, within-, and below canopy energy fluxes (green), as well as the ground heat flux, heat conduction through the soil, the geothermal heat flux (red), the meteorological forcing (red and blue), and water infiltration (blue).*

forcing data. The ground surface energy balance is replaced and now solved numerically by the forest module:

$$S_{\mathrm{in}_{\mathrm{canopy}}} + S_{\mathrm{out}_{\mathrm{ground}}} + L_{\mathrm{in}_{\mathrm{canopy}}} + L_{\mathrm{out}_{\mathrm{ground}}} + Q_{\mathrm{h}_{\mathrm{ground}}} + Q_{\mathrm{e}_{\mathrm{ground}}} - Q_{\mathrm{s}_{\mathrm{ground}}} = 0, \quad (2.6)$$

with $L_{\mathrm{in}_{\mathrm{canopy}}}$ and $S_{\mathrm{in}_{\mathrm{canopy}}}$ being the incoming long- and shortwave fluxes from the canopy module reaching the ground level. $S_{\mathrm{out}_{\mathrm{ground}}}$ is the outgoing shortwave flux from the ground, $L_{\mathrm{out}_{\mathrm{ground}}}$ the outgoing longwave flux, $Q_{\mathrm{e}_{\mathrm{ground}}}$ the latent heat flux, $Q_{\mathrm{h}_{\mathrm{ground}}}$ the sensible heat flux, and $Q_{\mathrm{s}_{\mathrm{ground}}}$ the storage heat flux at the ground surface. These sub-canopy components of the energy balance directly replace the previous surface energy balance components of the former CryoGrid versions (Equation 2.1). The storage heat flux ($Q_{\mathrm{s}_{\mathrm{ground}}}$) is calculated based on the temperature value of the uppermost ground (or snow) layers which are passed to the forest module from CryoGrid:

$$Q_{\mathrm{s}_{\mathrm{ground}}} = k\frac{T_{\mathrm{s}} - T_{\mathrm{ground}}}{\Delta z}, \tag{2.7}$$

where k is the soil thermal conductivity (or snow thermal conductivity in case of a snow layer) and $T_{\mathrm{s}}$ the soil surface temperature. $T_{\mathrm{ground}}$ is the actual ground temperature for the first layer below the surface and $\Delta z$ the soil or snow layer thickness. Following *Westermann et al.* (2013, 2016), the soil thermal conductivity is parameterized based on the *Cosenza et al.* (2003). The thermal conductivity of the soil is calculated as weighted power mean from the conductivities and volumetric fractions of the soil's water, ice, air, mineral and organic components.

The forest module receives ground state variables from the top CryoGrid soil layers. These state variables include the soil layer temperatures ($T_{\mathrm{ground}}$), the soil layer moisture ($W_{\mathrm{ground}}$), ice content ($I_{\mathrm{ground}}$), and soil layer conductivity ($k_{\mathrm{ground}}$). Accordingly, the vegetation transpiration fluxes are subtracted from ground soil layers within the rooting depth, and evaporation fluxes are subtracted from the ground surface.

Rain and snowfall is intercepted throughout the canopy with only a fraction reaching the ground directly as throughfall. The sum of the precipitation fraction reaching the ground ($W_{\mathrm{ground}_{\mathrm{s}}}$) is:

$$\frac{\delta W_{\mathrm{ground}_{\mathrm{s}}}}{\delta t} = fP_{\mathrm{R}} + D_{\mathrm{c}} - E_{\mathrm{c}} + D_{\mathrm{t}} - E_{\mathrm{t}} \tag{2.8}$$

consisting of direct throughfall ($fP_{\mathrm{R}}$), canopy drip ($D_{\mathrm{c}}$), canopy evaporation ($E_c$), the stemflow ($D_{\mathrm{t}}$) and the stem evaporation ($E_{\mathrm{t}}$). These values are based on the retained canopy water ($W_{\mathrm{c}}$):

$$\frac{\delta W_{\mathrm{c}}}{\delta t} = (1 - f - f_{\mathrm{t}})P_{\mathrm{R}} - E_{\mathrm{c}} - D_{\mathrm{c}}, \tag{2.9}$$

where $1 - f - f_t P_R$ is the precipitation, which is intercepted, and $W_t$ the retained trunk water:

$$\frac{\delta W_{\mathrm{t}}}{\delta t} = f_{\mathrm{t}}P_{\mathrm{R}} - E_{\mathrm{t}} - D_{\mathrm{t}}. \tag{2.10}$$

**Snow module**

While the permafrost model CryoGrid encompasses different snow schemes, the multilayer canopy has previously not been coupled to a snow scheme (*Bonan et al.*, 2018). The snow module employed within this thesis is based on *Zweigel et al.* (2021), which has extended CryoGrid with a CROCUS snow scheme-based snow microphysics parameterization (*Vionnet et al.*, 2012). As described in Article 1, the micro-structure of the snow-pack is characterized by grain size (gs, mm), sphericity (s, unitless, range 0-1), and dendricity (d, unitless, range 0-1). Snow density and properties of new snow layers are wind-speed and temperature-dependent. After deposition, the development of the snow-layers microstructure is based on temperature gradients and liquid water content. Based on the snow properties, an albedo value is calculated for the surface layer. Furthermore, an absorption coefficient is calculated for each layer, also based on the snow properties. Throughout the snow layers, the incoming solar radiation is gradually absorbed and the remainder is added to the lowest layer. Snow density and compaction are increased based on overload pressure and wind compression. In each timestep during snowfall, new snow is added on top and mixed with the old snow based on ice amount. A new snow layer is built once the snow water equivalent of the top layer exceeds 0.01 m, which equals a snow layer thickness of 0.03 m. For the first snowfall of the season and before the entire ground is covered by snow, the surface energy balance of the ground and the snow are calculated independently and added up based on their fractional cover. After the first snow layer is built, the surface energy balance is calculated for the snow-pack itself. The snow cover is built upon the ground below the forest canopy, and snow interception within and on top of the canopy are handled the same way as liquid precipitation (section 2.2.3). The top of the canopy wind speed is used to calculate the falling snow density. The surface temperature of the ground, the surface thermal conductivity, and the snow layer thickness are exchanged with the vegetation. Furthermore, the evaporative flux is subtracted from the snow surface.

### 2.2.4 Further model coupling to a dynamic vegetation model (Larix Vegetation Simulator (LAVESI))

In order to incorporate dynamic vegetation changes and study larch forest development, I have further advanced the multilayer-permafrost model to enable a coupling

with LAVESI, an individual based and spatially-explicit tree population model that simulates *Larix gmelinii* population dynamics. LAVESI was originally described in *Kruse et al.* (2016) and has been developed to simulate and understand local stand interactions in larch populations that can cause large scale population dynamics.

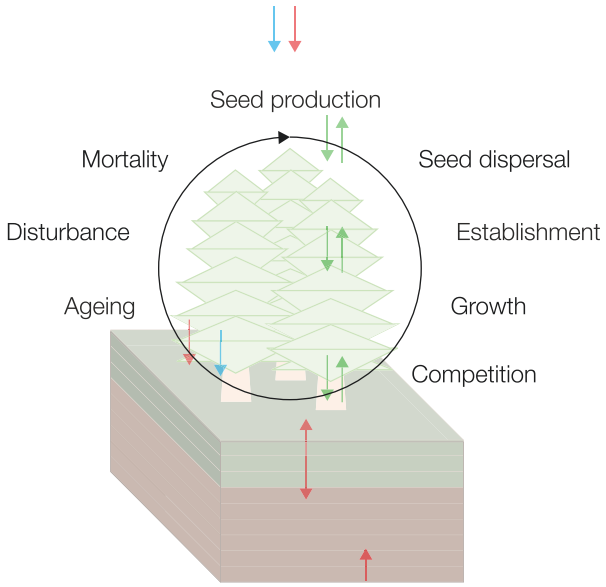


*Figure 2.5: Overview of the physical processes represented in the dynamic permafrost-multilayer canopy model coupled to LAVESI. The dynamic vegetation model LAVESI includes all life stages of Larix gmelinii as well as the integrated disturbance scenarios (surface and canopy fires, and logging).*

The model is based on a growth model where functions have been added successively, according to field observations. One simulation step equals one year, in which, environmental factors (weather and competition) and the different processes of growth, seed production, seed dispersal, establishment, and mortality are included (Figure 2.5). The coupled model system can (1) accurately assess the detailed thermal and hydrological fluxes between permafrost and the forest cover; and (2) simulate dynamic vegetation, including the full life-cycle (seed-seedling-mature tree), which leads to the non-linear behavior of population dynamics, and (3) includes a 3-D landscape resolution. The coupled model with an explicit representation of the permafrost table, active layer thickness, and the soil hydrology therein provides better results in terms of the vegetation dynamics because the permafrost is a major determinant for species occurrence and performance. To

couple the landscape resolution of LAVESI with the one-dimensional set-up of the forest-permafrost model, the study area used in LAVESI is separated into three sub-areas for which CryoGrid simulations are set up in parallel. The spatial variability of the forest cover is, thus, explicitly represented by an ensemble of three parallel CryoGrid instances. Stand specific state variables, such as leaf area index (LAI), plant area index (PAI), litter layer height, organic content in the organic soil layer, albedo, and the soil moisture content, are provided to CryoGrid by LAVESI. In exchange, LAVESI receives the yearly total plant-available groundwater in volume percent (PAW), and the maximum active layer thickness (ALT). The output generated by the three CryoGrid instances is extrapolated back to the original resolution of the environmental grid used in LAVESI (resolution of 0.2x0.2 m) (see Article 3 and *Kruse et al.* (2021) for additional model details).

### 2.2.5 Forcing data

The meteorological forcing data used by CryoGrid (air temperature, air pressure, wind speed, relative humidity, solid and liquid precipitation, incoming long- and shortwave radiation, and cloud cover) are obtained from ERA-interim (Article 1 and 2) and ERA-5 (Article 3) (ECMWF Reanalysis) extracted for our sites at a 1-hourly time-step (*Simmons et al.*, 2007; *Hersbach et al.*, 2018). In Article 3, I performed model simulations until 2050 under two projected climate change scenarios (SSP - Shared Socioeconomic Pathways): SSP1-2.6 (atmospheric CO2 around 420 parts per million (ppm), and global temperatures 1.3 - 1.9 °C above pre-industrial levels by 2100); and SSP5-8.5 (atmospheric CO2 around 935 parts per million (ppm), and global temperatures 4 - 6.1 °C above pre-industrial levels by 2100). Scenario data from the MPI-ESM1.2-HR model of the Max Planck Institute for Meteorology (*Müller et al.*, 2018) was applied (as 6-year monthly mean anomalies relative to the reference period 2015-2020) to the ERA5 data to generate forcing data for the projected timespan 2021-2050 and the two climate change scenarios (*Koven et al.*, 2015). The MPI-ESM1.2-HR (with a spatial resolution of 0.94 °EW x 0.94 °NS or approx. 100 km) model grid was interpolated to fit the ERA-5 grid. The temperature threshold for snow vs. rain is 0 °C, and minimum wind speed is set to the minimum value within the reference time frame (2015-2020). From the same data, the necessary forcing data of monthly mean temperature and precipitation sums for LAVESI were aggregated and 6-hourly wind speed and

direction were sampled. Before the ERA-5 time period (0-1978), LAVESI uses the monthly Climate Research Unit data set CRU TS 2.23 available at a 0.5° spatial resolution (*Harris et al.*, 2020).

### 2.2.6 Code and data availability

Model codes are available on Zenodo. The initial version of the coupled model used in Article 1 is available at DOI: 10.5281/zenodo.4317107. The code developments presented in Article 2, including fractional composition of deciduous and evergreen taxa, and a novel freeze curve parameterization are available at DOI: 10.5281/zenodo.4603668. The dynamic vegetation-permafrost model, including the coupling of LAVESI and the implementation of disturbance scenarios, is available at DOI: 10.5281/zenodo.5119987. Field data collected are available on Pangaea. The AWS and soil temperature data for August 2018 to August 2019 at Nyurba and Chukotka are available at DOI: 10.1594/PANGAEA.919859 (*Stuenzi et al.*, 2020). The soil surface temperature data (iButton) are available at DOI: 10.1594/PANGAEA.914327 (*Langer et al.*, 2020), and the forest inventories from 2018 are available at DOI: 10.1594/PANGAEA.923638 (*Kruse et al.*, 2020). The data for Spasskaya Pad is accessible through the Arctic Data archive System (ADS, http://ads.nipr.ac.jp/, last access: 3 September 2020) (*Maximov et al.*, 2019).

# Chapter 3

# Summary

In the previous chapters, I have explained the theory and background, research questions, and underlying methodology in this thesis. In the following chapter, I summarize the three research articles, which are provided in full in Part II, and outline how they build upon each other. Table 3.1 provides an overview of the methodologies used in the three articles.

## 3.1 Article 1

Within the first research article, I have adapted a one-dimensional land surface model (CryoGrid) for the application in vegetated areas by coupling a multilayer canopy model (CLM-ml v0; Community Land Model). This model is the methodological base of all three articles within my dissertation. In the first article, I have used this novel model setup to reproduce the energy transfer and thermal regime at a study site (N 63.08°, E 117.99°) in mixed boreal forest in eastern Siberia where an extensive measurement set was generated. The model was driven by meteorological forcing data reflecting present-day climatic conditions.

An extensive comparison between measured and modeled energy balance variables revealed a satisfactory model performance justifying its application to investigate the thermal regime; surface energy balance; and the vertical exchange of radiation, heat, and water in this complex ecosystem. I have further performed an extensive validation at an external study site.

I found that the forests exert a strong control on the thermal state of permafrost through changing the radiation balance and snow cover phenology. The forest cover alters the surface energy balance by inhibiting over 90% of the solar radiation

and suppressing turbulent heat fluxes. Additionally, the simulations revealed a surplus in longwave radiation by up to 20% trapped below the canopy, similar to a greenhouse, which lead to a magnitude in storage heat flux comparable to that simulated at the grassland site. Forested permafrost holds a higher groundwater content than the grassland site. Furthermore, I found that the end-of-season snow cover is three times greater at the forest site and that the onset of the snow-melting processes is delayed. In summary, the forest has a net stabilizing effect on the permafrost ground below. Canopy shading is the main controlling mechanism, along with enhanced longwave radiation, higher groundwater content, and a higher snowpack. These findings provided the baseline to further investigate the exchange processes and feedbacks between permafrost and boreal forests.

Stuenzi, S.M., Boike, J., Cable, W., Herzschuh, U., Kruse, S., Pestryakova, L. A., Schneider von Deimling, T., Westermann, S., Zakharov, E.S., and Langer, M. (2021): Variability of the surface energy balance in permafrost-underlain boreal forest, *Biogeosciences*, 18, 343–365,
DOI: 10.5194/bg-18-343-2021.

## 3.2 Article 2

In the second article, I analyzed future projections of forest density and plant functional type compositions based on simulation results of a Dynamic Global Vegetation Model (LPJ-GUESS) under global warming scenarios. I then used the detailed permafrost-multilayer canopy model, presented in Article 1, to study the spatial impact-variability of simulated future scenarios of forest densities and compositions for three study sites throughout eastern Siberia under current climate conditions.

The results showed that a change in forest density has a clear effect on the ground surface temperatures (GST) and the maximum active layer thickness (ALT) at all sites, but the direction depends on local climate conditions. At two sites, higher forest density leads to a significant decrease in GSTs in the snow-free period, while leading to an increase at the warmest site. Complete forest loss leads to a deepening of the ALT independently of local climatic conditions. Forest loss can

induce both – active layer wetting of up to four times or drying by 50% – depending on precipitation and substrate conditions. Deciduous-dominated canopies reveal lower GSTs compared to evergreen stands, which will play an important role in the spreading of evergreen taxa and the persistence of permafrost under warming conditions.

Our study highlighted that changing density and composition will significantly modify the thermal and hydrological state of the underlying permafrost. The induced soil changes will likely affect key forest functions such as the carbon pools, and related feedback mechanisms such as swamping, droughts, fires, or forest loss.

Stuenzi, S.M., Boike, J., Gädecke, A. , Herzschuh, U., Kruse, S., Pestryakova, L. A., Westermann, S., and Langer, M. (2021): Sensitivity of Ecosystem-Protected Permafrost Under Changing Boreal Forest Structures, *Environmental Research Letters*, 16, 084045,
DOI: 10.1088/1748-9326/ac153d.

## 3.3 Article 3

Forest disturbances and changing climate conditions can cause vegetation shifts and potentially destabilize the carbon stored within the vegetation and permafrost. Disturbed permafrost-forest ecosystems can (1) develop into dry or swampy bush- or grasslands, (2) shift towards broadleaf- or evergreen needleleaf-dominated forests, or (3) recover to the pre-disturbance state. An increase in the number and intensity of fires, as well as intensified logging activities could lead to the partial or complete ecosystem and permafrost degradation.

Within the first two articles, I treated forests as a static entity represented by observed or projected leaf and stem area indices, tree height, and plant functional type parameters. In the third Article, I integrated a dynamic vegetation model which allowed for dynamic tree growth. To study the dynamic evolution of larch forest covers under changing climatic conditions, I have further developed the model to enable the coupling to a dynamic forest model, LAVESI (“Larix vegetation simulator´´). I used this dynamic multilayer canopy-permafrost model to simulate a well-researched tree stand in eastern Siberia. I implemented expected mortality,

defoliation, and ground-surface changes of the most common disturbance scenarios (surface and canopy fires, and logging) to analyze the forest recovery's impact on the permafrost underneath.

The simulations revealed that forest loss induces soil drying of up to 50%, which leads to lower active layer thicknesses (ALTs) and abrupt or steady decline of larch forest cover, depending on the intensity of the disturbances. Only after surface fires, which induce low mortality rates and are the most common disturbances in these ecosystems, forests can successfully recover and even surpass pre-disturbance forest density values. This trajectory is nevertheless highly dependent on individual years following the disturbance, with years with low spring precipitation leading to larch forest loss.

Stuenzi, S.M., Kruse, S., Boike, J., Herzschuh, U., Oehme, A., Pestryakova, L. A., Westermann, S., and Langer, M. (2021): Thermohydrological impact of forest disturbances on ecosystem-protected permafrost, *submitted to Journal of Geophysical Research: Biogeosciences.*

*Table 3.1: Overview of the scope and methodology of the three articles.*

| | Article 1 | Article 2 | Article 3 |
|---|---|---|---|
| Thesis chapter | Chapter 5 | Chapter 6 | Chapter 7 |
| Study area | Nyurba<br>(63.19°N, 118.20°E)<br>Spasskaya Pad<br>(62.14°N, 129.37°E) | Nyurba<br>(63.19°N, 118.20°E)<br>Spasskaya Pad<br>(62.14°N, 129.37°E)<br>Chukotka<br>(67.40°N, 168.37°E) | Spasskaya Pad<br>(62.14°N, 129.37°E) |
| Dominant plant functional types | Mixed evergreen and deciduous needleleaf | Evergreen and deciduous needleleaf | Deciduous needleleaf |
| Climatic forcing | recent (2010-2019) | recent (2010-2019) | recent + future (2010-2050)<br>(RCP2.6, RCP4.5, RCP8.5) |
| Research objective | 1 | 1,2 | 1,3 |
| Model development | CryoGrid + Multilayer canopy coupling<br>Surface energy balance<br>Precipitation<br>Evapotranspiration<br>Crocus snow scheme | Fractional composition of deciduous and evergreen<br>Freeze curve | CryoGrid Multilayer canopy + Lavesi coupling<br>Disturbance scenarios |
| Model diagnostic | Ground surface temp.<br>Soil moist. content<br>Thaw depth<br>Snow height | Ground surface temp.<br>Plant-available soil moist.<br>Thaw depth<br>Snow height | Plant-available soil moist.<br>Thaw depth |
| Process explored | Surface energy balance below and above canopy | Permafrost-impact of change in forest density and composition | Permafrost persistence under forest cover<br>recovery after disturbance and<br>tipping points |

# Chapter 4

# Synthesis

The research presented within this dissertation has addressed the objectives outlined in Chapter 1.4. The three articles summarized in Chapter 3 and provided in Part II all contribute differently to answering the central research question of how the complex interactions and feedbacks between boreal forests and permafrost can be modeled to successfully make predictions on the future development of this ecosystem and its role under changing climate conditions. In the following, I synthesize the findings of the conducted research.

## 4.1 Physical processes and feedbacks in permafrost-affected boreal forests

The first research objective within this thesis was to gain a better understanding of the physical processes and feedbacks in permafrost-affected boreal forests by developing and validating a detailed forest-permafrost model. The presented model enables us to investigate the energy transfer and surface energy balance, and thereby quantify and study the impact of forest on the hydrothermal permafrost regime.

> In regards to the first research objective, the numerical modeling work I have conducted, revealed that the integration of detailed permafrost and canopy modeling schemes is essential for investigating the complex ecosystem interactions of boreal forests. The canopy fluxes significantly alter the below-canopy energy balance, snow cover dynamics, and the thermo-hydrological conditions of the ground.

> The coupling of two highly detailed and complex physical models offers new possibilities to identify and quantify the impact of control mechanisms and parameters within boreal permafrost ecosystems (Article 1-3). Compared to previous models, the developed model allows to quantify and trace vertical fluxes of radiation, heat, water, and snow through multiple canopy and ground layers. The layer structure of the model allows representing very specific forest characteristics (canopy structures and densities) and soil properties (organic layers) controlling the complex permafrost dynamics under boreal forest covers.

My work further reveals the importance of broad datasets derived from field measurements for model calibration and validation. The fieldwork conducted in the framework of this thesis includes measurements by automatic weather stations, stand-alone soil temperature sensors, soil sampling, soil temperature, and moisture profiles, tree sampling and surveying, as well as the acquisition of drone images, moss descriptions and sampling and ground vegetation analysis. All of the data has been made publicly available. The extensive data set adds to the sparse data records in eastern Siberian boreal-permafrost regions and is of great value for further model development and validation. In an extensive validation exercise in Article 1, measured and modeled energy balance variables revealed a highly satisfactory model performance justifying its application to investigate the thermal regime and surface energy balance at the selected study sites. Additionally, the model revealed further satisfactory agreement between modeled and measured components of the surface energy balance at the additional study sites used in Article 2.

## 4.2 Future development of permafrost affected boreal forests

The second objective of this thesis was to understand how the identified interactions between the forest cover and permafrost respond under changing forest conditions (forest density and composition changes). To understand and quantify the impacts of forest cover changes on permafrost, I have analyzed projected forest cover trajectories for eastern Siberia under different warming scenarios for two regions of interest (east and west) in Article 2 (Figure 4.1).

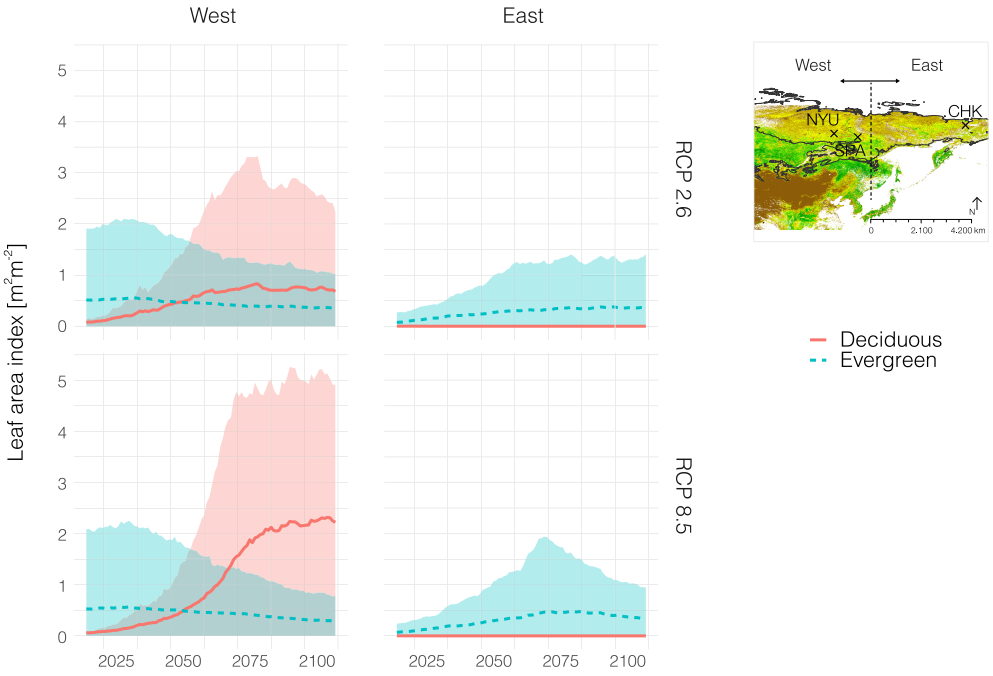


*Figure 4.1: Projected LAI for needleleaf evergreen (blue) and needleleaf deciduous (red) plant functional types under the two warming scenarios, RCP 2.6, and RCP 8.5 for the time frame 2006-2099. Data covers the region from E* $105 - 167°$ *and N* $45 - 70°$ *and are separated into two individual study regions, West (E* $105.25 - 137.25°$*, bottom) and East (E* $137.75 - 169.75°$*, top). The lines indicate mean values while the shaded areas show the corresponding 90th and 10th percentile.*

The biome projection data from LPJ-GUESS model simulations reveal an increase in needleleaf evergreen for the entire region of interest in eastern Siberia for the coming decade, followed by a decrease in the western region under all climate scenarios. In the western region, deciduous taxa will continue increasing until the end of the century under all climate forcing scenarios (see Article 2 in Chapter 6). By analyzing the current and projected forest covers under warming climate scenarios, I gained a clear idea of the direction of forest shifts. Based on these data, which are in agreement with other modeled forest cover projections for Eurasia (e.g. *Shuman et al.* (2014); *IPCC* (2019)), I was able to constrain the expected changes in plant functional type compositions and forest densities for the entire eastern Siberian boreal forest region underlain by permafrost east of 105° and north of 45°. The overall forest density is projected to increase with warming temperatures under all warming scenarios and for the entire region of interest.

> With respect to the second research objective, my analysis of the current and projected forest covers in eastern Siberia provided a clear picture of the projected forest covers. The conducted simulations underlined the importance of forest cover changes for permafrost thaw and conditions. Shifting forest covers significantly modify thermal and hydrological conditions of the underlying permafrost and the induced soil changes will likely affect key forest functions.

The research presented in detail in Article 2 enhances our understanding of how changing forest density and composition impact ecosystem-protected permafrost. This is especially relevant because of the forest's importance as a carbon pool and forest change-related feedbacks such as swamping, fires, and forest loss. The strong impact of forest cover transformations on the hydrological regime will further amplify climate-induced changes in near-surface temperature and precipitation. In consequence, the feedback loop might be further amplified by increasing fire probability and disease vulnerability due to additional water stress. Climate conditions and enhanced wetting can eventually lead to swamping and thermokarst causing forest die-back as observed in drunken forests. In light of the current discussion on boreal forests and their role in climate change mitigation, this dissertation provides important insights into the range of possible changes to the permafrost conditions that can be expected following landscape changes. Such changes can be deforestation through fires or other land-use change, afforestation in currently unforested grasslands, or the climate-induced densification and compositional changes of forested areas. My research shows that the structure and composition of forests are highly dependent on the local ecosystem resilience towards rising air temperatures, a decrease in precipitation, and an increasing frequency and intensity of forest fires. The favoring of different fire regimes between evergreen and deciduous taxa, as well as warmer and drier conditions, can lead to fast ecosystem shifts. Altered thermal conditions, higher soil wetness or soil drainage, enrichment in nutrients, and an increased active layer thickness can all have a favoring effect on either evergreen needleleaf or deciduous hardwood expansion, lead to the complete loss of forest cover or change the forest density. Furthermore, I demonstrate that these feedbacks will cause a significant shift in the thermal and hydrological permafrost state, which potentially destabilizes tightly coupled ecosystem functions.

## 4.3 Feedbacks and forest disturbances

In recent years forest and permafrost disturbances have become more visible in eastern Siberia (Figure 4.2) (*Boike et al.*, 2016; *Ulrich et al.*, 2017; *Kirillina et al.*, 2020; *Kirpotin et al.*, 2021). Such vegetation shifts and ecosystem changes are often related to anthropogenic influences. As discussed in Article 3, the majority of fires (70%) are initiated by humans (*Takahashi*, 2006). Furthermore, especially around settlements and roads deforestation through logging and infrastructure development can have a large ecosystem impact. Disturbances pose a threat to humans, wildlife, and biodiversity in general (*Kirpotin et al.*, 2021). From 1980-2018 *Kirillina et al.* (2020) have reported a lengthening of fire season, increased burned area extent, and an extension of the peak fire period in the Sakha Republic (Yakutia). Additionally, further disturbances such as pests and diseases (e.g. the Siberian moth) can easily spread in previously burned forests, especially under drought conditions (*Averensky et al.*, 2010). The 2020 and 2021 fire seasons, for example, have been particularly devastating. Nevertheless, the actual processes, trajectories, and thresholds are poorly studied.

> In regards to the third research objective, my research provides a first overview of possible, mid-term temporal permafrost and larch forest trajectories after a variety of disturbance scenarios that disrupt the tightly coupled ecosystem. These findings are particular to dry, larch-dominated, and permafrost-underlain boreal forests in eastern Siberia. Nevertheless, our study has implications for other boreal areas because it showcases how fragile the quasi-equilibrium between active layer thickness, plant-available soil moisture, and forest cover is.

The research presented is highly relevant in terms of increasing fire activity due to climatic changes, more extreme temperature, and precipitation events, and increased human activity in eastern Siberia. The simulations show that high-intensity disturbances, such as fires or logging can push the ecosystem into a very different state where e.g. larch cover and its permafrost-protecting abilities are lost. The modeling work further shows the sensitivity of the recovering ecosystems towards


*Figure 4.2: Photographs of disturbed ecosystems visible on expeditions to eastern Siberia. a) Surface fire near NYU (August 2019). b) Re-population led by broadleaf trees in former larch forest area after a complete canopy fire. c) Permafrost degradation due to human impact (e.g. off-road driving). d) Wetland intermixed with grassland in formerly forested area.*

small differences in the timing of precipitation events. As discussed in Article 3, the results are an indicator for tipping point behavior within the system's ability to recover pre-disturbance larch forest covers.

Boreal forests have often been included in the recent discussion on tipping elements within the Earth system (e.g. *Lenton et al.* (2008) or *Rey et al.* (2020)). Tipping elements have broadly been defined as "regional-scale features of climate that could exhibit a threshold behavior in response to climate change — that is, a small shift in background climate can trigger a large-scale shift towards a qualitatively different state of the system" (*Lenton et al.*, 2008). Increased water and summer heat stress are thought to cause increased mortality, and vulnerability to diseases and fires, as well as lower regrowth and forest collapse. Together, the climate-triggered changes could lead to large-scale die-back of boreal forests (*Lucht et al.*, 2006; *Lenton et al.*, 2008). A tipping point has been estimated to lay between 3 to 5 °C of global warming, but because of the various forcing mechanisms and complexities involved, this is only considered an uncertain estimate (*IPCC*, 2019). Here I show that, at a local scale, an increase in disturbances (fires or logging) can

lead to a tipping behavior in terms of larch forest recovery and fast changes in the permafrost conditions, especially the soil moisture and thus the water availability for plants. As discussed in Article 3, I only consider the loss of deciduous larch forest cover and their specific interactions with underlying permafrost rather than considering a loss of boreal forests altogether or the succession and new vegetation covers after disturbances.

The work conducted within this dissertation shows that larch forest loss could potentially trigger positive feedbacks that drive abrupt (local) or gradual (regional) permafrost thaw, a further ecosystem component that potentially meets the characteristics of a tipping element within the climate system (*Lenton et al.*, 2008). Substantial parts of permafrost are currently ecosystem-protected and a northward movement of the treeline and shrubification of current tundra areas will further increase the importance of vegetation in stabilizing permafrost (*Rogers et al.*, 2015). My simulations have also revealed that negative feedbacks such as the densification of vegetation covers, a change in species composition, or changes associated with surface albedo decrease (*Stuenzi and Schaepman-Strub*, 2020), and a potential increase in carbon sequestration (*D'Orangeville et al.*, 2018), could counteract, temporally, the local "tipping" of some permafrost due to changes in the protecting vegetation cover. Due to these dampening effects, which could counteract the positive feedbacks of larch forest on climate change, and because of the high variability in climate and landscapes, larch forest loss itself does not trigger global, abrupt permafrost loss. Nevertheless, my research suggests that changes in larch forest cover will potentially lead to local tipping behavior at different times, speeds, and irreversibilities.

## 4.4 Scientific contribution

In summary, this thesis contributes to a better understanding of boreal permafrost ecosystems with a focus on the characteristic larch forests of eastern Siberia. My work suggests that local, detailed, and specific land surface models, as well as field data and observations, are required to fully comprehend the complex dynamics in boreal permafrost ecosystems. Figure 4.3 provides an overview of the diverse interactions between the atmosphere, boreal forest cover, and permafrost identified and quantified within this thesis. The schematic illustration includes the mechanisms impacted by atmospheric changes (climatic change), boreal forest cover shifts, and modifications in the permafrost thermal and hydrological regime.

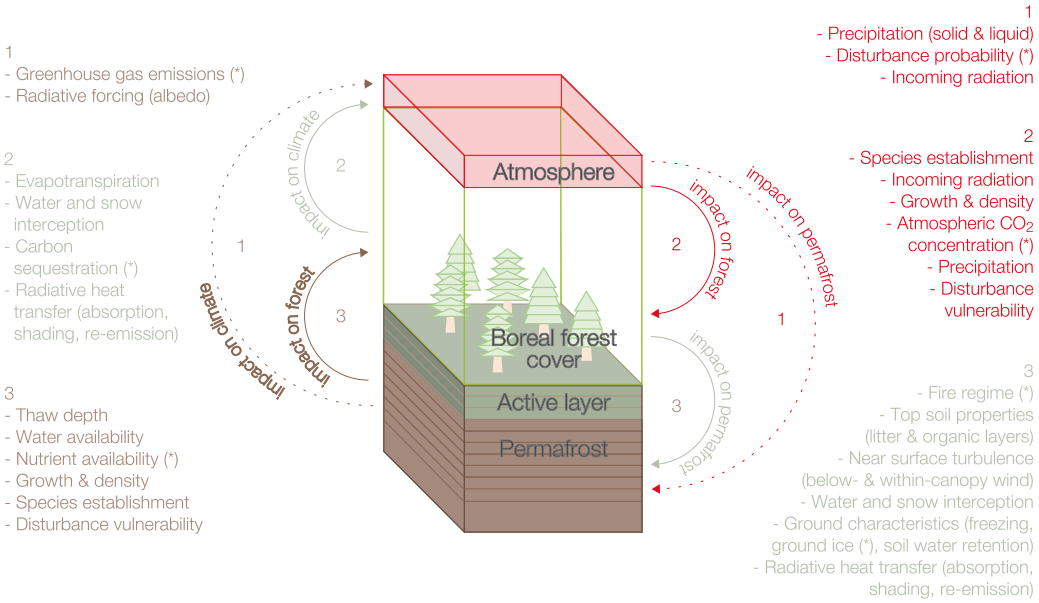


*Figure 4.3: Interactions between the atmosphere, boreal forest cover, and permafrost. In red (atmospheric impact), green (forest impact), and brown (permafrost impact) are all the mechanisms interacting between the three ecosystem components. Climatic change leads to a change in the forest density and structure, which leads to changes in all feedback processes between forest and permafrost. Additionally, climatic change leads to permafrost thawing and a change in the water availability, which also leads to forest density and structure changes. Interactions not directly simulated within this dissertation are marked with (*).*

Boreal forests do stabilize permafrost through a multitude of feedback mechanisms. Within this dissertation, I have been able to quantify the heat and water exchange processes that lead to the insulating effect boreal forests have on the thermal and hydrological conditions of underlying permafrost. This has enabled me to study the variation in the insulation effect of different forest types and forest densities, as well as the feedback mechanisms occurring after forest disturbances.

In particular, my work reveals the following main findings:

1. It is crucial to integrate detailed representations of both permafrost and multilayer canopy models to understand this complex ecosystem. The combination of these model entities has enabled me to quantify the individual physical dimensions of the interactions between different ecosystem components.

2. Changing forest density and composition will significantly modify the thermal and hydrological state of underlying permafrost. The induced soil changes will likely affect key forest functions such as the carbon pools and related feedback mechanisms such as swamping, droughts, fires, or forest loss.

3. Forest disturbances can induce soil drying of up to 50%, which leads to lower active layer thicknesses (ALTs) and abrupt or steady decline of larch forest cover, depending on the intensity of the disturbances. I have further found first indicators for tipping behavior in recovering larch forests. This tipping is closely related to the timing of precipitation events during dry spring seasons, likely triggering irreversible larch forest losses with potentially devastating effects on the underlying permafrost.

## 4.5 Outlook

By coupling existing models, I have developed a novel, detailed land surface model for the specific application in the complex and underrepresented boreal ecosystems of eastern Siberia. I will conclude this work with recommendations for future research directions based on the framework provided here.

As a next step, the presented model could readily be used at different boreal sites across the Arctic. The three study sites used for validation and model setup within this dissertation have displayed different responses to forest cover changes, especially in terms of the hydrological conditions in permafrost. Efforts, including additional validation exercises, could further evaluate the model capacities and improve parameterizations such as the timing of the needle-shedding of deciduous taxa or the rooting depths of different taxa. A logical next step would be to use the detailed, physically built model to parameterize a much quicker and pan-arctic-applicable model version for studies including larger ecosystem-protected permafrost areas. Recently, lots of progress has been made in terms of the use of neural networks, which can be trained with simulation data from process-based models (see e.g. *Irrgang et al.* (2021)), or with the optimization of model parameters and uncertainty assessment through the use of i.e. the Markov Chain Monte Carlo (MCMC) method in combination with machine learning algorithms (see e.g. *Sawada* (2020)). Such an approach could be used to build a computationally-efficient statistical surrogate model trained using the physically-based model described within this dissertation. This would allow the model setup to possibly be used for the improvement of permafrost-forest interactions in global land surface models.

Detailed analysis of the yearly cycle of ground surface temperatures (GST) in permafrost under boreal forests was conducted within Article 1. The snowmelt period in spring is biased at both the forest and grassland, sites and the ground warms up faster than simulated by the model. Under the forest canopy, this is likely caused by a wrong representation of snowpack compaction and snowmelt processes. The analysis revealed that the difference between modeled and measured GST in spring is only partially reduced by an extreme case of snow compaction. This points to more complex mechanisms currently not represented by the model but control snowmelt in the forest. It would therefore be highly desirable to obtain field

measurements of snow accumulation, snow density, and melting to gain a better understanding of snowmelt processes in boreal permafrost systems. Furthermore, the model does currently not represent moisture transport and migration in frozen ground or ice lens and excess ground ice formation. These processes could lead to further high impacts on the local micro-topography, the surface energy balance, or available plant water and root space. Lateral water fluxes were not investigated in the applied one-dimensional model setup. Nevertheless, lateral water flow and snow redistribution could be important processes controlling spatial heterogeneities in the ground thermal regime, as well as the snowpack development. The implementation of lateral water and energy fluxes would enable detailed analysis of multi-tile processes, as well as of boreal forest-permafrost feedbacks in topographically rich, mountainous areas. As detailed in Article 3, the lateral water fluxes at the dry Spasskaya Pad site are negligible, but at different sites, implementation of lateral heat- and water fluxes could be crucial.

Another direction for future research, which is already on its way, is the integration of broadleaf taxa, such as birch and aspen, as well as evergreen needleleaf taxa (in the coupled dynamic vegetation model 'LAVESI'), to cover the early-successional stages in boreal forest development/recovery. Additionally, the forest-permafrost model does so far not incorporate any chemical soil processes such as carbon sequestration and organic decomposition, or in other words, the C, N, and O cycling in the ground. These processes could be implemented at varying levels of complexities, especially since the used canopy module does already include such processes. These possible developments of the modeling scheme and the proposed fieldwork show the future research potential based on the framework provided within this dissertation.

# Part II

# Articles

# Chapter 5

# Variability of the surface energy balance in permafrost-underlain boreal forest

**Stuenzi, S.M., Boike, J., Cable, W., Herzschuh, U., Kruse, S., Pestryakova, L. A., Schneider von Deimling, T., Westermann, S., Zakharov, E.S., and Langer, M.**

*Biogeosciences* (2021), 18, 343–365, DOI: 10.5194/bg-18-343-2021.

Biogeosciences, 18, 343–365, 2021
https://doi.org/10.5194/bg-18-343-2021


Biogeosciences Open Access EGU

# Variability of the surface energy balance in permafrost-underlain boreal forest

**Simone Maria Stuenzi[1,2], Julia Boike[1,2], William Cable[1], Ulrike Herzschuh[1,3,8], Stefan Kruse[1], Luidmila A. Pestryakova[5], Thomas Schneider von Deimling[1,2], Sebastian Westermann[6,7], Evgenii S. Zakharov[4,5], and Moritz Langer[1,2]**

[1]Alfred Wegener Institute Helmholtz Centre for Polar and Marine Research, Telegrafenberg A45, 14473 Potsdam, Germany
[2]Geography Department, Humboldt-Universität zu Berlin, Unter den Linden 6, 10099 Berlin, Germany
[3]Institute of Environmental Science and Geography, University of Potsdam, 14476 Potsdam, Germany
[4]Institute for Biological Problems of Cryolithozone, Siberian Branch of the Russian Academy of Sciences, Yakutsk, Russia
[5]Institute of Natural Sciences, North-Eastern Federal University in Yakutsk, Belinskogo str. 58, 677000 Yakutsk, Russia
[6]Department of Geosciences, University of Oslo, Sem Sælands vei 1, 0316 Oslo, Norway
[7]Centre for Biogeochemistry in the Anthropocene, University of Oslo, Sem Sålands vei 1, 0316 Oslo, Norway
[8]Institute of Biochemistry and Biology, University of Potsdam, 14476 Potsdam, Germany

**Correspondence:** Simone Maria Stuenzi (simone.stuenzi@awi.de)

Received: 29 May 2020 – Discussion started: 18 June 2020
Revised: 23 November 2020 – Accepted: 1 December 2020 – Published: 18 January 2021

**Abstract.** Boreal forests in permafrost regions make up around one-third of the global forest cover and are an essential component of regional and global climate patterns. Further, climatic change can trigger extensive ecosystem shifts such as the partial disappearance of near-surface permafrost or changes to the vegetation structure and composition. Therefore, our aim is to understand how the interactions between the vegetation, permafrost and the atmosphere stabilize the forests and the underlying permafrost. Existing model setups are often static or are not able to capture important processes such as the vertical structure or the leaf physiological properties. There is a need for a physically based model with a robust radiative transfer scheme through the canopy. A one-dimensional land surface model (CryoGrid) is adapted for the application in vegetated areas by coupling a multilayer canopy model (CLM-ml v0; Community Land Model) and is used to reproduce the energy transfer and thermal regime at a study site (63.18946° N, 118.19596° E) in mixed boreal forest in eastern Siberia. An extensive comparison between measured and modeled energy balance variables reveals a satisfactory model performance justifying its application to investigate the thermal regime; surface energy balance; and the vertical exchange of radiation, heat and water in this complex ecosystem. We find that the forests exert a strong control on the thermal state of permafrost through changing the radiation balance and snow cover phenology. The forest cover alters the surface energy balance by inhibiting over 90 % of the solar radiation and suppressing turbulent heat fluxes. Additionally, our simulations reveal a surplus in longwave radiation trapped below the canopy, similar to a greenhouse, which leads to a magnitude in storage heat flux comparable to that simulated at the grassland site. Further, the end of season snow cover is 3 times greater at the forest site, and the onset of the snow-melting processes are delayed.

## 1 Introduction

Around 80 % of the world's boreal forest occurs in the circumpolar permafrost zone (Helbig et al., 2016). Despite little human interference and due to extreme climate conditions such as winter temperatures below −50 °C and very low precipitation, the biome is highly sensitive to climatic changes (ACIA, 2005; AMAP, 2011; IPCC, 2014) and thus prone to vegetation shifts. Boreal forest regions are expected to warm by 4 to 11 °C by 2100, coupled with a more modest precipitation increase (IPCC, 2014; Scheffer et al., 2012). Moreover, during 2007–2016 continuous-zone permafrost temper-

atures increased by 0.39 (±0.15) °C (Biskaborn et al., 2019; IPCC, 2019). The northeastern part of the Eurasian continent is dominated by such vast boreal forest – the taiga. Due to its sheer size, the biome is not only sensitive to climatic changes but also exerts a strong control on numerous climate feedback mechanisms through the altering of land surface reflectivity, the emission of biogenic volatile organic compounds and greenhouse gases, and the transfer of water to the atmosphere (Bonan et al., 2018; Zhang et al., 2011). The forests are usually considered to efficiently insulate the underlying permafrost (Chang et al., 2015). The canopy exerts shading by reflecting and absorbing most of the downward solar radiation, changes the surface albedo, and decreases the soil moisture by intercepting precipitation and increasing evapotranspiration (Vitt et al., 2000). Additionally, the forest promotes the accumulation of an organic surface layer which further insulates the soil from the atmosphere (Bonan and Shugart, 1989). Changing climatic conditions can promote an increasing active-layer depth or trigger the partial disappearance of the near-surface permafrost. Further, extensive ecosystem shifts such as a change in composition, density or the distribution of vegetation (Holtmeier and Broll, 2005; Pearson et al., 2013; Gauthier et al., 2015; Kruse et al., 2016; Ju and Masek, 2016) and resulting changes to the below- and within-canopy radiation fluxes (Chasmer et al., 2011) have already been reported. Changes to the vegetation – permafrost dynamics – can have a potentially high impact on the numerous feedback mechanisms between the two ecosystem components. Increased soil carbon release from thawing permafrost through the delivery of soil organic matter to the active carbon cycle (Schneider Von Deimling et al., 2012; Romanovsky et al., 2017) is modified by vegetation changes, which can compensate for carbon losses due to an increased $CO_2$ uptake (as observed at ice-rich permafrost sites in northwestern Canada and Alaska; Estop-Aragonés et al., 2018) or even further accelerate total carbon loss.

These vegetation–permafrost dynamics in eastern Siberia have been documented through exploratory and descriptive field studies showing a clear insulation effect of forests on soil temperatures (Chang et al., 2015). Further, the biogeophysical processes controlling the evolution of the ecosystem have been described by conceptual models (Beer et al., 2007; Zhang et al., 2011; Sato et al., 2016). Modeling schemes such as ORCHIDEE–CAN (Organising Carbon and Hydrology In Dynamic Ecosystems – CANopy; Chen et al., 2016), JULES (Joint UK Land Environment Simulator; Chadburn et al., 2015), Lund–Potsdam–Jena (LPJ DGVM – Dynamic Global Vegetation Model; Beer et al., 2007), NEST (Northern Ecosystem Soil Temperature; Zhang et al., 2003) or SiBCliM (Siberian BioClimatic Model; Tchebakova et al., 2009) have added a vegetation or canopy module, with defined exchange coefficients for the fluxes of mass and energy, to their soil modules. This is feasible for varying levels of complexity, and the models are capable of addressing a variety of different aspects such as forest establishment and mortality (Sato et al., 2016), unfrozen vs. frozen ground and fire disturbances (Zhang et al., 2011), or the evolution of the vegetation carbon density under diverse warming scenarios (Beer et al., 2007).

While all of these studies have significantly improved our understanding of essential mechanisms in boreal permafrost ecosystems, it is important to further understand how a dynamic evolution of the forest structure and canopy affects the thermal state and the snow regime of the ground, especially amid ongoing shifts in forest composition (Loranty et al., 2018). The existing model setups are often static or not able to capture important processes such as the vertical canopy structure or the leaf physiological properties which strongly control the energy transfer between the top-of-the-canopy atmosphere and the ground. To our knowledge, so far, none of the existing models is able to capture the important processes of the vertical canopy structure in combination with a physically based, highly advanced permafrost model. The novel, physically based model introduces a robust radiative transfer scheme through the canopy for a detailed analysis of the vegetation's impact on the hydro-thermal regime of the permafrost ground below. This allows us to quantify the surface energy balance dynamics below a complex forest canopy and its direct impact on the hydro-thermal regime of the permafrost ground below.

With a tailored version of a one-dimensional land surface model (CryoGrid – CG, Westermann et al., 2016) we perform and analyze numerical simulations and reproduce the energy transfer and surface energy balance in permafrost-underlain boreal forest of eastern Siberia. CryoGrid has, so far, not included a vegetation scheme but has been used to successfully describe atmosphere–ground energy transfer and the ground thermal regime in barren and grass-covered areas (Langer et al., 2016; Westermann et al., 2016; Nitzbon et al., 2019, 2020). In our study, we have adapted a state-of-the-art multilayer vegetation model (CLM-ml v0, originally developed for the Community Land Model – CLM – by Bonan et al., 2018). We tailor and implement this scheme to simulate the turnover of heat, water and snow between the atmosphere, forest canopy and ground. We take advantage of a detailed in situ data record from our primary study site as well as from a secondary, external study site. These data are used to provide model parameters, as well as for model validation by comparing field measurements with simulation results. The main objectives of this study are

1. to demonstrate the capabilities of a coupled multilayer forest–permafrost model to simulate vertical exchange of radiation, heat and water for boreal forests
2. to investigate the impact of the new canopy module on the surface energy balance of the underlying permafrost at a mixed boreal forest site in eastern Siberia.

## 2 Methods

### 2.1 Study area

Our primary study site is located southeast of Nyurba (63.18946° N, 118.19596° E) in a typical boreal forest zone intermixed with some grassland for horse grazing and shallow lakes. The forest is rather dense and mixed, with the dominant taxa being evergreen spruce (*Picea obovata*, 92 %), deciduous larch (*Larix gmelinii*, 7.3 %) and some hardwood birch (*Betula pendula*, < 1 %). The average tree height is 5.5 m for spruce and 12 m for larch, respectively. These boreal forest environments experience 6 to 8 months of freezing temperatures reaching extremes of −62 °C in winter and up to 35 °C between May and September. The low annual average temperatures result in continuous permafrost and are therefore poorly drained, podzolized and nutrient-poor soils (Chapin et al., 2011). Annual precipitation showed an increasing trend from 1900 until 1990, mainly due to an increase in wintertime precipitation. Between 1995 and 2002, summertime precipitation decreased by 16.9 mm in August and 4.2 mm in July (see Table 1 in Hayasaka, 2011, for further details). The temperature trend from 1970 to 2010 for the central Yakutian region is positive for spring, summer and fall and negative for winter (monthly surface temperature quantified using Climatic Research Unit (CRU) TS4.01 data; Harris et al., 2014; Stuenzi and Schaepman Strub, 2020). The treeline of northern Siberia is dominated by the deciduous needleleaf tree genus *Larix* Mill. up to 72.08° N, *Larix sibirica* Ledeb. from 60 to 90° E, *Larix gmelinii* Rupr. between 90 and 120° E, and *Larix cajanderi* Mayr. from 120 to 160° E (see Fig. 1). Larch competes effectively with other tree taxa because of its deciduous leaf habit and dense bark. In more southern margins of eastern Siberia, such as our study area, larch is mixed with evergreen conifers (Siberian pine (*Pinus sibirica* and *Pinus sylvestris*), spruce (*Picea obovata* Ledeb.) and fir (*Abies sibirica*)) and hardwood (*Betula pendula* Roth, *B. pubescens* Ehrh. and *Populus tremula* L.) (Kharuk et al., 2019). Moreover, the ground vegetation is poor in diversity and dominated by mosses and lichens that form carpets. Larch has shallow roots and grows on clay permafrost soils with an active layer of around 0.7 m and a maximum wetness of 20 %–40 %. Evergreen conifers and hardwood both prefer deeper active layers and a higher soil moisture availability (Ohta et al., 2001; Furyaev et al., 2001; Rogers et al., 2015). This study comprises a secondary site for complementary model validation which is situated 581 km east of the primary site (for further description see Appendix C).

### 2.2 Meteorological and soil physical measurements

An automatic weather station (AWS, Campbell Scientific; for a detailed list of sensors, see Table A1) is installed at 110 m a.s.l. on a meadow next to the forest patch described above. The grassland is grazed by horses in summer, and deforestation occurred more then 50 years ago. The AWS records air temperature and relative humidity at two heights (1.1 and 2.5 m) above the ground, while wind speed and direction are measured at 3.2 m above ground. In addition, the station measures liquid precipitation, snow depth, and incoming and outgoing short- and longwave radiation and is equipped as a Bowen ratio station ($B$, see Appendix A). All meteorological variables were recorded with 10 min resolution and stored as 30 min averages. In order to install soil temperature and moisture sensors in the ground a soil pit was excavated in the immediate vicinity (2.5 m) of the AWS. The O horizon has a depth of 0.04 m; the A horizon at 0.1 m contains undecomposed roots, dead moss remains, dense rooting and some organic humus. The mineral soil is podzolized, sandy and dominated by quartz. The rooting depth is 0.18 m. Iron-rich bands were found at 0.4, 0.7 and 1.1 m. The active-layer thickness was 2.3 m in mid-August 2018 and in early August 2019. In this soil pit, soil temperature and moisture measurement profiles are installed from the top to the bottom of the active layer, consisting of eight temperature sensors (0.07, 0.26, 0.88, 1.33, 1.28, 1.58, 1.98 and 2.28 m) and four moisture probes (0.07, 0.26, 0.88 and 1.33 m). In addition the conductive ground heat flux in the topsoil layer is measured with a heat flux plate installed at 0.02 m depth. Further, we record the near-surface ground temperature with five standalone temperature loggers (iButtons, see Table A1) with a measurement interval of 3 h. These are installed in the upper 0.03 m of the organic soil at our forest site. The forest soil has a litter layer of 0.08 m and an organic-rich A horizon reaching a depth of 0.16 m. It is rich in organic and undecomposed material. Mineral soil is podzolized, and the rooting depth is 0.20 m. The average active-layer thickness between spatially distributed point measurements was 0.75 m in mid-August 2018 and 0.73 m in early August 2019. In a vegetation survey along a 150 m transect from the grassland into the forest, the tree height of every tree within a 2 m distance was estimated. Trees < 2 m were measured with a measuring tape; trees > 2 m were measured with a clinometer or visually estimated after repeated comparisons with clinometer measurements. Together, the instrumentation, with a variety of different loggers, records the spatial and temporal variances across the two sites which are representative for a large area of the mixed boreal forest domain in eastern Siberia (https://doi.org/10.1594/PANGAEA.914327, Langer et al., 2020; https://doi.org/10.1594/PANGAEA.919859, Stuenzi et al., 2020b). In addition, we use a secondary study site, located 581 km east of Nyurba, with an extensive measurement record of radiation and temperature data from below the forest canopy, allowing for a comprehensive model validation (see Appendix C).

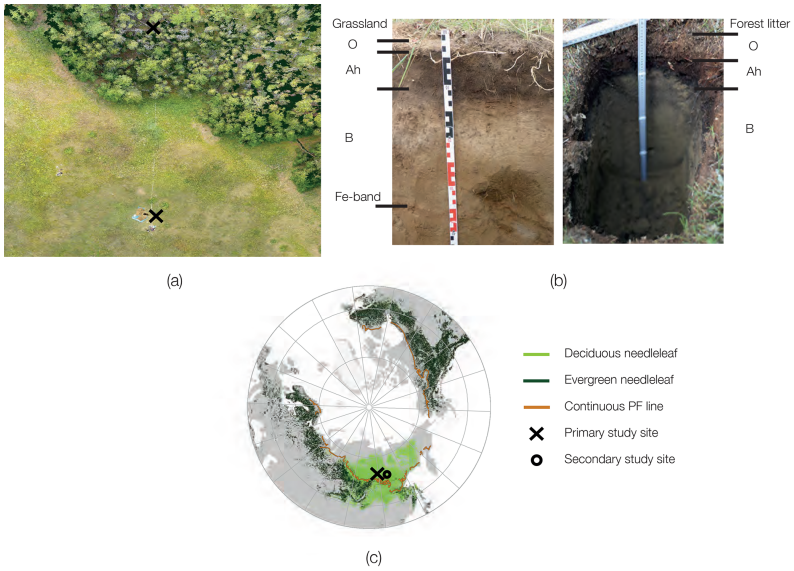


**Figure 1. (a)** Overview image of the location of the automatic weather station (AWS) in the grassland in the lower-right corner and the location of the instrumented forest site in the upper-left corner (Brieger et al., 2019a). **(b)** Respective soil profiles with the depths of the organic-matter-dominated O horizon, the top layer of the mineral soil containing the decomposed organic layer (Ah horizon), and the subsoil mineral layer (B horizon) at the grassland site (left) and at the forest site (right). **(c)** Global evergreen needleleaf (dark green) and summergreen needleleaf (light green) boreal forest distribution and the boundary line between the discontinuous and continuous permafrost extent in brown. The primary study site is marked with a black cross; our secondary study site is marked with a grey circle. Data: © ESA CCI Landcover classes, aggregated to summergreen and evergreen needleleaf classes (after Herzschuh, 2019) and permafrost extent from Land Resources of Russia – Maps of Permafrost and Ground Ice (after Kotlyakov and Khromova, 2002).

**Table 1.** Overview of the processes for which this study differs from the former CG parameterizations.

| Process or parameter | CG | CG Crocus and CLM-ml v0 |
|---|---|---|
| Surface energy balance | See Eq. (1) | Surface energy balance modulated by canopy, see Eq. (2), after Bonan et al. (2018) |
| Precipitation interception | Direct precipitation from forcing data of Westermann et al. (2016) | Precipitation modulated by canopy (canopy drip, canopy and stem evaporation, and stem flow and direct throughfall), see Eq. (4), after Bonan (2019) |
| Dynamic evapotranspiration | – | See Eq. (7) in Bonan et al. (2018) |
| Snow scheme | Westermann et al. (2016) | Crocus snow scheme, see Sect. 2.3.3, after Zweigel et al. (2020) |

## 2.3 Model description

### 2.3.1 Ground module

CryoGrid is a one-dimensional, numerical land surface model developed to simulate landscape processes related to permafrost such as surface subsidence, thermokarst and ice wedge degradation. The model version is originally described in Westermann et al. (2016) and has since been extended with different functionalities such as lake heat transfer (Langer et al., 2016), multi-tiling (Nitzbon et al., 2019, 2020) and an extensive snow scheme based on Crocus (Vionnet et al., 2012; Zweigel et al., 2020). The thermo-hydrological regime of the ground is simulated by numerically solving the one-dimensional heat equation with groundwater phase change, while groundwater flow is simulated with an explicit bucket scheme (Nitzbon et al., 2019). The exchange of sen-

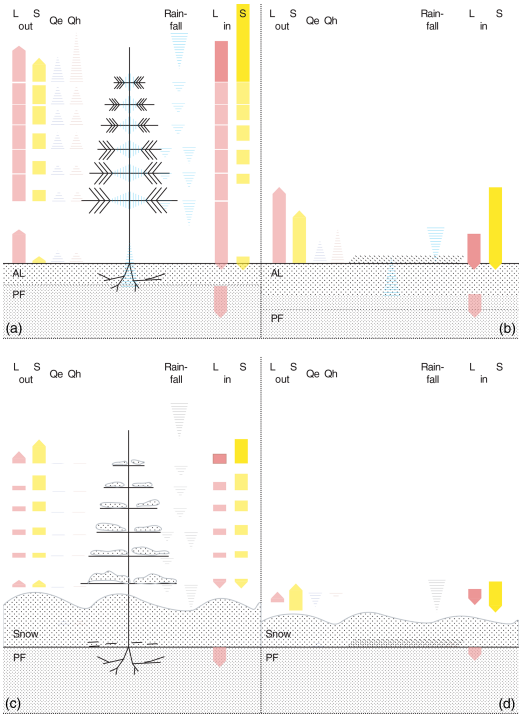


**Figure 2.** Schematic of the surface energy and water balance of the forest **(a, c)** and grassland **(b, d)** schemes for **(a, b)** the snow-free period and **(c, d)** the snow-covered period. The active layer (AL), the permafrost (PF), tree and grassland (dotted lines), and the snowpack (Snow) in the snow-covered period. In each of the four panels, incoming and outgoing longwave ($L_{in}$ and $L_{out}$), incoming and outgoing solar ($S_{in}$ and $S_{out}$), turbulent fluxes ($Q_h$ and $Q_e$), the storage heat flux ($Q_s$), and precipitation (and interception) of rain- and snowfall are shown.

sible and latent heat, radiation, evaporation, and condensation at the ground surface are simulated with a surface energy balance scheme based on atmospheric stability functions. In addition, the model encompasses different options for simulating the evolution of the snow cover including the Crocus snowpack scheme. The model is forced by standard meteorological variables which may be obtained from AWSs, reanalysis products or climate models. The required forcing variables include air temperature, wind speed, humidity, incoming short- and longwave radiation, air pressure, and precipitation (snow- and rainfall) (Westermann et al., 2016). The change of internal energy of the subsurface domain over time is controlled by fluxes across the upper and lower boundaries written as

$$\frac{\delta E}{\delta t} = S_{in} - S_{out} + L_{in} - L_{out} - Q_h - Q_e - Q_{h_{precip}}, \quad (1)$$

where the input to the uppermost grid cell is derived from the fluxes of shortwave radiation ($S_{in}$ and $S_{out}$) and longwave ($L_{in}$ and $L_{out}$) radiation at the same time regarding the latent ($Q_e$) and sensible ($Q_h$) heat added by precipitation ($Q_{precip}$) and storage heat flux ($Q_s$) between the atmosphere and the ground surface (Westermann et al., 2016).

For this study, we have adapted the multilayer canopy model developed by Bonan et al. (2014, 2018). The canopy model is coupled to CryoGrid by replacing its standard surface energy balance scheme, while soil state variables are passed back to the forest module. In the following, we describe the canopy module and its interaction with the existing CryoGrid soil and snow scheme. All differences towards former CryoGrid parameterizations are summarized in Table 1.

### 2.3.2 Canopy module

The multilayer canopy model provides a comprehensive parameterization of fluxes from the ground, through the canopy up to the roughness sublayer. The implementation of a roughness sublayer allows for the representation of different forest canopy structures and their impact on the transfer of vertical heat and moisture. The concept is similar to the multilayer approach in ORCHIDEE-CAN (Chen et al., 2016; Ryder et al., 2016). In an iterative manner, photosynthesis, leaf water potential, stomatal conductance, leaf temperature and leaf fluxes are calculated. This improves model performance in terms of capturing the stomatal conductance and canopy physiology, nighttime friction velocity, and diurnal radiative temperature cycle and sensible heat flux (Bonan et al., 2014, 2018). The within-canopy wind profile is calculated using above- and within-canopy coupling with a roughness sublayer (RSL) parameterization (see Bonan et al., 2018, for further detail).

The multilayer canopy model (Bonan et al., 2018) was developed based on the use with CLM soil properties. Following the notations summarized in Bonan (2019) we developed a CLM-independent multilayer canopy module which can be coupled to CryoGrid by integrating novel interactions and an adapted snow cover parameterization. In order to set necessary parameters of the canopy module, we make use of values defined for the CLM plant functional type of evergreen needleleaf forest. Please note that all parameters defining the canopy are set as constant values so that vegetation is not dynamic and that changes in forest composition or actual tree growth are not considered in this study.

### 2.3.3 Snow module

The snow module employed in this study is based on Zweigel et al. (2020) (submitted, available upon request). The CryoGrid model is extended with snow microphysics parameterizations based on the Crocus snow scheme (Vionnet et al., 2012), as well as lateral snow redistribution. The CLM-ml (v0) multilayer canopy model has not yet been coupled to a

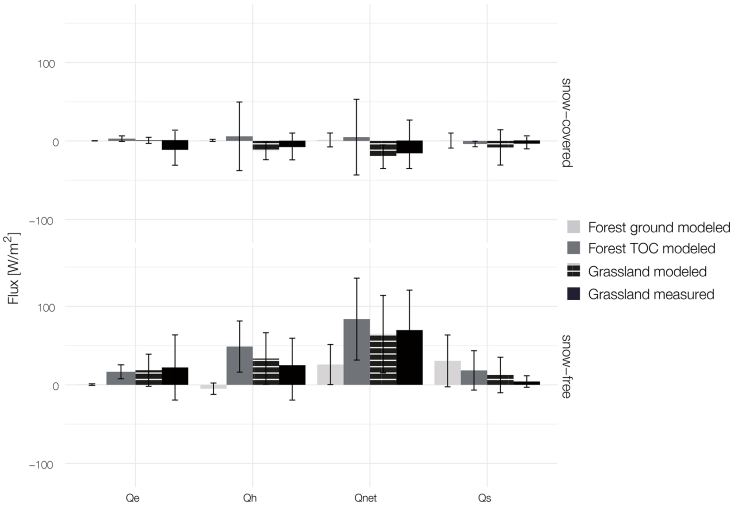


**Figure 3.** Surface energy balance for the snow-covered (28 October 2018–27 April 2019) and snow-free (10–27 October 2019 and 28 April–10 October 2019) periods at the ground surface of grassland and forest and at the top of the canopy of the forest (Forest TOC). Shown are the net radiation ($Q_{\mathrm{net}}$) and sensible ($Q_{\mathrm{h}}$), latent ($Q_{\mathrm{e}}$) and storage heat flux ($Q_{\mathrm{s}}$) for the model runs of the forest and grassland site as well as the measured values at the grassland site. The bars indicate mean values, while the whiskers show the corresponding standard deviations.

snow scheme (Bonan et al., 2018). Following Vionnet et al. (2012) the microstructure of the snowpack is characterized by grain size (gs, mm), sphericity ($s$, unitless, range 0–1) and dendricity ($d$, unitless, range 0–1). Fresh snow is added on top of the existing snow layers with temperature- and wind-speed-dependent density and properties. After deposition the development of each layers' microstructure occurs based on temperature gradients and liquid water content (Vionnet et al., 2012). Snow albedo for the surface layer and an absorption coefficient for each layer are calculated based on the snow properties. Solar radiation is gradually absorbed throughout the snow layers, and the remaining radiation is added to the lowest cell. Additionally, the two mechanical processes of mechanical settling due to overload pressure and wind compression increase snow density and compaction. During snowfall, new snow is added to the top layer in each time step and mixed with the old snow based on the amount of ice. Once a cell exceeds the snow water equivalent of 0.01 m, which equals a snow layer thickness of 0.03 m, a new snow layer is built. Here, snow accumulates on the ground under the forest canopy. During the first snowfall, the surface energy balance of the ground and snow is calculated for each respective cover fraction. After reaching a snow layer thickness of 0.03 m, the ground surface energy balance is calculated for the snowpack itself (see Table A2). Variables exchanged based on the snow cover are the ground surface temperature, surface thermal conductivity and layer thickness of the layer directly under vegetation. Evaporation flux is subtracted from the snow surface. Top-of-the-canopy wind speed is used to calculate the density of the falling snow. Additionally, snow interception is handled like liquid precipitation interception described in Eq. (4).

#### 2.3.4 Interactions between the modules

The vegetation module forms the upper boundary layer of the coupled vegetation–permafrost model and replaces the surface energy balance equation used for common CryoGrid representations. The top-of-the-canopy (TOC) surface energy balance is calculated by the vegetation module based on atmospheric forcing. The forest module numerically solves the energy balance of the ground surface below the canopy defined as

$$S_{\mathrm{in}_{\mathrm{canopy}}} - S_{\mathrm{out}_{\mathrm{ground}}} + L_{\mathrm{in}_{\mathrm{canopy}}} - L_{\mathrm{out}_{\mathrm{ground}}} - Q_{\mathrm{h}_{\mathrm{ground}}} - Q_{\mathrm{e}_{\mathrm{ground}}} - Q_{\mathrm{s}_{\mathrm{ground}}} = 0, \quad (2)$$

where $L_{\mathrm{in}_{\mathrm{canopy}}}$ and $S_{\mathrm{in}_{\mathrm{canopy}}}$ are the incoming long- and shortwave radiation at the ground surface and the lower boundary fluxes of the multilayer canopy module, $S_{\mathrm{out}_{\mathrm{ground}}}$ is the outgoing shortwave flux from the ground, $L_{\mathrm{out}_{\mathrm{ground}}}$ is the outgoing longwave flux, $Q_{\mathrm{h}_{\mathrm{ground}}}$ is the sensible heat flux, $Q_{\mathrm{e}_{\mathrm{ground}}}$ is the latent heat flux, and $Q_{\mathrm{s}_{\mathrm{ground}}}$ is the storage heat flux at the ground surface. The first six components of the sub-canopy energy balance directly replace the respective components surface energy balance scheme of CryoGrid (see Eq. 1). $Q_{\mathrm{s}_{\mathrm{ground}}}$ is calculated based on temperatures of the

uppermost ground or snow layers that are passed from CryoGrid to the forest module. The storage heat flux is calculated as

$$Q_{s_{\text{ground}}} = k\frac{T_s - T_{\text{ground}}}{\Delta z}, \tag{3}$$

where $k$ is the soil thermal conductivity, $T_s$ is the soil surface temperature, $T_{\text{ground}}$ is the actual ground temperature for the first layer below the surface and $\Delta z$ is the layer thickness. Soil thermal conductivity is parameterized following Westermann et al. (2013, 2016) and is based on the parameterization in Cosenza et al. (2003). The thermal conductivity of the soil is calculated as the weighted power mean from the conductivities and volumetric fractions of the soil constituents water, ice, air, mineral and organic (Cosenza et al., 2003). In Fig. 2 the energy fluxes expected for a forested and a grassland site in the snow-covered and snow-free periods each are illustrated schematically.

In the novel model setup which allows for soil–vegetation interaction, the vegetation module receives ground state variables of the top 0.7 m of the soil layers. These state variables are soil layer temperature ($T_{\text{ground}}$) and soil layer moisture ($W_{\text{ground}}$), as well as the diagnostic variables soil layer conductivity ($k_{\text{ground}}$) and ice content ($I_{\text{ground}}$). The vegetation transpiration fluxes are subtracted from the ground soil layers within the rooting depth and evaporation fluxes from the ground surface.

Following the notation in Bonan et al. (2018) the rain and snow fraction reaching the ground ($W_{\text{ground}_s}$) is described as follows

$$\frac{\delta W_{\text{ground}_s}}{\delta t} = f P_R + D_c - E_c + D_t - E_t \tag{4}$$

and consists of the direct throughfall ($f P_R$), the canopy drip ($D_c$), the canopy evaporation ($E_c$), the stemflow ($D_t$) and the stem evaporation ($E_t$), which are based on the retained canopy water ($W_c$) as

$$\frac{\delta W_c}{\delta t} = (1 - f - f_t) P_R - E_c - D_c, \tag{5}$$

where $1 - f - f_t P_R$ is the intercepted precipitation, and the retained trunk water ($W_t$) is represented as

$$\frac{\delta W_t}{\delta t} = f_t P_R - E_t - D_t, \tag{6}$$

respectively. Lateral water fluxes are neglected in this baseline, one-dimensional model setup.

### 2.4 Model setup and simulations

We ran model simulations for forested and non-forested scenarios based on in situ measurements recorded in 2018 and 2019. The subsurface stratigraphies used in CryoGrid is described by the mineral and organic content, natural porosity, field capacity, and initial water and ice content. Some of these parameters could be measured at the forest and grassland sites and were used to set the initial soil profiles in the model. Table A3 summarizes all parameter choices for soil stratigraphies, and Table A4 summarizes constants used. The subsurface stratigraphy extends to 100 m below the surface, where the geothermal heat flux is set to 0.05 W m$^{-2}$ (Langer et al., 2011b). The ground is divided into separate layers in the model. The uppermost 8 m section has a layer thickness of 0.05 m, followed by 0.1 m for the next 20, 0.5 m up to 50 and 1 m thereafter. The remaining CryoGrid parameters were adopted from previous studies using CryoGrid (see Table A2) (Langer et al., 2011a, b, 2016; Westermann et al., 2016; Nitzbon et al., 2019, 2020). We use ground surface temperature (GST) as the target variable for model validation. GST results from the surface energy balance at the interface between the canopy, snow cover and ground and provides an integrative measure of the different model components. In addition it is the most important variable determining the thermal state of permafrost.

For the canopy stratigraphy, we follow the parameterizations in Bonan et al. (2018) for the plant functional type evergreen needleleaf (see Table A5 and A6). This canopy stratigraphy can be described by two parameters: the leaf area index (LAI) measured at the bottom of the canopy defines the total leaf area. The leaf area density function on the other hand describes the foliage area per unit volume of canopy space, which is the vertical distribution of leaf area. Leaf area density is measured by evaluating the amount of the leaf area between two heights in the canopy separated by the distance. This function can be expressed by the beta distribution probability density function which provides a continuous representation of leaf area for use with multilayer models (see Bonan, 2019, for further information). Here, we use the beta distribution parameters for needleleaf trees ($p = 3.5$, $q = 2$), which resembles a cone-like tree shape. LAI can be estimated from satellite data and calculated from below-canopy light measurements or by harvesting leaves and relating their mass to the canopy diameter. Ohta et al. (2001) have described the monitored deciduous–needleleaf forest site at the Spasskaya Pad research station (our secondary study site, see Appendix C), which has comparable climate conditions but is larch-dominated. The value of the tree plant area index (PAI), obtained from fish-eye imagery and confirmed by litter fall observations, varied between 3.71 m$^2$ m$^{-2}$ in the foliated season and 1.71 m$^2$ m$^{-2}$ in the leafless season. This value does not include the ground vegetation cover. Further, Chen et al. (2005) compared ground-based LAI measurements to MODIS values at an evergreen-dominated study area (57.3° N, 91.6° E) southwest of the region discussed here, around the city of Krasnoyarsk. The mixed forest consists of spruce, fir, pine and some occasional hardwood species (birch and aspen). They find LAI values between 2 and 7 m$^2$ m$^{-2}$. To assess the LAI we use data from the literature and experience from the repeated fieldwork at the described site. Following Kobayashi et al. (2010), who

conducted an extensive study using satellite data, the average LAI for our forest type is set to $4\,m^2\,m^{-2}$, and the stem area index (SAI) is set to $0.05\,m^2\,m^{-2}$, resulting in a plant area index (PAI) of $4.05\,m^2\,m^{-2}$ and nine vegetation layers for model simulations. The lower atmospheric boundary layer is simulated by 4 m of atmospheric layers.

We perform simulations over a 5-year period from August 2014 to August 2019. The model runs are initialized with a typical temperature profile of 0 m depth at 0 °C, 2 m at 0 °C, 10 m at −9 °C, 100 m at 5 °C, 5000 m at 20 °C. Spin-up period prior to the validation period is 4 years before we compare modeled and measured data. Test runs with a longer spin-up period of 10 years confirmed that only 4 years are sufficient when focusing on GST. The meteorological forcing data required by the model include air temperature, relative humidity, air pressure, wind speed, liquid and solid precipitation, incoming short- and longwave radiation, and cloud cover. ERA-Interim (ECMWF Reanalysis) data for the coordinate 63.18946° N, 118.19596° E were used to obtain forcing data for the total available period from 1979 to 2019 (Simmons et al., 2007).

## 3 Results

### 3.1 Model validation and in situ measurements

At our primary study site, the model is validated against ground surface temperature (GST) measurements of forested and non-forested study sites. The dataset used covers one complete annual cycle from 10 August 2018 to 10 August 2019. In addition, the model output is compared to radiation, snow depth, conductive heat flux, precipitation and temperature measurements of the AWS at the grassland site. The AWS was set up on 5 August 2018 and taken down on 26 August 2019. Data were recorded continuously, except for 40 d in late May and early June due to a power cut. The mean annual air temperature was −7.3 °C with a maximum temperature of 33.1 °C, a minimum of −54.0 °C and an average relative humidity of 70.5 %. Precipitation is $129.8\,mm\,yr^{-1}$ (liquid). The maximum snow height at the grassland site is measured to be 0.5 m in February, and the ground was snow-covered for 181 d from 28 October 2018 to 27 April 2019 (values above 0.05 m snow height). A quality check of the radiation data revealed partly inconsistent incoming longwave radiation measurements for the time span of 1 November 2018–26 February 2019. During this period it is likely that the sensor is partially covered by snow, making it necessary to discard those measurements from the record. High-quality $Q_{net}$ and $L_{in}$ and $L_{out}$ measurements, thus, only exist for the periods 28 to 30 October 2018 and 27 February 2018 to 27 April 2019. This data gap consequently also limits the period for which Bowen ratios are calculated and sensible heat fluxes ($Q_h$) and latent heat fluxes ($Q_e$) can be derived. The mean annual grassland albedo is 0.35 with an average of 0.30 during the snow-free and 0.48 during the snow-covered season. From December to February the albedo reaches its highest values with a mean of 0.7. Mean annual GST at 0.07 m depth is −2.6 °C (range from 19.1 to −24.9 °C) with an average of −11.4 °C in the snow-covered period and 8.0 °C in the snow-free period. The average annual GST recorded in forested areas at a depth of 0.03 m is 1.9 °C (range from 15.6 to −23.4 °C) with an average of −9.3 °C in the snow-covered period and 5.6 °C in the snow-free period.

We acknowledge that the target variable GST does not allow a detailed evaluation of the surface energy balance. Therefore, we further validate the model performance with additional measurements from an external study site (see Appendix C). Through the Arctic Data archive System (ADS) we have been provided with meteorological and radiation data from beneath and above the larch-dominated forest canopy at Spasskaya Pad for 2017–2018 (Maximov et al., 2019). These data are used for additional model validation and are added to the Appendix of our paper. Overall our analysis reveals a satisfactory agreement between modeled and measured components of the surface energy balance below the canopy. Thus, we argue that the performance of the model at the external study site justifies its application at the primary study site in Nyurba, where below-canopy fluxes were not acquired (see Appendix C).

#### 3.1.1 Surface energy balance

In a first step we assess the surface energy balance by comparing the modeled net radiation ($Q_{net}$), sensible heat flux ($Q_h$), latent heat flux ($Q_e$) and storage heat flux ($Q_s$) at the forested site and the modeled and measured fluxes at the grassland site (see Fig. 3 and Appendix A). Turbulent fluxes at the forest ground are close to zero for both the snow-free and snow-covered periods. The TOC sensible heat flux is highest in the snow-free period ($48.6\,W\,m^{-2}$), resulting in the highest net radiation flux ($83.5\,W\,m^{-2}$). Forest ground net radiation flux is only a third ($25.8\,W\,m^{-2}$) of the TOC flux. The latent heat flux in the snow-free period is similar for the forest TOC ($16.5\,W\,m^{-2}$) and grassland sites (measured value of $22.1\,W\,m^{-2}$ and modeled value of $18.5\,W\,m^{-2}$). During the snow-covered season, forest TOC and ground turbulent heat fluxes and net radiation are close to zero. Net radiation flux in the snow-covered period is smallest at the grassland site (modeled value of $-20.0\,W\,m^{-2}$ and measured value of $9.7\,W\,m^{-2}$). The resulting storage flux is more than double at the forest ground ($30.4\,W\,m^{-2}$) for the snow-free period and slightly positive ($0.5\,W\,m^{-2}$) during the snow-covered period.

The average measured Bowen ratio ($B$) at the AWS is 1.04, with an average of 1.94 for the snow-free and 0.35 for the snow-covered periods. At the grassland site the model predicts a $B$ of 1.8 for the snow-free period and −16.54 for the snow-covered period. This sums up to an annual average $B$ of 1.09 for grassland. Modeled annual average $B$ at the for-

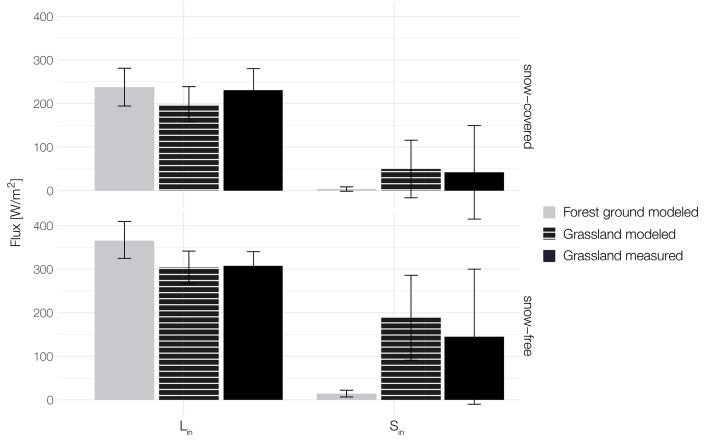


**Figure 4.** Modeled incoming solar and longwave radiation for the snow-covered (28 October 2018–27 April 2019) and snow-free (10–27 October 2019 and 28 April–10 October 2019) periods at the ground surface of forest (grey) and grassland (striped). Measured (black) incoming solar (for the same time periods) and longwave radiation (for 28–30 October 2018 and 27 February 2018–27 April 2019) are shown for the grassland site. The bars indicate mean values, while the whiskers show the corresponding standard deviations.

est ground is more than double with 2.85 for the snow-free period and 2.01 for the snow-covered period. The top-of-the-canopy modeled annual average $B$ is 2.99, with an average of $-0.77$ in the snow-covered period and 3.93 in the snow-free period.

More detailed insights into differences of available radiation at the ground surface are presented in Fig. 4. Here, the incoming short- and longwave radiation measured at the grassland site and modeled for the forest and grassland are shown. The longwave radiation dominates the incoming part of the radiation balance at both sites throughout the year. In the snow-free period, downward longwave radiation flux is $44.2\,\mathrm{W\,m^{-2}}$ higher at the forest ground. In the snow-covered period downward longwave radiation flux is $40.7\,\mathrm{W\,m^{-2}}$ higher at the forest ground. This results in a surplus of energy of $+9.6\,\mathrm{W\,m^{-2}}$ for the snow-covered and $+16.7\,\mathrm{W\,m^{-2}}$ for the snow-free periods under the forest canopy compared to the grassland. The shortwave radiation reaching the forest ground is very small for both periods ($9.9\,\mathrm{W\,m^{-2}}$ for the snow-free and $2.8\,\mathrm{W\,m^{-2}}$ for the snow-covered periods), showing that the canopy effectively intercepts (absorbs and reflects) most of the incoming shortwave radiation. Shortwave downward radiation at the grassland site is more than 19 times higher in the snow-free period and 18 times higher in the snow-covered period.

### 3.1.2 Thermal regime of the ground near the surface

In a second step, we compare the annual average GST in the snow-free and snow-covered periods to understand the overall model performance and the relative temperature differences between the forest and grassland sites (see Fig. 5). We further discuss the annual cycle of the thermal development of the permafrost ground, the modeled and measured active-layer thickness, and the volumetric groundwater content at both of our study sites.

Measured and modeled average GST values are summarized in Fig. 5. The highest deviation between modeled and measured GST is found at the grassland site. Here, the model shows a cold bias of $-4.1\,^{\circ}\mathrm{C}$ for the snow-covered period. Also, there is a cold bias of $-2.8\,^{\circ}\mathrm{C}$ in the snow-free period in the forest. Overall, we find an average annual difference of $0.7\,^{\circ}\mathrm{C}$ between the two sites. This difference is $5.2\,^{\circ}\mathrm{C}$ for the snow-free season and $6.7\,^{\circ}\mathrm{C}$ for the snow-covered period, respectively.

For a more detailed understanding of the annual cycle of the thermal evolution of permafrost ground at our study sites, we compare the weekly averaged GST at the grassland and forest site (see Fig. 6). The more detailed analysis of the annual cycle reveals periods with distinct differences between the model simulations and the measured values. For both study sites the model produces a slight GST overestimation in summer and a prolonged thawing period in spring. The measured data show a much faster ground warming in spring. This difference is over 20 d at the forest site and 15 d at the grassland site. In addition, there is a cold bias by $5\,^{\circ}\mathrm{C}$ in January at the grassland site. This bias is not seen at the forest site. Thawing starts later in model simulations than in measured values.

To further investigate the temporal evolution of the permafrost ground, we compare modeled and measured active-layer thicknesses at both study sites. In the grassland, the

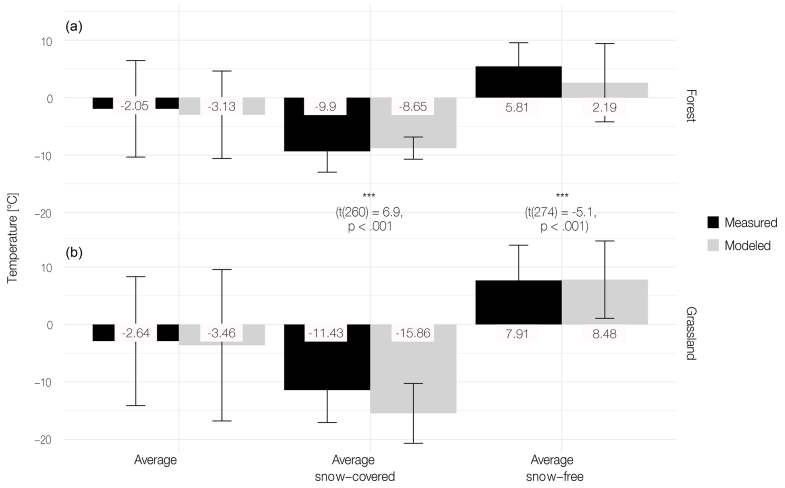


**Figure 5.** Average measured and modeled GST in the snow-covered period, average measured and modeled GST in the snow-free period, annual average measured and modeled GST, and the respective standard deviations in forest (**a** at 0.03 m depth) and grassland (**b** at 0.07 m depth) over a measurement period of 1 year (10 August 2018–10 August 2019). The bars indicate mean values, while the whiskers show the corresponding standard deviations. Unpaired *t* test between modeled forest and grassland GST shows a statistically significant temperature difference for the snow-covered and snow-free periods.

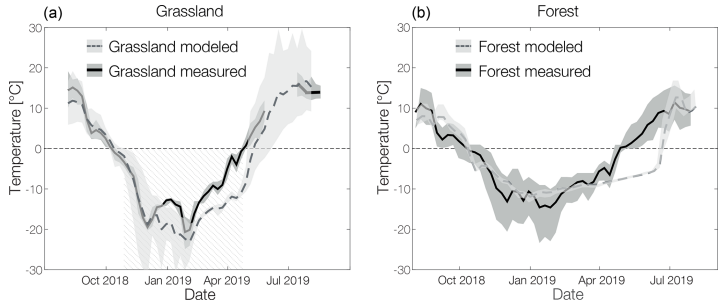


**Figure 6. (a)** Modeled (grey) and measured (black) average weekly GST in 0.03 m depth in forest and **(b)** in grassland in 0.07 m depth with standard deviations for modeled (light grey) and measured (dark grey) values. In addition, the measured duration of the snow-covered period is shaded at the grassland site. Please note that there is a data gap in the measured data at the grassland site in May–June (see Sect. 3.1 for further details).

modeled maximum active-layer thickness (ALT) is 2.35 m between 13 and 24 October 2018, with complete freezing occurring on 9 November and topsoil thawing starting on 3 May. The measured ALT in the grassland was 2.3 m in mid-August 2018 and early August 2019. The measured ALT in the forest was between 0.5 and 1.1 m in mid-August 2018. In the forest, the modeled maximum ALT is 2.05 m in October 2018 with freezing being completed on the 14 November. Topsoil thawing began on 23 June, 51 d later than in grassland. The modeled ALT in August 2018 was between 0.4 and 1.8 m and therefore overestimated by 0.3 m compared to the point measurements taken in August 2018 (see Fig. 7).

Moreover, the measured volumetric water content (VWC) in grassland reaches its maximum of 0.2 in August. The averaged measured VWC at the forest site in August 2018 was 0.3. The model can broadly reproduce this difference, but there is a model bias towards higher VWC for both sites. The modeled maximum water content in forest is 0.5 between the end of June and the beginning of July and is about 0.2 higher than in grassland, where the simulation shows a maximum VWC of 0.3 in August. The modeled winter ice

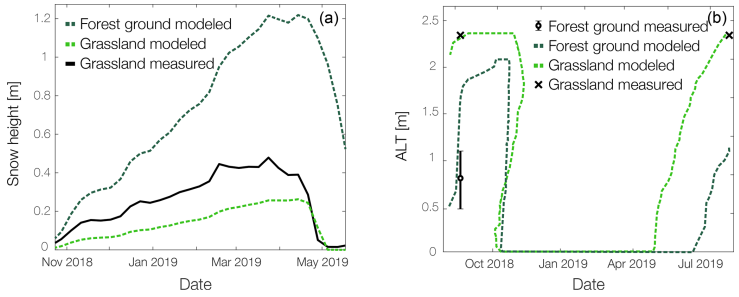


**Figure 7. (a)** Measured snow depth at AWS (black solid line) in the grassland, modeled snow depth in grassland (dashed light green) and modeled snow depth in forest (dashed dark green). **(b)** Active-layer thickness (ALT) dynamics, measured ALT at the grassland and forest sites (black, point measurements in 2018 and 2019 (grassland only)), modeled ALT in forest (dashed light green), and modeled ALT in grassland (dashed dark green) sites. Topsoil freezing starts at the beginning of October.

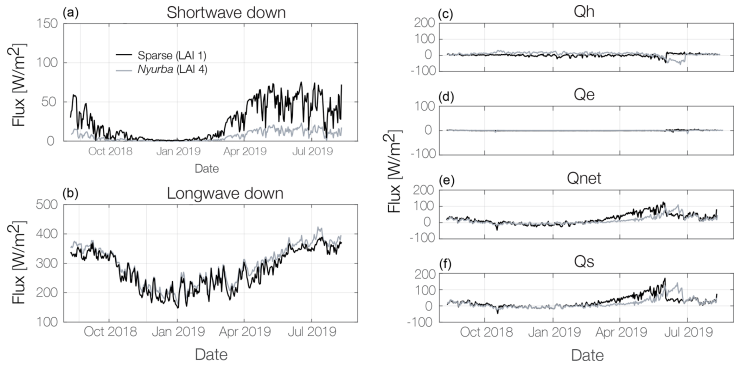


**Figure 8. (a)** Modeled longwave and solar radiation at the forest ground for an LAI of $1\,m^2\,m^{-2}$ (Sparse, black) and LAI of $4\,m^2\,m^{-2}$ (*Nyurba*, grey). **(b)** Modeled turbulent fluxes ($Q_h$ and $Q_e$), net radiation ($Q_{net}$) and storage heat flux at the forest ground ($Q_s$).

content reaches a maximum value of 0.36 in grassland and 0.42 in forest.

## 4 Discussion

The model presented here is found to be capable of simulating the differences in the ground thermal regime between a forested and a non-forested site for permafrost underneath boreal forests. This can provide important insights into the range of spatial differences and possible temporal changes that can be expected following current and future landscape changes such as deforestation through fires, anthropogenic influences and afforestation in currently unforested grasslands or the densification of forested areas. The implemented scheme is able to simulate the physical processes that define the vertical exchange of radiation, heat, water and snow between permafrost and the canopy. Our simulations show that the forests exert a strong control on the thermal state of permafrost. At the grassland site, we find a much larger ground surface temperature (GST) amplitude of 60.35 °C over the annual cycle, which is 32 °C higher than at the forest site. This vegetation dampening effect on soil temperature is well-described in the literature (Oliver et al., 1987; Balisky and Burton, 1993; Chang et al., 2015). Earlier work by Bonan and Shugart (1989) found that forest soils generally thaw later and less deeply and are cooler than in open areas. In the winter, forested soils are typically warmer relative to open areas. The tree cover can maintain stable permafrost under otherwise unstable thermal conditions (Bonan and Shugart, 1989). Our results are in agreement with these observations but further demonstrate that the impact of mixed boreal forest on the GST is strongest during the snow period and the summer peak with the warmest months. Our model reveals an average of 6.7 °C higher GST during the snow-covered period and 5.2 °C lower GST during the snow-free period. Measurements reveal an average of 2 °C higher GST in forest during the snow-covered period and 2.3 °C lower GST during

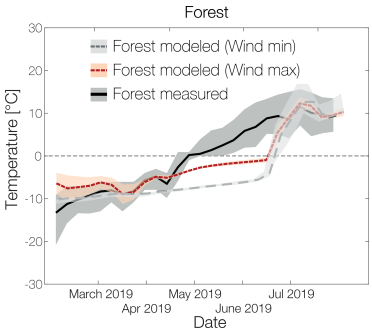


**Figure 9.** Modeled (Wind min (grey) and Wind max (red)) and measured (black) average weekly GST in 0.03 m depth in forest with standard deviations for modeled (light grey and light red) and measured (dark grey) values. Red represents a simulation using the wind speed at the top of the canopy as the input value for snow compaction. Grey shows the standard model simulation using the wind speed at the canopy bottom for the snow compaction mechanisms.

the snow-free period. Our model simulations show that the strong control on the thermal state of permafrost is a result of the combined effects of canopy shading, the suppression of turbulent heat fluxes, below-canopy longwave enhancement, increased soil moisture and distinct snow cover dynamics. These relevant processes controlling forest insulation will be discussed individually in the following subsections followed by a detailed discussion on model applicability and limitations.

### 4.1 Canopy shading and longwave enhancement

The surface energy balances simulated by the model are very different for grassland and forest. The forest canopy reflects and absorbs over 92 % of incoming solar radiation for both the snow-free and snow-covered periods. The forest ground albedo therefore has little influence on the energy balance. This canopy shading effect makes the longwave radiation the largest source of radiative energy at the forest site for both time periods. A surplus of longwave radiation of over 20 % is largely trapped below the canopy due to extremely low turbulent heat fluxes, similar to a greenhouse. The increased longwave radiation results in a relatively strong storage heat flux. Despite shading, the storage heat flux at the forest site is similar in magnitude to that simulated at the grassland site. This explains the small difference in the modeled depths of the active layer at both sites. The heat flux plate used for measuring the conductive heat flux at the grassland site is designed for use in mineral soil. Due to a certain amount of organic content in the upper soil layer, under- or overestimated heat fluxes are possible (Ochsner et al., 2006). This could explain to some extent the difference between measurements and simulations. We further find that during the snow-free period, the sensible and latent heat flux at the canopy top are high, while they are close to zero at the forest ground. In summary, we show that the canopy effectively absorbs and reflects the majority of incoming solar radiation, making canopy shading one of the main controlling mechanisms, and that the canopy enhances the longwave radiation at the forest ground because of extremely low turbulent heat fluxes.

### 4.2 Soil moisture, canopy interception and evapotranspiration

According to the majority of studies, tree growth in permafrost areas is limited by summer air temperatures and available water from snowmelt, water accumulated within the soil in the previous year and permafrost thaw water (Kharuk et al., 2015; Sidorova et al., 2007). The amount of precipitation in the eastern Siberian taiga is characteristically small compared to other areas; therefore it is expected that permafrost plays an important role in the existence of these forests (Sugimoto et al., 2002). Sugimoto et al. (2002) found that plants used rainwater during wet summers but meltwater from permafrost during drought summers. This indicates that permafrost provides the direct source of water for plants in drought summers and retains surplus water in the soil until the next summer. They conclude that if this system is disturbed by future warming, the forest stands might be seriously damaged in severe drought summers (Sugimoto et al., 2002). Our grassland site, which was supposedly forested until the 1950s, has dried up and has a much smaller organic layer and a maximum active-layer thickness of 2.30 m. The volumetric water content in forest soil is 10 %–20 % higher despite the same amount of precipitation and a higher evaporative flux during the growing season. This points to the conclusion that permafrost plays an important role in regulating the hydrological conditions in this boreal forest area by holding the water table close to the surface, which improves plant water supply.

### 4.3 Insulating the litter and moss layer

The existence of a thick moss and organic layer on the forest ground can significantly lower ground temperatures due to the high insulation impact (Bonan and Shugart, 1989). The low bulk density and low thermal conductivity of the organic mat effectively insulate the mineral soil, causing lower soil temperatures and maintaining a high permafrost table. A thick moss–organic layer on the forest floor is an important structural component of the forest–permafrost relationship, controlling energy flow, nutrient cycling, water relations, and, through these, stand productivity and dynamics (Bonan and Shugart, 1989). At our forest site the moss coverage was found to range between 0 % and 40 % with thicknesses ranging from 0.005 to 0.02 m. This is a comparably thin moss layer, but it was taken into account in the ground setup for the forest site.

### 4.4 Snowpack dynamics

Snow cover dynamics on the other hand seem to be a highly important factor in regard to the thermal evolution of the underlying permafrost ground (Gouttevin et al., 2012). Snow cover is an essential ecosystem component, acting as a radiation shield, insulator and seasonal water reservoir. The forest canopy exerts a strong control on snow accumulation due to interception and reduced wind speeds (Price, 1988). To analyze characteristics in the snow cover evolution, we compare modeled and measured snow depths at the AWS (grassland site) with the modeled snow depth at the forest site. Snow depth modeled in grassland agrees well with the measured snow depth and reaches a maximum value of 0.26 m in late April (see Fig. 7). Towards spring, the snowpack in the forest accumulates to 1.2 m. The melting of snow starts around the same period but lasts longer up until the end of May. The snowpack at the forest site exhibits different characteristics than at the grassland site. The found differences are clearly induced by the canopy structure controlling snow interception within the canopy, mass unload from the branches to the ground, sublimation and snow compaction.

In addition, our simulations at the forest site show an increase in longwave radiation, a decrease in solar radiation and the oppression of turbulent fluxes, which additionally lead to the slower melting of snow, less snow compaction and therefore a higher snowpack. This is in agreement with earlier work on snowpack modeling in coniferous forests (Price, 1988). For example, Beer et al. (2007) note that vegetation effects such as solar radiation extinction and atmospheric turbulence have a far greater influence on snow cover dynamics in boreal forests of eastern Siberia than snow interception alone. In addition, Grippa et al. (2005) found that the leaf area index (LAI) and snow depth are highly connected.

To understand the high impact that coupling the vegetation has on the snow cover, we next study the surface energy balance simulated by our model for our specific forest study site and a hypothetical, sparse canopy with an LAI of $1\,m^2\,m^{-2}$, while keeping all other parameters the same (see Fig. 8). In snow-free periods the mean incoming solar radiation at the ground is 5 times higher in the sparse canopy simulation, which leads to a higher net radiation flux ($Q_{net}$). Turbulent fluxes ($Q_h$ and $Q_e$) are similar, which suggests that air circulation is blocked, even in a very sparse canopy. The high longwave radiation at the forest ground is persistent for the hypothetical sparse canopy as well, and longwave radiation remains the dominant energy component.

Snow depth analysis further reveals that for a sparse forest canopy the maximum snow depth reaches 0.23 m only, resulting in a maximum ALT of 0.88 m and an annual average $\delta T$ of 0.8 °C. This confirms that the thermal differences between forest and grassland sites are largely controlled by the impact of the canopy density on snow depth and density.

The snowpack at our primary site (mixed forest) reaches a maximum thickness of 1.2 m, which is in accordance with studies of boreal forest snow depths in other boreal regions such as in Canadian boreal regions, where, i.e., Kershaw and McCulloch (2007) found varying mean snowpack depths between 0.73 and 1.3 m in different forest types and depths of only 0.08 m in a tundra landscape. Further, Fortin et al. (2015) measured maximum snowpack heights between 0.7 and 0.9 m in a black-spruce-dominated forest–tundra ecotone. Similar values were also found in a study in mixed boreal forests in northeastern China (Chang et al., 2015) and in a more general large-scale approach for the circumpolar north (Zhang et al., 2018). This strong variability and heterogeneity in snow distribution has already been identified as a very important driver of the subsurface and hydrological regimes and runoff in unforested permafrost regions (Nitzbon et al., 2019).

Nevertheless, the strong delay between observed and modeled top ground thawing at the forest site (see Fig. 6) demands further investigation. The snow compaction currently used in the snow module is dependent on wind speed only (see Sect. 2.3.3). Due to the coupled forest canopy, modeled wind speed at ground level is strongly reduced to the minimum value of $0.1\,m\,s^{-1}$. Consequently, the snow compaction is remarkably low. To understand how much of the difference between modeled and measured spring GST can be explained by the underestimated snow compaction, we simulate an extreme case, using the above-canopy wind speed for the snow compaction processes (see Fig. 9). The use of the above-canopy wind speed and the resulting high snow compaction reduces the difference between modeled and measured GST in spring by about 50 %. This reduction arises from the lower insulation capacity of the thinner snowpack. However, the timing of topsoil thawing does not improve. This may be explained by the fact that the snow cover has, on the one hand, a lower depth but, on the other hand, a higher density, which results in the same snow water equivalent and an equally high amount of energy needed to melt the snow cover completely.

### 4.5 Applicability and model limitations

The presented model is largely able to reproduce recorded GSTs in forests. The detailed analysis of the annual cycle shows that the snowmelt period in spring is biased at the forest and grassland sites. In reality, the ground warms up faster than is modeled. In the forest this is most likely caused by a wrong representation of snowpack compaction and snowmelt. Our analysis reveals that an extreme case of snow compaction only partly reduces the difference between modeled and measured GST in spring. This points to more complex processes that control snowmelt in forest than are currently represented by the model. Thus, it would be highly desirable to obtain further field measurements in order to gain a better understanding of snowmelt processes in boreal forests.

An aspect not represented in the model is the moisture transport and migration in frozen ground including the form-

ing of ice lenses and excess ground ice, which can have a high impact on the local micro-topography and the surface energy balance. Furthermore, lateral water flow and snow redistribution may be important processes to be investigated in the future, since they can strongly modify the ground thermal regime as well as the snowpack development.

Additionally, more detailed field studies and modeling exercises on the variation of canopy densities and structures should be carried out in order to obtain a better understanding of the impact of dynamic forest stand development on permafrost and vice versa. In combination, the above model limitations could explain a great part of the described GST and ALT differences between measurements and modeled simulations.

To simulate the needle tossing of deciduous larch, we have incorporated a leaf area index threshold between needle tossing and leaf-out (10 October–30 May) for simulations at our external validation site at Spasskaya Pad (see Appendix C). This tunes the model towards a more detailed representation of larch-dominated forests, which are particular to the secondary study site and large parts of eastern Siberia. The analysis reveals a satisfactory agreement between modeled and measured components of the surface energy balance below the predominantly deciduous forest canopy. The mixed forest cover at our primary study site only contains 7 % of deciduous larch trees. The LAI reduction implemented is therefore very small and had no noticeable effect on our results. This modification can be used to study further taxa-specific interactions with permanently frozen ground. It would also be desirable to implement a spatially explicit, dynamic vegetation model, such as the larch forest simulator (LAVESI – Larix Vegetation Simulator, Kruse et al., 2016), to further analyze the dynamic vegetation distribution under the recognition of the found interactions. This would allow us to simulate the vegetation response to changes in permafrost temperature and hydrology dynamically over a large timescale and across a wide range of boreal forest ecosystems in eastern Siberia.

## 5 Conclusions

This study presents a specific application of a novel, coupled multilayer forest–permafrost model which enables us to investigate the energy transfer and surface energy balance in permafrost-underlain boreal forest of eastern Siberia. By simulating interactions between the vegetation cover and permafrost, our modeling approach allows us to quantify and study the impact of the forest on the hydro-thermal regime of the permafrost ground below. An extensive comparison between measured and modeled energy balance variables (GST, $Q_e$, $Q_h$, $Q_{net}$, $S_{in}$ and $S_{out}$) reveals a satisfactory model performance justifying its application to investigate the thermal regime and surface energy balance in this complex ecosystem. Despite overall good performance, the field measurements reveal model shortcomings during the snowmelt period. Based on this modeling exercise and field measurements, we investigate the thermal conditions of two landscape entities as they typically occur in the boreal zone. In regard to the forest insulation effect on permafrost and ongoing land cover transitions, this study delivers important insights into the range of spatial differences and possible temporal changes that can be expected following landscape changes such as deforestation through fires, anthropogenic influences, and afforestation in currently unforested grasslands or the densification of forested areas. The detailed vegetation model successfully calculates the canopy radiation and water budgets, leaf fluxes, and canopy turbulence and aerodynamic conductance. These canopy fluxes alter the below-canopy surface energy balance, the ground thermal conditions and the snow cover dynamics. We find a strong dampening effect of over 30 °C on the annual ground surface temperature amplitude of the permafrost. Further, forested permafrost maintains a higher soil water content by controlling water storage in the ground. The forest cover alters the surface energy balance by inhibiting most of the solar radiation and suppressing turbulent heat fluxes. Additionally, we reveal that the canopy leads to a surplus in longwave radiation trapped below the canopy, similar to a greenhouse. Therefore and despite the canopy shading, the storage heat flux at the forest site is similar in magnitude to that simulated at the grassland site. In summary, we identify the following key points.

i. The forest canopy effectively absorbs and reflects over 90 % of incoming solar radiation, making canopy shading one of the main controlling mechanisms.

ii. The vegetation cover suppresses the majority of the turbulent heat fluxes in the below-canopy space.

iii. The forest canopy enhances the longwave radiation below the canopy by up to 20 %, similar to a greenhouse, which results in a comparable magnitude of storage heat flux for both the forest and the grassland sites.

iv. Forested permafrost holds a higher groundwater content than the dry grassland site.

v. Forest canopy shading leads to the slower melting of snow, less snow compaction and therefore a higher snowpack.

vi. The differences in the thermal development of the forest and grassland sites are highly influenced by the depth, density and resulting insulation capacities of the snow cover, which are in turn controlled by the forest canopy density.

## Appendix A: Bowen ratio and turbulent heat flux calculation

With the AWS equipped as a Bowen ratio station, $B$ is calculated following Foken (2016) as

$$B = \frac{c_p}{L_v} \times \frac{\Delta T}{\Delta q}, \tag{A1}$$

where the specific heat at constant pressure for moist air ($c_p$) is $1.006\,\mathrm{kJ\,kg^{-1}\,K^{-1}}$ and the latent heat of vaporization of water ($L_v$) is $2260\,\mathrm{kJ\,kg^{-1}}$; $\Delta T$ is the temperature difference between the two air temperature sensors at heights 0.115 and 0.252 m; and $\Delta q$ is the difference in specific humidity calculated from measured relative humidity ($\phi$), temperature and pressure.

Thereafter, latent heat flux ($Q_e$) is calculated as

$$Q_e = \frac{Q_s - Q_g}{1 + B}, \tag{A2}$$

and sensible heat flux ($Q_h$) is

$$Q_h = (Q_s - Q_g)\frac{B}{1 + B}, \tag{A3}$$

with the storage heat flux ($Q_s$) being

$$Q_s = L_{in} + S_{in} - L_{out} - S_{out}, \tag{A4}$$

and $Q_g$ being the convective ground heat flux.

**Table A1.** Sensors used for field measurements.

| Sensor | Brand | Measurement | Accuracy |
|---|---|---|---|
| Temperature and relative humidity probe (HMP155A) | Vaisala | Air temperature and relative humidity | ±1% (15–25 °C) |
| Alpine wind monitor (05103-45) | R. M. Young Company | Wind speed and direction | 1 % of reading |
| Sonic ranging sensor (SR50A) | Campbell | Snow depth | 0.4 % of height |
| Barometric sensor (CS100) | Setra | Barometric pressure | ±0.5 mbar (20 °C) |
| Four-component net radiometer (NR01) | Hukseflux | Short- and longwave in and out | 10 % daily totals |
| Thermistor probe (107) | Campbell | Soil temperature | 0.2 °C |
| Heat flux sensor (HFP01) | Hukseflux | Ground heat flux | ±3% |
| Rain gauge tipping bucket, unheated (52 203) | R. M. Young C. | Precipitation (liquid) | 2 % up to 25 $\mathrm{mm\,h^{-1}}$ |
| Water content reflectometer (CS616) | Campbell | Soil moisture | ±2.5% VWC |
| HOBO four-channel data logger and temperature sensor | Onset | Soil temperature | ±2 mV ± 2.5 % of absolute reading |
| iButton (DS1922L) | Maxim Integrated | Soil temperature | ±0.5 °C (−10–65 °C) |

**Table A2.** Overview of the CryoGrid parameters used.

| Process or parameter | | Value | Unit | Source |
|---|---|---|---|---|
| Density of falling snow | $\rho_{snow}$ | 300 | $\mathrm{kg\,m^{-3}}$ | Kershaw and McCulloch (2007) |
| Albedo at ground | $\alpha$ | 0.3 | – | Field measurement |
| Roughness length | $z_0$ | 0.001 | m | Westermann et al. (2016) |
| Roughness length of snow | $z0_{snow}$ | 0.0001 | m | Boike et al. (2019) |
| Geothermal heat flux | $F_{lb}$ | 0.05 | $\mathrm{W\,m^{-2}}$ | Westermann et al. (2016) |
| Thermal conductivity of mineral soil fraction | $k_{mineral}$ | 3.0 | $\mathrm{W\,m^{-1}\,K^{-1}}$ | Westermann et al. (2016) |
| Emissivity | $\epsilon$ | 0.99 | – | Langer et al. (2011a) |
| Root depth | $D_T$ | 0.2 | m | Field measurement |
| Evaporation depth | $D_E$ | 0.1 | m | Nitzbon et al. (2019) |
| Hydraulic conductivity | $K$ | $10^{-5}$ | $\mathrm{m\,s^{-1}}$ | Boike et al. (2019) |

**Table A3.** Ground setup for simulations. Depth in meters with all others in unitless volumetric fractions.

| | Top depth | Water or ice | Mineral | Organic | Field capacity | Natural porosity |
|---|---|---|---|---|---|---|
| Forest | 0 | 0.6 | 0 | 0.2 | 0.5 | 0.8 |
| | 0.08 | 0.6 | 0.1 | 0.2 | 0.5 | 0.7 |
| | 0.16 | 0.6 | 0.4 | 0 | 0.5 | 0.6 |
| Grassland | 0 | 0.5 | 0.4 | 0.1 | 0.5 | 0.5 |
| | 0.04 | 0.4 | 0.6 | 0 | 0.5 | 0.4 |
| | 0.1 | 0.4 | 0.6 | 0 | 0.5 | 0.4 |

**Table A4.** Constants.

| Constants | Value | Unit |
|---|---|---|
| Von Kármán | 0.4 | – |
| Freezing point water (normal pressure) | 273.15 | K |
| Latent heat of vaporization | $2.501 \times 10^6$ | $\mathrm{J\,kg^{-1}}$ |
| Molecular mass of water | 18.016/1000 | $\mathrm{kg\,mol^{-1}}$ |
| Molecular mass of dry air | 28.966/1000 | $\mathrm{kg\,mol^{-1}}$ |
| Specific heat of dry air (constant pressure) | 1004.64 | $\mathrm{J\,kg^{-1}\,K^{-1}}$ |
| Density of fresh water | 1000 | $\mathrm{kg\,m^{-3}}$ |
| Density of ice | 917 | $\mathrm{kg\,m^{-3}}$ |
| Heat of fusion for water at 0 °C | $0.334 \times 10^6$ | $\mathrm{J\,kg^{-1}}$ |
| Thermal conductivity of water | 0.57 | $\mathrm{m^{-1}\,K^{-1}}$ |
| Thermal conductivity of ice | 2.29 | $\mathrm{W\,m^{-1}\,K^{-1}}$ |
| Kinematic viscosity of air (0 °C, 1013.25hPa) | 0.0000133 | $\mathrm{m^2\,s^{-1}}$ |
| Specific heat of water vapor (constant pressure) | 1810 | $\mathrm{J\,kg^{-1}\,K^{-1}}$ |

**Table A5.** Multilayer canopy parameters. PFT: plant functional type. VIS: visible. NIR: near-infrared. NET: needleleaf evergreen boreal.

| Parameter PFT NET boreal | Value | Unit | Source |
|---|---|---|---|
| Leaf angle depth from spherical | 0.01 | – | Bonan (2002) |
| Leaf reflectance (VIS–NIR) | 0.07/0.35 | – | Bonan (2002) |
| Stem reflectance (VIS–NIR) | 0.16/0.39 | – | Bonan (2002) |
| Leaf transmittance (VIS–NIR) | 0.05/0.01 | – | Bonan (2002) |
| Stem transmittance (VIS–NIR) | 0.001/0.001 | – | Bonan (2002) |
| Maximum carboxylation rate (25 °C) | 43 | $\mu mol\,m^{-2}\,s^{-1}$ | Bonan (2002) |
| Photosynthetic pathway | C3 | – | Bonan (2002) |
| Leaf emissivity | 0.98 | – | Bonan (2002) |
| Quantum efficiency $a$ | 0.06 | $\mu mol\ CO_2\ \mu mol\ photon^{-1}$ | Bonan (2002) |
| Slope $m$ | 6 | – | Bonan (2002) |
| Leaf dimension | 0.04 | m | Bonan (2002) |
| Roughness length | 0.055 | m | Bonan (2002) |
| Displacement height | 0.67 | m | Bonan (2002) |
| Root distribution parameters | 7.0/2.0 | – | Bonan (2002) |
| Minimum vapor pressure deficit | 100 | Pa | Bonan (2019) |
| Plant capacitance | 2500 | $mmol\ H_2O\ m^{-2}$ leaf area $MPa^{-1}$ | Bonan (2019) |
| Minimum leaf water potential | −2 | MPa | Bonan (2019) |
| Stem hydraulic conductance | 4 | $mmol\ H_2O\ m^{-2}$ leaf area $s^{-1}\,MPa^{-1}$ | Bonan (2019) |
| Atmospheric $CO_2$ | 380 | $\mu mol\ mol^{-1}$ | Bonan (2019) |
| Atmospheric $O_2$ | 209 | $\mu mol\,mol^{-1}$ | Bonan (2019) |
| Soil evaporative resistance | 3361.509 | $s\,m^{-1}$ | Bonan (2019) |
| Specific heat of dry–wet soil | 1396 | $J\,kg^{-1}\,K^{-1}$ | Oleson et al. (2013) |
| Specific heat of fresh $H_2O$ | 4188 | $J\,kg^{-1}\,K^{-1}$ | Oleson et al. (2013) |
| Specific leaf area at the top of the canopy | 0.01 | $m^2\,g^{-1}$ C | Bonan et al. (2018) |
| Fine root biomass | 500 | g biomass $m^{-2}$ | Bonan (2019) |
| Leaf drag coefficient | 0.25 | – | Bonan (2019) |
| Foliage clumping index | 0.7 | – | Bonan (2019) |

**Table A6.** Further ground parameters needed by the vegetation.

| Soil parameters (sandy clay loam) | Value | Unit | Source |
|---|---|---|---|
| Soil layer Clapp–Hornberger b (empirical parameter) | 4.05, 4.38, 10.4 | – | Bonan (2019) |
| Alpha (empirical parameter) | 0.059 | $cm^{-3}$ | Bonan (2019) |
| $n$ (pore size distributed index) | 1.48 | – | Bonan (2019) |
| Initial porosity | 0.8, 0.7, 0.6 | $m^3\,m^{-3}$ | Bonan (2019) |
| Soil layer depth or thickness | 0.1, 0.1, 0.7 | m | – |
| Interface depth | 0.05, 0.15, 0.45 | m | – |
| Number of soil layers | 3 | – | – |

## Appendix B: Direct and diffuse solar radiation components from cloud cover data

ERA-Interim cloud cover data ($N$) allow us to use a simple approach to differentiate the incoming shortwave radiation ($S_{\text{in}}$) into diffuse,

$$S_{\text{in}_{\text{diffuse}}} = S_{\text{in}} \times \left(0.3 + 0.7 \times (N/8)^2\right), \tag{B1}$$

and direct,

$$S_{\text{in}_{\text{direct}}} = S_{\text{in}} - S_{\text{in}_{\text{diffuse}}}, \tag{B2}$$

components, based on Younes and Muneer (2007).

## Appendix C: External validation site "Spasskaya Pad"

Further validation of the model performance is performed for a well-studied research site at Spasskaya Pad at 62.14° N, 129.37° E. This additional validation site is located 581 km from our primary study site but allows for validating further model variables due to additional observational data. Spasskaya Pad is a continuous permafrost region, and the active-layer depth is about 1.2 m in larch-dominated forests. The main tree species is Dahurian larch (*Larix gmelinii*), and there is a stand density of 840 trees $\text{ha}^{-1}$. The understory vegetation (*Vaccinium*) is dense and 0.05 m high. In 1996 a 32 m observation tower was installed (Ohta et al., 2001) in larch-dominated forest. Through the Arctic Data archive System (ADS, http://ads.nipr.ac.jp/, last access: 3 September 2020) we have been provided with the most recent available meteorological and radiation data from beneath and above the larch-dominated forest canopy for the time period 2017–2018 (Maximov et al., 2019). Each variable used here is measured at exactly 5 min intervals, except radiation (1 min). Ventilated shelters cover air temperature and humidity sensors. Net all-wave radiation and the four components of radiation are measured every minute, and the data loggers record average, maximum and minimum values. Upward and downward longwave radiation is corrected using the sensed temperature at domes and sensor bodies. Ground temperature is measured at seven depths, and soil moisture is measured at five depths. A more detailed description of the sensors can be found in Table 1 in Ohta et al. (2001). We have set up and run a 6-year simulation for this study site (2013–2019), using ERA-Interim forcing data using the grid cell closest to the coordinate 62.14° N, 129.37° E. The measurement tower is situated in larch-dominated forest so that a simple leaf-off parameterization is implemented. Following Ohta et al. (2001) we define a partial leaf-off period from 10 October–30 May, resulting in a reduced winter LAI of 0.5 $\text{m}^2\,\text{m}^{-2}$. The summer LAI is set to a constant value of 1.9 $\text{m}^2\,\text{m}^{-2}$, and we use the measured average tree height of 18 m for setting up the canopy structure. In order to ensure consistent model validation with the primary study site we used identical soil parameters for the external study site. All soil parameters used are summarized in Table A3, while Table A4 summarizes the constants used. We make use of canopy parameters defined by the PFT deciduous needleleaf due to the dominance of deciduous larch. The subsurface (soil) stratigraphy extends to 100 m below the surface, where the geothermal heat flux is set to a standard value of 0.05 $\text{W}\,\text{m}^{-2}$ (Langer et al., 2011b). The ground is divided into separate layers in the model. The uppermost 8 m have a layer thickness of 0.05 m, followed by 0.1 m for the next 20, 0.5 m up to 50 and 1 m thereafter. All remaining model parameters were set to default values as defined in previous studies (see Table A2) (Langer et al., 2011a, b, 2016; Westermann et al., 2016; Nitzbon et al., 2019, 2020). Similar to the primary study site we use ground surface temperature (GST) as one of the target variables for model validation, measured and modeled at 0.2 m. In addition we use air temperature below the canopy, measured at the height of 1.2 m, net radiation ($Q_{\text{net}}$), latent ($Q_{\text{e}}$) and sensible ($Q_{\text{h}}$) heat flux, and incoming ($S_{\text{in}}$) and outgoing ($S_{\text{out}}$) shortwave radiation flux at the ground surface as additional target variables allowing for a comprehensive validation of the modeled heat and moisture exchange processes within and below the canopy.

We assess the surface energy balance by comparing the median weekly values of modeled and measured net radiation ($Q_{\text{net}}$), sensible heat flux ($Q_{\text{h}}$), latent heat flux ($Q_{\text{e}}$), and incoming ($S_{\text{in}}$) and outgoing ($S_{\text{out}}$) solar radiation at the forested site (see Fig. C1).

Modeled turbulent fluxes below the canopy are small during the snow-covered period, and measurement data are not available during this period. Modeled and measured sensible heat flux in the snow-free period differ by 0.1 $\text{W}\,\text{m}^{-2}$ only. Modeled latent heat flux is only a fourth of the measured value and therefore underestimated in our model. Modeled net radiation in the snow-free period (25.7 $\text{W}\,\text{m}^{-2}$) is slightly above measured net radiation (19.4 $\text{W}\,\text{m}^{-2}$). For the snow-covered period, median modeled net radiation is slightly below the measured median value. The incoming shortwave radiation measured and modeled for the forest site fit well with differences well below 10 $\text{W}\,\text{m}^{-2}$. The standard deviation of measured values is higher for all variables except snow-covered net radiation.

In a second step, we compare the modeled and measured annual median GST for the snow-free and snow-covered periods and air temperature below the canopy to understand the overall model performance regarding the thermal regime of the surface and the ground and the relative temperature differences between the model and measurements (see Fig. C2).

The highest deviation between modeled and measured temperatures is found in the GST of the snow-free period. Here, the model shows a cold bias of −2 °C. For the snow-covered period the difference is 1.8 °C. For the air temperature below the canopy the difference between modeled and measured in the snow-free period is 1.5 °C; for the snow-covered period, the difference is again 1.8 °C. This falls into

the range of 1.5–2 °C that is commonly used for validation purposes (Langer et al., 2013; Westermann et al., 2016).

Overall our analysis reveals a satisfactory agreement between modeled and measured components of the surface energy balance below the canopy. Thus, we argue that the performance of the model at the external study site justifies its application at the primary study site in Nyurba, where below-canopy fluxes were not acquired.

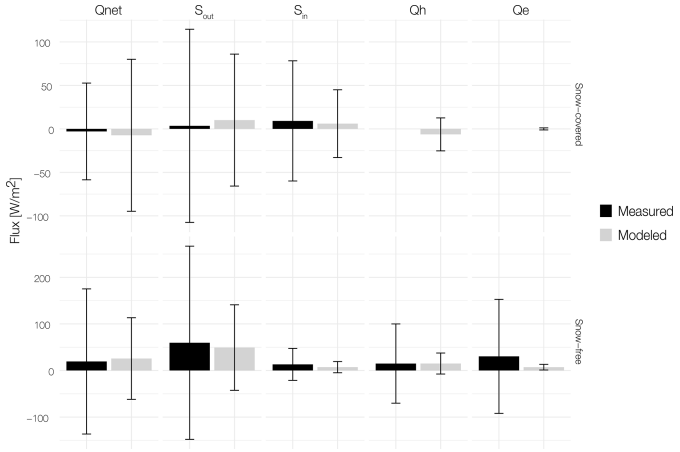


**Figure C1.** Modeled (grey) incoming and outgoing solar radiation ($S_{in}$ and $S_{out}$) and turbulent fluxes ($Q_h$, $Q_e$ and $Q_{net}$) for the snow-covered (28 October 2017–27 April 2018, above) and snow-free (10–27 October 2017 and 28 April–10 October 2018, below) periods at the ground surface of forest. The bars indicate median values, while the whiskers show the corresponding standard deviations.

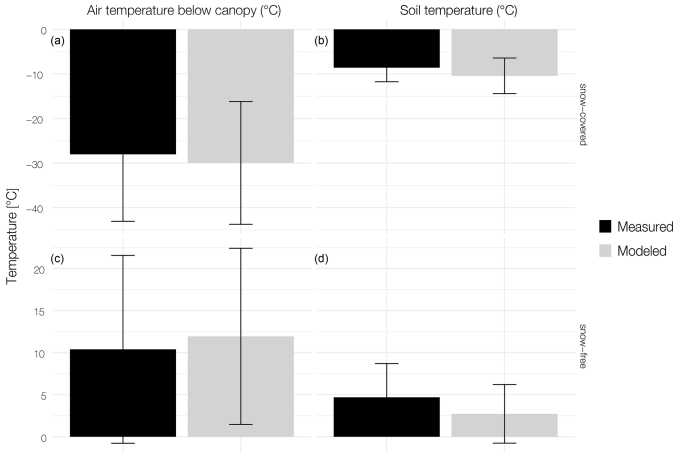


**Figure C2. (a)** Modeled (grey) and measured (black) air temperature (°C) below the canopy and **(b)** ground surface temperature (°C) for both the snow-covered (28 October 2017–27 April 2018, above) and snow-free (10–27 October 2017 and 28 April–10 October 2018, below) periods at the forest site at Spasskaya Pad. The bars indicate median values, while the whiskers show the corresponding standard deviations.

*Code and data availability.* The code is available at http://github.com/CryoGrid/CryoGrid/tree/vegetation (last access: 4 December 2020) and https://doi.org/10.5281/zenodo.4317107 (Stuenzi et al., 2020a). The iButton soil temperature data are available at https://doi.org/10.1594/PANGAEA.914327 (Langer et al., 2020). The AWS data are available at https://doi.org/10.1594/PANGAEA.919859 (Stuenzi et al., 2020b). The data for high-resolution photogrammetric point clouds used in Fig. 1 are available at https://doi.org/10.1594/PANGAEA.902259 (Brieger et al., 2019b).

*Author contributions.* SMS designed the study, developed and implemented the numerical model, carried out and analyzed the simulations, prepared the results figures, and led the paper preparation. ML, SW, JB, UH and SK co-designed the study and interpreted the results. SMS, ML and TSvD implemented the code in the model and designed the model simulations. SMS, WC, LAP, ESZ, UH and SK prepared and conducted the fieldwork in 2018; SMS and EZ conducted the fieldwork in 2019. SMS wrote the paper with contributions from all co-authors. UH, ML and JB secured funding.

*Competing interests.* The authors declare that they have no conflict of interest.

*Acknowledgements.* Simone Maria Stuenzi is thankful to the POLMAR graduate school, the Geo.X Young Academy and the WiNS program at Humboldt-Universität zu Berlin for providing a supportive framework for her PhD project and helpful courses on scientific writing and project management. Further, Simone Maria Stuenzi is very grateful for the help during fieldwork in 2018 and 2019, especially for the help from Levina Sardana Nikolaevna, Alexey Nikolajewitsch, Lena Ushnizkaya, Luise Schulte, Frederic Brieger, Stuart Vyse, Elisbeth Dietze, Nadine Bernhard, Boris K. Biskaborn and Iuliia Shevtsova, as well as for the help from her co-authors Luidmila Pestryakova and Evgeniy Zakharov. Additionally, Simone Maria Stuenzi would like to thank Stephan Jacobi, Alexander Oehme, Niko Borneman, Peter Schreiber and her co-author William Cable for their help in preparing for fieldwork and the entire PermaRisk and SPARC research groups for their ongoing support. Finally, Simone Maria Stuenzi would like to thank the editor, Alexey V. Eliseev, the reviewer Manuel Helbig and two further anonymous reviewers for their comments and suggestions which have greatly improved the paper.

*Financial support.* This study has been supported by the ERC consolidator grant Glacial Legacy to Ulrike Herzschuh (no. 772852). Further, the work was supported by the Federal Ministry of Education and Research (BMBF) of Germany through a grant to Moritz Langer (no. 01LN1709A). Funding was additionally provided by the Helmholtz Association in the framework of MOSES (Modular Observation Solutions for Earth Systems). Luidmila A. Pestryakova was supported by the Russian Foundation for Basic Research (grant no. 18–45-140053 r_a) and Ministry of Science and Higher Education of Russia (grant no. FSRG-2020-0019). Sebastian Westermann acknowledges funding by Permafost4Life (Research Council of Norway, grant no. 301639).

The article processing charges for this open-access publication were covered by a Research Centre of the Helmholtz Association.

*Review statement.* This paper was edited by Alexey V. Eliseev and reviewed by Manuel Helbig and two anonymous referees.

## References

ACIA: Arctic Climate Impact Assessment. ACIA overview report, available at: http://www.amap.no/documents/doc/arctic-arctic-climate-impact-assessment/796 (last access: 30 August 2018), 2005.

AMAP: Arctic Monitoring and Assessment Program 2011: Mercury in the Arctic, Cambridge University Press, https://doi.org/10.1017/CBO9781107415324.004, 2011.

Balisky, A. C. and Burton, P. J.: Distinction of soil thermal regimes under various experimental vegetation covers, Can. J. Soil Sci., 73, 411–420, https://doi.org/10.4141/cjss93-043, 1993.

Beer, C., Lucht, W., Gerten, D., Thonicke, K., and Schmullius, C.: Effects of soil freezing and thawing on vegetation carbon density in Siberia: A modeling analysis with the Lund-Potsdam-Jena Dynamic Global Vegetation Model (LPJ-DGVM), Global Biochem. Cy., 21, GB1012, https://doi.org/10.1029/2006GB002760, 2007.

Biskaborn, B. K., Smith, S. L., Noetzli, J., Matthes, H., Vieira, G., Streletskiy, D. A., Schoeneich, P., Romanovsky, V. E., Lewkowicz, A. G., Abramov, A., Allard, M., Boike, J., Cable, W. L., Christiansen, H. H., Delaloye, R., Diekmann, B., Drozdov, D., Etzelmüller, B., Grosse, G., Guglielmin, M., Ingeman-Nielsen, T., Isaksen, K., Ishikawa, M., Johansson, M., Johannsson, H., Joo, A., Kaverin, D., Kholodov, A., Konstantinov, P., Kröger, T., Lambiel, C., Lanckman, J. P., Luo, D., Malkova, G., Meiklejohn, I., Moskalenko, N., Oliva, M., Phillips, M., Ramos, M., Sannel, A. B. K., Sergeev, D., Seybold, C., Skryabin, P., Vasiliev, A., Wu, Q., Yoshikawa, K., Zheleznyak, M., and Lantuit, H.: Permafrost is warming at a global scale, Nat. Commun., 10, 1–11, https://doi.org/10.1038/s41467-018-08240-4, 2019.

Boike, J., Nitzbon, J., Anders, K., Grigoriev, M., Bolshiyanov, D., Langer, M., Lange, S., Bornemann, N., Morgenstern, A., Schreiber, P., Wille, C., Chadburn, S., Gouttevin, I., Burke, E., and Kutzbach, L.: A 16-year record (20022017) of permafrost, active-layer, and meteorological conditions at the Samoylov Island Arctic permafrost research site, Lena River delta, northern Siberia: an opportunity to validate remote-sensing data and land surface, snow, and permafrost models, Earth Syst. Sci. Data, 11, 261–299, https://doi.org/10.5194/essd-11-261-2019, 2019.

Bonan, G. B.: Ecological climatology: concepts and applications, Cambridge University Press, Cambridge, UK, 2002.

Bonan, G. B.: Climate Change and Terrestrial Ecosystem Modeling, Cambridge University Press, https://doi.org/10.1017/9781107339217, 2019.

Bonan, G. B. and Shugart, H. H.: Environmental Factors and Ecological Processes in Boreal Forests, Tech. rep., available at: http://www.annualreviews.org (last access: 11 May 2020), 1989.

Bonan, G. B., Williams, M., Fisher, R. A., and Oleson, K. W.: Modeling stomatal conductance in the earth system: linking leaf water-use efficiency and water transport along the soil-plant-atmosphere continuum, Geosci. Model Dev., 7, 2193–2222, https://doi.org/10.5194/gmd-7-2193-2014, 2014.

Bonan, G. B., Patton, E. G., Harman, I. N., Oleson, K. W., Finnigan, J. J., Lu, Y., and Burakowski, E. A.: Modeling canopy-induced turbulence in the Earth system: a unified parameterization of turbulent exchange within plant canopies and the roughness sublayer (CLM-ml v0), Geosci. Model Dev., 11, 1467–1496, https://doi.org/10.5194/gmd-11-1467-2018, 2018.

Brieger, F., Herzschuh, U., Pestryakova, L. A., Bookhagen, B., Zakharov, E. S., and Kruse, S.: Advances in the Derivation of Northeast Siberian Forest Metrics Using High-Resolution UAV-Based Photogrammetric Point Clouds, Remote Sens.-Basel, 11, 1447, https://doi.org/10.3390/rs11121447, 2019a.

Brieger, F., Herzschuh, U., Pestryakova, L. A., Bookhagen, B., Zakharov, E. S., and Kruse, S.: High-resolution photogrammetric point clouds from northeast Siberian forest stands. Alfred-Wegener-Institute research expedition "Chukotka 2018", PANGAEA, https://doi.org/10.1594/PANGAEA.902259, 2019b.

Chadburn, S. E., Burke, E. J., Essery, R. L. H., Boike, J., Langer, M., Heikenfeld, M., Cox, P. M., and Friedlingstein, P.: Impact of model developments on present and future simulations of permafrost in a global land-surface model, The Cryosphere, 9, 1505–1521, https://doi.org/10.5194/tc-9-1505-2015, 2015.

Chang, X., Jin, H., Zhang, Y., He, R., Luo, D., Wang, Y., Lü, L., and Zhang, Q.: Thermal Impacts of Boreal Forest Vegetation on Active Layer and Permafrost Soils in Northern da Xing'Anling (Hinggan) Mountains, Northeast China, Arct. Antarct. Alp. Res., 47, 267–279, https://doi.org/10.1657/AAAR00C-14-016, 2015.

Chapin, F. S., Matson, P. A., and Vitousek, P. M.: Earth's Climate System, in: Principles of Terrestrial Ecosystem Ecology, pp. 23–62, Springer, New York, NY, https://doi.org/10.1007/978-1-4419-9504-9_2, 2011.

Chasmer, L., Quinton, W., Hopkinson, C., Petrone, R., and Whittington, P.: Vegetation Canopy and Radiation Controls on Permafrost Plateau Evolution within the Discontinuous Permafrost Zone, Northwest Territories, Canada, Permafrost Periglac., 22, 199–213, https://doi.org/10.1002/ppp.724, 2011.

Chen, Y., Ryder, J., Bastrikov, V., McGrath, M. J., Naudts, K., Otto, J., Ottlé, C., Peylin, P., Polcher, J., Valade, A., Black, A., Elbers, J. A., Moors, E., Foken, T., van Gorsel, E., Haverd, V., Heinesch, B., Tiedemann, F., Knohl, A., Launiainen, S., Loustau, D., Ogée, J., Vessala, T., and Luyssaert, S.: Evaluating the performance of land surface model ORCHIDEE-CAN v1.0 on water and energy flux estimation with a single- and multi-layer energy budget scheme, Geosci. Model Dev., 9, 2951–2972, https://doi.org/10.5194/gmd-9-2951-2016, 2016.

Cosenza, P., Guerin, R., and Tabbagh, A.: Relationship between thermal conductivity and water content of soils using numerical modelling, Eur. J. Soil Sci., 54, 581–588, 2003.

Estop-Aragonés, C., Cooper, M. D., Fisher, J. P., Thierry, A., Garnett, M. H., Charman, D. J., Murton, J. B., Phoenix, G. K., Treharne, R., Sanderson, N. K., Burn, C. R., Kokelj, S. V., Wolfe, S. A., Lewkowicz, A. G., Williams, M., and Hartley, I. P.: Limited release of previously-frozen C and increased new peat formation after thaw in permafrost peatlands, Soil Biol. Biochem., 118, 115–129, https://doi.org/10.1016/j.soilbio.2017.12.010, 2018.

Foken, T.: Angewandte Meteorologie – Mikrometeorologische Methoden, Springer Spektrum, Berlin, Heidelberg, 3rd Edn., https://doi.org/10.1007/978-3-662-05743-8_8, 2016.

Fortin, V., Jean, M., Brown, R., and Payette, S.: Predicting Snow Depth in a Forest-Tundra Landscape using a Conceptual Model Allowing for Snow Redistribution and Constrained by Observations from a Digital Camera, Atmos. Ocean, 53, 200–211, https://doi.org/10.1080/07055900.2015.1022708, 2015.

Furyaev, V., Vaganov, E., Tchebakova, N., and Valendik, E.: Effects of Fire and Climate on Successions and Structural Changes in The Siberian Boreal Forest, Eur. J. Forest Res., 2, 1–15, 2001.

Gauthier, S., Bernier, P., Kuuluvainen, T., Shvidenko, A. Z., and Schepaschenko, D. G.: Boreal forest health and global change, Science, 349, 819–822, https://doi.org/10.1126/science.aaa9092, 2015.

Gouttevin, I., Menegoz, M., Dominé, F., Krinner, G., Koven, C., Ciais, P., Tarnocai, C., and Boike, J.: How the insulating properties of snow affect soil carbon distribution in the continental pan-Arctic area, J. Geophys. Res.-Biogeo., 117, 1–11, https://doi.org/10.1029/2011JG001916, 2012.

Grippa, M., Kergoat, L., Le Toan, T., Mognard, N. M., Delbart, N., L'Hermitte, J., and Vicente-Serrano, S. M.: The impact of snow depth and snowmelt on the vegetation variability over central Siberia, Geophys. Res. Lett., 32, L21412, https://doi.org/10.1029/2005GL024286, 2005.

Harris, I., Jones, P., Osborn, T., and Lister, D.: Updated high-resolution grids of monthly climatic observations – the CRU TS3.10 Dataset, Int. J. Climatol., 34, 623–642, https://doi.org/10.1002/joc.3711, 2014.

Hayasaka, H.: Recent Vegetation Fire Incidence in Russia, Global Environ. Res., 15, 5–13, 2011.

Helbig, M., Pappas, C., and Sonnentag, O.: Permafrost thaw and wildfire: Equally important drivers of boreal tree cover changes in the Taiga Plains, Canada, Geophys. Res. Lett., 43, 1598–1606, https://doi.org/10.1002/2015GL067193, 2016.

Herzschuh, U.: Legacy of the Last Glacial on the present-day distribution of deciduous versus evergreen boreal forests, Global Ecol. Biogeogr., 29, 198–206, https://doi.org/10.1111/geb.13018, 2019.

Kotlyakov, V. and Khromova, T.: Land Resources of Russia – Maps of Permafrost and Ground Ice, Version 1, GGD600, Boulder, Colorado, USA, NSIDC: National Snow and Ice Data Center, https://doi.org/10.7265/zpm9-j983, 2002.

Holtmeier, F. K. and Broll, G.: Sensitivity and response of northern hemisphere altitudinal and polar treelines to environmental change at landscape and local scales, Global Ecol. Biogeogr., 14, 395–410, https://doi.org/10.1111/j.1466-822X.2005.00168.x, 2005.

IPCC: Climate Change 2014 Synthesis Report. Contribution of Working Groups I, II and III to the Fifth Assessment Report of the Intergovernmental Panel on Climate Change, IPCC, Geneva, Switzerland, available at: http://ar5-syr.ipcc.ch/ipcc/ipcc/resources/pdf/IPCC_SynthesisReport.pdf (last access: 20 September 2018), 2014.

IPCC: Summary for Policymakers, in: IPCC Special Report on the Ocean and Cryosphere in a Changing Climate, edited by: Pörtner, H.-O., Roberts, D. C., Masson-Delmotte, V., Zhai, P., Tig-

nor, M., Poloczanska, E., Mintenbeck, K., Alegría, A., Nicolai, M., Okem, A., Petzold, J., Rama, B., and Weyer, N. M., in press, 2019.

Ju, J. and Masek, J. G.: The vegetation greenness trend in Canada and US Alaska from 1984–2012 Landsat data, Remote Sens. Environ., 176, 1–16, https://doi.org/10.1016/j.rse.2016.01.001, https://doi.org/10.1016/j.rse.2016.01.001, 2016.

Kershaw, G. P. and McCulloch, J.: Midwinter Snowpack Variation Across the Arctic Treeline, Churchill, Manitoba, Canada, Arct. Antarct. Alp. Res., 39, 9–15, https://doi.org/10.1657/1523-0430(2007)39[9:MSVATA]2.0.CO;2, 2007.

Kharuk, V. I., Ranson, K. J., Im, S. T., and Petrov, I. A.: Climate-induced larch growth response within the central Siberian permafrost zone, Environ. Res. Lett., 10, 125009, https://doi.org/10.1088/1748-9326/10/12/125009, 2015.

Kharuk, V. I., Ranson, K. J., Petrov, I. A., Dvinskaya, M. L., Im, S. T., and Golyukov, A. S.: Larch (Larix dahurica Turcz) growth response to climate change in the Siberian permafrost zone, Reg. Environ. Change, 19, 233–243, https://doi.org/10.1007/s10113-018-1401-z, 2019.

Kobayashi, H., Delbart, N., Suzuki, R., and Kushida, K.: A satellite-based method for monitoring seasonality in the overstory leaf area index of Siberian larch forest, J. Geophys. Res.-Biogeo., 115, 1–14, https://doi.org/10.1029/2009JG000939, 2010.

Kruse, S., Wieczorek, M., Jeltsch, F., and Herzschuh, U.: Treeline dynamics in Siberia under changing climates as inferred from an individual-based model for Larix, Ecol. Model., 338, 101–121, https://doi.org/10.1016/j.ecolmodel.2016.08.003, 2016.

Langer, M., Westermann, S., Muster, S., Piel, K., and Boike, J.: The surface energy balance of a polygonal tundra site in northern Siberia Part 2: Winter, The Cryosphere, 5, 509–524, https://doi.org/10.5194/tc-5-509-2011, 2011a.

Langer, M., Westermann, S., Muster, S., Piel, K., and Boike, J.: The surface energy balance of a polygonal tundra site in northern Siberia Part 2: Winter, The Cryosphere, 5, 509–524, https://doi.org/10.5194/tc-5-509-2011, 2011b.

Langer, M., Westermann, S., Heikenfeld, M., Dorn, W., and Boike, J.: Satellite-based modeling of permafrost temperatures in a tundra lowland landscape, Remote Sens. Environ., 135, 12–24, https://doi.org/10.1016/j.rse.2013.03.011, 2013.

Langer, M., Westermann, S., Boike, J., Kirillin, G., Grosse, G., Peng, S., and Krinner, G.: Rapid degradation of permafrost underneath waterbodies in tundra landscapes – Toward a representation of thermokarst in land surface models, J. Geophys. Res.-Earth, 121, 2446–2470, https://doi.org/10.1002/2016JF003956, 2016.

Langer, M., Kaiser, S., Stuenzi, S. M., Schneider von Deimling, T., Oehme, A., and Jacobi, S.: Soilsurface temperatures in 2 cm depth between summer 2018 and 2019 with iButton-sensors in the North Slope of Alaska (USA), around Churchill (Canada) and the region of Illirney and Lena-Viluy (Russia), PANGAEA, https://doi.org/10.1594/PANGAEA.914327, 2020.

Loranty, M. M., Abbott, B. W., Blok, D., Douglas, T. A., Epstein, H. E., Forbes, B. C., Jones, B. M., Kholodov, A. L., Kropp, H., Malhotra, A., Mamet, S. D., Myers-Smith, I. H., Natali, S. M., O'Donnell, J. A., Phoenix, G. K., Rocha, A. V., Sonnentag, O., Tape, K. D., and Walker, D. A.: Reviews and syntheses: Changing ecosystem influences on soil thermal regimes in northern high-latitude permafrost regions, Biogeosciences, 15, 5287–5313, https://doi.org/10.5194/bg-15-5287-2018, 2018.

Maximov, T., Petrov, R., Iijima, Y., Hiyama, T., Ohta, T., Kotani, A., and Nakai, T.: Meteorological data at larch forest in eastern Siberia [Spasskaya Pad, 2016–2019], available at: https://ads.nipr.ac.jp/dataset/A20191107-009 (last access: 3 September 2020), 2019.

Nitzbon, J., Langer, M., Westermann, S., Martin, L., Aas, K. S., and Boike, J.: Pathways of ice-wedge degradation in polygonal tundra under different hydrological conditions, The Cryosphere, 13, 1089–1123, https://doi.org/10.5194/tc-13-1089-2019, 2019.

Nitzbon, J., Westermann, S., Langer, M., Martin, L. C. P., Strauss, J., Laboor, S., and Boike, J.: Fast response of cold ice-rich permafrost in northeast Siberia to a warming climate, Nat. Commun., 11, 2201, https://doi.org/10.1038/s41467-020-15725-8, 2020.

Ochsner, T. E., Sauer, T. J., and Horton, R.: Field tests of the soil heat flux plate method and some alternatives, Agron. J., 98, 1005–1014, https://doi.org/10.2134/agronj2005.0249, 2006.

Ohta, T., Hiyama, T., Tanaka, H., Kuwada, T., Maximov, T. C., Ohata, T., and Fukushima, Y.: Seasonal variation in the energy and water exchanges above and below a larch forest in eastern Siberia, Hydrol. Process., 15, 1459–1476, https://doi.org/10.1002/hyp.219, 2001.

Oleson, K. W., Lead, D. M. L., Bonan, G. B., Drewniak, B., Huang, M., Koven, C. D., Levis, S., Li, F., Riley, W. J., Subin, Z. M., Swenson, S. C., Thornton, P. E., Bozbiyik, A., Fisher, R., Heald, C. L., Kluzek, E., Lamarque, J.-F., Lawrence, P. J., Leung, L. R., Lipscomb, W., Muszala, S., Ricciuto, D. M., Sacks, W., Sun, Y., Tang, J., and Yang, Z.-L.: Technical description of version 4.5 of the Community Land Model (CLM) (No. NCAR/TN-503+STR), https://doi.org/10.5065/D6RR1W7M, 2013.

Oliver, S. A., Oliver, H. R., Wallace, J. S., and Roberts, A. M.: Soil heat flux and temperature variation with vegetation, soil type and climate, Agr. Forest Meteorol., 39, 257–269, https://doi.org/10.1016/0168-1923(87)90042-6, 1987.

Pearson, R. G., Phillips, S. J., Loranty, M. M., Beck, P. S., Damoulas, T., Knight, S. J., and Goetz, S. J.: Shifts in Arctic vegetation and associated feedbacks under climate change, Nat. Clim. Change, 3, 673–677, https://doi.org/10.1038/nclimate1858, 2013.

Price, A. G.: Prediction of Snowmelt Rates in a Deciduous Forest, J. Hydrol., 101, 145–157, 1988.

Rogers, B. M., Soja, A. J., Goulden, M. L., and Randerson, J. T.: Influence of tree species on continental differences in boreal fires and climate feedbacks, Nat. Geosci., 8, 228–234, https://doi.org/10.1038/ngeo2352, 2015.

Romanovsky, V., Smith, S., Shiklomanov, N., Streletskiy, D., Isaksen, K., Kholodov, A., Christiansen, H., Drozdov, D., Malkova, G., and Marchenko, S.: Terrestrial Permafrost in State of the Climate in 2016, B. Am. Meteorol. Soc., 98, 147–149, https://doi.org/10.1175/2017BAMSStateoftheClimate.1, 2017.

Ryder, J., Polcher, J., Peylin, P., Ottlé, C., Chen, Y., van Gorsel, E., Haverd, V., McGrath, M. J., Naudts, K., Otto, J., Valade, A., and Luyssaert, S.: A multi-layer land surface energy budget model for implicit coupling with global atmospheric simulations, Geosci. Model Dev., 9, 223–245, https://doi.org/10.5194/gmd-9-223-2016, 2016.

Sato, H., Kobayashi, H., Iwahana, G., and Ohta, T.: Endurance of larch forest ecosystems in eastern Siberia under warming trends, Ecol. Evol., 6, 5690–5704, https://doi.org/10.1002/ece3.2285, 2016.

Scheffer, M., Hirota, M., Holmgren, M., Van Nes, E. H., and Chapin, F. S.: Thresholds for boreal biome transitions, P. Natl. Acad. Sci, USA, 109, 21384–21389, https://doi.org/10.1073/pnas.1219844110, 2012.

Schneider von Deimling, T., Meinshausen, M., Levermann, A., Huber, V., Frieler, K., Lawrence, D. M., and Brovkin, V.: Estimating the near-surface permafrost-carbon feedback on global warming, Biogeosciences, 9, 649–665, https://doi.org/10.5194/bg-9-649-2012, 2012.

Sidorova, O. V., Vaganov, E. A., Naurzbaev, M. M., Shishov, V. V., and Hughes, M. K.: Regional features of the radial growth of larch in north central Siberia according to millennial tree-ring chronologies, Russ. J. Ecol.+, 38, 90–93, https://doi.org/10.1134/S106741360702004X, 2007.

Simmons, A., Uppala, S., Dee, D., and Kobayashi, S.: ERA-Interim: New ECMWF reanalysis 20 products from 1989 onwards, Tech. rep., ECMWF Newsletter, 110, https://doi.org/10.21957/pocnex23c6, 2007.

Stuenzi, S. M. and Schaepman Strub, G.: Vegetation Trajectories and Shortwave Radiative Forcing following Boreal Forest Disturbance in Eastern Siberia, J. Geophys. Res.-Biogeo., 125, e2019JG005395, https://doi.org/10.1029/2019jg005395, 2020.

Stuenzi, S. M., Boike, J., Cable, W., Herzschuh, U., Kruse, S., Pestryakova, L. A., Schneider von Deimling, T., Westermann, S., Zakharov, E. S., and Langer, M.: Coupled multilayer canopy-permafrost model (CryoGrid) for the use in permafrost underlain boreal forests, Zenodo, https://doi.org/10.5281/zenodo.4317107, 2020a.

Stuenzi, S. M., Cable, W. L., Kruse, S., Boike, J., Herzschuh, U., Langer, M., Schulte, L., Brieger, F., Vyse, S. A., Bernhard, N., Dietze, E., Pestryakova, L. A., Zakharov, E. S., Nikolajewitsch, A., Ushnizkaya, L., and Levina, S.: Automatic weather stations and stand-alone soil temperature sensors (Hobo logger) between August 2018 and August 2019 at two boreal forest sites in the region of Lake Ilirney and Lena-Viluy in Eastern Siberia, PANGAEA, https://doi.org/10.1594/PANGAEA.919859, 2020b.

Sugimoto, A., Yanagisawa, N., Naito, D., Fujita, N., and Maximov, T. C.: Importance of permafrost as a source of water for plants in east Siberian taiga, Ecol. Res., 17, 493–503, https://doi.org/10.1046/j.1440-1703.2002.00506.x, 2002.

Tchebakova, N. M., Parfenova, E., and Soja, A. J.: The effects of climate, permafrost and fire on vegetation change in Siberia in a changing climate, Environ. Res. Lett., 4, 045013, https://doi.org/10.1088/1748-9326/4/4/045013, 2009.

Vionnet, V., Brun, E., Morin, S., Boone, A., Faroux, S., Le Moigne, P., Martin, E., and Willemet, J.-M.: The detailed snowpack scheme Crocus and its implementation in SURFEX v7.2, Geosci. Model Dev., 5, 773–791, https://doi.org/10.5194/gmd-5-773-2012, 2012.

Vitt, D. H., Halsey, L. A., Bauer, I. E., and Campbell, C.: Spatial and temporal trends in carbon storage of peatlands of continental western Canada through the Holocene, Can. J. Earth Sci., 37, 683–693, https://doi.org/10.1139/e99-097, 2000.

Westermann, S., Schuler, T. V., Gisnås, K., and Etzelmüller, B.: Transient thermal modeling of permafrost conditions in Southern Norway, The Cryosphere, 7, 719–739, https://doi.org/10.5194/tc-7-719-2013, 2013.

Westermann, S., Langer, M., Boike, J., Heikenfeld, M., Peter, M., Etzelmüller, B., and Krinner, G.: Simulating the thermal regime and thaw processes of ice-rich permafrost ground with the land-surface model CryoGrid 3, Geosci. Model Dev., 9, 523–546, https://doi.org/10.5194/gmd-9-523-2016, 2016.

Younes, S. and Muneer, T.: Comparison between solar radiation models based on cloud information, Int. J. Sust. Ener., 26, 121–147, https://doi.org/10.1080/14786450701549824, 2007.

Zhang, N., Yasunari, T., and Ohta, T.: Dynamics of the larch taiga-permafrost coupled system in Siberia under climate change, Environ. Res. Lett., 6, 024003, https://doi.org/10.1088/1748-9326/6/2/024003, 2011.

Zhang, Y., Chen, W., and Cihlar, J.: A process-based model for quantifying the impact of climate change on permafrost thermal regimes, J. Geophys. Res.-Atmos., 108, 4695, https://doi.org/10.1029/2002JD003354, 2003.

Zhang, Y., Sherstiukov, A. B., Qian, B., Kokelj, S. V., and Lantz, T. C.: Impacts of snow on soil temperature observed across the circumpolar north, Environ. Res. Lett., 13, 044012, https://doi.org/10.1088/1748-9326/aab1e7, 2018.

Zweigel, R., Westermann, S., Nitzbon, J., Langer, M., Boike, J., Etzelmüller, B., and Schuler, T. V.: Simulating snow redistribution and its effect on the ground thermal regime at a high-Arctic site on Svalbard, J. Geophys. Res.-Earth, in press, 2020.

# Chapter 6

# Sensitivity of Ecosystem-Protected Permafrost Under Changing Boreal Forest Structures

**Stuenzi, S.M., Boike, J., Gädecke, A. , Herzschuh, U., Kruse, S., Pestryakova, L. A., Westermann, S., and Langer, M.**

*Environmental Research Letters* (2021), 16, 084045, DOI: 10.1088/1748-9326/ac153d.

IOP Publishing Environ. Res. Lett. 16 (2021) 084045 https://doi.org/10.1088/1748-9326/ac153d

ENVIRONMENTAL RESEARCH
LETTERS

LETTER

# Sensitivity of ecosystem-protected permafrost under changing boreal forest structures

Simone M Stuenzi[1,2,*], Julia Boike[1,2], Anne Gädeke[6], Ulrike Herzschuh[1,3,8], Stefan Kruse[1], Luidmila A Pestryakova[7], Sebastian Westermann[4,5] and Moritz Langer[1,2]

[1] Alfred Wegener Institute, Helmholtz Centre for Polar and Marine Research, Telegrafenberg A45, 14473 Potsdam, Germany
[2] Geography Department, Humboldt-Universität zu Berlin, Unter den Linden 6, Berlin 10099, Germany
[3] Institute of Environmental Science and Geography, University of Potsdam, 14476 Potsdam, Germany
[4] Department of Geosciences, University of Oslo, Sem Sælands vei 1, 0316 Oslo, Norway
[5] Centre for Biogeochemistry in the Anthropocene, University of Oslo, Sem Sålands vei 1, 0316 Oslo, Norway
[6] Potsdam Institute for Climate Impact Research, Member of the Leibniz Association, Telegrafenberg, Potsdam 14412, Germany
[7] Institute of Natural Sciences, North-Eastern Federal University in Yakutsk, Belinskogo str. 58, 677000 Yakutsk, Russia
[8] Institute of Biochemistry and Biology, University of Potsdam, 14476 Potsdam, Germany
[*] Author to whom any correspondence should be addressed.

**E-mail:** simone.stuenzi@awi.de

**Keywords:** global warming impact, boreal forest, permafrost

OPEN ACCESS

RECEIVED
31 March 2021

REVISED
9 June 2021

ACCEPTED FOR PUBLICATION
16 July 2021

PUBLISHED
2 August 2021



## Abstract

Boreal forests efficiently insulate underlying permafrost. The magnitude of this insulation effect is dependent on forest density and composition. A change therein modifies the energy and water fluxes within and below the canopy. The direct influence of climatic change on forests and the indirect effect through a change in permafrost dynamics lead to extensive ecosystem shifts such as a change in composition or density, which will, in turn, affect permafrost persistence. We derive future scenarios of forest density and plant functional type composition by analyzing future projections provided by the dynamic global vegetation model (LPJ-GUESS) under global warming scenarios. We apply a detailed permafrost-multilayer canopy model to study the spatial impact-variability of simulated future scenarios of forest densities and compositions for study sites throughout eastern Siberia. Our results show that a change in forest density has a clear effect on the ground surface temperatures (GST) and the maximum active layer thickness (ALT) at all sites, but the direction depends on local climate conditions. At two sites, higher forest density leads to a significant decrease in GSTs in the snow-free period, while leading to an increase at the warmest site. Complete forest loss leads to a deepening of the ALT up to 0.33 m and higher GSTs of over 8 °C independently of local climatic conditions. Forest loss can induce both, active layer wetting up to four times or drying by 50%, depending on precipitation and soil type. Deciduous-dominated canopies reveal lower GSTs compared to evergreen stands, which will play an important factor in the spreading of evergreen taxa and permafrost persistence under warming conditions. Our study highlights that changing density and composition will significantly modify the thermal and hydrological state of the underlying permafrost. The induced soil changes will likely affect key forest functions such as the carbon pools and related feedback mechanisms such as swamping, droughts, fires, or forest loss.

## 1. Introduction

The boreal forest cover exerts a strong control on numerous climate feedback mechanisms (Bonan *et al* 2018, Zhang *et al* 2018). Globally, 80% of boreal forests are underlain by permafrost (Helbig *et al* 2016). The forest cover is considered to efficiently insulate the underlying, ecosystem-protected permafrost (Chang *et al* 2015) and therefore play an important role in the development of boreal regions and the stability of permafrost in a warming climate. Boreal regions are projected to warm between 4 °C and 11 °C by 2100, with a modest precipitation increase (Scheffer *et al* 2012, Meredith *et al* 2019). The change

in air temperature and precipitation directly influences the vegetation cover development (Esper *et al* 2010, Kharuk *et al* 2015, Sato *et al* 2016, Ito *et al* 2020) and permafrost thaw (Meredith *et al* 2019), directly affecting soil water availability and root space limitation (Carpino *et al* 2018). The changing thermo-hydrological soil conditions may provoke changes in forest density and forest composition (Takahashi 2006, Kharuk *et al* 2013, Liu *et al* 2017, Kropp *et al* 2021) leading to extensive ecosystem shifts (Pearson *et al* 2013, Gauthier *et al* 2015, Boike *et al* 2016, Kruse *et al* 2016).

Forest composition and density exert a strong control on permafrost stability (Yi *et al* 2007, Chasmer *et al* 2011, Fisher *et al* 2016) and a direct feedback mechanism is expected to control the temporal ecosystem evolution (Bonan *et al* 1992, Carpino *et al* 2018, Loranty *et al* 2018). This feedback mechanism (figure A1) is, however, poorly understood and broad-scale vulnerability studies do not yet exist. The canopy exerts shading by reflecting and absorbing most downward solar radiation and by suppressing the majority of turbulent heat fluxes in the below-canopy space (Chang *et al* 2015). Further, the canopy controls the surface albedo, which is much lower than in grasslands especially during snow-covered periods (Bonan and Shugart 1989). The canopy decreases soil moisture and leads to a reduced thermal conductivity through precipitation interception (Thomas and Rowntree 1992) and higher evapotranspiration (Vitt *et al* 2000). Additionally, the canopy slows snow melting in spring and reduces snow compaction because of the suppressed turbulent fluxes, which therefore leads to higher snowpacks under denser canopies (Stuenzi *et al* 2021). Finally, the vegetation cover promotes the accumulation of an organic surface layer (Bonan and Shugart 1989, Yi *et al* 2007) which further insulates the topsoil from the atmosphere. A change in the forest density modifies the within- and below-canopy energy and water fluxes (Chasmer *et al* 2011, Stuenzi *et al* 2021). The forest composition also has an impact on the ground surface energy and water balance. Most boreal forests are dominated by evergreen needleleaf taxa, but wide areas of the north-eastern Eurasian continent are dominated by deciduous needleleaf taxa. The needle-shedding of deciduous taxa impacts the within and below canopy fluxes (Tanaka *et al* 2008, Zhang *et al* 2011, Peng *et al* 2020, Stuenzi *et al* 2021), the litter and organic surface layers (Bonan and Shugart 1989) and the fire regime (Rogers *et al* 2015). Since evergreen and deciduous taxa can establish under similar climate conditions (Esper and Schweingruber 2004, Kharuk *et al* 2009) the successful spread of evergreen taxa into currently larch dominated areas and vice-versa, mainly depends on the frequency of disturbance events, which have increased over the past decades (Shuman *et al* 2011, Mekonnen *et al* 2019, Meredith *et al* 2019).

Detailed modeling studies are needed to incorporate the local, heterogeneous, and complex feedback mechanisms, caused by the vegetation type and its relationship with topsoil temperature, active layer thickness (ALT), and available plant water (Tchebakova *et al* 2009, Schuur and Mack 2018, Kropp *et al* 2021, Stuenzi *et al* 2021). It has been shown that the integration of ecosystem components such as permafrost is highly relevant for projections on biomass and vegetation cover (Ito *et al* 2020). Here, we fill this gap between vegetation cover model projections and the actual physical impact this vegetation cover change has on permafrost ground, and present a detailed coupled permafrost-multilayer canopy model, developed for use in permafrost-underlain boreal forest systems.

We analyze (a) the trends of the two ecosystem changes, boreal forest densification and plant functional type composition, based on biome LPJ-GUESS model projections for north-eastern Siberia. Based on the projected trends in ecosystem changes, we use CryoGrid to simulate the projected ranges of (b) forest densities and (c) plant functional type compositions for three different study sites throughout north-eastern Siberia to investigate the impact of canopy variability on the ground thermal and hydrological regime. We thereby study the effect of the projected trends over an extensive range of predominantly deciduous-dominated boreal forests, as well as over different climate characteristics within the polar climate regime. This study delivers important insights into the range of spatial differences and possible temporal changes to the permafrost condition that can be expected following landscape changes such as deforestation through fires or other anthropogenic influences, afforestation in currently unforested grasslands, or the climate-induced densification of forested areas.

## 2. Methods

### 2.1. Study region

The treeline of north-eastern Siberia is dominated by the deciduous needleleaf tree genus *Larix* Mill. (figure 1), even though in mixed forest stands, larch taxa are out-competed by evergreen taxa, which is thought to represent the late-successional stage (Kharuk *et al* 2007). Once established, larch forests are likely to stabilize through a complex vegetation-permafrost-climate feedback system. Mainly shallow active layer depths hinder the establishment of evergreen taxa (Herzschuh 2019) and in more southern regions of eastern Siberia, larch is mixed with evergreen conifers (pine, spruce, fir) and hardwoods (Kharuk *et al* 2019). The ground vegetation is generally dominated by mosses and lichens that form carpets. Larch has shallow roots and preferably grows on clay permafrost soils with a shallow ALT and

IOP Publishing Environ. Res. Lett. 16 (2021) 084045 S M Stuenzi et al

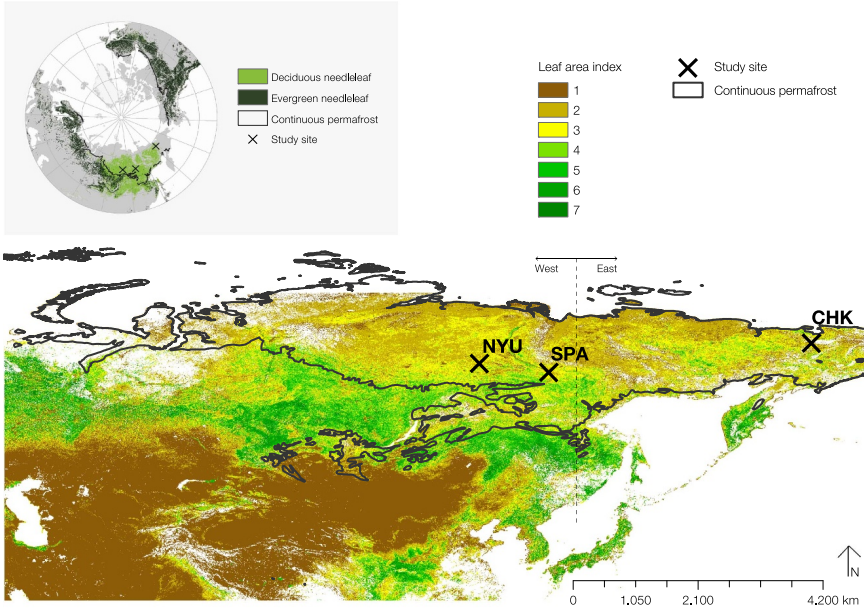


**Figure 1.** Main map: leaf area index ($m^2 m^{-2}$) from satellite imagery and permafrost extent in north-eastern Siberia. The three study sites are marked with black crosses (Nyurba (NYU), Spasskaya Pad (SPA), and Chukotka (CHK)). Additionally, the dotted line indicates the two individual study regions, West (E 105.25°–137.25°) and East (E 137.75°–169.75°) as used in the biome projection data analysis. Top left corner: spatial distribution of current deciduous and evergreen boreal forest dominance and the study sites. Data: ESA CCI Land Cover classes. ESA. Land Cover CCI Product User Guide Version 2. Tech. Rep. (2017) (after (Herzschuh 2019)), permafrost extent from Land Resources of Russia—Maps of permafrost and Ground Ice (after Kotlyakov and Khromova (2002)), and Copernicus Global Land Service, Leaf Area Index (LAI), (after Copernicus Global Land Operations (2021)). Adapted from Stuenzi *et al* (2021). CC BY 4.0.

maximum wetness of 20%–40%. Evergreen conifers and hardwood both prefer deeper active layers and a higher soil moisture availability (Ohta *et al* 2001, Rogers *et al* 2015). To capture these spatial differences across boreal forests, we study the current forest composition and structure along a east-west transect represented by three different sites as specified in table 1, figure 1, and appendix B with figure B1.

### 2.2. Projected forest evolution

We use ESA CCI Land Cover satellite data to parameterize forest composition and Copernicus Global Land Service leaf area index (LAI) data to parameterize forest density under current climate conditions (figure 1). To understand the current plant functional type distribution and the projected changes we study projections of LAI and plant functional types simulated by the LPJ-GUESS model as part of ISIMIP2b (Frieler *et al* 2017). We analyze the forest change scenarios from 2006 until 2099 under three global warming scenarios (RCP 2.6, RCP 6.0, RCP 8.5). The LPJ-GUESS dynamic vegetation model combines an individual- and patch-based representation of forest dynamics with biogeochemical cycling from regional to global scales and is further described in Smith *et al* (2014). The model is forced with bias-adjusted climate data from the Hadgem2-es earth system model. The EWEMBI dataset (Lange 2019) served as the basis for the trend-preserving bias adjustment of the GCMs at a daily time step (as detailed in Frieler *et al* (2017)). The data selected cover a region from E 105°–167° and N 45°–70° at a spatial resolution of 0.5° × 0.5°. We have separated this area into two individual study regions: West (E 105.25°–137.25°) and East (E 137.75°–169.75°) (figure 1), because of the differences in temperature and current vegetation cover between these two regions. We analyze projected LAI for needleleaf evergreen and needleleaf deciduous plant functional types under the three warming scenarios at the transect sites. Note that these LAI values are averaged annual values over the entire study sites, and do not represent the full summer LAI in deciduous forests. Therefore, we also study the projected monthly LAI (only available for the combination of all PFTs) for August, which corresponds to the maximum LAI of deciduous taxa plus the LAI of all other PFTs, including needleleaf evergreen and hardwoods, under the available warming scenarios (RCP 6.0, RCP 8.5) for the period 2006–2099 (figure B2).

IOP Publishing Environ. Res. Lett. 16 (2021) 084045 S M Stuenzi et al

**Table 1.** Description of different study sites. Adapted from Stuenzi *et al* (2021). CC BY 4.0.

| Study site | Nyurba (NYU) | Spasskaya Pad (SPA) | Chukotka (CHK) |
|---|---|---|---|
| Lat | N 63.08° | N 62.14° | N 67.40° |
| Lon | E 117.99° | E 129.37° | E 168.37° |
| Elevation (m asl) | 117 | 237 | 603 |
| Mean annual air temperature (°C) | −3.69 | −5.97 | −11.69 |
| Mean snow-covered air temperature (°C) | −9.6 | −12.7 | −17.7 |
| Mean snow-free air temperature (°C) | 13.6 | 13.7 | 6.0 |
| Solid precipitation (mm) | 101 | 84 | 116 |
| Liquid precipitation (mm) | 180 | 170 | 292 |
| Dominant plant functional type | Evergreen | Deciduous | Deciduous |
| Tree height (m) | 8 | 12 | 11 |
| Leaf area index ($m^2m^{-2}$) | 3 | 3 | 1 |
| Study regions | West | West | East |

### 2.3. Coupled permafrost-vegetation model

The model setup is based on the permafrost model CryoGrid (originally described in Westermann *et al* (2016)), a one-dimensional, numerical land surface model that simulates the thermo-hydrological regime of permafrost ground by numerically solving the heat-conduction equation (Nitzbon *et al* 2019). The CryoGrid model was extended by a multilayer canopy module developed by Bonan *et al* (2014) for the use in permafrost regions (appendix C and Stuenzi *et al* (2021) for model details). Here, we add a parameterization for deciduous forest to simulate the leafless state of deciduous-dominated regions outside of the short vegetative period in summer. This is achieved by allowing for separate leaf area index controlled by static time windows defining leaf-on and leaf-off season (10 October–10 April) following literature values for east Siberia (Spasskaya Pad) (Ohta *et al* 2001). Further, a more realistic canopy structure is simulated by allowing fractional composition of deciduous and evergreen taxa within the simulated forest stand. In addition, we test a parameterization for coupling forest density (LAI) to fine root biomass ($R_{\text{total}}$, ($gm^{-2}$)) (appendix D). Further, we have implemented a new relationship for phase partitioning of water in frozen soil (freeze curve) based on Painter and Karra (2014) (appendix C).

### 2.4. Model simulations and setup

We ran model simulations for a wide range of forest types and forest compositions at the three transect sites. Parameters defining the canopy, snow, and soil properties were set according to literature values, model documentation, and own measurements (appendix for details). Tables E2 and E4 summarize the ground and vegetation parameter choices for all three sites. Table E3 summarizes constants used. We perform model simulations over a time period of five years from August 2014 to August 2019. This equals a spin-up period of four years before comparing modeled and measured data. The meteorological forcing data (air temperature, air pressure, wind speed, relative humidity, solid and liquid precipitation, incoming long- and shortwave radiation, and cloud cover) are obtained from ERA-Interim (ECMWF Reanalysis) extracted for the three sites (N 63.08°, E 117.99°, N 62.14°, E 129.37°, and N 67.40°, E 168.37°) (Simmons *et al* 2007). We use ground surface temperature (GST, top 0.4 m of the soil column) as the major target variable for model validation (appendix D). We further analyze maximum yearly ALT and the available water for plants within this active layer (PAW).

For each study site, we conduct 70 simulations representing different forest types and forest compositions (figure 2). The range of different forest types considered are bench-marked based on the projected ISIMIP2b data described by canopy density (leaf area index, LAI ($m^2m^{-2}$)) between 0 and 7 $m^2m^{-2}$ and fractions between deciduous needleleaf and evergreen needleleaf taxa (0%–90% deciduous) (figure 2). To test the statistical significance of the differences between the simulated mean GSTs for varying forest densities and compositions, we apply variance analysis (one-way ANOVA) with a significance level of 0.001. Data are controlled for normal distribution and homogeneous variance across all groups. Statistical analyzes were performed using R software (R Core Team 2016).

## 3. Results

### 3.1. Forest evolution under climatic warming

The biome projection data from LPJ-GUESS model simulations data reveal that in the eastern sub-domain of our study region an increase in evergreen taxa are projected for all warming scenarios (RCP 2.6, RCP 6.0, RCP 8.5), with a peak in the yearly mean value of 0.5 $m^2m^{-2}$ and a maximum value of 2 $m^2m^{-2}$, and 1.8 $m^2m^{-2}$ around 2075 respectively, for the RCP 6.0 and RCP 8.5 scenarios, followed by a decrease towards the end of the century (figure 3). In the western sub-domain, the three global warming scenarios project an increase in deciduous taxa. The overall LAI for August under the RCP 8.5 warming scenario increases by 2 $m^2m^{-2}$ in the western region

IOP Publishing Environ. Res. Lett. 16 (2021) 084045 S M Stuenzi et al

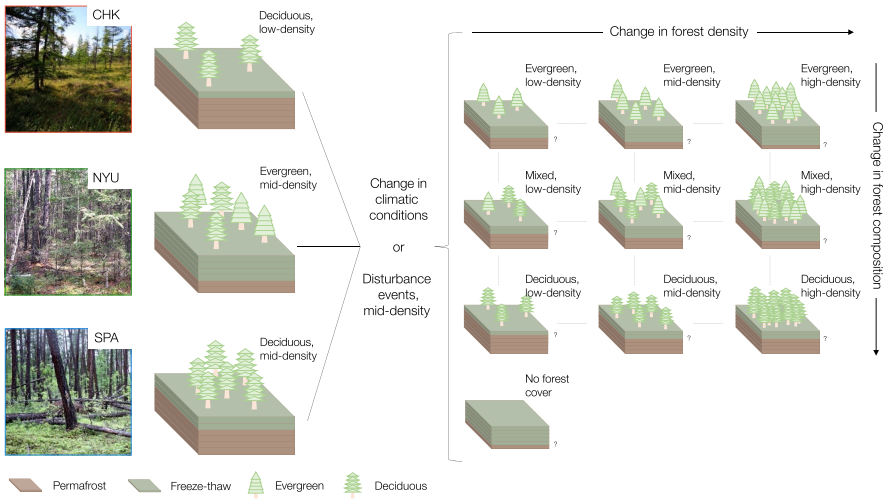


**Figure 2.** Schematic of the simulated vegetation trajectories and the possible impact on the thermal development of the permafrost. Left: photographs from the three study sites and the respective model set-ups for Nyurba (NYU), mixed forest with a LAI of 3 $m^2m^{-2}$ (mid-density), for Spasskaya (SPA), deciduous-dominated forest with a LAI of 3 $m^2m^{-2}$ (mid-density), and for Chukotka (CHK), deciduous-dominated with a LAI of 1 $m^2m^{-2}$ (low-density). Right: schematic illustration of the range of possible forest cover scenarios (Forest density: low-density to high density, and forest composition: evergreen, mixed (10%–50% of deciduous taxa) or deciduous dominated (60%–90% of deciduous taxa), and no forest cover) caused by either, climatic changes and/or disturbance events such as i.e. an extreme drought, a fire event, logging, or pest infestation. Each forest cover scenario is simulated at each of the three sites, NYU, SPA and CHK.

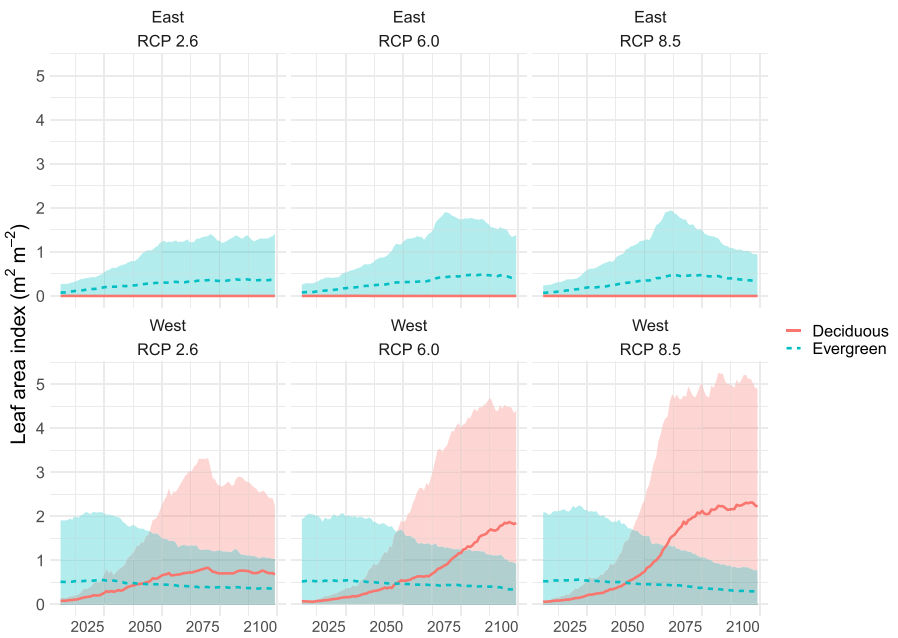


**Figure 3.** Projected LAI for needleleaf evergreen (blue) and needleleaf deciduous (red) plant functional types under the three warming scenarios, RCP 2.6, RCP 6.0, and RCP 8.5 for the time frame 2006–2099. Data covers the region from E 105° − 167° to N 45° − 70° and is separated into two individual study regions, West (E 105.25°–137.25°, bottom) and East (E 137.75°–169.75°, top). The lines indicate mean values while the shaded areas show the corresponding 90th and 10th percentile.

IOP Publishing Environ. Res. Lett. 16 (2021) 084045 S M Stuenzi et al

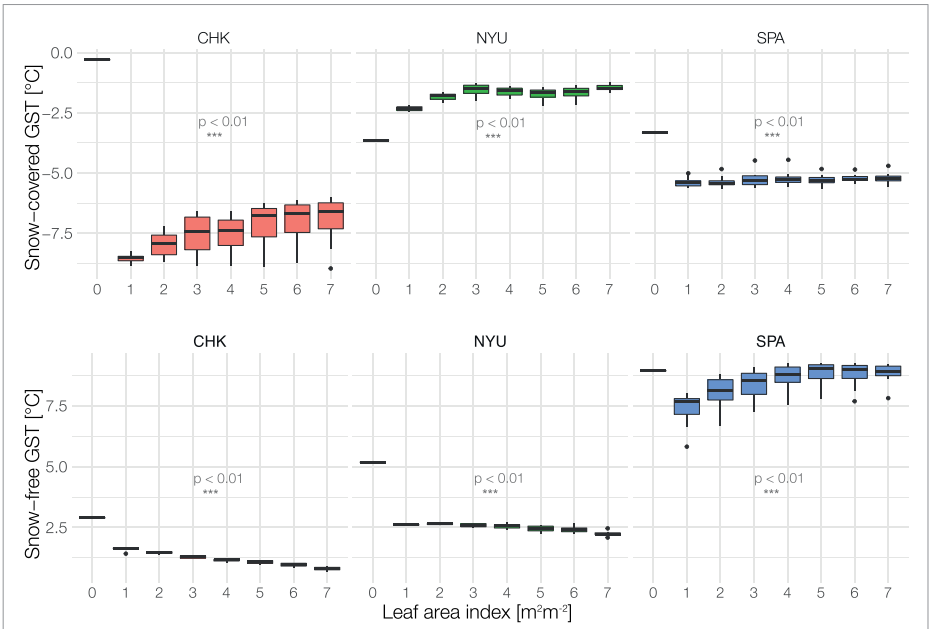


**Figure 4.** Averaged modeled snow-covered period GST, average modeled snow-free period GST and the respective spread for different forest canopy densities (LAI = 2 − 7 $m^2m^{-2}$) and no forest cover (LAI = 0 $m^2m^{-2}$) at the three study sites over 1 year (10 August 2018–10 August 2019). Statistical significance of each trend is based on ANOVA analysis (significance codes: *** = 0.001, ** = 0.01, * = 0.05). The bars indicate mean values while the whiskers show the corresponding standard deviations.

and doubles in the eastern region (appendix B). Currently, we find mean values around 3 $m^2m^{-2}$ for the western study region and 1 $m^2m^{-2}$ in the east. According to the annual data (figure 3), the mean LAI is currently dominated by evergreen taxa. In the western region, this dominance switches around 2050 under all three climate forcing scenarios. Under the strongest climatic warming scenario, deciduous LAI increases to a mean value of 2.4 $m^2m^{-2}$, a value three times higher than the end of the century deciduous taxa projection under RCP 2.6. The projection data reveals an increase in needleleaf evergreen taxa at both sites for the coming decade, followed by a decrease in the western region under all climate scenarios. In the eastern region, the increase continues until 2060, where-after the LAI of needleleaf evergreen taxa stays constant under RCP 2.6 and decreases under both the RCP 6.0 and 8.5 scenarios. In the western region, deciduous taxa will continue increasing until the end of the century under all climate forcing scenarios. Based on these data, which are in agreement with other model projections for Eurasia (Shuman *et al* 2014, Meredith *et al* 2019), we can constrain the expected changes in plant functional type compositions and forest densities for the entire eastern Siberian permafrost underlain boreal forest region east of 105° and north of 45°. The overall forest density is projected to increase with warming temperatures under all warming scenarios and for both study regions.

### 3.2. Permafrost sensitivity under changing forest density

The simulations clearly demonstrate that higher forest density leads to lower mean GST in the snow-free period. This trend is highly significant with $p < 0.01$ for Chukotka and Nyurba. The average snow-free GST is 1 °C colder for the simulations with the densest canopy covers. For Spasskaya Pad (SPA), this trend is reversed, showing an increasing GST for denser canopies ($p < 0.01$). In the snow-covered period mean GST increase with larger LAI values at Chukotka and Nyurba ($p < 0.01$) (figure 4). Temperature values for the simulations without forest are higher at all sites and for both time periods except for the snow-covered period at the Nyurba site, where the simulation without forest cover is 1.3 °C colder. The maximum difference between a sparse forest cover and no forest cover is a temperature increase of 8.3 °C in the snow-covered period at Chukotka.

Our model simulations show that the projected forest development alone exerts a strong control on the thermal state of the permafrost, in addition to the expected effect of a warmer and dryer climate itself. At two study sites, higher forest density leads to a significant decrease in ground surface temperatures in the

IOP Publishing Environ. Res. Lett. 16 (2021) 084045 S M Stuenzi et al

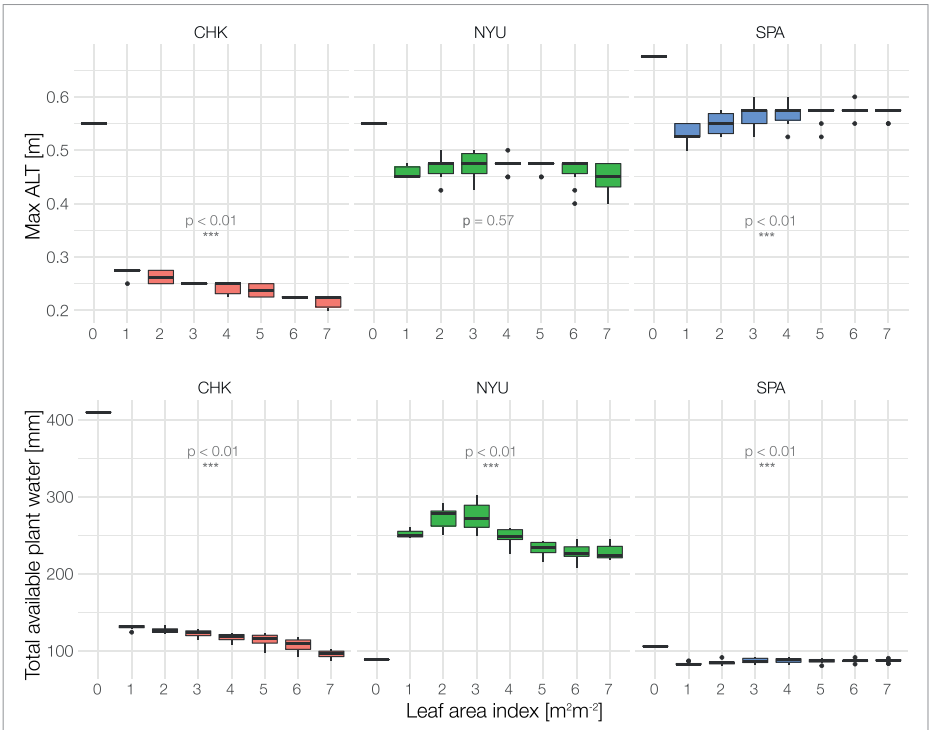


**Figure 5.** Top: Averaged modeled maximum ALT and the spread for different forest canopy densities (LAI $= 2-7\ m^2m^{-2}$) and no forest cover (LAI $= 0\ m^2m^{-2}$) at the three study sites over 1 year (10 August 2018–10 August 2019). Bottom: total modeled available plant water in the ALT and the spread for different densities (LAI $= 2-7\ m^2m^{-2}$) and no forest cover (LAI $= 0\ m^2m^{-2}$) at the three study sites over 1 year (10 August 2018–10 August 2019). Statistical significance of each trend is based on ANOVA analysis (significance codes: *** $= 0.001$, ** $= 0.01$, * $= 0.05$). The bars indicate mean values while the whiskers show the corresponding standard deviations.

snow-free period, while leading to an increase at the warmest site, SPA.

The magnitude of the insulation effect on the annual GST change from no forest cover to a dense forest cover is −6.3 °C at Chukotka, −0.2 °C at Nyurba, and −2.5 °C at Spasskaya.

The impact of forest density on GST consequently alters the annual ALT dynamics. We find a decline in maximum ALT with increasing canopy density for two sites in our study region. Highest maximum ALT of 0.68 m is found at the Spasskaya site with a LAI of $0\ m^2m^{-2}$. The lowest maximum ALT is simulated at the Chukotka site with a value of 0.2 m only for LAI $7\ m^2m^{-2}$ (figure 5). We find a significant trend ($p < 0.01$) of a decrease in ALT with an increasing canopy density in Chukotka but an insignificant trend in Nyurba. At the SPA site, our model predicts an increasing maximum ALT with an increasing canopy density from LAI $1-4\ m^2m^{-2}$. The maximum ALT for the simulations without a forest cover is higher at all sites. The difference between LAI $1\ m^2m^{-2}$ and no forest cover is up to 0.33 m in Chukotka. The decrease in snow-free period insulation with higher forest density is strongest at the coldest site of Chukotka. Here, the average maximum ALT of all simulations at highest forest density ($7\ m^2m^{-2}$) is 0.22 m, while average ALT is 0.27 m for a low LAI ($1\ m^2m^{-2}$). The maximum ALT under a dense forest canopy is thus found 0.05 m (−19%) lower than under a sparse canopy. At Nyurba we find an average maximum ALT value of 0.45 m for a sparse canopy as well as for a dense canopy. At SPA low-density forest results in a maximum ALT of 0.54 m, which is considerably lower than the mean value of 0.57 m (−5%) for high-density forest.

In order to analyze the impact of forest density on soil hydrology, we investigate the total yearly available plant water within the active layer. We find a clear and significant trend at Chukotka and Nyurba, with a decrease in available plant water for higher forest densities. The Chukotka site reveals the available plant water to be three times higher for the simulation without forest cover. The soil moisture in the active layer steadily decreases with increasing forest density at Chukotka and Nyurba, whereas it remains constantly low for SPA. SPA is the driest site, both in terms of liquid and solid precipitation, which leads to a very low amount of available plant water together

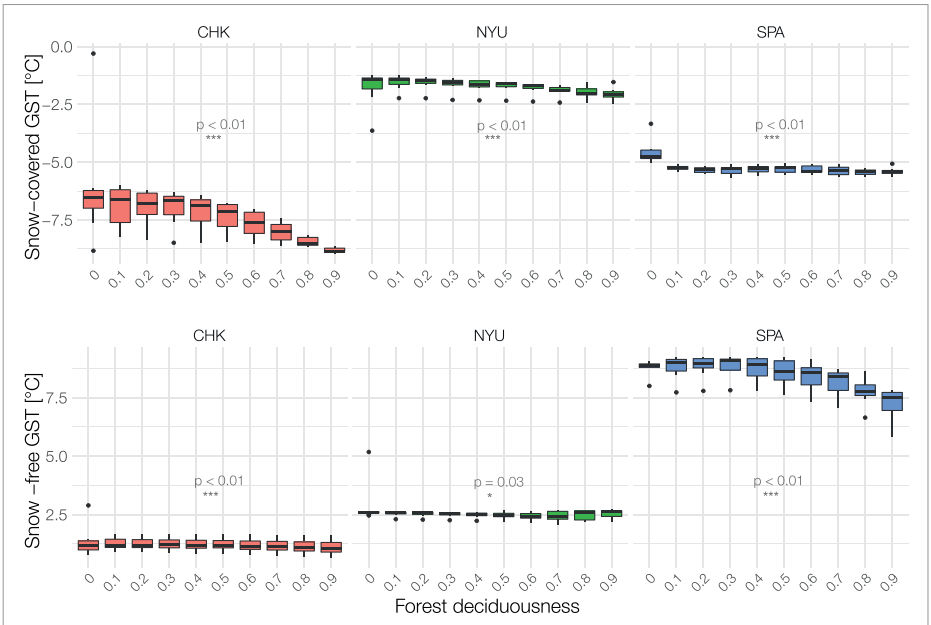


**Figure 6.** Averaged modeled snow-covered period GST, average modeled snow-free period GST and the respective spread for different percentages of deciduous taxa (90%–0%) at the three study sites over 1 year (10 August 2018–10 August 2019). Statistical significance of each trend is based on ANOVA analysis (significance codes: *** = 0.001, ** = 0.01, * = 0.05). The bars indicate mean values while the whiskers show the corresponding standard deviations.

with a relatively shallow snow cover (< 0.2 m) during winter.

The available plant water found is up to four times higher for the non-forested simulation at the Chukotka site and up to two times higher at the Spasskaya site. This indicates that forest loss may trigger the development of wetter and potentially swampy soil conditions depending on precipitation, evaporation, and ALT. In contrast, forest cover loss leads to a reduction in available plant water (up to 50%) at Nyurba which is characterized by climate conditions similar to Spasskaya. These contrasting hydrological impacts were observed in the vicinity of the respective study sites of Spasskaya and Nyurba. The performed simulations, thus, reveal that boreal forest loss can amplify both the wetting and drying of sub-Arctic regions.

### 3.3. Permafrost sensitivity under changing forest composition

Across the three study sites, we find a significant trend ($p < 0.01$) in lower GST's with an increasing percentage of deciduous taxa in the snow-covered period (figure 6). A lower percentage of deciduous taxa leads to a significant increase in the mean wintertime GST at Chukotka and Nyurba. The forest enhanced insulation effect of evergreen canopies, compared to deciduous cover, reaches up to +2.7 °C during the snow-covered period at Chukotka. A cooling trend of lower percentages of deciduous taxa in the summer period is found at SPA and Chukotka ($p < 0.01$).

The magnitude of the insulation on the annual GST change from evergreen to deciduous forest cover is −2.3 °C at Chukotka, −0.3 °C at Nyurba, and −1.2 °C at Spasskaya.

Changes in deciduousness also affect maximum ALT and the available plant water (figure 7). At SPA, Chukotka and Nyurba we find statistically significant trends ($p < 0.01$) towards higher maximum ALTs with decreasing deciduous taxa. The difference in ALT between 90% and 0% deciduous taxa are +0.04 m (+15%) at Chukotka, +0.05 m (+11%) at Nyurba and +0.07 m (+11%) at SPA. We find statistically significant trends ($p < 0.01$) towards higher available plant water with decreasing deciduous taxa at Chukotka and Spasskaya.

## 4. Discussion

About 55% of the total global permafrost area is covered by boreal forest (Gruber 2012, Helbig *et al* 2016). The forest cover plays an important role in insulating and stabilizing the permafrost underneath. The magnitude of this is highly dependent on the forest density as well as on the forest composition and structure but this relationship has not yet been studied in depth (McGuire *et al* 2002, Fisher *et al* 2016, Stuenzi *et al* 2021). Our results provide a detailed examination of the exact impact of boreal forest on

IOP Publishing Environ. Res. Lett. 16 (2021) 084045 S M Stuenzi et al

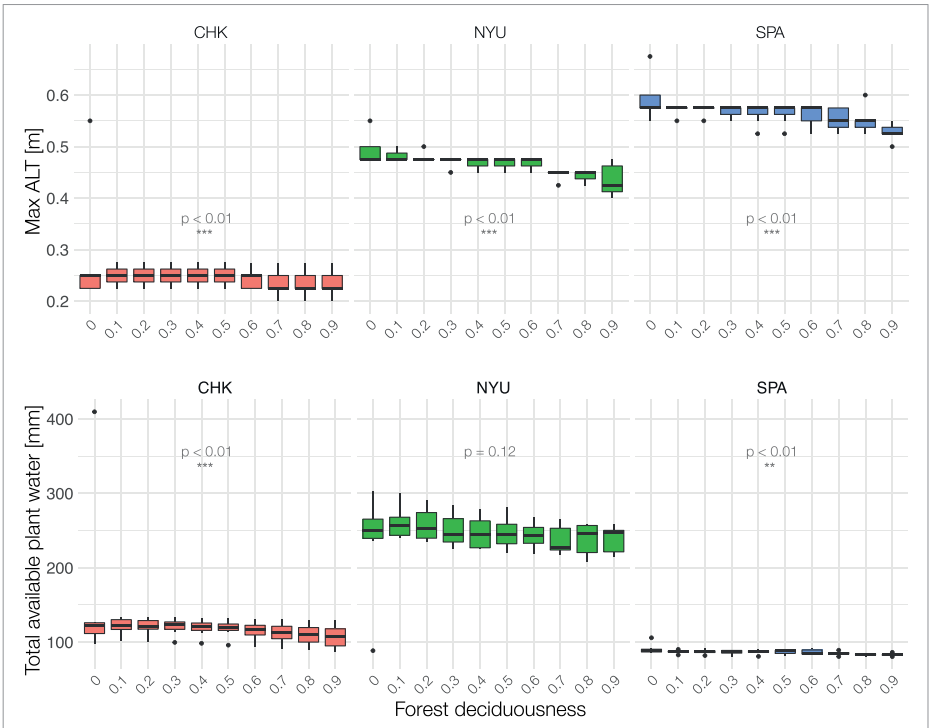


**Figure 7.** Top: Averaged modeled maximum ALT and the spread for different percentages of deciduous taxa (100%–0%) at the three study sites over 1 year (10 August 2018–10 August 2019). Bottom: Total modeled available plant water in the ALT and the spread for different percentages of deciduous taxa (90%–0%) at the three study sites over 1 year (10 August 2018–10 August 2019). Statistical significance of each trend is based on ANOVA analysis (significance codes: *** = 0.001, ** = 0.01, * = 0.05). The bars indicate mean values while the whiskers show the corresponding standard deviations.

permafrost by covering a wide variety of forest densities and plant functional type compositions.

We find forest density to significantly control the ground thermohydrological conditions at all sites, whereby trends strongly differ in magnitude and direction. The cooling trends of denser canopies at the wetter sites, and the warming trend at the driest site, are reflected in the ALT dynamics. At the coldest site, the maximum ALT under a dense canopy is 19% lower than under a sparse canopy. Forest loss leads to higher snow-free GSTs at all sites and higher snow-covered GST at Chukotka and Spasskaya, with a maximum temperature increase of +8.3 °C. In just five years the forest cover loss leads to a warming of the GSTs at the same order of magnitude as the projected temperature increase for boreal regions 4 °C–11 °C until 2100 (Meredith *et al* 2019). In the snow-covered period, a lower share of deciduous trees was found to lead to warmer GSTs at all three sites. This difference in insulation capacity between deciduous- and evergreen-dominated canopies is up to +2.7 °C at the Chukotka site and +1.5 °C at SPA. Deciduousness has a higher effect on the average GSTs in cold regions (Chukotka) and a significant effect on the snow-covered GSTs at all sites. We show that in addition to the previously described change in fire regime (Rogers *et al* 2015) and albedo decrease (Bonan and Shugart 1989), the lower insulation capacity of evergreen canopies will be an important factor in the spreading of evergreen taxa in eastern Siberia. The actual thermal and hydrological impact of the forest cover is therefore determined by the forest density and structure, highly dependent on the local climate and hydrological conditions, and therefore varies greatly between our study sites. We find that forest loss can amplify wetting as well as drying of the soil. The available plant water after forest cover loss is four times higher at the coldest site, two times higher at the warmest site, and 50% reduced at the driest site. Depending on precipitation and soil type, forest cover loss can induce both drying and wetting. Generally, the reduction in transpiration after forest loss leads to wetter soils (O'Donnell *et al* 2011, Loranty *et al* 2018) which we find at both Spasskaya and Chukotka. A further important factor determining the hydrological conditions is the nature of the soil type (Boike *et al* 2016, Loranty *et al* 2018, Holloway *et al* 2020). Very sandy soils explain the good draining conditions and the resulting drying trajectory at Nyurba, while the clay-containing soils at Spasskaya and Chukotka

are drained less, and hence the forest cover change can lead to wetting.

In this study, we focus on the direct physical impact of forest change on the detailed thermal and hydrological conditions of permafrost ground underneath, rather than investigating the exact timing of these ecosystem changes because the simulations themselves are decoupled from projected climate forcing data. Because of the difference found in the forest cover's impact on the thermal regime of the permafrost ground, we argue, that specific, local and detailed land-surface models are needed to understand the complex dynamics in permafrost underlain boreal ecosystems. Further, higher detail in the simulated change to the thermal and hydrological conditions could be achieved by incorporating a change in the thickness or composition of the litter, moss, and organic layers over time, and by additionally simulating the plant functional type broadleaf, which can establish wherever sufficient precipitation is available (Kharuk *et al* 2009, Shuman *et al* 2011).

While knowledge about carbon sequestration through boreal forests is well-established, more and more studies have found that different processes can counteract the boreal forest's role as a carbon sink (Betts 2000, Bonan 2008). As such, a decreasing albedo due to afforestation has been found to lead to a positive climate forcing for certain regions (Bonan 2008, Stuenzi and Schaepman-Strub 2020). Further, forest loss can lead to reduced evapotranspiration and a resulting short-term positive forcing effect (Liu *et al* 2019), as well as to an increased surface albedo, mainly in the snow-covered-period, and hence, a strong cooling effect (Lyons *et al* 2008, Rogers *et al* 2015, Chen *et al* 2018, Liu *et al* 2019). We argue that the development of the forest cover does not only influence the future of the boreal forest's function as a carbon sink but also plays an important role in the stability of permafrost. We show that varying density and tree composition have a significant effect on the thermal and hydrological state of permafrost. The insulating effect of the forest cover depends on the local climatic conditions but significant impact was found at all sites. Finally, the structure and composition of forests are highly dependent on the local ecosystem resilience towards an increasing frequency and intensity of forest fires, rising air temperatures, and a decrease in precipitation (Shuman *et al* 2011, Mekonnen *et al* 2019). Especially, the favoring of different fire regimes between evergreen and deciduous taxa, as well as warmer and drier conditions, can lead to fast ecosystem shifts. Altered thermal conditions, soil drainage or higher soil wetness, enrichment in nutrients, and an increased active layer depth can all have a favoring effect on either evergreen needleleaf or deciduous hardwood expansion, lead to the complete loss of forest cover, or change the forest density (Takahashi 2006, Kharuk *et al* 2013, Liu *et al* 2017, Kropp *et al* 2021). Here, we show that these changes will cause a shift in the thermal and hydrological permafrost state, which potentially destabilizes tightly coupled ecosystem functions.

### 4.1. Conclusions

In this study, we can underlay the tightly coupled interplay between forest and permafrost development with a physically-based model and make predictions on the progression of ecosystem-protected permafrost under a variety of forest change scenarios. In summary, we identify the following key points:

(a) A change in forest density clearly affects the ground surface temperatures at all sites. Temperature differences are highest at the coldest site and in the snow-free period. This is further reflected by a decrease in the maximum ALT of up to 0.05 m or 19% at the two colder sites. The direction of this trend highly depends on local climate conditions.
(b) At all sites, simulations without a forest cover reveal higher maximum ALTs of up to 0.33 m and higher GSTs of more than 8 °C after only five years. The thermal impact of forest cover loss is on the same order of magnitude as the climate warming projected for the region until 2100. Complete forest loss is found to lead to a deepening of the ALT and a warming of GSTs at all sites, independent of local climatic conditions.
(c) Depending on precipitation and soil type, forest cover loss can induce both drying and wetting. After forest cover loss, the available plant water is four times higher at the coldest site, two times higher at the warmest site, and 50% reduced at the driest site.
(d) At all sites, deciduous dominated canopies reveal lower GSTs, especially during the snow-covered period. This difference in insulation capacity reaches up to +2.7 °C for pure evergreen stands and is likely an important factor controlling the spreading of evergreen taxa and controlling the resilience of ecosystem-protected permafrost.

In the light of increasing disturbances (such as fires and diseases) in boreal forests our conclusions have strong implications regarding permafrost-vegetation-climate feedback mechanisms. Our simulations indicate a positive feedback between the successive establishment of evergreen taxa and active layer deepening which may accelerate further forest transformation and permafrost thaw. In addition, forest cover transformation will have a strong impact on the hydrological regime, which may further amplify climate-induced changes in near surface temperature and precipitation. In consequence, the feedback loop might be further amplified by increasing fire probability and disease vulnerability due to additional water stress. On the other hand, under wetter

climate conditions, enhanced wetting can eventually lead to swamping and thermokarst causing forest dieback as observed in drunken forests.

SMS designed the study, developed and implemented the numerical model, carried out and analyzed the simulations, prepared the results figures and led the paper preparation. ML, SW, JB, UH and SK co-designed the study, and supported the interpretation of the results. SMS, ML, and SW implemented the code in the model and designed the model simulations. AG prepared the land cover projection data. SMS, UH and SK prepared and conducted the field work in 2018, SMS conducted the field work in 2019. SMS wrote the paper with contributions from all co-authors. UH, ML and JB secured funding.

No competing interests are present.

## Data availability statement

The code is available on Zenodo (DOI: https://doi.org/10.5281/zenodo.4603.668). The iButton soil temperature data are available at https://doi.org/10.1594/PANGAEA.914327 (Langer *et al* 2020). The AWS data are available at https://doi.pangaea.de/10.1594/PANGAEA.918074 (Stuenzi *et al* 2020).

## Acknowledgments

SMS is thankful to the POLMAR graduate school, the Geo.X Young Academy and the WiNS program at the Humboldt University of Berlin for providing a supportive framework for her PhD project and helpful courses on scientific writing and project management. SMS would like to acknowledge the help from AG, Kirsten Thonicke, Christopher Reyer and Martin Gutsch in acquiring the land cover projection data. Further, SMS is very grateful for the help during fieldwork in 2018 and 2019, especially for the help from Levina Sardana Nikolaevna, Alexey Nikolajewitsch Pestryakov, Lena Ushnizkaya, Luise Schulte, Frederic Brieger, Stuart Vyse, Elisbeth Dietze, Nadine Bernhard, Boris K. Biskaborn, Iuliia Shevtsova, as well as Luidmila Pestryakova and Evgeniy Zakharov. Additionally, SMS would like to thank Stephan Jacobi, Alexander Oehme, Niko Borneman, Peter Schreiber and William Cable for their help in preparing for field work and the entire PermaRisk and Sparc research groups for their ongoing support.

This study has been supported by the ERC consolidator grant Glacial Legacy to Ulrike Herzschuh (No. 772852). Further, the work was supported by the Federal Ministry of Education and Research (BMBF) of Germany through a grant to Moritz Langer (No. 01LN1709A). Funding was additionally provided by the Helmholtz Association in the framework of MOSES (Modular Observation Solutions for Earth Systems). Luidmila A. Pestryakova was supported by the Russian Foundation for Basic Research (Grant No. 18-45-140053 ra) and Ministry of Science and Higher Education of Russia (Grant No. FSRG-2020-0019). Sebastian Westermann acknowledges funding by Permafost4Life (Research Council of Norway, Grant No. 301639) and ESA PermafrostCCI (climate.esa.int/en/projects/permafrost/). AG received funding by the German Federal Ministry of Education and Research (BMBF) and the European Research Area for Climate Services ERA4CS with project funding reference 518, No.01LS1711C (ISIPedia project).

IOP Publishing Environ. Res. Lett. 16 (2021) 084045 S M Stuenzi et al

## Appendix A. Interactions between the atmosphere, boreal forest and permafrost

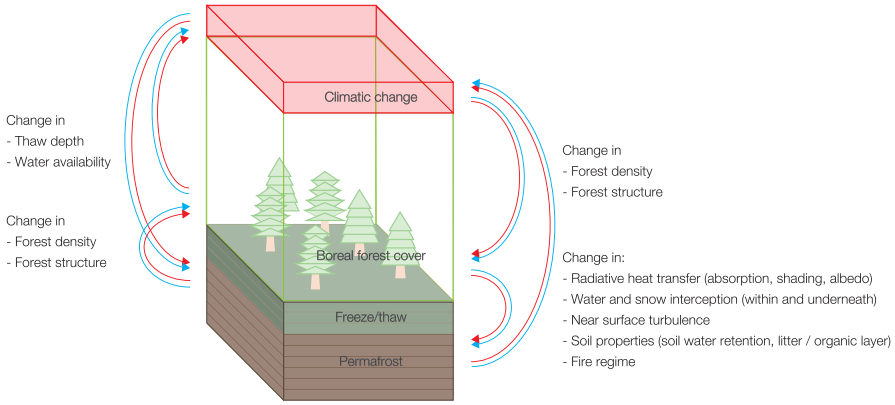


**Figure A1.** Interactions between the atmosphere, boreal forest cover, and permafrost. In red (energy) and blue (hydrology) are all the mechanisms changing due to climatic changes. Climatic change leads to a change in the forest density and structure, which leads to changes in all feedback processes between forest and permafrost. Additionally, climatic change leads to permafrost thawing and a change in the water availability, which also leads to forest density and structure changes.

## Appendix B. Study sites and their climate

### B.1. Study sites

*B.1.1. Nyurba*

The most western study site is located south east of Nyurba at N 63.08°, E 117.99°, and 117 m asl, in a continuous permafrost boreal forest zone intermixed with some grassland, agricultural usage, and shallow lakes. The soils are sandy, and nutrient-poor (Chapin *et al* 2011). The forest soil has a litter layer of 0.07 m and an A-horizon reaching a depth of 0.16 m. It is rich in organic and undecomposed material. Mineral soil is podzolized. The rooting depth is 0.20 m. The average ALT between spatially distributed point measurements was 0.75 m in mid-August 2018 and 0.73 m in early August 2019. The forest is rather dense and mixed, with evergreen spruce *Picea obovata* Ledeb. and deciduous larch *Larix gmelinii* Rupr. The average tree height is 8 m (6 m for spruce and 12 m for larch). This site has been used as the main validation site in Langer *et al* (2020), Stuenzi *et al* (2020, 2021).

*B.1.2. Spasskaya Pad*

The central study site is the well-described forest research site in SPA at N 62.14°, E 129.37°, at 237 masl (Ohta *et al* 2001, Maximov 2015). SPA is located in a continuous permafrost region, and the active-layer depth is around 1.2 m in larch-dominated forests. The soils are sandy loam, and nutrient-poor. The forest soil has a litter layer of 0.08 m and an A-horizon reaching a depth of 0.16 m, mineral soil is podzolized. The measured average tree height is 12 m. Understory vegetation (*Vaccinium* L.) is dense and 0.05 m high. This site has been used as an external validation site in Stuenzi *et al* (2021).

*B.1.3. Chukotka*

The most northern study area is located at Lake Ilirney in Chukotka at N 67.40°, E 168.37°, and 603 m asl. The treeline here is dominated by deciduous larch and underlain by continuous permafrost. The soil is clay dominated with a litter layer of undecomposed *Betula* roots, dead moss, and dense rooting (0.01 m). The organic horizon consist of organic black humus with highly decomposed organic material, moss remains, and good rooting (−0.18 m). The thawed mineral sediment layer had a thickness of (0.37 m) with little roots, dark grey clay matrix (40%), and clasts (60%). The average measured tree height is 11 m.

IOP Publishing Environ. Res. Lett. 16 (2021) 084045 S M Stuenzi et al

### B.2. Monthly forest cover projection data

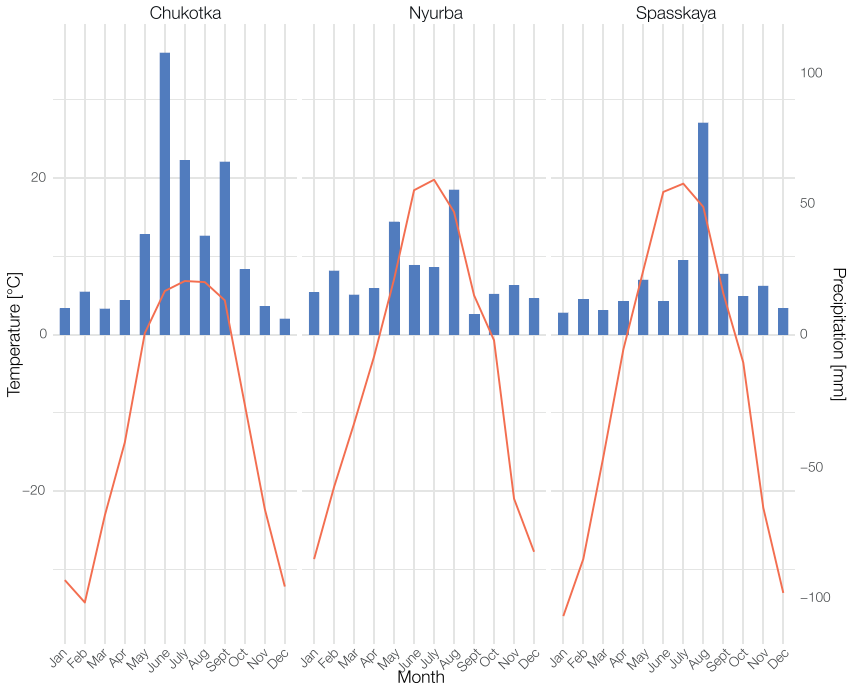


**Figure B1.** Monthly average temperature (red) and total monthly solid and liquid precipitation (blue) for the three study sites (based on ERA-Interim (ECMWF Reanalysis) data for the study site coordinates).

IOP Publishing Environ. Res. Lett. 16 (2021) 084045 S M Stuenzi et al

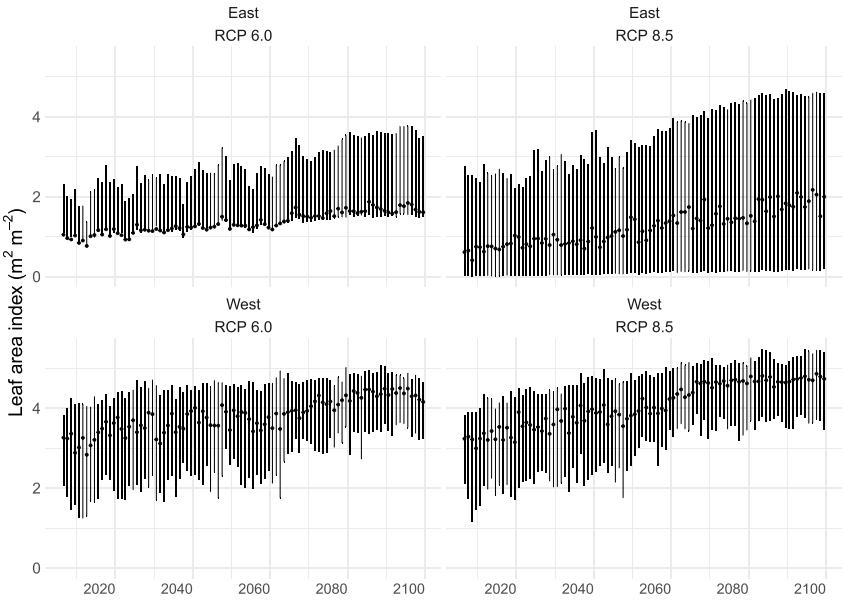


**Figure B2.** Projected LAI for the month of August, which corresponds to the maximum LAI of deciduous taxa, under the two warming scenarios, RCP 6.0 and RCP 8.5 for the time frame 2006-2099. Data covers the region from E 105.25 − 169.75° and N 45.25 − 69.75° and is separated into two individual study regions, West (E 105.25 − 137.25°, bottom) and East (E 137.75 − 169.75°, top). The points indicate median values while the bars show the corresponding 90th and 10th percentile.

## Appendix C. Coupled multilayer-permafrost model

### C.1. Coupled multilayer-permafrost model

The canopy model has been coupled to CryoGrid by replacing its standard surface energy balance scheme while soil state variables are passed back to the forest module. The vegetation module forms the upper boundary layer of the coupled model and replaces the surface energy balance equation used for common CryoGrid representations. The multilayer canopy model provides a comprehensive parameterization of fluxes from the ground, through the canopy up to the roughness sublayer, which allows the representation of different forest canopy structures and their impact on the vertical heat and moisture transfer.

The exchange of sensible heat, radiation, evaporation, and condensation at the ground surface are simulated with an surface energy balance scheme based on atmospheric stability functions. In addition, the model encompasses different options to simulate the evolution of the snow cover including the Crocus snowpack scheme (Vionnet *et al* 2012) as implemented by Zweigel *et al* (2021). The model is forced by standard meteorological variables which may be obtained from AWSs, reanalysis products, or climate models. The required forcing variables include air temperature, wind speed, humidity, incoming short-and longwave radiation, air pressure and precipitation (snow- and rainfall) (Westermann *et al* 2016) and cloud cover (Stuenzi *et al* 2021). We implement an updated model for the phase partitioning among liquid water, water vapor and ice based on the paramterization in Painter and Karra (2014). The proposed relationship for phase partitioning of water in frozen soil shows an improved performance for unsaturated ground conditions by smoothing the thermodynamically derived relationship to eliminate jump discontinuity at freezing. The flow in freezing soil is solved by a modified nonisothermal Richards equation. This constitutive relationship is more applicable for soils with very low total water content, which is the case for some regions in south and eastern Siberia, or high gas content. Following experimental results in Painter and Karra (2014), the ratio of ice-liquid to liquid-air surface tensions for noncolloidal soil, $\beta = 2.2$, and the smoothing parameter, $\omega = 0$, with $n$ and $\alpha$ following the parameterization in the van Genuchten-Mualem model (van Genuchten 1980). This leads to an improved model performance for very dry ground conditions at boreal study sites in eastern Siberia.

The subsurface stratigraphy extends to 100 m, where the geothermal heat flux is set to 0.05 W m$^{-2}$ (Langer *et al* 2011b). The ground is divided into separate layers in the model, the top 8 m have a layer thickness of 0.05 m, followed by 0.1 m for the

IOP Publishing Environ. Res. Lett. 16 (2021) 084045 S M Stuenzi et al

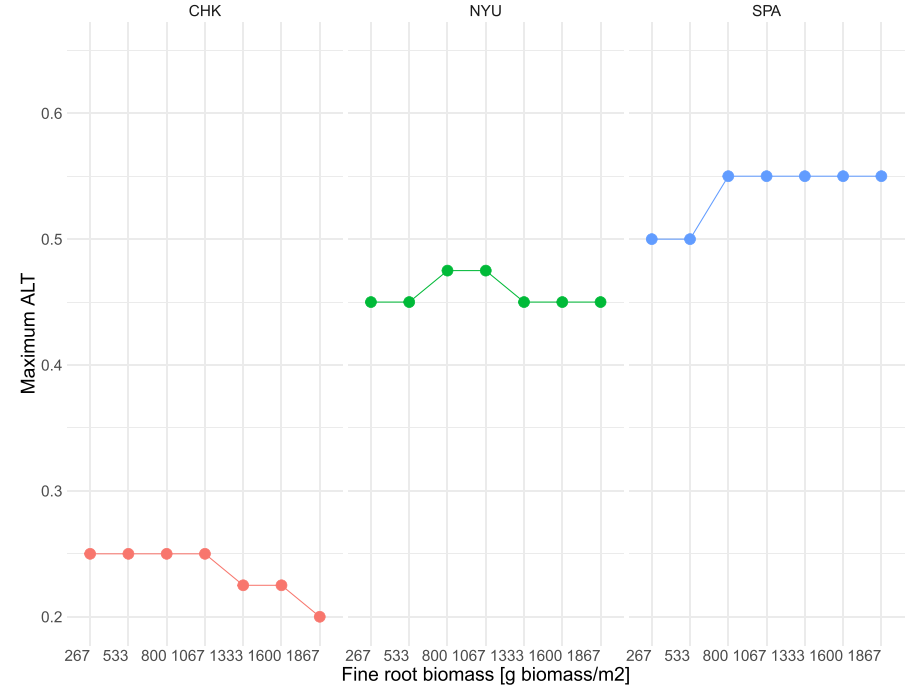


**Figure C1.** Averaged modeled maximum ALT and the spread for increasing root biomass and canopy density (Root biomass = 267–1867 g biomass $m^{-2}/m^2$ and LAI = 1–7 $m^2 m^{-2}$) at the three study sites over a period of 1 year (10 August 2018–10 August 2019). The bars indicate mean values while the whiskers show the corresponding standard deviations.

next 20 m, 0.5 m up to 50 m and 1 m thereafter. The remaining CryoGrid parameters were adopted from previous studies using CryoGrid (table E1) (Langer *et al* 2011a, Westermann *et al* 2016, Nitzbon *et al* 2019, Stuenzi *et al* 2021). The model runs are initialized with a typical temperature profile of 0 m depth: 0 °C, 2 m: 0 °C, 10 m: −9 °C, 100 m: 5 °C, 5000 m: 20 °C. The remaining CryoGrid parameters were adopted from previous studies using CryoGrid (Langer *et al* 2011a, 2011b, 2016, Westermann *et al* 2016, Nitzbon *et al* 2019, 2020, Stuenzi *et al* 2021). The subsurface stratigraphy is described by the mineral and organic content, natural porosity, field capacity and initial water/ice content. Some of these parameters could be measured at the forest sites and were used to set the initial soil profiles and current canopy cover (tree height, forest composition) in the model (AsiaFlux 2017, Langer *et al* 2020, Stuenzi *et al* 2020).

### C.2. Fine root biomass

Here, we use root/shoot ratio ($R_{RS}$) of 0.32 as defined in Jackson *et al* (1996) to calculate the fine root biomass correspondent to each LAI value to evaluate the importance of constraining this parameter.

$$R_{total} = R_{RS} \times LAI \times \frac{1}{SLA_{d/e}} \times \frac{1}{F_{carbon}} \times \frac{1}{(1 - F_{water})}, \quad (C.1)$$

with the specific leaf area at the top of canopy $SLA_d = 0.008\,m^2\,g^{-1}C$ for deciduous and $SLA_e = 0.008\,m^2\,g^{-1}C$ for evergreen taxa, respectively. The carbon content of the dry biomass is $F_{carbon} = 0.5\,gC\,g^{-1}$ and the ratio of the fresh biomass that is water $F_{water} = 0.7\,gH_2O\,g^{-1}$ (Bonan *et al* 2018). Simulation results for LAI = 1–7 $m^2 m^{-2}$ and corresponding root biomass = 267–1867 g biomass $m^{-2}/m^2$ reveal no consistent trend across the three study sites (figure C1). The change in ALT caused by an increasing root biomass is up to 0.05 m at Chukotka and SPA and therefore on the same order of magnitude as found for forest deciduousness. We argue that root biomass needs to be constrained further but this is outside of the scope of this study.

IOP Publishing Environ. Res. Lett. 16 (2021) 084045 S M Stuenzi et al

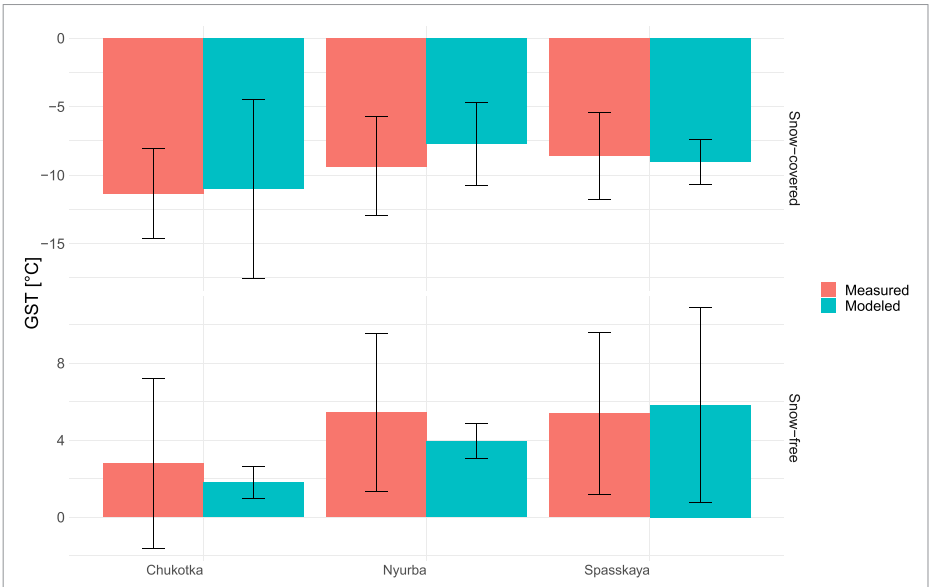


**Figure D1.** Top, averaged modeled (blue) and measured (red) snow-covered period GST, and bottom, average modeled and measured snow-free period GST and the respective spread at the three study sites over a period of 1 year (1 September 2018–10 August 2019 for Nyurba and Chukotka and 1 September 2017 to 10 August 2018 for SPA). The bars indicate mean values while the whiskers show the corresponding standard deviations.

### C.3. Canopy description

The canopy is described by the leaf area index, the stem area index, and the leaf density function. LAI describes the total leaf area, which can be measured by harvesting leaves and calculating the total mass to canopy diameter ratio or estimated from below-canopy light measurements. The most common form of LAI estimation is from satellite data and the variance in values is rather high. LAI is measured at the bottom of the canopy and defines the total one-sided leaf area or the total projected needle leaf area ($m^2m^{-2}$) of all leaves per unit ground area (Myneni *et al* 2002, Chen *et al* 2005). LAI can be estimated from satellite data, calculated from below-canopy light measurements or by harvesting leaves and relating their mass to the the canopy diameter. To assess the LAI in our study region we use data from literature and satellite data. Following Kobayashi *et al* 2010) who conducted an extensive study using satellite data, the average LAI of the forest types in our study region vary between 1 $m^2m^{-2}$ and 7 $m^2m^{-2}$. Stem area index is not varied here and set to 0.05 $m^2m^{-2}$, following Bonan (2019) and Stuenzi *et al* (2021). The leaf area density function is also not varied here and describes the foliage area per unit volume of canopy space which is the vertical distribution of leaf area. Leaf area density is measured by evaluating the amount of leaf area between two heights in the canopy separated by the distance. This function can be expressed by the beta distribution probability density function which provides a continuous representation of leaf area for the use with multilayer models ((Bonan 2019) for further information). Here, we use the beta distribution parameters for needleleaf trees ($p = 3.5$, $q = 2$) which resembles a cone-like tree shape. Further, the lower atmospheric boundary layer is simulated by 4 m of atmospheric layers.

## Appendix D. Model validation and in-situ measurements

We compare modeled and measured annual, snow-free and snow-covered mean GST to understand the overall model performance regarding the thermal regime of the surface and the ground and the relative temperature differences between the model and measurements. GST results from the surface energy balance at the interface between canopy, snow cover, and ground, and provides an integrative measure of the different model components. In addition, it is the most important variable determining the thermal state of permafrost. The model has previously been validated against GST, radiation, snow depth, conductive heat flux, precipitation and temperature measurements for Nyurba and Spasskaya (Stuenzi *et al* 2021). To validate the model for all study sites used here, the model is validated against GST measurements at all sites. The data sets used for Nyurba and Chukotka cover one complete annual cycle from 10 August 2018 to 10 August 2019 (iButton (DS1922L), Maxim Integrated, accuracy: 0.5 °C

IOP Publishing Environ. Res. Lett. 16 (2021) 084045 S M Stuenzi et al

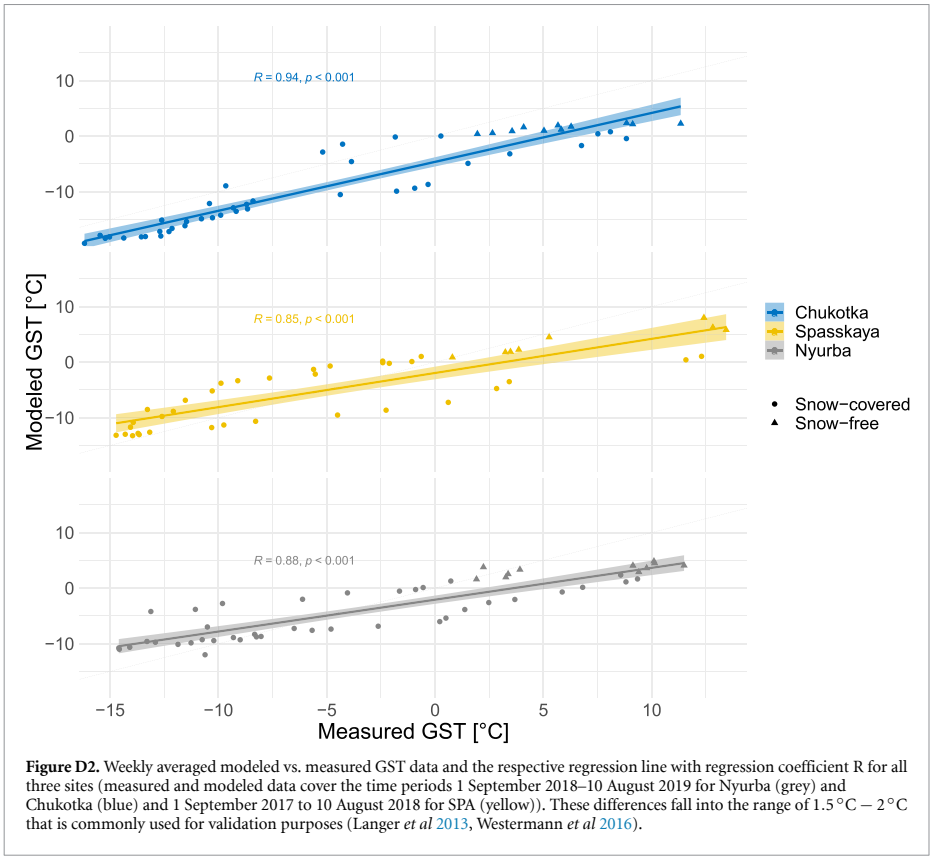


**Figure D2.** Weekly averaged modeled vs. measured GST data and the respective regression line with regression coefficient R for all three sites (measured and modeled data cover the time periods 1 September 2018–10 August 2019 for Nyurba (grey) and Chukotka (blue) and 1 September 2017 to 10 August 2018 for SPA (yellow)). These differences fall into the range of 1.5 °C – 2 °C that is commonly used for validation purposes (Langer *et al* 2013, Westermann *et al* 2016).

(−10 °C to 65 °C, (Langer *et al* 2020, Stuenzi *et al* 2020)). For SPA we have soil temperature measurements acquired through the AsiaFlux Network and the most recent data available and covering one entire year was used (August 2017–August 2018) (AsiaFlux 2017). The average annual GST recorded at the warmest study site in Nyurba at a depth of 0.03 m is 2 °C with an average of −9.4 °C in the snow-covered period and 5.4 °C in the snow-free period. Chukotka is the coldest study site with average snow-covered GST of −11.3 °C and 2.8 °C for the snow-free period, 1.9 °C colder than Nyurba and 0.5 °C colder than SPA. Here, the average snow-covered GST is −8.6 °C (figure D1). The model can reproduce these GSTs at all sites with a slight cold bias for the snow-free periods in Nyurba (−1.4 °C) and Chukotka (−1 °C) and a warm bias for the snow-covered period in Nyurba (+1.5 °C). These differences fall into the range of 1.5 °C – 2 °C that is commonly used for validation purposes (Langer *et al* 2013, Westermann *et al* 2016).

IOP Publishing Environ. Res. Lett. 16 (2021) 084045 S M Stuenzi et al

## Appendix E. Model parameters used and constants

**Table E1.** Overview of the CryoGrid parameters used.

| Process / Parameter | | Value | Unit | Source |
|---|---|---|---|---|
| Density falling snow | $\rho_{snow}$ | 80–200 | kg m$^{-3}$ | Kershaw and McCulloch (2007) |
| Albedo ground | $\alpha$ | 0.3 | — | Field measurement |
| Roughness length | $z_0$ | 0.001 | m | Westermann *et al* (2016) |
| Roughness length snow | $z_{0\,snow}$ | 0.0001 | m | Boike *et al* (2019) |
| Geothermal heat flux | $F_{lb}$ | 0.05 | W m$^{-2}$ | Westermann *et al* (2016) |
| Thermal cond. mineral soil | $k_{mineral}$ | 3.0 | W m$^{-1}$ K$^{-1}$ | Westermann *et al* (2016) |
| Emissivity | $\varepsilon$ | 0.99 | — | Langer *et al* (2011a) |
| Root depth | $D_T$ | 0.2 | m | Field measurement |
| Evaporation depth | $D_E$ | 0.1 | m | Nitzbon *et al* (2019) |
| Hydraulic conductivity | $K$ | $10^{-5}$ | m s$^{-1}$ | Boike *et al* (2019) |

**Table E2.** Parameter set-up for different study sites.

| Study site | Tree height (m) | Soil layer depth (Litter/organic /mineral) | Respective soil type | ERA-interim coordinate | Snow-free period |
|---|---|---|---|---|---|
| Nyurba | 8 | 0/0.07/0.16 | Peat/clay/sand | N 63.08°, E 117.99° | June-October |
| Spasskaya | 12 | 0/0.08/0.16 | Peat/clay/sand | N 62.14°, E 129.37° | June-September |
| Chukotka | 11 | 0/0.01/0.18 | Peat/clay/sand | N 67.40°, E 168.37° | July-September |

**Table E3.** Constants.

| Constants | Value | Unit |
|---|---|---|
| von Karman | 0.4 | — |
| Freezing point water (normal pres.) | 273.15 | K |
| Latent heat of vaporization | $2.501 \times 10^6$ | J kg$^{-1}$ |
| Molecular mass of water | 18.016/1000 | kg mol$^{-1}$ |
| Molecular mass of dry air | 28.966/1000 | kg mol$^{-1}$ |
| Specific heat dry air (const. pres.) | 1004.64 | J kg$^{-1}$ K$^{-1}$ |
| Density of fresh water | 1000 | kg m$^{-3}$ |
| Heat of fusion for water at 0 °C | $0.334 \times 10^6$ | J kg$^{-1}$ |
| Thermal conductivity of water | 0.57 | W m$^{-1}$ K$^{-1}$ |
| Thermal conductivity of ice | 2.2 | W m$^{-1}$ K$^{-1}$ |
| Kinem. visc. air (0 °C, 1013.25 hPa) | 0.0000 133 | m$^2$ s$^{-1}$ |
| Sp. heat water vapor (const. pr.) | 1810 | J kg$^{-1}$ K$^{-1}$ |

IOP Publishing Environ. Res. Lett. 16 (2021) 084045 S M Stuenzi et al

**Table E4.** Multilayer canopy parameters for deciduous needleleaf (NDT) and evergreen needleleaf (NET) plant functional types.

| Parameter | Value | Unit | Source |
|---|---|---|---|
| Leaf angle dep. from spherical | 0.01 | — | Bonan (2002) |
| Leaf reflectance (VIS/NIR) | 0.07/0.35 | — | Bonan (2002) |
| Stem reflectance (VIS/NIR) | 0.16/0.39 | — | Bonan (2002) |
| Leaf transmittance (VIS/NIR) | 0.05/0.01 | — | Bonan (2002) |
| Stem transmittance (VIS/NIR) | 0.001/0.001 | — | Bonan (2002) |
| Max. carboxylation rate (25 °C) | 43 | $\mu$mol m$^{-2}$ s$^{-1}$ | Bonan (2002) |
| Photosynthetic pathway | C3 | — | Bonan (2002) |
| Leaf emissivity | 0.98 | — | Bonan (2002) |
| Quantum efficiency a | 0.06 | $\mu$mol $CO_2$ $\mu$mol photon$^{-1}$ | Bonan (2002) |
| Slope m | 6 | — | Bonan (2002) |
| Leaf dimension | 0.04 | m | Bonan (2002) |
| Roughness length | 0.055 | m | Bonan (2002) |
| Displacement height | 0.67 | m | Bonan (2002) |
| Root distribution (a/b) | 7.0/2.0 | — | Bonan (2002) |
| Min. vapor pressure deficit | 100 | Pa | Bonan (2019) |
| Plant capacitance | 2500 | mmol $H_2O$ m$^{-2}$ leaf area MPa$^{-1}$ | Bonan (2019) |
| Minimum leaf water potential | −2 | MPa | Bonan (2019) |
| Stem hydraulic conductance | 4 | mmol $H_2O$ m$^{-2}$ s$^{-1}$ leaf area MPa$^{-1}$ | Bonan (2019) |
| Atmospheric $CO_2$ | 380 | $\mu$mol mol$^{-1}$ | Bonan (2019) |
| Atmospheric $O_2$ | 209 | mmol mol$^{-1}$ | Bonan (2019) |
| Soil evaporative resistance | 3361.509 | s m$^{-1}$ | Bonan (2019) |
| Specific heat of dry-wet soil | 1396 | J kg$^{-1}$ K$^{-1}$ | Oleson *et al*(2013) |
| Specific heat of fresh $H_2O$ | 4188 | J kg$^{-1}$ K$^{-1}$ | Oleson *et al*(2013) |
| Specific leaf area (TOC) | 0.008 (NET)<br>0.024 (NDT) | m$^2$ g$^{-1}$ C | Bonan *et al*(2018) |
| Fine root biomass | 500 | g biomass m$^{-2}$ | Bonan (2019) |
| Leaf drag coefficient | 0.25 | — | Bonan (2019) |
| Foliage clumping index | 0.7 | — | Bonan (2019) |

## ORCID iDs

Simone M Stuenzi https://orcid.org/0000-0002-6071-289X
Julia Boike https://orcid.org/0000-0002-5875-2112
Anne Gädeke https://orcid.org/0000-0003-0514-2908
Ulrike Herzschuh https://orcid.org/0000-0003-0999-1261
Stefan Kruse https://orcid.org/0000-0003-1107-1958
Luidmila A Pestryakova https://orcid.org/0000-0001-5347-4478
Sebastian Westermann https://orcid.org/0000-0003-0514-4321
Moritz Langer https://orcid.org/0000-0002-2704-3655

## References

AsiaFlux 2017 Yakutsk Spasskaya Pad larch forest data (Site Code: YLF) (available at: http://asiaflux.net/index.php?pageid=121)
Betts R A 2000 *Nature* **408** 187–90
Boike J *et al* 2019 *Earth Syst. Sci. Data* **11** 261–99
Boike J, Grau T, Heim B, Günther F, Langer M, Muster S, Gouttevin I and Lange S 2016 *Glob. Planet. Change* **139** 116–27
Bonan G B 2002 *Ecological Climatology: Concepts and Applications* (Cambridge: Cambridge University Press)
Bonan G B 2008 *Science* **320** 1444–9
Bonan G B 2019 *Climate Change and Terrestrial Ecosystem Modeling* (Cambridge: Cambridge University Press)
Bonan G B, Patton E G, Harman I N, Oleson K W, Finnigan J J, Lu Y and Burakowski E A 2018 *Geosci. Model Dev.* **11** 1467–96
Bonan G B, Pollard D and Thompson S L 1992 *Nature* **359** 716–18
Bonan G B and Shugart H H 1989 Environmental factors and ecological processes in boreal forests *Annual Review of Ecology and Systematics* **20** 1–28
Bonan G B, Williams M, Fisher R A and Oleson K W 2014 *Geosci. Model Dev.* **7** 2193–222
Carpino O A, Berg A A, Quinton W L and Adams J R 2018 *Environ. Res. Lett.* **13** 084018
Chang X, Jin H, Zhang Y, He R, Luo D, Wang Y, Lü L and Zhang Q 2015 *Arctic Antarct. Alpine Res.* **47** 267–79
Chapin F S, Matson P A and Vitousek P M 2011 *Principles of Terrestrial Ecosystem Ecology* (New York: Springer) pp 23–62
Chasmer L, Quinton W, Hopkinson C, Petrone R and Whittington P 2011 *Permafrost Periglacial Process.* **22** 199–213
Chen D, Loboda T V, He T, Zhang Y and Liang S 2018 *Sci. Rep.* **8** 1–10
Chen X, Vierling L, Deering D and Conley A 2005 *Int. J. Remote Sens.* **26** 5433–51

Copernicus Global Land Operations 2021 Leaf Area Index (LAI) Collection, 300 m, Version 1.1, Issue I 1.01 (available at: https://land.copernicus.eu/global/sites/cgls.vito.be/files/products/CGLOPS1PUMLAI300m-V1.1I1.01.pdf)
Esper J, Frank D, Büntgen U, Verstege A, Hantemirov R and Kirdyanov A V 2010 *Glob. Change Biol.* **16** 386–98
Esper J and Schweingruber F H 2004 *Geophys. Res. Lett.* **31** L06202
Fisher J P, Estop-Aragonés C, Thierry A, Charman D J, Wolfe S A, Hartley I P, Murton J B, Williams M and Phoenix G K 2016 *Glob. Change Biol.* **22** 3127–40
Frieler K *et al* 2017 *Geosci. Model Dev* **10** 4321–45
Gauthier S, Bernier P, Kuuluvainen T, Shvidenko A Z and Schepaschenko D G 2015 *Science* **349** 819–22
Gruber S 2012 *Cryosphere* **6** 221–33
Helbig M, Pappas C and Sonnentag O 2016 *Geophys. Res. Lett.* **43** 1598–606
Herzschuh U 2019 *Glob. Ecol. Biogeogr.* **29** 198–206
Holloway J E, Lewkowicz A G, Douglas T A, Li X, Turetsky M R, Baltzer J L and Jin H 2020 *Permafrost Periglacial Process.* **31** 371–82
Ito A *et al* 2020 *Environ. Res. Lett.* **15** 044006
Jackson R B, Canadell J, Ehleringer J R, Mooney H A, Sala O E and Schulze E D 1996 *Oecologia* **108** 389–411
Kershaw G P and McCulloch J 2007 *Arctic Antarct. Alpine Res.* **39** 9–15
Kharuk V I, Ranson K J, Im S T and Dvinskaya M L 2009 *Scand. J. Forest Res.* **24** 130–9
Kharuk V I, Ranson K J, Im S T, Oskorbin P A, Dvinskaya M L and Ovchinnikov D V 2013 *Arctic Antarct. Alpine Res.* **45** 526–37
Kharuk V I, Ranson K J, Im S T and Petrov I A 2015 *Environ. Res. Lett.* **10** 125009
Kharuk V I, Ranson K J, Petrov I A, Dvinskaya M L, Im S T and Golyukov A S 2019 *Reg. Environ. Change* **19** 233–43
Kharuk V, Ranson K and Dvinskaya M 2007 *Eurasian J. For. Res* **10** 163–71 (https://eprints.lib.hokudai.ac.jp/dspace/bitstream/2115/30308/1/10(2)_163-171.pdf)
Kobayashi H, Delbart N, Suzuki R and Kushida K 2010 *J. Geophys. Res.: Biogeosci.* **115** 1–14
Kotlyakov V and Khromova T 2002 Land Resources of Russia—Maps of Permafrost and Ground Ice, Version 1 (https://doi.org/10.7265/zpm9-j983)
Kropp H *et al* 2021 *Environ. Res. Lett.* **16** 015001
Kruse S, Wieczorek M, Jeltsch F and Herzschuh U 2016 *Ecol. Model.* **338** 101–21
Lange S 2019 EartH2Observe, WFDEI and ERA-Interim data Merged and Bias-corrected for ISIMIP (EWEMBI). V. 1.1. (https://doi.org/10.5880/pik.2019.004)
Langer M, Kaiser S, Stuenzi S M, Schneider Von Deimling T, Oehme A and Jacobi S 2020 Soilsurface temperatures in 2 cm depth between summer 2018 and 2019 with iButton-sensors in the North Slope of Alaska (USA), around Churchill (Canada) and the region of Illirney and Lena-Viluy (Russia) (https://doi.org/10.1594/PANGAEA.914327)
Langer M, Westermann S, Boike J, Kirillin G, Grosse G, Peng S and Krinner G 2016 *J. Geophys. Res.: Earth Surf.* **121** 2446–70
Langer M, Westermann S, Heikenfeld M, Dorn W and Boike J 2013 *Remote Sens. Environ.* **135** 12–24
Langer M, Westermann S, Muster S, Piel K and Boike J 2011a *Cryosphere* **5** 151–71
Langer M, Westermann S, Muster S, Piel K and Boike J 2011b *Cryosphere* **5** 509–24
Liu Y *et al* 2017 *Remote Sens. Environ.* **201** 256–74
Liu Z, Ballantyne A P and Cooper L A 2019 *Nat. Commun.* **10** 1–9
Loranty M M *et al* 2018 *Biogeosciences* **15** 5287–313
Lyons E A, Jin Y and Randerson J T 2008 *J. Geophys. Res.: Biogeosci.* **113** 1–15
Maximov T 2015 Elgeeii Forest Station (available at: www.isaaffik.org/users/elgeeii-forest-station)
McGuire A D *et al* 2002 *J. Vegetation Sci.* **13** 301–14
Mekonnen Z A, Riley W J, Randerson J T, Grant R F and Rogers B M 2019 *Nat. Plants* **5** 952–8
Meredith M *et al* 2019 Pörtner H-O *et al* (eds) *IPCC Special Report* on the Ocean and Cryosphere in a Changing Climate
Myneni R *et al* 2002 *Remote Sens. Environ.* **83** 214–31
Nitzbon J, Langer M, Westermann S, Martin L, Aas K S and Boike J 2019 *Cryosphere* **13** 1089–123
Nitzbon J, Westermann S, Langer M, Martin L C P, Strauss J, Laboor S and Boike J 2020 *Nat. Commun.* **11** 2201
O'Donnell J A, Harden J W, McGuire A D and Romanovsky V E 2011 *Biogeosciences* **8** 1367–82
Ohta T, Hiyama T, Tanaka H, Kuwada T, Maximov T C, Ohata T and Fukushima Y 2001 *Hydrol. Process.* **15** 1459–76
Oleson K W *et al* 2013 Technical description of version 4.5 of the Community Land Model (CLM) (No. NCAR/TN-503+STR) *Technical Report*
Painter S L and Karra S 2014 *Vadose Zone J.* **13** vzj2013.04.0071
Pearson R G, Phillips S J, Loranty M M, Beck P S, Damoulas T, Knight S J and Goetz S J 2013 *Nat. Clim. Change* **3** 673–7
Peng X, Zhang T, Frauenfeld O W, Wang S, Qiao L, Du R and Mu C 2020 *J. Geophys. Res.: Biogeosci.* **125** 1-20
R Core Team 2016 R: A language and environment for statistical computing (available at: www.r-project.org/)
Rogers B M, Soja A J, Goulden M L and Randerson J T 2015 *Nat. Geosci.* **8** 228–34
Sato H, Kobayashi H, Iwahana G and Ohta T 2016 *Ecol. Evol.* **6** 5690–704
Scheffer M, Hirota M, Holmgren M, Van Nes E H and Chapin F S 2012 *Proc. Natl Acad. Sci. USA* **109** 21384–9
Schuur E A G and Mack M C 2018 *Ann. Rev. Ecol. Evol. Systematics* **49** 279–301
Shuman J K, Shugart H H and O'Halloran T L 2011 *Glob. Change Biol.* **17** 2370–84
Shuman J K, Tchebakova N M, Parfenova E I, Soja A J, Shugart H H, Ershov D and Holcomb K 2014 *Can. J. Forest Res.* **45** 175–84
Simmons A, Uppala S, Dee D and Kobayashi S 2007 ERA-Interim: New ECMWF reanalysis 20 products from 1989 onwards *Technical Report* ECMWF Newsletter, 110
Smith B, Wårlind D, Arneth A, Hickler T, Leadley P, Siltberg J and Zaehle S 2014 *Biogeosciences* **11** 2027–54
Stuenzi S M *et al* 2020 Automatic weather stations and stand-alone soil temperature sensors (Hobo logger) between August 2018 and August 2019 at two boreal forest sites in the region of Lake Illirney and Lena-Viluy in Eastern Siberia (availabel at: https://doi.pangaea.de/10.1594/PANGAEA.919859)
Stuenzi S M *et al* 2021 *Biogeosciences* **18** 343–65
Stuenzi S M and Schaepman-Strub G 2020 *J. Geophys. Res.: Biogeosci.* **125** e2019JG005395
Takahashi K 2006 *Symptom Environ. Change Siberian Permafrost* pp 163–70 (http://lab.agr.hokudai.ac.jp/env/ctc_siberia/book.html)
Tanaka H, Hiyama T, Kobayashi N, Yabuki H, Ishii Y, Desyatkin R V, Maximov T C and Ohta T 2008 *Agric. Forest Meteorol.* **148** 1954–67
Tchebakova N M, Parfenova E and Soja A J 2009 *Environ. Res. Lett.* **4** 045013
Thomas G and Rowntree P R 1992 *Q. J. R. Meteorol. Soc.* **118** 469–97
van Genuchten M T 1980 *Soil Sci. Soc. Am. J.* **44** 892–8
Vionnet V, Brun E, Morin S, Boone A, Faroux S, Le Moigne P, Martin E and Willemet J M 2012 *Geosci. Model Dev.* **5** 773–91
Vitt D H, Halsey L A, Bauer I E and Campbell C 2000 *Can. J. Earth Sci.* **37** 683–93
Westermann S, Langer M, Boike J, Heikenfeld M, Peter M, Etzelmüller B and Krinner G 2016 *Geosci. Model Dev.* **9** 523–46
Yi S, Woo M k and Arain M A 2007 *Geophys. Res. Lett.* **34** L16504
Zhang N, Yasunari T and Ohta T 2011 *Environ. Res. Lett.* **6** 024003
Zhang Y, Sherstiukov A B, Qian B, Kokelj S V and Lantz T C 2018 *Environ. Res. Lett.* **13** 044012
Zweigel R B, Westermann S, Nitzbon J, Langer M, Boike J, Etzelmüller B and Schuler T V 2021 *J. Geophys. Res.: Earth Surf.* **126** e2020JF005673

# Chapter 7

# Thermohydrological impact of forest disturbances on ecosystem-protected permafrost

**Stuenzi, S.M., Kruse, S., Boike, J., Herzschuh, U., Oehme, A., Pestryakova, L. A., Westermann, S., and Langer, M.**

*JGR: Biogeosciences, in Review.*

manuscript submitted to *JGR: Biogeosciences*

# Thermohydrological impact of forest disturbances on ecosystem-protected permafrost

**S. M. Stuenzi[1,2], S. Kruse[1], J. Boike[1,2], U. Herzschuh[1,3,7], A. Oehme[1,2], L. A. Pestryakova[6], S. Westermann[4,5]and M. Langer[1,2]**

[1]Alfred Wegener Institute, Helmholtz Centre for Polar and Marine Research, Telegrafenberg A45, 14473 Potsdam, Germany
[2]Humboldt-Universitt zu Berlin, Geography Department, Unter den Linden 6, 10099 Berlin, Germany
[3]Institute of Environmental Science and Geography, University of Potsdam, 14476 Potsdam, Germany
[4]Department of Geosciences, University of Oslo, Sem Slands vei 1, 0316 Oslo, Norway
[5]Centre for Biogeochemistry in the Anthropocene, University of Oslo, Sem Slands vei 1, 0316 Oslo, Norway
[6]Institute of Natural Sciences, North-Eastern Federal University in Yakutsk, Belinskogo str. 58, 677000 Yakutsk, Russia
[7]Institute of Biochemistry and Biology, University of Potsdam, 14476 Potsdam, Germany

**Key Points:**

- We demonstrate a dynamic forest-permafrost model to investigate the interplay between boreal larch forest, permafrost, and disturbances.
- Canopy fires and logging induce soil drying which leads to abrupt or steady decline of larch forest cover.
- Survival of larch forests after surface fires is dependent on the timing of precipitation events.

Corresponding author: S. M. Stuenzi, `simone.stuenzi@awi.de`

## Abstract

Boreal forests cover over half of the global permafrost area and are considered to protect underlying permafrost. Boreal forest development, therefore, has an important impact on permafrost evolution, especially under a warming climate. Forest disturbances and changing climate conditions cause vegetation shifts and can potentially destabilize the carbon stored within the vegetation and permafrost. Disturbed permafrost-forest ecosystems can develop into dry or swampy bush- or grasslands, shift towards broadleaf- or evergreen needleleaf-dominated forests, or recover to the pre-disturbance state. An increase in the number and intensity of fires, as well as intensified logging activities could lead to partial or complete ecosystem and permafrost degradation.

We study the impact of forest disturbances (logging, surface and canopy fires) on the thermal and hydrological permafrost conditions and the ecosystem resilience. We use a dynamic multilayer canopy-permafrost model to simulate different scenarios at a study site in eastern Siberia. We implement expected mortality, defoliation, and ground surface changes and analyze the interplay between forest recovery and permafrost.

We find that forest loss induces soil drying of up to 44%, leading to lower active layer thicknesses and abrupt or steady decline of larch forest, depending on disturbance intensity. Only after surface fires, which induce low mortality rates and are the most common disturbances, forests are able to successfully recover and even overpass pre-disturbance forest density values. We find that the recovery trajectory is highly dependent on post-disturbance years, with years with low spring precipitation leading to no larch forest reestablishment within the analyzed time period.



## Plain Language Summary

Boreal forests of eastern Siberia, cover more than half of the global permafrost area and insulate the underlying frozen ground. The development of the forest cover is important for the state and evolution of permafrost. Forest disturbances such as fires or droughts and climate change can cause changes in this ecosystem. Potentially such shifts can destabilize the carbon stored within the vegetation and permafrost. Disturbed permafrost-forest ecosystems can then develop into dry or swampy bush- or grasslands, shift towards different forest types, or recover. An increase in the number and intensity of fires, as well as intensified logging, could lead to partial or complete permafrost degradation. We study the interactions between forest disturbances, permafrost, and forests. We use a forest-permafrost model and simulate disturbances at a study site in eastern Siberia. We implement mortality, defoliation, and ground surface changes of different disturbances. We then analyze the forest recovery's impact on the permafrost underneath. We find that forest loss can cause soil drying and abrupt or steady decline of forest cover, depending on the intensity of the disturbance. Only after a surface fire, which has low mortality rates and is the most common disturbance, forests can successfully recover.


## 1 Introduction

Boreal forests hold more than one third of global terrestrial carbon and cover about 55% of the total global permafrost area (Helbig et al., 2016). The forest cover is considered to efficiently insulate the underlying, ecosystem-protected permafrost (Chang et al., 2015) and therefore play an important role in the development of boreal regions and the stability of permafrost in a warming climate. Despite little human interference and due to extreme climate conditions such as winter temperatures below $-50\,^{\circ}$C and very low precipitation, the biome is highly sensitive to climatic changes and thus prone to vegetation shifts (Meredith et al., 2019). Large forested regions in eastern Siberia, which make up around 20% of the global boreal forest cover, are larch (deciduous needleleaf) dominated and foster a unique interplay between the forest cover, the underlying per-

mafrost, disturbances, and climate. Recently, lots of permafrost destabilization and vegetation shifts have become visible in this vast ecosystem-protected permafrost region (Ulrich et al., 2017). Often, the observed permafrost dynamics are related to anthropogenic deforestation, fires and forest dynamics but the exact processes and thresholds are poorly studied.

Forest composition and density exert a strong control on permafrost stability (Yi et al., 2007; Chasmer et al., 2011; Fisher et al., 2016) and a direct feedback mechanism is expected to control the temporal ecosystem evolution (Bonan et al., 1992; Loranty et al., 2018; Carpino et al., 2018). Previous studies have found that the vegetation cover has a significant impact on the development and stability of the permafrost ground underneath (Stuenzi, Boike, Gädeke, et al., 2021), and vice-versa, the thermal and hydrological conditions of the ground determine the state of the vegetation cover. Anthropogenically-caused disturbances and changing climate conditions are leading to shifts in this ecosystem which could potentially destabilize the carbon stored within the vegetation and permafrost. Disturbed permafrost-forest ecosystems can potentially develop into dry or swampy bush- or grasslands, shift towards broadleaf- or evergreen needleleaf-dominated forests (Takahashi, 2006), or recover to the pre-disturbance state. An increase in the number and/or intensity of fires, and the lengthening of the fire season (Meredith et al., 2019; Narita et al., 2020), as well as intensified logging activities could lead to partial or complete permafrost degradation (Meredith et al., 2019) and vegetation shifts away from deciduous-dominated forest stands (Kharuk et al., 2019). Especially permafrost at the southern margin might not remain resilient under warming climate because of its dependence on ecosystem protection (Yershov, 2004). While larch growth increments and a positive gross primary production suggests an increase in carbon sequestration in the future (Kharuk et al., 2019), an increase in fires and carbon emissions might convert the vast larch forest into a carbon source especially in years of extreme fires (Kharuk et al., 2021).

Previous modeling set-ups have coupled dynamic vegetation to permafrost models with a focus on the forest development rather than the permafrost stability (see i.e. Tchebakova et al. (2009); Zhang et al. (2011); Sato et al. (2016). Sato et al. (2010) (SEIB-DGVM) have simulated post-fire successional patterns at Spasskaya Pad without incorporating or studying permafrost dynamics and the impact of the forest change on permafrost. Zhang et al. (2011) used a coupled permafrost-dynamic vegetation model to study the interactions between permafrost and forest biomass under current and future climate scenarios. Tchebakova et al. (2009) used SibClim to simulate vegetation shifts across eastern Siberia. Zhang et al. (2009) used FAREAST to model the responses of eastern Eurasian forests to climatic change to understand the compositional and structural sensitivity at several locations. FAREAST does not account for the permafrost effected water balance but simply uses a correction factor (Xiaodong & Shugart, 2005). Takahashi (2006) used artificial fire at Spasskaya Pad to study fire dynamics and succession and describe the common patterns within these ecosystems. In Canadian boreal forest areas, Rey et al. (2020) have found that the pre-disturbance soil conditions are key factors controlling the thawing and talik formation processes and wildfire initiated talik-development is already substantial. In summary, former studies on stand-replacing and surface fires and other disturbances in eastern Siberia have focused on their implications on the carbon budget (Soja et al., 2004; Schulze et al., 2012) or their potential impact through albedo and related surface radiative forcing (Chen & Loboda, 2018; Chen et al., 2018; Stuenzi & Schaepman Strub, 2020), or have not incorporated detailed permafrost dynamics.

Further work is therefore needed to identify the post-disturbance response of permafrost (Holloway et al., 2020), and the related interplay between the living forest and the permafrost (Li et al., 2021). We couple the one-dimensional permafrost land surface model CryoGrid adapted for use in boreal forest ecosystems (Stuenzi, Boike, Cable, et al., 2021; Stuenzi, Boike, Gädeke, et al., 2021), with the individual-based and spatially explicit larch forest model LAVESI (Kruse et al., 2016). The coupled model forms a dy-

namic vegetation-permafrost model which is able to reproduce the complex interplay between larch forests and the dynamically changing thermo-hydrological soil conditions linked to permafrost. We reconstruct vegetation disturbances (surface and canopy fires, and logging) reported over the past century and simulate such scenarios at a specific, well-described site in central Yakutia. We study the interplay between forest disturbances, larch recovery, and the thermo-hydrological ecosystem factors. We shift the focus from vegetation succession towards the assessment of the impact different disturbances have on the hydro-thermal regime of permafrost and its interactions with deciduous larch forest on a mid-term temporal scale (30 years, until 2050). We investigate the complex interplay between forest disturbances, permafrost degradation, and changing ecological factors which control larch forest stand recovery and permafrost dynamics to understand how certain disturbances, in combination with projected changing climatic conditions, can push this tightly coupled system out of balance.

The main objectives of this study are

1. to demonstrate the capabilities of a coupled, dynamic multilayer forestpermafrost model to simulate the interplay within the highly sensitive system formed by dynamic boreal larch forest and permafrost
2. to investigate which disturbances and intensities occur in our study region and under which climatic circumstances they trigger the tightly coupled system to get out of balance, and
3. to study if, when and how the thermal and hydrological conditions of the underlying permafrost and the larch forest cover itself can reach a new state.

## 2 Materials and Methods

### 2.1 Study region

We used a site previously used for model validation at the southern margin of continuous permafrost to evaluate the permafrost's resilience towards forest disturbance scenarios. Our study site Spasskaya Pad (SPA) is located at N 62.14°, E 129.37°, about 20 km north of Yakutsk, on the western side of the central Lena river, at an elevation of 237 ma.s.l. (Maximov et al., 2019). The region is underlain by continuous permafrost and the majority of the forested area is dominated by the deciduous species Dahurian larch *Larix gemelinii* ($89-90\%$), while 6% are covered by Scots pine *Pinus sylvestris*, which prefer sandier soils. The rest of the area is vegetated by the willow birch, a successful early-successor after forest disturbances. Especially after disturbances, deciduous species such as Alnus or Betula can also grow in the forest stands. Average tree height is 18 m, with dense understory vegetation such as *Vaccinium vitis-idaea* growing 0.05 m tall. Sugimoto et al. (2002) report a stem density of 836 stemsperha and a basal area of 27.12 $m^2 ha^{-1}$ for larch. Leaf-out of deciduous larch taxa has been observed in mid-May, with a growing period until late August. Topography is quite flat with an incline of 1.6 towards the north-east. Mean annual air temperature reaches $-5.97\,^\circ$ C, with an average of $-12.7\,^\circ$ C during the snow-covered and $13.7\,^\circ$ C during the snow-free periods. Liquid precipitation adds up to around 170 mm and solid precipitation to 84 mm (Simmons et al., 2007). In very dry and harsh conditions, larch trees restrict growth and photosynthetic capacity, by using water efficiently through stomata closure regulation (Baldocchi et al., 2004). Additionally, they can use snow and ground ice melt water from the seasonally thawing frozen ground (Kelliher et al., 1998). Therefore their physiological conditions are closely linked to the soil moisture dynamics. Active layer thickness is typically 1.0−1.4 m under larch forest. The ecological optimum of Siberian larch species is far from the cold climate and frozen soils but in the milder climatic conditions they are outcompeted by stronger competitors such as evergreen spruce or pine, and thus pushed out to the less favourable sites, first of all to the north (Abaimov et al., 1998). Their main rooting mass (80%) is concentrated in the upper, 0.3 m deep soil layer (Stuenzi, Boike, Cable, et al.,

2021; Stuenzi, Boike, Gädeke, et al., 2021). On warmed up and well drained plots the roots of *Larix gemelinii* can penetrate to the depth of 0.8−1 m. Under optimal ecological conditions the tallest trees of *Larix gemelinii* can reach the height of 35−40 m (Abaimov et al., 1998).

### 2.2 Forest disturbance scenarios

In the following, different disturbances occurring in boreal forests are introduced. Based on impact size and frequency we focus on two main disturbance classes: forestry and fire (see Fig. 1). We further specify different intensity classes based on literature values on mortality and defoliation, organic and litter layer damage, and a change in surface albedo (Kirichenko et al., 2009; Shvidenko & Nilsson, 2000; Averensky et al., 2010; Narita et al., 2020).

A relevant factor in the development of boreal forests is the importance of logging. In Yakutia, the forestry industry started recovering around 2000 after a sharp reduction between 1990 and 2000. In 2015, $1'000'000\,m^3$ of wood have been sold (Narita et al., 2020). Low-developed transport infrastructure and remoteness of the foreign and domestic markets hinder large-scale timber production in the Sakha republic, which is therefore not of importance to the republics economy and only accounts for roughly 1% of the exports. Accordingly, 97% of the harvested wood goes to the domestic market (Oleg Tomshin, personal communication, October 31, 2017). Based on this, it is assumed that logging does not account for a substantial part of the regions forest loss, but accessible forest stands in the vicinity of settlements and roads are prone to small- and large scale deforestation. We divide logging into three classes of intensity from a thinning where a quarter of trees are removed to a clear cut with 100% tree removal.

The most prominent disturbance in terms of area size and occurrences are forest fires. In Yakutia, the annual average fire area between 2015 and 2018 was estimated to $10'405\,km^2$ (Narita et al., 2020). Forest fires are the largest cause of forest loss or forest destruction in eastern Siberia. Fires are caused by dry thunderstorms, and human factors such as agricultural burning. The causes of ignition are hard to backtrack but it is assumed that around 70% of fires are anthropogenic (Takahashi, 2006). Larch are generally well adapted to wildfires and protected by their thick bark. Additionally, larch drop low-hanging branches which limits the chances of a fire spreading into the canopy. Finally, the low canopy closure additionally lowers the chance of high severity canopy fires (Schulze et al., 2012). There are different types of fires, which are classified into the two categories, surface and canopy fires. Most common are surface fires which are quick and result in a low energy output. They do not necessarily harm living trees, and are therefore rather nondestructive with mortality rates from 12 to 50%. Nevertheless they have a large effect on the forest development especially by reducing the organic and litter layers and impacting the surface albedo. In a study using artificial fires at SPA the canopy photosynthesis was not affected the year after a surface fire, but the mortality was increased for the following years (Takahashi, 2006). Tree die-back is increased for up to 5 years and mortality for up to 10 years (Shvidenko & Nilsson, 2000). Less common but more destructive are canopy fires, consuming most trees, including their crowns, and leading to mortality's between 60 and 100%. The variation in the mortality caused by forest fires is very high. Therefore, we use 6 different categories, making a distinction between surface and canopy fires and intensities. A low intensity surface fire causes the forest to go through natural thinning, where the smallest and weakest, or pre-damaged trees die. After a medium intensity fire the seeds of some trees survive and can trigger the regeneration of the coniferous forest. After a high intensity crown fire the trees are killed and dry out, resulting in high fuel accumulation, and widespread degradation (Shvidenko & Nilsson, 2000). The long-term effects of fire on the soil thermal regime are poorly understood. It is speculated that the organic layer is fully reestablished after 10-25 years (Bonan & Shugart, 1989). Wildfires elevate albedo through different mechanisms such

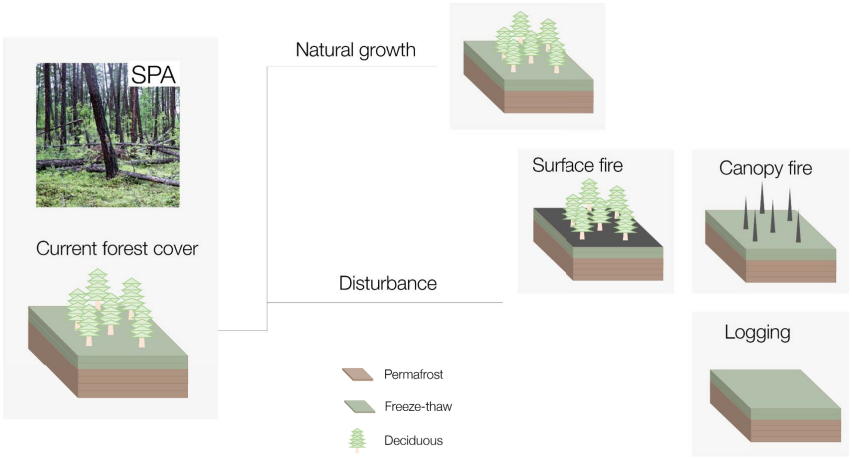


Figure 1: Left: Photograph and schematic illustration of the current forest cover at the study site, SPA. Right: Different development trajectories and their impact on the ecosystem including natural growth without any external disruptions, and the main disturbances, logging and fires (surface and canopy).

as the exposure of the previously shielded forest floor, an elevated snow season albedo due to a (partly) missing forest canopy, and the dominance of early-succession species such as birch or aspen with a higher albedo than needleleaf (Randerson et al., 2006; Stuenzi & Schaepman Strub, 2020). Jin et al. (2012) found that the higher spring albedo and large albedo increases in areas that had burned more severely were sustained for at least 7 years after fire.

### 2.3 Coupled permafrost-vegetation model

We couple a detailed permafrost-multilayer vegetation model described in (Stuenzi, Boike, Cable, et al., 2021; Stuenzi, Boike, Gädeke, et al., 2021), based on CryoGrid (Westermann et al., 2016), to LAVESI, an individual-based larch vegetation simulator, originally described in Kruse et al. (2016).

### 2.4 CryoGrid

The permafrost model is based on a one-dimensional, numerical land surface model that simulates the thermo-hydrological regime of permafrost ground (Nitzbon et al., 2019). The thermo-hydrological regime is simulated by numerically solving the one-dimensional heat equation with ground water phase change. We use a modified nonisothermal Richards equation to solve flow in freezing soil based on the paramterization in Painter and Karra (2014). This relationship for phase partitioning of water in frozen soil shows an improved performance for unsaturated ground conditions by smoothing the thermodynamically derived relationship to eliminate jump discontinuity at freezing. The exchange of sensible and latent heat, radiation, evaporation, and condensation at the ground surface are simulated with an surface energy balance scheme based on atmospheric stability functions. In addition, the model encompasses different options to simulate the evolution of the snow cover including the Crocus snowpack scheme.

This model has previously been extended by a multilayer canopy module developed by Bonan et al. (2014) for the use in permafrost regions (see Stuenzi, Boike, Cable, et al. (2021) and Stuenzi, Boike, Gädeke, et al. (2021) for model details). The multilayer canopy model provides a comprehensive parameterization of fluxes from the ground, through the canopy up to the roughness sublayer. In an iterative manner, photosynthesis, leaf water potential, stomatal conductance, leaf temperature and leaf fluxes are calculated. This improves model performance in terms of capturing the stomatal conductance and canopy physiology, nighttime friction velocity and the diurnal radiative temperature cycle and sensible heat flux (Bonan et al., 2014, 2018). The within-canopy wind profile is calculated using above- and within-canopy coupling with a roughness sublayer (RSL) parameterization (see Bonan et al. (2018) for further detail). The canopy model has been coupled to CryoGrid by replacing its standard surface energy balance scheme while soil state variables are passed back to the forest module. The vegetation module forms the upper boundary layer of the coupled model and replaces the surface energy balance equation used for common CryoGrid representations. CryoGrid operates at a 1D spatial resolution, and a 5-min time-step. Please note that our model does not account for lateral water fluxes. These fluxes are extremely small at this dry and homogeneous study site and therefore do not play an important role in the permafrost hydrology here. It requires a minimum LAI of $0.7\,\mathrm{m^2 m^{-2}}$ and a minimum height of 1 m to set up a full canopy structure required for the radiative transfer scheme, therefore forest covers below these thresholds are considered forest cover free.

### 2.5 LAVESI

To dynamically update the vegetation cover we couple this vegetation-permafrost energy transfer model to the *Larix Vegetation Simulator* (LAVESI). LAVESI is an individual-based, spatially-explicit model that can simulate larch-dominated stand dynamics originally described in Kruse et al. (2016). The relevant processes (growth, seed production and dispersal, establishment and mortality) are incorporated and adjusted to observation data gained from field surveys and literature. LAVESI simulates the forest cover dynamics at a yearly temporal resolution. Here, we use a plot size of $1250x1250\,\mathrm{m}$. This simulated forest patch in LAVESI is coupled to the one-dimensional CryoGrid set-up by separating the study plot area into three sub-areas. The spatial variability of the forest cover is, thus, explicitly represented by an ensemble of three parallel CryoGrid instances. Stand specific state variables such as, leaf area index (LAI), plant area index (PAI), litter layer height, organic content in the organic soil layer, albedo and the soil moisture content are provided to CryoGrid by LAVESI. In exchange, LAVESI receives the yearly total plant available ground water in percent (PAW), and the maximum active layer thickness (ALT). The output generated by the three CryoGrid instances is extrapolated back to the original resolution of the environmental grid used in LAVESI with a resolution of $0.2x0.2\,\mathrm{m}$ (see Kruse et al. (2021) for additional model details). The optimum plant available water levels for growth for the simulated *Larix gmelinii* tree species is between 21.1% to 40% (Sato et al., 2010). When actual levels fall below 15% or exceed 60%, trees get a growth penalty of 10% and with this a higher mortality rate. Further LAVESI parameters are provided in the original descriptions in Kruse et al. (2016), Kruse et al. (2018) and Kruse et al. (2021). Newly introduced parameters are provided in Table A2.

### 2.6 Model simulations

We use this coupled, dynamic vegetation-permafrost model to study permafrost conditions under natural, disturbance-driven and climate change induced forest cover dynamics. We run model simulations for disturbance scenarios under two different climate scenarios at a typical, larch-dominated forest patch at our study site SPA. Additionally, we run reference simulations without any disturbances (see Fig. 2). Based on the most

common disturbances and their impact on the vegetation in terms of increased mortality or defoliation, we simulate a variety of forest stand scenarios to understand threshold values in the forest-permafrost dynamics. We implemented the disturbance scenarios at a fixed date in 2020. Tables A1, A3, and A5 summarize the ground and vegetation parameter setups. Table A4 summarizes all constants used.

The disturbance scenarios are implemented in LAVESI at the export stage where data is compiled for CryoGrid. For all scenarios we split the total simulated area into three equally-sized subareas to represent the three scenario intensities (see Fig. 2). For each, LAVESI aggregates the necessary output to call CryoGrid. Leaf area index (LAI), stem area index (SAI), the 75-percentile tree height, and litter layer height are exported. Additionally, the other state variables (albedo and organic content) are set based on literature values as detailed in the following and visualized in Fig. 2. In the natural growth scenario there is no increased mortality or defoliation, and no litter layer damage. Albedo is set to the standard value of 0.15, the organic layer is undamaged. In the logging scenario, trees are removed randomly with a probability of 25% (subarea 2.1), 50% (2.2) and 100% (2.3). There is no additional defoliation and no litter layer damage, albedo is at the standard value of 0.15, and the organic layer is undamaged. In the surface fire scenario trees are removed randomly with a probability of 12% (3.1), 20% (3.2) and 50% (3.3) (Shvidenko & Nilsson, 2000). Albedo is set to the increased value of 0.4 for a total of 7 years (Jin et al., 2012). The organic layer is reduced to 10% (3.2), and completely removed (3.3), growing back linearly within 10 years (Bonan & Shugart, 1989). For the crown fire scenario, trees are removed randomly with a probability of 60% (4.1), 75% (4.2) and 100% (4.3) (Shvidenko & Nilsson, 2000). Trees are additionally completely defoliated (Shvidenko & Nilsson, 2000). Albedo is set to 0.4, coming back to the standard value of 0.15 after 7 years (Jin et al., 2012). The organic layer thickness is reduced to 10% (4.1) and completely removed in the other subareas (4.2 and 4.3), growing back linearly within 10 years (Bonan & Shugart, 1989).

### 2.7 Meteorological forcing data

The meteorological forcing data used by CryoGrid (air temperature, air pressure, wind speed, relative humidity, solid and liquid precipitation, incoming long- and shortwave radiation, and cloud cover) are obtained from ERA-5 (ECMWF Reanalysis) extracted for the site (N 62.14°, E 129.37°) at a 1-hourly time-step (Hersbach et al., 2018). Scenario data from the MPI-ESM1.2-HR model of the Max Planck Institute for Meteorology (Müller et al., 2018) was then applied as 6-year monthly mean anomalies relative to the reference period 2015-2020 to the ERA5 data to generate forcing data for the projected time span 2021-2050 and the two climate change scenarios (SSP - Shared Socioeconomic Pathways, SSP1-2.6 and SSP5-8.5) (Koven et al., 2015). The MPI-ESM1.2-HR (with a spatial resolution of 0.94 ° EW x 0.94 ° NS or approx. 100 km) model grid was interpolated to fit the ERA-5 grid. Temperature threshold for snow vs. rain is 0 ° C, and minimum wind speed is set to the minimum value within the reference time frame (2015-2020). We perform model simulations until 2050 under two projected climate change scenarios (SSP - Shared Socioeconomic Pathways) SSP1-2.6 (atmospheric CO2 around 420 parts per million (ppm) and global temperatures 1.3 to 1.9 ° C above pre-industrial levels by 2100), and SSP5-8.5 (atmospheric CO2 around 935 parts per million (ppm) and global temperatures 4 - 6.1 ° C above pre-industrial levels by 2100). From the same data the necessary forcing data of monthly mean temperature and precipitation sums for LAVESI were aggregated and 6-hourly wind speed and direction were sampled. Prior to the ERA-5 time period (0-1978) we use the monthly Climate Research Unit data set CRU TS 2.23 available at a 0.5° resolution (Harris et al., 2020).

manuscript submitted to *JGR: Biogeosciences*

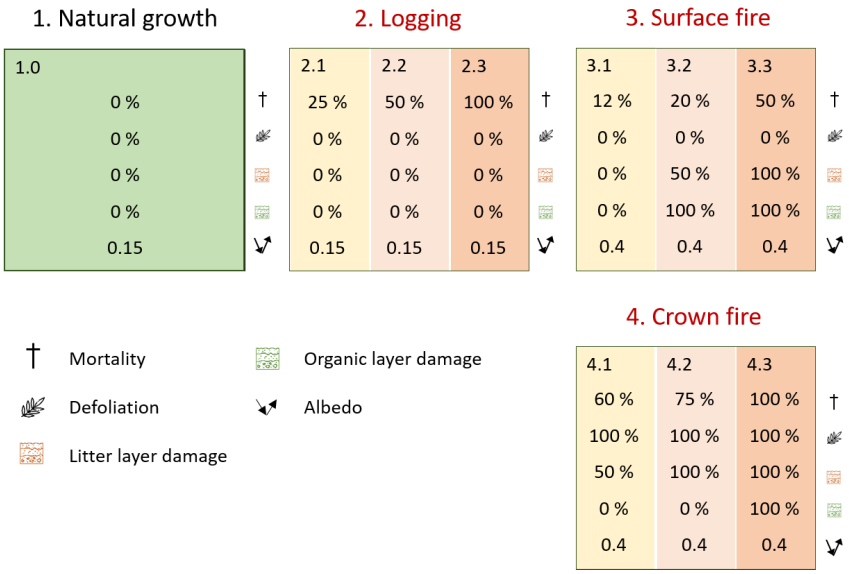


Figure 2: Schematic of the four simulations with the respective values for mortality, defoliation, change in litter layer height, existence of an organic layer and albedo change. Left: Undisturbed, natural vegetation growth. Middle/right: Implementation of the three disturbance scenarios, logging, surface fire, crown fire.

# 3 Results

We first discuss the model validation for the study site, and give an overview of the projected climatic changes. We then report on the forest stand developments under natural and disturbance-driven conditions. Lastly, we focus on the post-disturbance thydrological and thermal regimes of permafrost.

## 3.1 Model validation

The multilayer canopy-permafrost model has previously been validated against GST, radiation, snow depth, conductive heat flux, precipitation and temperature measurements for SPA in Stuenzi, Boike, Cable, et al. (2021). Site-specific LAVESI model validation for SPA is performed by comparing modeled and field-based forest density values, in number of trees (stand density). The initial parameters set in the current LAVESI model version simulated a larch forest similar to the present stands at SPA. Modeled summer LAI reached $3.56\,\mathrm{m^2 m^{-2}}$ after model spin-up which compares very well with the measured LAI value of $3.66\,\mathrm{m^2 m^{-2}}$ at SPA (Ohta et al., 2001; Sugimoto et al., 2002) (further model validation is provided in Kruse et al. (2021)). LAVESI spin-up is 2015 years before the forest cover variables are provided to CryoGrid to achieve larch forest stands that are in equilibrium with climate. For the first year of coupling (2015), CryoGrid runs for a total of 5 years, from 2010-2015, following Stuenzi, Boike, Cable, et al. (2021). This equals a spin-up period of four years before delivering ALT and PAW values for the year 2015 to LAVESI.

## 3.2 Climatic changes

The average annual air temperature projected for 2020-2050 at our study site is $-7.4\,^\circ$ C under the SSP1-2.6 scenario and $-6.4\,^\circ$ C under SSP5-8.5. Under SSP5-8.5 a maximum annual average air temperature of $-4.5\,^\circ$ C is projected for 2050 (see Fig. 3), $+2.9\,^\circ$ C above the 2021 annual average. Under SSP1-2.6 the change from 2021 to 2050 is $+1.0\,^\circ$ C. The average total yearly liquid precipitation is 487 mm under SSP1-2.6 and 401 mm under SSP5-8.5. The average total yearly solid precipitation is 196 mm under SSP1-2.6 and 186 mm under SSP5-8.5 respectively. The average total yearly precipitation (both liquid and solid) is therefore 961 mm higher under SSP1-2.6.

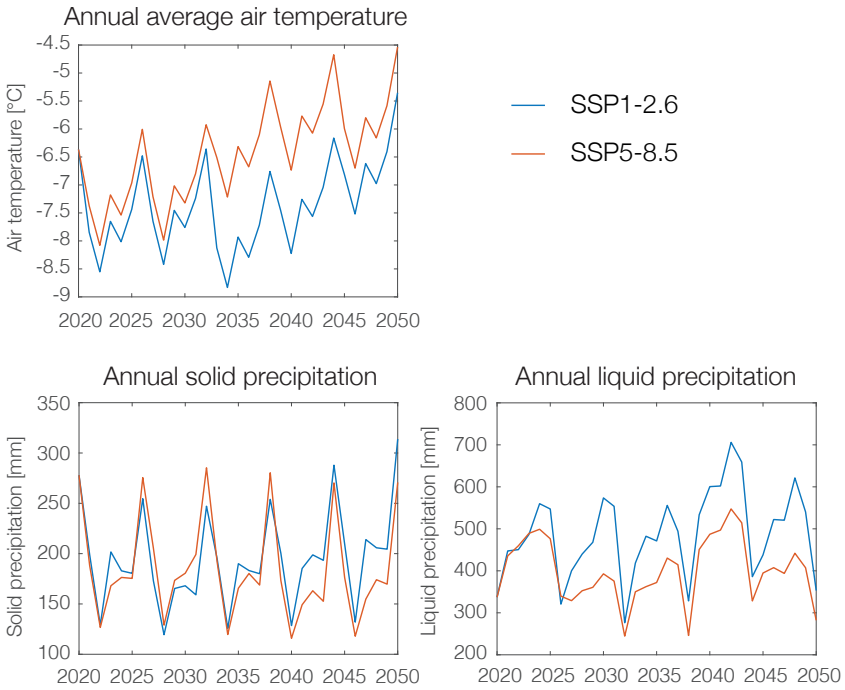


Figure 3: Comparison of the climate data forcing of SSP1-2.6 (blue) and SSP5-8.5 (red) for annual average air temperature, annual summed liquid and solid precipitation for the time period 2020-2050.

### 3.3 Forest stand development

In the natural growth scenario, where climate is the only varying factor, with yearly average temperatures rising between 1.0 and 2.9 °C, we see a very stable development of both active layer thickness (ALT) and plant available water (PAW, volumetric water content [%]). The system stays in an equilibrium state under both climate scenarios, SSP1-2.6 and 5-8.5, for the 30 years analyzed (see Fig. 4). While liquid and solid precipitation do not follow a clear trend until 2050, tree density and tree height balance out the temperature changes leaving the ALT and PAW at a constant level throughout the 30 year period. The ALT of the natural growth scenario shows the lowest variation and is 0.96 m (with a standard deviation (sd) of ±0.1) under SSP1-2.6, and 0.99 m (sd: ±0.1) under SSP5-8.5, respectively. PAW has a mean value of 17.24% (±1.3) under SSP1-2.6, and 17.03% (±1) under SSP5-8.5, also resulting in the lowest variations compared to the other scenarios. We show a decadal height decrease of −0.4 and LAI decrease of −1.2 under SSP1-2.6 climate forcing and a decadal height increase of +2 (SSP5-8.5) and LAI increase of +1.4 under SSP5-8.5. Tree density stays constant throughout the entire 30-year period analyzed. In most disturbance scenarios inducing forest loss the larch forest cover can not reestablish to pre-disturbance state within the 30 years analyzed, which will be explained in detailed in the following paragraphs on soil moisture. Under SSP5-8.5 forcing we see a faster larch density and height decrease for the logging scenario. Nevertheless, in the majority of intensity classes of the surface fire scenario we see forest densification compared to the pre-disturbance state. The surface fire disturbance results in an increasing tree height and LAI for two intensity classes under SSP1-2.6 and all three intensities under SSP5-8.5. This points out that a surface fire can have a positive effect on larch growth within the affected forest patch.

### 3.4 Post-disturbance hydrological regime of the ground

We find that a change in larch forest cover has a consistently large impact on the hydrological regime of permafrost at our study site. Under the SSP1-2.6 climate scenario the average PAW after every disturbance is lower than before with decreases from −2 to −7% (volumetric water content [%]). The largest decrease is simulated for the canopy fire scenario 4.3, where we see complete forest loss just one year post-disturbance. The loss in PAW occurs within the first year after complete forest cover loss. For the natural growth scenario PAW values of up to 20% are simulated. Under SSP5-8.5 forcing post-disturbance PAW is also lower, with decreases from −1 to −7%. The largest decrease is simulated for scenario 4 where the pre-disturbance PAW of 16% (±3) decreases to 9% (±1).

### 3.5 Post-disturbance thermal regime of the ground

Under SSP1-2.6 the average ALT after disturbance is lower than before with decreases up to −0.1 m in all scenarios. This equals an ALT decrease of −2 to −4%. The biggest decrease is simulated for the canopy fire scenario 4.3. Under SSP5-8.5 forcing the average post-disturbance ALT is higher for scenario 3 (+0.1 m) and lower for all other scenarios, with decreases up to −0.1 m. At this very dry site the latent heat content related to ground ice is small and therefore we do not see large varieties in the ALT over the studied time period. The increases in larch density following the surface fire scenario have no large impact on the ALT. The simulated differences between SSP1-2.6 and 5-8.5 are surprisingly small with ALT differences below 0.1 m.

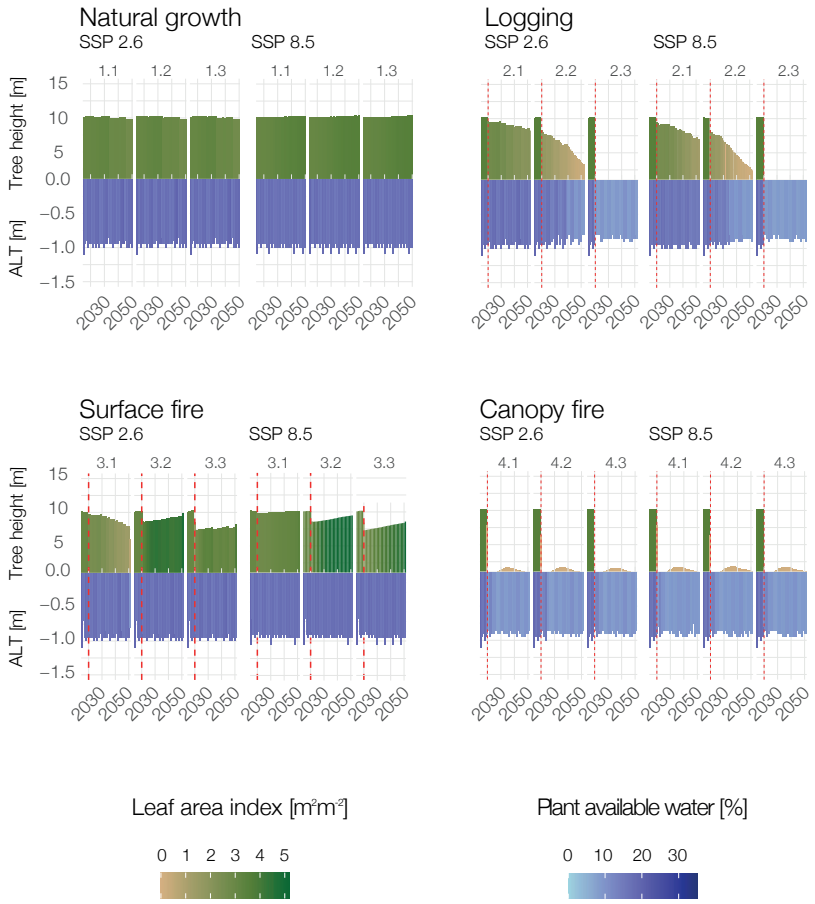


Figure 4: Active layer thickness, tree height, LAI and plant available water trajectories for the natural growth scenario, and the logging, and fire (surface and canopy) disturbances under the two climate forcing scenarios SSP2.6 and SSP8.5. Shown is the time period from 2015-2050 with the disturbance occurring in 2021 (dotted red line) followed by 29 years of recovery.

# 4 Discussion

## 4.1 Larch forest recovery and disturbances under a warming climate

Our natural growth simulations show that larch height and density play an important role in controlling the permafrost conditions underneath and maintaining the ecosystem's stable conditions. Under natural growth our model simulates a stable development under both climate scenarios until 2050. At SPA this stable trajectory was also found in a previous study by Sato et al. (2016). Larch forest is declining in some southern, drought-prone regions, while expanding at the northern treeline (i.e. Mamet et al. (2019)). In central Yakutia this trend is not visible for the studied time period. Further, we find that the plant available water (PAW) and the thawing conditions control the growth of larch forest cover. Our modeled values (ALT: 0.96−0.99 m (±0.1) and PAW: 17.03−17.24% (±1 − 1.3)) show a good agreement with measured values for SPA presented in Sato et al. (2016) where ALT under larch forest was 1.04 m and soil wetness was 20.7% in the top 0.5 m. The disturbance scenarios all lead to a change in forest cover and PAW at varying degrees. Logging and canopy fire scenarios with high mortality rates lead to a consistent loss of larch forest cover and very low PAW values. Generally, lower LAI leads to decreasing transpiration through the vegetation which can lead to a wetting of the ground (O'Donnell et al., 2011) but sandy soil offers good drainage conditions which further enhance the drying of the ground at this study site (see also i.e. Zhang et al. (2011)). In previous studies we have additionally found higher snowpacks in dense forest hence there is a higher availability of melt water in spring (Stuenzi, Boike, Cable, et al., 2021). The substantial decrease in soil moisture presented here cannot sustain constant larch forest covers nor trigger the reestablishment of pre-disturbance larch tree heights and densities. A decline in larch cover is consistent for all intensities of the logging and canopy fire scenarios. This is in agreement with the study conducted by Takahashi (2006) at Spasskaya Pad where they state a post-fire reforestation period of 30-35 years with a likely change in dominant species. We find that this is not the case in a majority of intensities of the surface fire scenario. Here, the slight decrease in forest density and average stand height is not followed by an immediate decline in plant available water. The forest cover is slowly able to recover in five out of six intensities of the surface fire scenario. Surface fire is a regular phenomenon that is important for the stability, productivity and carbon sequestration in the fire-adapted coniferous forests of Siberia. Accordingly, deciduous larch are less vulnerable to surface fires than other conifers and the ecosystem is most accustomed to this type of disruption because it is the most common disturbance (Schulze et al., 2012; Takahashi, 2006). Our simulations reveal decadal LAI increases up to +3.8 (SSP1-2.6) and +9.5 (SSP5-8.5) and height increases up to +0.9 (SSP1-2.6) and +1.5 (SSP5-8.5). This reveals that larch forests generally thrive after surface fires which could therefore be an important factor for larch forest persistence.

Interestingly, the lowest intensity surface fire implemented leads to contrasting forest cover trajectories between the two climate scenarios even though the differences in precipitation and air temperature are small for the studied period until 2050 (see Fig. 5). In scenario 3.1, the lowest intensity surface fire scenario, LAI shows a decadal trend of −4.8 (SSP1-2.6) and +1.9 (SSP5-8.5), and a tree height decadal trend of −1.8 (SSP1-2.6) and +0.4 (SSP5-8.5). Two understand how these two, very similar climate scenarios can cause such a difference in larch forest growth we need to study the different factors involved. Studying the plant available water (PAW) values exchanged between our models, we see a high sensibility of LAI towards small decreases in PAW (see Fig. 5). In scenario 3.1, PAW values under SSP1-2.6 scenario are lower than under SSP5-5.8 for a number of years starting in the year 2021, one year after the disturbance. At this point in time the LAI trajectories separate and larch forest can not recover under SSP1-2.6.

The annual sum of solid and liquid precipitation as well as the annual average air temperature for 2021 (where the LAI trajectories divide) are extremely similar. We therefore study the weekly 2021 solid and liquid precipitation patterns in more detail to un-

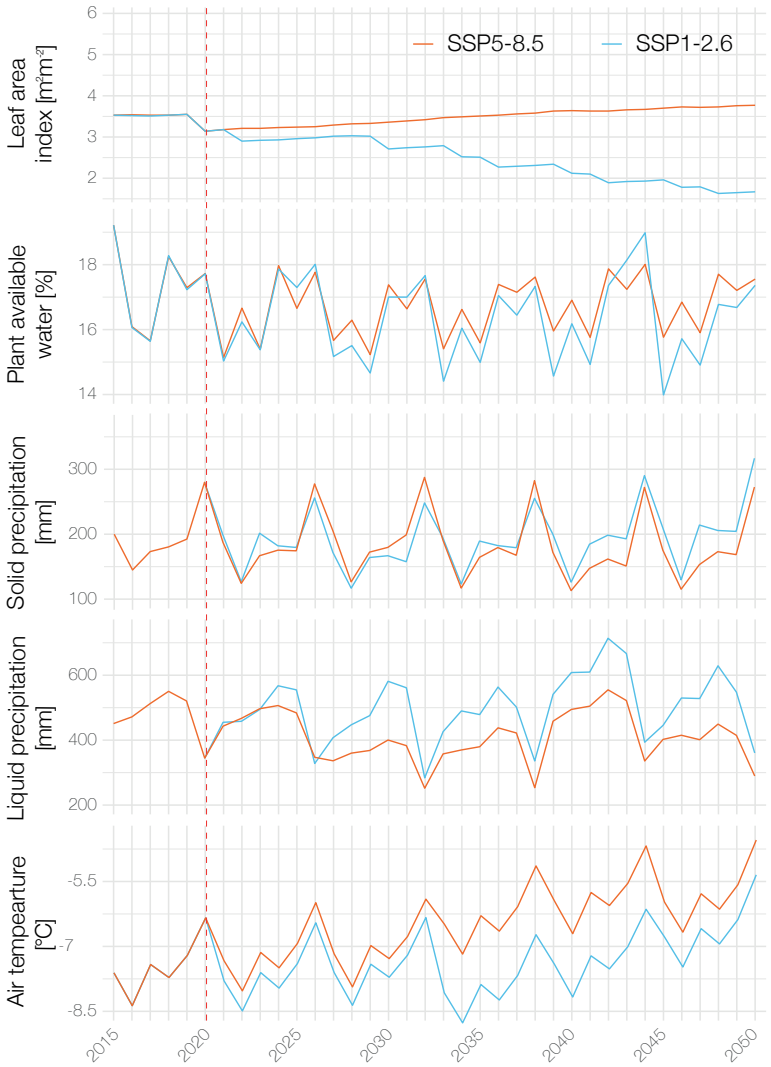


Figure 5: LAI and plant available water trajectories and the forcing for the surface fire scenario 3.1 under the two climate scenarios SSP1-2.6 and SSP5-8.5. Shown is the time period from 2015-2050 with the disturbance occurring in 2020 followed by 30 years of recovery.

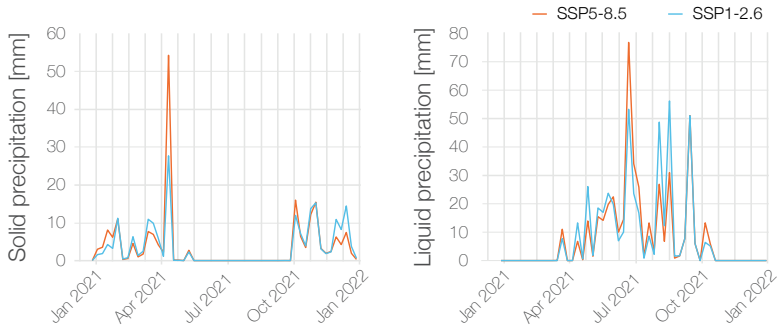


Figure 6: LAI and plant available water trajectories and the forcing for the surface fire scenario 3.1 under the two climate scenarios SSP1-2.6 and SSP5-8.5. Shown is the weekly 2021 solid (left) and liquid (right) precipitation pattern for both climate forcing scenarios.

derstand how these small differences in PAW, which eventually lead to the divergence in LAI, can be explained. Fig. 6 does reveal very different precipitation patterns between the two climate scenarios. While SSP1-2.6 shows higher solid precipitation values in December and January, the SSP5-8.5 scenario shows extremely high values of solid precipitation in late April. Similarly, under SSP5-8.5, we see an above-average intensity liquid precipitation phase mid-June, while higher liquid precipitation values occur under SSP1-2.6 in fall and early spring. So while the sum of liquid and solid precipitation show no differences between the two climate forcings, we conclude that the timing of precipitation events can define the entire larch forest recovery trajectory. As such, spring precipitation is much more important for larch forest recovery and persistence than precipitation throughout the rest of the year.

Notably, small differences in weather, such as these differences in the timing of precipitation events found here, or extreme weather events can also be dampened in a natural forest, i.e. because of bushy undergrowth which impacts snow depth, snow redistribution, lateral surface water flow, shading, etc. Nevertheless ou simulations reveal that a week of high precipitation, in combination with light disturbances in the previous year, can potentially change the trajectory of the tightly coupled forest/permafrost ecosystem. Further, it is clearly visible that LAI decreases every time PAW values reach the critical threshold of 15%. We recognize that this is a set parameter within our model setup which is highly important for the forest trajectory. This value is derived from the literature value of the lower boundaries of the optimum water availability which is 21.1% for larch as defined by (Sato et al., 2010). In both other intensities of the surface fire scenario, PAW values are very similar under both climate scenarios and LAI can recover or even surpass pre-disturbance conditions because the critical value of 15% is rarely reached. Wherever this is the case such as for the 3.3 subarea, in the years 2032 and 2044, we also see the expected 10% mortality with its related LAI decrease. We conclude that the set threshold value of 15% is highly relevant in terms of larch forest trajectories. This value should be further evaluated to make even better projections for larch forest development. Nevertheless, we see clear indications for a feedback behaviour between plant available

water and larch growth. Wherever the exact threshold value occurs in nature, drought-like states under-passing this value can trigger an unstoppable larch forest decline. Regeneration in the North is slow due to slow turnover rates and short growing seasons. Stand-replacing disturbances cause succession with a change in dominant species as reported by Takahashi (2006). A typical progression for larch-dominated ecosystems goes from deciduous needleleaf towards deciduous broadleaf to mixed deciduous and evergreen needleleaf. In our simulations we do not specifically account for the successional stage of deciduous broadleaf trees such as birch or aspen, which also have an effect on the surface energy balance of the ground. We rather study if the larch-dominated forests can return to the pre-disturbance, stable state. We show that this depends on the permafrost dynamics, mainly the hydrological conditions of the ground, and individual dry or wet years as well as on the exact timing of precipitation events. Further, we focus on the main disturbances while there are many more scenarios to be studied, among others droughts, windfall, or pests, which have also been reported to increase with climatic changes (Kharuk et al., 2021).

## 5 Conclusions

We find that ecosystem resilience towards different disturbances depends on the intensity and the type of disturbance event. We use a coupled larch dynamics permafrost model and apply different disturbance scenarios, such as surface and canopy fires, and logging. Our modeling study is in agreement with observations which show large resilience against regional, typical fire regimes, such as the surface fire scenario implemented here. In contrary, the larch forest remains severely disturbed after all other disturbances studied here. Such events usually trigger ecosystem scale changes such as total vegetation/litter layer and organic layer removal, no immediate larch forest recovery and drying up of the soil. We find that after such severe disturbances the larch forests are not recovering to pre-disturbance larch densities or return to larch dominance within the 29 years analyzed. We further find that the timing of precipitation events within the individual years after disturbances can have a deciding effect on the larch forest trajectory. This points at a threshold-bound tipping behaviour to changes in plant available soil moisture.

The main findings of our study can be summarized as follows:

- We find that disturbances with high mortality rates, such as canopy fires and logging, lead to a reduction in plant available soil water by up to $-44\%$, which results in a continuous decline of larch forest cover.
- Only surface fires, the most common disturbance type, can lead to an increased larch density and constant soil moisture values over the studied time period of 29 years.
- Finally, we find that the trajectory of larch forests after disturbances is highly dependent on single years with dry spring conditions. Such years drastically change the direction of the larch forest development within the studied time period.

Here, we demonstrate the capabilities of a dynamic multilayer-forest-permafrost model in simulating the complex interactions and feedbacks between boreal forest cover, permafrost, climate and disturbances. Our study provides an overview of possible, mid-term permafrost and larch forest trajectories after a variety of disturbance scenarios which disrupt the tightly coupled ecosystem. These finding are particular to dry, larch-dominated, and permafrost-underlain larch forests in eastern Siberia. Nevertheless, our study has implications for other boreal areas such as evergreen-dominated forests because our model showcases how fragile the quasi-equilibrium between active layer thickness, plant available soil moisture and forest cover is.

## Appendix A Model parameters used and constants

Table A1: Overview of the CryoGrid parameters used.

| Process / Parameter | | Value | Unit | Source |
|---|---|---|---|---|
| Density falling snow | $\rho_{snow}$ | 80-200 | kg m$^{-3}$ | Kershaw and McCulloch (2007) |
| Albedo ground | $\alpha$ | 0.3 | - | *field measurement* |
| Roughness length | $z_0$ | 0.001 | m | *Westermann et al. (2016)* |
| Roughness length snow | $z_{0snow}$ | 0.0001 | m | *Boike et al. (2019)* |
| Geothermal heat flux | $F_{lb}$ | 0.05 | W m$^{-2}$ | Westermann et al. (2016) |
| Thermal cond. mineral soil | $k_{mineral}$ | 3.0 | W m$^{-1}$ K$^{-1}$ | Westermann et al. (2016) |
| Emissivity | $\epsilon$ | 0.99 | - | Langer et al. (2011) |
| Root depth | $D_T$ | 0.2 | m | *field measurement* |
| Evaporation depth | $D_E$ | 0.1 | m | Nitzbon et al. (2019) |
| Hydraulic conductivity | $K$ | $10^{-5}$ | m s$^{-1}$ | Boike et al. (2019) |

Table A2: Overview of the LAVESI parameters used.

| Parameter | *Larix gmelinii* | Reference |
|---|---|---|
| Minimum active layer | 20 | Abaimov et al. (1998) |
| January threshold temperature | -45C | Kruse et al. (2016, 2018, 2019) |
| Minimum soil water | 21.1 % vol. | Sato et al. (2010) |
| Mortality drought | 0.237805 | Kruse et al. (2016, 2018, 2019) |
| Rooting depth | 50 | Abaimov et al. (1998) |
| Maximum age | 609 | Kruse et al. (2016, 2018, 2019) |
| Mortality age | 8.18785 | Kruse et al. (2016, 2018, 2019) |
| Resprouting | 0.01 | Kruse et al. (2016, 2018, 2019) |

Table A3: Parameter set-up for the study site.

| Study site | Tree height (m) | Soil layer depth (Litter/Organic /Mineral) | Respective soil type | ERA-interim coordinate |
|---|---|---|---|---|
| Spasskaya | 12 | 0/0.08/0.16 | Peat/Clay/Sand | N 62.14, E 129.37 |

Table A4: Constants.

| Constants | Value | Unit |
|---|---|---|
| von Karman | 0.4 | - |
| Freezing point water (normal pres.) | 273.15 | K |
| Latent heat of vaporization | 2.501 x 10^6 | J $kg^{-1}$ |
| Molecular mass of water | 18.016 | g $mol^{-1}$ |
| Molecular mass of dry air | 28.966 | g $mol^{-1}$ |
| Specific heat dry air (const. pres.) | 1004.64 | J $kg^{-1}$ $K^{-1}$ |
| Density of fresh water | 1000 | kg $m^{-3}$ |
| Heat of fusion for water at 0 ° C | 0.334 x 10^6 | J $kg^{-1}$ |
| Thermal conductivity of water | 0.57 | W $m^{-1}$ $K^{-1}$ |
| Thermal conductivity of ice | 2.2 | W $m^{-1}$ $K^{-1}$ |
| Kinem. visc. air (0 ° C, 1013.25 hPa) | 0.0000133 | $m^2$ $s^{-1}$ |
| Sp. heat water vapor (const. pr.) | 1810 | J $kg^{-1}$ $K^{-1}$ |

Table A5: Multilayer canopy parameters for deciduous needleleaf (NDT) plant functional type.

| Parameter | Value | Unit | Source |
|---|---|---|---|
| Leaf angle dep. from spherical | 0.01 | - | Bonan (2002) |
| Leaf reflectance (VIS/NIR) | 0.07/0.35 | - | Bonan (2002) |
| Stem reflectance (VIS/NIR) | 0.16/0.39 | - | Bonan (2002) |
| Leaf transmittance (VIS/NIR) | 0.05/0.01 | - | Bonan (2002) |
| Stem transmittance (VIS/NIR) | 0.001/0.001 | - | Bonan (2002) |
| Max. carboxylation rate (25 ° C) | 43 | $\mu$mol $m^{-2}$ $s^{-1}$ | Bonan (2002) |
| Photosynthetic pathway | C3 | - | Bonan (2002) |
| Leaf emissivity | 0.98 | - | Bonan (2002) |
| Leaf dimension | 0.04 | m | Bonan (2002) |
| Roughness length | 0.055 | m | Bonan (2002) |
| Displacement height | 0.67 | m | Bonan (2002) |
| Root distribution (a/b) | 7.0/2.0 | - | Bonan (2002) |
| Min. vapor pressure deficit | 100 | Pa | Bonan (2019) |
| Plant capacitance | 2500 | mmol $H_2O$ $m^{-2}$ leaf area $MPa^{-1}$ | Bonan (2019) |
| Minimum leaf water potential | -2 | MPa | Bonan (2019) |
| Stem hydraulic conductance | 4 | mmol $H_2O$ $m^{-2}$ $s^{-1}$ leaf area $MPa^{-1}$ | Bonan (2019) |
| Atmospheric $CO_2$ | 380 | $\mu$mol $mol^{-1}$ | Bonan (2019) |
| Atmospheric $O_2$ | 209 | mmol $mol^{-1}$ | Bonan (2019) |
| Soil evaporative resistance | 3361.509 | s $m^{-1}$ | Bonan (2019) |
| Specific heat of dry-wet soil | 1396 | J $kg^{-1}$ $K^{-1}$ | Oleson et al. (2013) |
| Specific heat of fresh $H_2O$ | 4188 | J $kg^{-1}$ $K^{-1}$ | Oleson et al. (2013) |
| Specific leaf area (TOC) | 0.024 | $m^2$ $g^{-1}$ C | Bonan et al. (2018) |
| Fine root biomass | 500 | g biomass $m^{-2}$ | Bonan (2019) |
| Leaf drag coefficient | 0.25 | - | Bonan (2019) |
| Foliage clumping index | 0.7 | - | Bonan (2019) |

**Acknowledgments**

The CryoGrid code is available on Zenodo (https://doi.org/10.5281/zenodo.5119987). The source code of LAVESI is available on https://github.com/StefanKruse/LAVESI/tree/CryoGrid_multispecies and the latest commit used for the coupled simulations with scenarios is 93a9767. Hersbach, H. et al., (2018) was downloaded from the Copernicus Climate Change Service (C3S) Climate Data Store. The results contain modified Copernicus Climate Change Service information 2020. Neither the European Commission nor ECMWF is responsible for any use that may be made of the Copernicus information or data it contains.

SMS is thankful to the POLMAR graduate school, the Geo.X Young Academy and the WiNS program at the Humboldt Universitt zu Berlin for providing a supportive framework for her PhD project and helpful courses on scientific writing and project management. SMS is very grateful for the help during fieldwork in 2018 and 2019, especially for the help from Levina Sardana Nikolaevna, Alexey Nikolajewitsch Pestryakov, Lena Ushnizkaya, Luise Schulte, Frederic Brieger, Stuart Vyse, Elisbeth Dietze, Nadine Bernhard, Boris K. Biskaborn, Iuliia Shevtsova, as well as Luidmila Pestryakova and Evgeniy Zakharov. Additionally, SMS would like to thank Stephan Jacobi, Alexander Oehme, Niko Borneman, Peter Schreiber and William Cable for their help in preparing for field work and the entire PermaRisk and Sparc research groups for their ongoing support. This study has been supported by the ERC consolidator grant Glacial Legacy to Ulrike Herzschuh (no. 772852). Further, the work was supported by the Federal Ministry of Education and Research (BMBF) of Germany through a grant to Moritz Langer (no. 01LN1709A). Funding was additionally provided by the Helmholtz Association in the framework of MOSES (Modular Observation Solutions for Earth Systems). Sebastian Westermann acknowledges funding by Permafost4Life (Research Council of Norway, grant no. 301639) and ESA Permafrost_CCI (climate.esa.int/en/projects/permafrost/).

No competing interests are present.

## References

Abaimov, A. P., Lesinski, J. A., Martinsson, O., & Milyutin, L. I. (1998). *Variability and ecology of Siberian larch species* (Tech. Rep.). Swedish University of Agricultural Sciences, (SLU), Department of Silviculture. Retrieved from `https://www.osti.gov/etdeweb/servlets/purl/10147794`

Averensky, A., Chikidov, I. I., & Ermakova, Y. V. (2010). Insect Impact on Vegetation. In E. I. Troeva (Ed.), *The far north: Plant biodiversity and ecology of yakutia, plant and vegetation* (3rd ed., pp. 297–316). Springer. doi: 10.1007/978-90-481-3774-9

Baldocchi, D. D., Xu, L., & Kiang, N. (2004). How plant functional-type, weather, seasonal drought, and soil physical properties alter water and energy fluxes of an oakgrass savanna and an annual grassland. *Agricultural and Forest Meteorology*, *123*(123), 13–39. Retrieved from `https://pubs.giss.nasa.gov/docs/2004/2004{\_}Baldocchi{\_}ba03100m.pdf` doi: 10.1016/j.agrformet.2003.11.006

Boike, J., Nitzbon, J., Anders, K., Grigoriev, M., Bolshiyanov, D., Langer, M., ... Kutzbach, L. (2019). A 16-year record (2002-2017) of permafrost, active-layer, and meteorological conditions at the Samoylov Island Arctic permafrost research site, Lena River delta, northern Siberia: an opportunity to validate remote-sensing data and land surface, snow, and . *Earth Syst. Sci. Data*, *11*, 261–299. Retrieved from `https://doi.org/10.5194/essd-11-261-2019` doi: 10.5194/essd-11-261-2019

Bonan, G. B. (2002). *Ecological climatology: concepts and applications.* Cambridge, UK: Cambridge University Press.

Bonan, G. B. (2019). *Climate Change and Terrestrial Ecosystem Modeling.* Cambridge University Press. doi: 10.1017/9781107339217

Bonan, G. B., Patton, E. G., Harman, I. N., Oleson, K. W., Finnigan, J. J., Lu, Y., & Burakowski, E. A. (2018). Modeling canopy-induced turbulence in the Earth system: A unified parameterization of turbulent exchange within plant canopies and the roughness sublayer (CLM-ml v0). *Geoscientific Model Development*, *11*(4), 1467–1496. doi: 10.5194/gmd-11-1467-2018

Bonan, G. B., Pollard, D., & Thompson, S. L. (1992, oct). Effects of boreal forest vegetation on global climate. *Nature*, *359*(6397), 716–718. Retrieved from `http://www.nature.com/doifinder/10.1038/359716a0` doi: 10.1038/359716a0

Bonan, G. B., & Shugart, H. H. (1989). *Environmental Factors and Ecological Processes in Boreal Forests* (Vol. 20; Tech. Rep.). Retrieved from `https://www.annualreviews.org/doi/pdf/10.1146/annurev.es.20.110189.000245`

Bonan, G. B., Williams, M., Fisher, R. A., & Oleson, K. W. (2014). Modeling stomatal conductance in the earth system: Linking leaf water-use efficiency and water transport along the soil-plant-atmosphere continuum. *Geoscientific Model Development*, *7*(5), 2193–2222. doi: 10.5194/gmd-7-2193-2014

Carpino, O. A., Berg, A. A., Quinton, W. L., & Adams, J. R. (2018). Climate change and permafrost thaw-induced boreal forest loss in northwestern Canada. *Environmental Research Letters*, *13*. Retrieved from `https://doi.org/10.1088/1748-9326/aad74e` doi: 10.1088/1748-9326/aad74e

Chang, X., Jin, H., Zhang, Y., He, R., Luo, D., Wang, Y., ... Zhang, Q. (2015). Thermal Impacts of Boreal Forest Vegetation on Active Layer and Permafrost Soils in Northern da Xing'Anling (Hinggan) Mountains, Northeast China. *Arctic, Antarctic, and Alpine Research*, *47*(2), 267–279. Retrieved from `https://www.tandfonline.com/action/journalInformation?journalCode=uaar20` doi: 10.1657/AAAR00C-14-016

Chasmer, L., Quinton, W., Hopkinson, C., Petrone, R., & Whittington, P. (2011). Vegetation Canopy and Radiation Controls on Permafrost Plateau Evolution within the Discontinuous Permafrost Zone, Northwest Territories, Canada. *Permafrost and Periglacial Processes*, *22*(3), 199–213. doi: 10.1002/ppp.724

Chen, D., & Loboda, T. V. (2018). Surface forcing of non-stand-replacing fires in Siberian larch forests. *Environmental Research Letters*, *13*(4), 2002–2011. doi: 10.1088/1748-9326/aab443

Chen, D., Loboda, T. V., He, T., Zhang, Y., & Liang, S. (2018). Strong cooling induced by stand-replacing fires through albedo in Siberian larch forests. *Scientific Reports*, *8*(1), 1–10. doi: 10.1038/s41598-018-23253-1

Fisher, J. P., Estop-Aragonés, C., Thierry, A., Charman, D. J., Wolfe, S. A., Hartley, I. P., ... Phoenix, G. K. (2016). The influence of vegetation and soil characteristics on active-layer thickness of permafrost soils in boreal forest. *Global Change Biology*, *22*(9), 3127–3140. doi: 10.1111/gcb.13248

Harris, I., Osborn, T. J., Jones, P., & Lister, D. (2020). Version 4 of the CRU TS monthly high-resolution gridded multivariate climate dataset. *Scientific Data*, *7*(109). Retrieved from `www.nature.com/scientificdata` doi: 10.1038/s41597-020-0453-3

Helbig, M., Pappas, C., & Sonnentag, O. (2016, feb). Permafrost thaw and wildfire: Equally important drivers of boreal tree cover changes in the Taiga Plains, Canada. *Geophysical Research Letters*, *43*(4), 1598–1606. Retrieved from `http://doi.wiley.com/10.1002/2015GL067193` doi: 10.1002/2015GL067193

Hersbach, H., Bell, B., Berrisford, P., Biavati, G., Hanányi, A., Munoz Sabater, J., ... Thépaut, J.-N. (2018). *ERA5 hourly data on single levels from 1979 to present. Copernicus Climate Change Service (C3S) Climate Data Store (CDS).* doi: 10.24381/cds.adbb2d47

Holloway, J. E., Lewkowicz, A. G., Douglas, T. A., Li, X., Turetsky, M. R., Baltzer, J. L., & Jin, H. (2020). Impact of wildfire on permafrost landscapes: A review of recent advances and future prospects. *Permafrost and Periglacial Processes*, *31*(3), 371–382. doi: 10.1002/ppp.2048

Jin, Y., Randerson, J. T., Goetz, S. J., Beck, P. S., Loranty, M. M., & Goulden, M. L. (2012, mar). The influence of burn severity on postfire vegetation recovery and albedo change during early succession in North American boreal forests. *Journal of Geophysical Research: Biogeosciences*, *117*(1). doi: 10.1029/2011JG001886

Kelliher, E., Schulze, E.-D., Bauer, G., & Arneth, A. (1998). Forest-atmosphere carbon dioxide exchange in eastern Siberia. *Agricultural and Forest Meteorology*, *90*, 291–306. Retrieved from `https://www.fs.fed.us/ne/durham/4104/papers/Hollinger{\_}Kelliher{\_}1998.pdf`

Kershaw, G. P., & McCulloch, J. (2007, feb). Midwinter Snowpack Variation Across the Arctic Treeline, Churchill, Manitoba, Canada. *Arctic, Antarctic, and Alpine Research*, *39*(1), 9–15. doi: 10.1657/1523-0430(2007)39[9:MSVATA]2.0.CO;2

Kharuk, V. I., Ponomarev, E. I., Ivanova, G. A., Dvinskaya, M. L., Coogan, S. C., & Flannigan, M. D. (2021). Wildfires in the Siberian taiga. *Ambio*. doi: 10.1007/s13280-020-01490-x

Kharuk, V. I., Ranson, K. J., Petrov, I. A., Dvinskaya, M. L., Im, S. T., & Golyukov, A. S. (2019, jan). Larch (Larix dahurica Turcz) growth response to climate change in the Siberian permafrost zone. *Regional Environmental Change*, *19*(1), 233–243. doi: 10.1007/s10113-018-1401-z

Kirichenko, N. I., Baranchikov, Y. N., & Vidal, S. (2009, aug). Performance of the potentially invasive Siberian moth Dendrolimus superans sibiricus on coniferous species in Europe. *Agricultural and Forest Entomology*, *11*(3), 247–254. Retrieved from `http://doi.wiley.com/10.1111/j.1461-9563.2009.00437.x` doi: 10.1111/j.1461-9563.2009.00437.x

Koven, C. D., Schuur, E. A. G., Schädel, C., Bohn, T. J., Burke, E. J., Chen, G., ... Turetsky, M. (2015). A simplified, data-constrained approach to estimate the permafrost carbon-climate feedback. *Phil. Trans. R. Soc*, *373*(20140423). Retrieved from `http://dx.doi.org/10.1098/rsta.2014.0423` doi: 10.1098/rsta.2014.0423

Kruse, S., Gerdes, A., Kath, N. J., & Herzschuh, U. (2018). Implementing spatially explicit wind-driven seed and pollen dispersal in the individual-based larch simulation model: LAVESI-WIND 1.0. *Geosci. Model Dev*, *11*, 4451–4467. Retrieved from `https://doi.org/10.5194/gmd-11-4451-2018` doi: 10.5194/gmd-11-4451-2018

Kruse, S., Stuenzi, S. M., Boike, J., Langer, M., Gloy, J., & Herzschuh, U. (2021). Novel coupled permafrost-forest model revealing the interplay between permafrost, vegetation and climate across eastern Siberia. *Submitted to Geoscientific Model Development*.

Kruse, S., Wieczorek, M., Jeltsch, F., & Herzschuh, U. (2016). Treeline dynamics in Siberia under changing climates as inferred from an individual-based model for Larix. *Ecological Modelling*, *338*, 101–121. Retrieved from `http://dx.doi.org/10.1016/j.ecolmodel.2016.08.003` doi: 10.1016/j.ecolmodel.2016.08.003

Langer, M., Westermann, S., Muster, S., Piel, K., & Boike, J. (2011). The surface energy balance of a polygonal tundra site in northern Siberia - Part 1: Spring to fall. *Cryosphere*, *5*, 151–171. doi: 10.5194/tc-5-509-2011

Li, X. Y., Jin, H. J., Wang, H. W., Marchenko, S. S., Shan, W., Luo, D. L., ... Jia, N. (2021, feb). *Influences of forest fires on the permafrost environment: A review* (Vol. 12) (No. 1). National Climate Center. Retrieved from `www.sciencedirect.comwww.keaipublishing.com/en/journals/`

accr/https://doi.org/10.1016/j.accre.2021.01.0011674-9278/ doi: 10.1016/j.accre.2021.01.001

Loranty, M. M., Abbott, B. W., Blok, D., Douglas, T. A., Epstein, H. E., Forbes, B. C., ... Walker, D. A. (2018). Reviews and syntheses: Changing ecosystem influences on soil thermal regimes in northern high-latitude permafrost regions. *Biogeosciences*, *15*, 5287–5313. Retrieved from https://doi.org/10.5194/bg-15-5287-2018 doi: 10.5194/bg-15-5287-2018

Mamet, S. D., Brown, C. D., Trant, A. J., & Laroque, C. P. (2019, jan). Shifting global Larix distributions: Northern expansion and southern retraction as species respond to changing climate. *Journal of Biogeography*, *46*(1), 30–44. doi: 10.1111/JBI.13465

Maximov, T., Petrov, R., Iijima, Y., Hiyama, T., Ohta, T., Kotani, A., & Nakai, T. (2019). *Meteorological data at larch forest in eastern Siberia [Spasskaya Pad, 2016-2019].* Retrieved 2020-09-05, from https://ads.nipr.ac.jp/dataset/A20191107-009

Meredith, M., Sommerkorn, M., Cassotta, S., Derksen, C., Ekaykin, A., Hollowed, A., ... Schuur, E. (2019). Polar Regions. In H.-O. Pörtner et al. (Eds.), *Ipcc special report on the ocean and cryosphere in a changing climate.*

Müller, W. A., Jungclaus, J. H., Mauritsen, T., Baehr, J., Bittner, M., Budich, R., ... Marotzke, J. (2018). A Higher-resolution Version of the Max Planck Institute Earth System Model (MPI-ESM1.2-HR). *Journal of Advances in Modeling Earth Systems*, *10*, 1383–1413. Retrieved from https://doi.org/10.1029/2017MS001217 doi: 10.1029/2017MS001217

Narita, D., Gavrilyeva, T., & Isaev, A. (2020). Impacts and management of forest fires in the Republic of Sakha, Russia: A local perspective for a global problem. *Polar Science*. Retrieved from https://doi.org/10.1016/j.polar.2020.100573 doi: 10.1016/j.polar.2020.100573

Nitzbon, J., Langer, M., Westermann, S., Martin, L., Aas, K. S., & Boike, J. (2019). Pathways of ice-wedge degradation in polygonal tundra under different hydrological conditions. *Cryosphere*, *13*(4), 1089–1123. doi: 10.5194/tc-13-1089-2019

O'Donnell, J. A., Harden, J. W., McGuire, A. D., & Romanovsky, V. E. (2011). Exploring the sensitivity of soil carbon dynamics to climate change, fire disturbance and permafrost thaw in a black spruce ecosystem. *Biogeosciences*, *8*(5), 1367–1382. Retrieved from www.biogeosciences.net/8/1367/2011/ doi: 10.5194/bg-8-1367-2011

Ohta, T., Hiyama, T., Tanaka, H., Kuwada, T., Maximov, T. C., Ohata, T., & Fukushima, Y. (2001). Seasonal variation in the energy and water exchanges above and below a larch forest in eastern Siberia. *Hydrological Processes*, *15*(8), 1459–1476. doi: 10.1002/hyp.219

Oleson, K. W., Lead, D. M. L., Bonan, G. B., Drewniak, B., Huang, M., Koven, C. D., ... Yang, Z.-L. (2013). *Technical description of version 4.5 of the Community Land Model (CLM) (No. NCAR/TN-503+STR)* (Tech. Rep.). doi: 10.5065/D6RR1W7M

Painter, S. L., & Karra, S. (2014). Constitutive Model for Unfrozen Water Content in Subfreezing Unsaturated Soils. *Vadose Zone Journal*, *13*(4), vzj2013.04.0071. doi: 10.2136/vzj2013.04.0071

Randerson, J. T., Liu, H., Flanner, M. G., Chambers, S. D., Jin, Y., Hess, P. G., ... Zender, C. S. (2006). The Impact of Boreal Forest Fire on Climate Warming. *Science*, *314*. Retrieved from https://www.ess.uci.edu/sites/default/files/pictures/Science-2006-Randerson-1130-2.pdf

Rey, D. M., Walvoord, M. A., Minsley, B. J., Ebel, B. A., Voss, C. I., & Singha, K. (2020, aug). WildfireInitiated Talik Development Exceeds Current Thaw Projections: Observations and Models From Alaska's Continuous Permafrost Zone. *Geophysical Research Letters*, *47*(15). Retrieved from

https://onlinelibrary.wiley.com/doi/10.1029/2020GL087565 doi: 10.1029/2020GL087565

Sato, H., Kobayashi, H., & Delbart, N. (2010). Simulation study of the vegetation structure and function in eastern Siberian larch forests using the individual-based vegetation model SEIB-DGVM. *Forest Ecology and Management*, *259*(3), 301–311. doi: 10.1016/j.foreco.2009.10.019

Sato, H., Kobayashi, H., Iwahana, G., & Ohta, T. (2016). Endurance of larch forest ecosystems in eastern Siberia under warming trends. *Ecology and Evolution*, *6*(16), 5690–5704. doi: 10.1002/ece3.2285

Schulze, E.-D., Wirth, C., Mollicone, D., Von, N., Upke, L. ., Ziegler, W., ... Scherbina, S. (2012). Factors promoting larch dominance in central Siberia: fire versus growth performance and implications for carbon dynamics at the boundary of evergreen and deciduous conifers. *Biogeosciences*, *9*, 1405–1421. Retrieved from www.biogeosciences.net/9/1405/2012/ doi: 10.5194/bg-9-1405-2012

Shvidenko, A. Z., & Nilsson, S. (2000). Extent, Distribution, and Ecological Role of Fire in Russian Forests. In *Fire, climate change, and carbon cycling in the boreal forest* (pp. 132–150). Springer, New York, NY. Retrieved from https://link.springer.com/chapter/10.1007/978-0-387-21629-4{_}8 doi: 10.1007/978-0-387-21629-4_8

Simmons, A., Uppala, S., Dee, D., & Kobayashi, S. (2007). *ERA-Interim: New ECMWF reanalysis 20 products from 1989 onwards* (Tech. Rep.). ECMWF Newsletter, 110. Retrieved from https://www.ecmwf.int/sites/default/files/elibrary/2007/17713-era-interim-new-ecmwf-reanalysis-products-1989-onwards.pdf doi: 10.21957/pocnex23c6

Soja, A. J., Cofer, W. R., Shugart, H. H., Sukhinin, A. I., Stackhouse, P. W., McRae, D. J., & Conard, S. G. (2004, jul). Estimating fire emissions and disparities in boreal Siberia (1998-2002). *Journal of Geophysical Research D: Atmospheres*, *109*(14). doi: 10.1029/2004JD004570

Stuenzi, S. M., Boike, J., Cable, W., Herzschuh, U., Kruse, S., Pestryakova, L. A., ... Langer, M. (2021). Variability of the surface energy balance in permafrost-underlain boreal forest. *Biogeosciences*, *18*, 343–365. Retrieved from https://doi.org/10.5194/bg-18-343-2021 doi: 10.5194/bg-18-343-2021

Stuenzi, S. M., Boike, J., Gädeke, A., Herzschuh, U., Kruse, S., Pestryakova, L. A., ... Langer, M. (2021, aug). Sensitivity of ecosystem-protected permafrost under changing boreal forest structures. *Environmental Research Letters*, *16*(8), 084045. Retrieved from https://iopscience.iop.org/article/10.1088/1748-9326/ac153dhttps://iopscience.iop.org/article/10.1088/1748-9326/ac153d/meta doi: 10.1088/1748-9326/AC153D

Stuenzi, S. M., & Schaepman Strub, G. (2020, apr). Vegetation Trajectories and Shortwave Radiative Forcing following Boreal Forest Disturbance in Eastern Siberia. *Journal of Geophysical Research: Biogeosciences*. doi: 10.1029/2019jg005395

Sugimoto, A., Yanagisawa, N., Naito, D., Fujita, N., & Maximov, T. C. (2002, jul). Importance of permafrost as a source of water for plants in east Siberian taiga. *Ecological Research*, *17*(4), 493–503. Retrieved from http://doi.wiley.com/10.1046/j.1440-1703.2002.00506.x doi: 10.1046/j.1440-1703.2002.00506.x

Takahashi, K. (2006). Future perspective of forest management in a Siberian permafrost area. *Symptom of Environmental Change in Siberian Permafrost*, 163–170. Retrieved from http://www.agr.hokudai.ac.jp/env/ctc{_}siberia/pdf{_}book/18{_}Takahashi.pdf

Tchebakova, N. M., Parfenova, E., & Soja, A. J. (2009). The effects of climate, permafrost and fire on vegetation change in Siberia in a changing climate. *Environmental Research Letters*, *4*(4). doi: 10.1088/1748-9326/4/4/045013

Ulrich, M., Matthes, H., Schirrmeister, L., Schütze, J., Park, H., Iijima, Y.,

& Fedorov, A. N. (2017, feb). Differences in behavior and distribution of permafrost-related lakes in Central Yakutia and their response to climatic drivers. *Water Resources Research*, *53*(2), 1167–1188. doi: 10.1002/2016WR019267

Westermann, S., Langer, M., Boike, J., Heikenfeld, M., Peter, M., Etzelmüller, B., & Krinner, G. (2016). Simulating the thermal regime and thaw processes of ice-rich permafrost ground with the land-surface model CryoGrid 3. *Geoscientific Model Development*, *9*(2), 523–546. doi: 10.5194/gmd-9-523-2016

Xiaodong, Y., & Shugart, H. H. (2005, aug). FAREAST: a forest gap model to simulate dynamics and patterns of eastern Eurasian forests. *Journal of Biogeography*, *32*(9), 1641–1658. Retrieved from `http://doi.wiley.com/10.1111/j.1365-2699.2005.01293.x` doi: 10.1111/j.1365-2699.2005.01293.x

Yershov, E. (2004). *General Geocryology* (P. J. Williams, Ed.). Cambridge University Press. Retrieved from `https://babibokony.mypaperypaper.icu/general-geocryology-book-1381mu.php`

Yi, S., Woo, M.-k., & Arain, M. A. (2007, aug). Impacts of peat and vegetation on permafrost degradation under climate warming. *Geophysical Research Letters*, *34*(16). Retrieved from `http://doi.wiley.com/10.1029/2007GL030550` doi: 10.1029/2007GL030550

Zhang, N., Shugart, H. H., & Yan, X. (2009, aug). Simulating the effects of climate changes on Eastern Eurasia forests. *Climatic Change*, *95*(3-4), 341–361. doi: 10.1007/s10584-009-9568-4

Zhang, N., Yasunari, T., & Ohta, T. (2011). Dynamics of the larch taiga-permafrost coupled system in Siberia under climate change. *Environmental Research Letters*, *6*(2). doi: 10.1088/1748-9326/6/2/024003

# Bibliography


Abaimov, A. P., J. A. Lesinski, O. Martinsson, and L. I. Milyutin, Variability and ecology of Siberian larch species, *Tech. rep.*, Swedish University of Agricultural Sciences, (SLU), Department of Silviculture, 1998.

Achard, F., D. Mollicone, H.-J. Stibig, D. Aksenov, L. Laestadius, Z. Li, P. Popatov, and A. Yaroshenko, Areas of rapid forest-cover change in boreal Eurasia, *Forest Ecology and Management*, *237*(1-3), 322–334, https://doi.org/10.1016/j.foreco.2006.09.080, 2006.

ACIA, *Arctic Climate Impact Assessment. ACIA overview report*, 1020 pp. pp., 2005.

AMAP, *Arctic Monitoring and Assessment Program 2011: Mercury in the Arctic*, 1–210 pp., https://doi.org/10.1017/CBO9781107415324.004, 2011.

AsiaFlux, Yakutsk Spasskaya Pad larch forest data (Site Code: YLF), 2017.

Averensky, A., I. I. Chikidov, and Y. V. Ermakova, Insect Impact on Vegetation, in *The Far North: Plant Biodiversity and Ecology of Yakutia, Plant and Vegetation*, edited by E. I. Troeva, 3 ed., chap. 5, pp. 297–316, Springer, https://doi.org/10.1007/978-90-481-3774-9, 2010.

Baldocchi, D. D., L. Xu, and N. Kiang, How plant functional-type, weather, seasonal drought, and soil physical properties alter water and energy fluxes of an oak–grass savanna and an annual grassland, *Agricultural and Forest Meteorology*, *123*(123), 13–39, https://doi.org/10.1016/j.agrformet.2003.11.006, 2004.

Balisky, A. C., and P. J. Burton, Distinction of soil thermal regimes under various experimental vegetation covers, *Canadian Journal of Soil Science*, *73*, 411–420, https://doi.org/10.4141/CJSS93043, 1993.

Baltzer, J. L., T. Veness, L. E. Chasmer, A. E. Sniderhan, and W. L. Quinton, Forests on thawing permafrost: fragmentation, edge effects, and net forest loss, *Global Change Biology*, *20*(3), 824–834, https://doi.org/10.1111/GCB.12349, 2014.

Beer, C., W. Lucht, D. Gerten, K. Thonicke, and C. Schmullius, Effects of soil freezing and thawing on vegetation carbon density in Siberia: A modeling analysis with the Lund-Potsdam-Jena Dynamic Global Vegetation Model (LPJ-DGVM), *Global Biochemical Cycles*, *21*, https://doi.org/10.1029/2006GB002760, 2007.

Betts, R. A., Offset of the potential carbon sink from boreal forestation by decreases in surface albedo, *Nature*, *408*(6809), 187–190, https://doi.org/10.1038/35041545, 2000.

Biskaborn, B. K., et al., Permafrost is warming at a global scale, *Nature Communications*, *10*(1), 1–11, https://doi.org/10.1038/s41467-018-08240-4, 2019.

Blyth, E. M., et al., Advances in Land Surface Modelling, *Current Climate Change Reports*, *7*, 45–71, https://doi.org/10.1007/s40641-021-00171-5/Published, 2021.

Boike, J., T. Grau, B. Heim, F. Günther, M. Langer, S. Muster, I. Gouttevin, and S. Lange, Satellite-derived changes in the permafrost landscape of central Yakutia, 2000-2011: Wetting, drying, and fires, *Global and Planetary Change*, *139*, 116–127, https://doi.org/10.1016/j.gloplacha.2016.01.001, 2016.

Boike, J., et al., Baseline characteristics of climate, permafrost and land cover from a new permafrost observatory in the Lena River Delta, Siberia (1998-2011), *Biogeosciences*, *10*(3), 2105–2128, https://doi.org/10.5194/bg-10-2105-2013, 2013.

Boike, J., et al., A 16-year record (2002-2017) of permafrost, active-layer, and meteorological conditions at the Samoylov Island Arctic permafrost research site, Lena River delta, northern Siberia: an opportunity to validate remote-sensing data and land surface, snow, and , *Earth Syst. Sci. Data*, *11*, 261–299, https://doi.org/10.5194/essd-11-261-2019, 2019.

Boike, J., et al., Standardized monitoring of permafrost thaw: a user-friendly, multi-parameter protocol, *Arctic Science*, *8*, https://doi.org/10.1139/as-2021-0007, 2021.

Bonan, G. B., *Ecological climatology: concepts and applications*, 678 pp., Cambridge University Press, Cambridge, UK, https://doi.org/10.1017/CBO9781107339200, 2002.

Bonan, G. B., Forests and Climate Change: Forcings, Feedbacks, and the Climate Benefits of Forests, *Science*, *320*(5882), 1444–1449, https://doi.org/10.1126/science.1155121, 2008.

Bonan, G. B., *Climate Change and Terrestrial Ecosystem Modeling*, Cambridge University Press, https://doi.org/10.1017/9781107339217, 2019.

Bonan, G. B., and H. H. Shugart, Environmental Factors and Ecological Processes in Boreal Forests, *Annu. Rev. Ecol. Syst*, *20*, 1–28, https://doi.org/10.1146/annurev.es.20.110189.000245, 1989.

Bonan, G. B., D. Pollard, and S. L. Thompson, Effects of boreal forest vegetation on global climate, *Nature*, *359*(6397), 716–718, https://doi.org/10.1038/359716a0, 1992.

Bonan, G. B., S. Levis, L. Kergoat, and K. W. Oleson, Landscapes as patches of plant functional types: An integrating concept for climate and ecosystem models, *Global Biogeochemical Cycles*, *16*(2), 5–1–5–23, https://doi.org/10.1029/2000gb001360, 2002.

Bonan, G. B., M. Williams, R. A. Fisher, and K. W. Oleson, Modeling stomatal conductance in the earth system: Linking leaf water-use efficiency and water transport along the soil-plant-atmosphere continuum, *Geoscientific Model Development*, *7*(5), 2193–2222, https://doi.org/10.5194/gmd-7-2193-2014, 2014.

Bonan, G. B., E. G. Patton, I. N. Harman, K. W. Oleson, J. J. Finnigan, Y. Lu, and E. A. Burakowski, Modeling canopy-induced turbulence in the Earth system: A unified parameterization of turbulent exchange within plant canopies and the roughness sublayer (CLM-ml v0), *Geoscientific Model Development*, *11*(4), 1467–1496, https://doi.org/10.5194/gmd-11-1467-2018, 2018.

Bonan, G. B., E. G. Patton, J. J. Finnigan, D. D. Baldocchi, and I. N. Harman, Moving beyond the incorrect but useful paradigm : reevaluating big-leaf and multilayer plant canopies to model biosphere-atmosphere

fluxes – a review, *Agricultural and Forest Meteorology*, *306*(April), 108,435, https://doi.org/10.1016/j.agrformet.2021.108435, 2021.

Brieger, F., U. Herzschuh, L. A. Pestryakova, B. Bookhagen, E. S. Zakharov, and S. Kruse, Advances in the Derivation of Northeast Siberian Forest Metrics Using High-Resolution UAV-Based Photogrammetric Point Clouds, *Remote Sensing*, *11*(12), https://doi.org/https://doi.org/10.3390/rs11121447, 2019.

Carpino, O. A., A. A. Berg, W. L. Quinton, and J. R. Adams, Climate change and permafrost thaw-induced boreal forest loss in northwestern Canada, *Environmental Research Letters*, *13*, https://doi.org/10.1088/1748-9326/aad74e, 2018.

Chadburn, S. E., E. J. Burke, R. L. Essery, J. Boike, M. Langer, M. Heikenfeld, P. M. Cox, and P. Friedlingstein, Impact of model developments on present and future simulations of permafrost in a global land-surface model, *Cryosphere*, *9*(4), 1505–1521, https://doi.org/10.5194/tc-9-1505-2015, 2015.

Chang, X., H. Jin, Y. Zhang, R. He, D. Luo, Y. Wang, L. Lü, and Q. Zhang, Thermal Impacts of Boreal Forest Vegetation on Active Layer and Permafrost Soils in Northern da Xing'Anling (Hinggan) Mountains, Northeast China, *Arctic, Antarctic, and Alpine Research*, *47*(2), 267–279, https://doi.org/10.1657/AAAR00C-14-016, 2015.

Chapin, F. S., P. A. Matson, and P. M. Vitousek, *Principles of Terrestrial Ecosystem Ecology*, Springer New York, New York, NY, https://doi.org/10.1007/978-1-4419-9504-9, 2011.

Chapin, F. S., et al., Role of land-surface changes in arctic summer warming, *Science*, *310*(5748), 657–660, https://doi.org/10.1126/science.1117368, 2005.

Chasmer, L., W. Quinton, C. Hopkinson, R. Petrone, and P. Whittington, Vegetation Canopy and Radiation Controls on Permafrost Plateau Evolution within the Discontinuous Permafrost Zone, Northwest Territories, Canada, *Permafrost and Periglacial Processes*, *22*(3), 199–213, https://doi.org/10.1002/ppp.724, 2011.

Chen, D., and T. V. Loboda, Surface forcing of non-stand-replacing fires in Siberian larch forests, *Environmental Research Letters*, *13*(4), 2002–2011, https://doi.org/10.1088/1748-9326/aab443, 2018.

Chen, D., T. V. Loboda, A. Krylov, and P. V. Potapov, Mapping stand age dynamics of the Siberian larch forests from recent Landsat observations, *Remote Sensing of Environment*, *187*, 320–331, https://doi.org/10.1016/j.rse.2016.10.033, 2016a.

Chen, D., T. V. Loboda, T. He, Y. Zhang, and S. Liang, Strong cooling induced by stand-replacing fires through albedo in Siberian larch forests, *Scientific Reports*, *8*(1), 1–10, https://doi.org/10.1038/s41598-018-23253-1, 2018.

Chen, X., L. Vierling, D. Deering, and A. Conley, Monitoring boreal forest leaf area index across a Siberian burn chronosequence: A MODIS validation study, *International Journal of Remote Sensing*, *26*(24), 5433–5451, https://doi.org/10.1080/01431160500285142, 2005.

Chen, Y., et al., Evaluating the performance of land surface model ORCHIDEE-CAN v1.0 on water and energy flux estimation with a single- and multi-layer energy budget scheme, *Geoscientific Model Development*, *9*(9), 2951–2972, https://doi.org/10.5194/gmd-9-2951-2016, 2016b.

Copernicus Global Land Operations, Leaf Area Index (LAI) Collection, 300m, Version 1.1, Issue I 1.01, 2021.

Cosenza, P., R. Guerin, and A. Tabbagh, Relationship between thermal conductivity and water content of soils using numerical modelling, *Eur. J. Soil Sci.*, *54*, 581–588, https://doi.org/10.1046/j.1365-2389.2003.00539.x, 2003.

Dickinson, E., A. Henderson-Sellers, and J. Kennedy, Biosphere-atmosphere Transfer Scheme (BATS) Version 1e as Coupled to the NCAR Community Climate Model, *NCAR Tech. Rep. NCAR/TN-3871STR, 72*, (August), 77, https://doi.org/10.5065/D67W6959, 1993.

D'Orangeville, L., D. Houle, L. Duchesne, R. P. Phillips, Y. Bergeron, and D. Kneeshaw, Beneficial effects of climate warming on boreal tree growth may be transitory, *Nature Communications*, *9*(1), 1–10, https://doi.org/10.1038/s41467-018-05705-4, 2018.

Ekici, A., et al., Site-level model intercomparison of high latitude and high altitude soil thermal dynamics in tundra and barren landscapes, *Cryosphere*, *9*(4), 1343–1361, https://doi.org/10.5194/tc-9-1343-2015, 2015.

Esper, J., and F. H. Schweingruber, Large-scale treeline changes recorded in Siberia, *Geophysical Research Letters*, *31*(6), https://doi.org/10.1029/2003gl019178, 2004.

Esper, J., D. Frank, U. Büntgen, A. Verstege, R. Hantemirov, and A. V. Kirdyanov, Trends and uncertainties in Siberian indicators of 20th century warming, *Global Change Biology*, *16*(1), 386–398, https://doi.org/10.1111/j.1365-2486.2009.01913.x, 2010.

Estop-Aragonés, C., et al., Limited release of previously-frozen C and increased new peat formation after thaw in permafrost peatlands, *Soil Biology and Biochemistry*, *118*(December 2017), 115–129, https://doi.org/10.1016/j.soilbio.2017.12.010, 2018.

Fisher, J. P., C. Estop-Aragonés, A. Thierry, D. J. Charman, S. A. Wolfe, I. P. Hartley, J. B. Murton, M. Williams, and G. K. Phoenix, The influence of vegetation and soil characteristics on active-layer thickness of permafrost soils in boreal forest, *Global Change Biology*, *22*(9), 3127–3140, https://doi.org/10.1111/gcb.13248, 2016.

Foken, T., *Micrometeorology*, second ed., 1–306 pp., Springer Berlin Heidelberg, https://doi.org/10.1007/978-3-540-74666-9, 2017.

Fortin, V., M. Jean, R. Brown, and S. Payette, Predicting Snow Depth in a Forest-Tundra Landscape using a Conceptual Model Allowing for Snow Redistribution and Constrained by Observations from a Digital Camera, *Atmosphere-Ocean*, *53*(2), 200–211, https://doi.org/10.1080/07055900.2015.1022708, 2015.

Frieler, K., et al., Assessing the impacts of 1.5°C global warming-simulation protocol of the Inter-Sectoral Impact Model Intercomparison Project (ISIMIP2b), *Geosci. Model Dev*, *10*, 4321–4345, https://doi.org/10.5194/gmd-10-4321-2017, 2017.

Furyaev, V., E. Vaganov, N. Tchebakova, and E. Valendik, Effects of Fire and Climate on Successions and Structural Changes in The Siberian Boreal Forest, *Eurasian Journal of Forest Research*, *2*, 1–15, 2001.

Gauthier, S., P. Bernier, T. Kuuluvainen, A. Z. Shvidenko, and D. G. Schep-

aschenko, Boreal forest health and global change, *Science*, *349*(6250), 819–822, https://doi.org/10.1126/science.aaa9092, 2015.

Gorokhov, A. N., and A. N. Fedorov, Current Trends in Climate Change in Yakutia, *Geography and Natural Resources*, *39*(2), 153–161, https://doi.org/10.1134/S1875372818020087, 2018.

Grippa, M., L. Kergoat, T. Le Toan, N. M. Mognard, N. Delbart, J. L'Hermitte, and S. M. Vicente-Serrano, The impact of snow depth and snowmelt on the vegetation variability over central Siberia, *Geophysical Research Letters*, *32*(21), L21,412, https://doi.org/10.1029/2005GL024286, 2005.

Gruber, S., Derivation and analysis of a high-resolution estimate of global permafrost zonation, *The Cryosphere*, *6*, 221–233, https://doi.org/10.5194/tc-6-221-2012, 2012.

Harman, I. N., and J. J. Finnigan, Scalar Concentration Profiles in the Canopy and Roughness Sublayer, *Boundary-Layer Meteorology*, *129*, 323–351, https://doi.org/10.1007/s10546-008-9328-4, 2008.

Harris, I., P. Jones, T. Osborn, and D. Lister, Updated high-resolution grids of monthly climatic observations - the CRU TS3.10 Dataset, *International Journal of Climatology*, *34*(3), 623–642, https://doi.org/10.1002/joc.3711, 2014.

Harris, I., T. J. Osborn, P. Jones, and D. Lister, Version 4 of the CRU TS monthly high-resolution gridded multivariate climate dataset, *Scientific Data*, *7*(109), https://doi.org/10.1038/s41597-020-0453-3, 2020.

Hayasaka, and Hiroshi, Recent Vegetation Fire Incidence in Russia, *Global Environmental Research*, *15*(1), 5–13, 2011.

Helbig, M., C. Pappas, and O. Sonnentag, Permafrost thaw and wildfire: Equally important drivers of boreal tree cover changes in the Taiga Plains, Canada, *Geophysical Research Letters*, *43*(4), 1598–1606, https://doi.org/10.1002/2015GL067193, 2016.

Hersbach, H., et al., ERA5 hourly data on single levels from 1979 to present. Copernicus Climate Change Service (C3S) Climate Data Store (CDS), https://doi.org/10.24381/cds.adbb2d47, 2018.

Herzschuh, U., Legacy of the Last Glacial on the present-day distribution of deciduous versus evergreen boreal forests, *Global Ecology and Biogeography*, *29*(2), 198–206, https://doi.org/10.1111/geb.13018, 2019.

Herzschuh, U., H. J. B. Birks, T. Laepple, A. Andreev, M. Melles, and J. Brigham-Grette, Glacial legacies on interglacial vegetation at the Pliocene-Pleistocene transition in NE Asia, *Nature Communications*, *7*(May 2015), 1–11, https://doi.org/10.1038/ncomms11967, 2016.

Hiyama, T., et al., Lessons learned from more than a decade of greenhouse gas flux measurements at boreal forests in eastern Siberia and interior Alaska, *Polar Science*, *27*, 100,607, https://doi.org/10.1016/J.POLAR.2020.100607, 2021.

Hollinger, D., E. Kelliher, E.-D. Schulze, G. Bauer, and A. Arneth, Forest-atmosphere carbon dioxide exchange in eastern Siberia, *Agricultural and Forest Meteorology*, *90*, 291–306, 1998.

Holloway, J. E., A. G. Lewkowicz, T. A. Douglas, X. Li, M. R. Turetsky, J. L. Baltzer, and H. Jin, Impact of wildfire on permafrost landscapes: A review of recent advances and future prospects, *Permafrost and Periglacial Processes*, *31*(3), 371–382, https://doi.org/10.1002/ppp.2048, 2020.

Holtmeier, F. K., and G. Broll, Sensitivity and response of northern hemisphere altitudinal and polar treelines to environmental change at landscape and local scales, *Global Ecology and Biogeography*, *14*(5), 395–410, https://doi.org/10.1111/j.1466-822X.2005.00168.x, 2005.

Hugelius, G., et al., Estimated stocks of circumpolar permafrost carbon with quantified uncertainty ranges and identified data gaps, *Biogeosciences*, *11*(23), 6573–6593, https://doi.org/10.5194/bg-11-6573-2014, 2014.

IPCC, *IPCC: Climate Change 2014 Synthesis Report. Contribution of Working Groups I, II and III to the Fifth Assessment Report of the Intergovernmental Panel on Climate Change*, 151 pp., IPCC, Geneva, Switzerland, 2014.

IPCC, *Summary for Policymakers. In: IPCC Special Report on the Ocean and Cryosphere in a Changing Climate*, IPCC, 2019.

IPCC, IPCC, 2021: Climate Change 2021: The Physical Science Basis. Contribution of Working Group I to the Sixth Assessment Report of the Intergovernmental Panel on Climate Change, *Tech. rep.*, 2021.

Irrgang, C., N. Boers, M. Sonnewald, E. A. Barnes, C. Kadow, J. Staneva, and J. Saynisch-Wagner, Towards neural Earth system modelling by integrating artificial intelligence in Earth system science, *Nature Machine Intelligence 2021 3:8*, *3*(8), 667–674, https://doi.org/10.1038/s42256-021-00374-3, 2021.

Ito, A., et al., Pronounced and unavoidable impacts of low-end global warming on northern high-latitude land ecosystems, *Environmental Research Letters*, *15*(4), 044,006, https://doi.org/10.1088/1748-9326/ab702b, 2020.

Jackson, R. B., J. Canadell, J. R. Ehleringer, H. A. Mooney, O. E. Sala, and E. D. Schulze, A global analysis of root distributions for terrestrial biomes, *Oecologia*, *108*(3), 389–411, https://doi.org/10.1007/BF00333714, 1996.

Jin, Y., J. T. Randerson, S. J. Goetz, P. S. Beck, M. M. Loranty, and M. L. Goulden, The influence of burn severity on postfire vegetation recovery and albedo change during early succession in North American boreal forests, *Journal of Geophysical Research: Biogeosciences*, *117*(1), 1036, https://doi.org/10.1029/2011JG001886, 2012.

Ju, J., and J. G. Masek, The vegetation greenness trend in Canada and US Alaska from 1984-2012 Landsat data, *Remote Sensing of Environment*, *176*, 1–16, https://doi.org/10.1016/j.rse.2016.01.001, 2016.

Kajimoto, T., Root System Development of Larch Trees Growing on Siberian Permafrost, in *Permafrost Ecosystems. Ecological Studies (Analysis and Synthesis), vol. 209*, edited by A. Osawa, O. Zyryanova, Y. Matsuura, T. Kajimoto, and R. Wein, pp. 303–330, Springer, Dordrecht, https://doi.org/10.1007/978-1-4020-9693-8_16, 2010.

Kasischke, E. S., Boreal Ecosystems in the Global Carbon Cycle, pp. 19–30, https://doi.org/10.1007/978-0-387-21629-4_2, 2000.

Kershaw, G. P., and J. McCulloch, Midwinter Snowpack Variation Across the Arctic Treeline, Churchill, Manitoba, Canada, *Arctic, Antarc-*

*tic, and Alpine Research*, *39*(1), 9–15, https://doi.org/10.1657/1523-0430(2007)39[9:MSVATA]2.0.CO;2, 2007.

Kharuk, V., K. Ranson, and M. Dvinskaya, Evidence of Evergreen Conifer Invasion into Larch Dominated Forests During Recent Decades in Central Siberia, *Eurasian J. For. Res*, *10*(2), 163–171, 2007.

Kharuk, V. I., M. L. Dvinskaya, K. J. Ranson, and S. T. Im, Expansion of evergreen conifers to the larch-dominated zone and climatic trends, *Russian Journal of Ecology*, *36*(3), 164–170, https://doi.org/10.1007/s11184-005-0055-5, 2005.

Kharuk, V. I., K. J. Ranson, S. T. Im, and M. L. Dvinskaya, Response of Pinus sibirica and Larix sibirica to climate change in southern Siberian alpine forest-tundra ecotone, *Scandinavian Journal of Forest Research*, *24*(2), 130–139, https://doi.org/10.1080/02827580902845823, 2009.

Kharuk, V. I., K. J. Ranson, S. T. Im, P. A. Oskorbin, M. L. Dvinskaya, and D. V. Ovchinnikov, Tree-line structure and dynamics at the northern limit of the larch forest: Anabar Plateau, Siberia, Russia, *Arctic, Antarctic, and Alpine Research*, *45*(4), 526–537, https://doi.org/10.1657/1938-4246-45.4.526, 2013.

Kharuk, V. I., K. J. Ranson, S. T. Im, and I. A. Petrov, Climate-induced larch growth response within the central Siberian permafrost zone, *Environmental Research Letters*, *10*(12), https://doi.org/10.1088/1748-9326/10/12/125009, 2015.

Kharuk, V. I., K. J. Ranson, I. A. Petrov, M. L. Dvinskaya, S. T. Im, and A. S. Golyukov, Larch (Larix dahurica Turcz) growth response to climate change in the Siberian permafrost zone, *Regional Environmental Change*, *19*(1), 233–243, https://doi.org/10.1007/s10113-018-1401-z, 2019.

Kharuk, V. I., E. I. Ponomarev, G. A. Ivanova, M. L. Dvinskaya, S. C. Coogan, and M. D. Flannigan, Wildfires in the Siberian taiga, *Ambio*, https://doi.org/10.1007/s13280-020-01490-x, 2021.

Kirichenko, N. I., Y. N. Baranchikov, and S. Vidal, Performance of the potentially invasive Siberian moth *Dendrolimus superans sibiricus* on coniferous species in Europe, *Agricultural and Forest Entomology*, *11*(3), 247–254, https://doi.org/10.1111/j.1461-9563.2009.00437.x, 2009.

Kirillina, K., E. G. Shvetsov, V. V. Protopopova, L. Thiesmeyer, and W. Yan, Consideration of anthropogenic factors in boreal forest fire regime changes during rapid socio-economic development: case study of forestry districts with increasing burnt area in the Sakha Republic, Russia, *Environmental Research Letters*, *15*(3), 035,009, https://doi.org/10.1088/1748-9326/AB6C6E, 2020.

Kirpotin, S. N., et al., Impacts of environmental change on biodiversity and vegetation dynamics in Siberia, *Ambio*, https://doi.org/10.1007/s13280-021-01570-6, 2021.

Kobayashi, H., N. Delbart, R. Suzuki, and K. Kushida, A satellite-based method for monitoring seasonality in the overstory leaf area index of Siberian larch forest, *Journal of Geophysical Research: Biogeosciences*, *115*(1), 1–14, https://doi.org/10.1029/2009JG000939, 2010.

Kotlyakov, V., and T. Khromova, Land Resources of Russia – Maps of Permafrost and Ground Ice, Version 1, https://doi.org/https://doi.org/, 2002.

Koven, C. D., et al., A simplified, data-constrained approach to estimate the permafrost carbon-climate feedback, *Phil. Trans. R. Soc*, *373*(20140423), https://doi.org/10.1098/rsta.2014.0423, 2015.

Kropp, H., et al., Shallow soils are warmer under trees and tall shrubs across Arctic and Boreal ecosystems, *Environmental Research Letters*, *16*, https://doi.org/10.1088/1748-9326/abc994, 2021.

Kruse, S., M. Wieczorek, F. Jeltsch, and U. Herzschuh, Treeline dynamics in Siberia under changing climates as inferred from an individual-based model for Larix, *Ecological Modelling*, *338*, 101–121, https://doi.org/10.1016/j.ecolmodel.2016.08.003, 2016.

Kruse, S., A. Gerdes, N. J. Kath, and U. Herzschuh, Implementing spatially explicit wind-driven seed and pollen dispersal in the individual-based larch simulation model: LAVESI-WIND 1.0, *Geosci. Model Dev*, *11*, 4451–4467, https://doi.org/10.5194/gmd-11-4451-2018, 2018.

Kruse, S., U. Herzschuh, L. Schulte, S. M. Stuenzi, F. Brieger, E. S. Zakharov, and L. A. Pestryakova, Forest inventories on circular plots on the expedition Chukotka 2018, NE Russia, https://doi.org/10.1594/PANGAEA.923638, 2020.

Kruse, S., S. M. Stuenzi, J. Boike, M. Langer, J. Gloy, and U. Herzschuh, Novel coupled permafrost-forest model revealing the interplay between permafrost, vegetation and climate across eastern Siberia, *Submitted to Geoscientific Model Development*, https://doi.org/10.5194/gmd-2021-304, 2021.

Lange, S., EartH2Observe, WFDEI and ERA-Interim data Merged and Bias-corrected for ISIMIP (EWEMBI). V. 1.1., https://doi.org/10.5880/pik.2019.004, 2019.

Langer, M., S. Westermann, S. Muster, K. Piel, and J. Boike, The surface energy balance of a polygonal tundra site in northern Siberia - Part 2: Winter, *Cryosphere*, *5*(2), 509–524, https://doi.org/10.5194/tc-5-509-2011, 2011a.

Langer, M., S. Westermann, S. Muster, K. Piel, and J. Boike, The surface energy balance of a polygonal tundra site in northern Siberia - Part 1: Spring to fall, *Cryosphere*, *5*, 151–171, https://doi.org/10.5194/tc-5-509-2011, 2011b.

Langer, M., S. Westermann, M. Heikenfeld, W. Dorn, and J. Boike, Satellite-based modeling of permafrost temperatures in a tundra lowland landscape, *Remote Sensing of Environment*, *135*, 12–24, https://doi.org/10.1016/j.rse.2013.03.011, 2013.

Langer, M., S. Westermann, J. Boike, G. Kirillin, G. Grosse, S. Peng, and G. Krinner, Rapid degradation of permafrost underneath waterbodies in tundra landscapes—Toward a representation of thermokarst in land surface models, *Journal of Geophysical Research: Earth Surface*, *121*(12), 2446–2470, https://doi.org/10.1002/2016JF003956, 2016.

Langer, M., S. Kaiser, S. M. Stuenzi, T. Schneider Von Deimling, A. Oehme, and S. Jacobi, Soilsurface temperatures in 2 cm depth between summer 2018 and 2019 with iButton-sensors in the North Slope of Alaska (USA), around Churchill (Canada) and the region of Illirney and Lena-Viluy (Russia), https://doi.org/10.1594/PANGAEA.914327, 2020.

Lenton, T. M., H. Held, E. Kriegler, J. W. Hall, W. Lucht, S. Rahmstorf, and H. J. Schellnhuber, Tipping elements in the Earth's climate system, *Proceedings of the National Academy of Sciences*, *105*(6), 1786–1793, https://doi.org/10.1073/PNAS.0705414105, 2008.

Li, X. Y., et al., Influences of forest fires on the permafrost environment: A review, https://doi.org/10.1016/j.accre.2021.01.001, 2021.

Liu, Y., et al., Evaluation of the VIIRS BRDF, Albedo and NBAR products suite and an assessment of continuity with the long term MODIS record, *Remote Sensing of Environment*, *201*, 256–274, https://doi.org/10.1016/j.rse.2017.09.020, 2017.

Liu, Z., A. P. Ballantyne, and L. A. Cooper, Biophysical feedback of global forest fires on surface temperature, *Nature Communications*, *10*(1), 1–9, https://doi.org/10.1038/s41467-018-08237-z, 2019.

Loranty, M., S. Davydov, H. Kropp, H. Alexander, M. Mack, S. Natali, and N. Zimov, Vegetation Indices Do Not Capture Forest Cover Variation in Upland Siberian Larch Forests, *Remote Sensing*, *10*(11), 1686, https://doi.org/10.3390/rs10111686, 2018a.

Loranty, M. M., et al., Reviews and syntheses: Changing ecosystem influences on soil thermal regimes in northern high-latitude permafrost regions, *Biogeosciences*, *15*, 5287–5313, https://doi.org/10.5194/bg-15-5287-2018, 2018b.

Lucht, W., S. Schaphoff, T. Erbrecht, U. Heyder, and W. Cramer, Terrestrial vegetation redistribution and carbon balance under climate change, *Carbon Balance and Management 2006 1:1*, *1*(1), 1–7, https://doi.org/10.1186/1750-0680-1-6, 2006.

Lyons, E. A., Y. Jin, and J. T. Randerson, Changes in surface albedo after fire in boreal forest ecosystems of interior Alaska assessed using MODIS satellite observations, *Journal of Geophysical Research: Biogeosciences*, *113*(2), 1–15, https://doi.org/10.1029/2007JG000606, 2008.

Mamet, S. D., C. D. Brown, A. J. Trant, and C. P. Laroque, Shifting global Larix distributions: Northern expansion and southern retraction as species respond to changing climate, *Journal of Biogeography*, *46*(1), 30–44, https://doi.org/10.1111/JBI.13465, 2019.

Maximov, T., Spasskaya Pad Scientific Research Station, Station Information, 2015.

Maximov, T., R. Petrov, Y. Iijima, T. Hiyama, T. Ohta, A. Kotani, and T. Nakai, Meteorological data at larch forest in eastern Siberia [Spasskaya Pad, 2016-2019], 2019.

McGuire, A. D., et al., Environmental variation, vegetation distribution, carbon dynamics and water/energy exchange at high latitudes, *Journal of Vegetation Science*, *13*(3), 301–314, https://doi.org/10.1111/j.1654-1103.2002.tb02055.x, 2002.

Mekonnen, Z. A., W. J. Riley, J. T. Randerson, R. F. Grant, and B. M. Rogers, Expansion of high-latitude deciduous forests driven by interactions between climate warming and fire, *Nature Plants*, *5*(9), 952–958, https://doi.org/10.1038/s41477-019-0495-8, 2019.

Meredith, M., et al., Polar Regions, in *IPCC Special Report on the Ocean and Cryosphere in a Changing Climate*, edited by H.-O. Pörtner, D. Roberts, V. Masson-Delmotte, P. Zhai, M. Tignor, E. Poloczanska, K. Mintenbeck, A. Alegría, M. Nicolai, A. Okem, J. Petzold, B. Rama, and N. Weyer, p. In Press, 2019.

Meyer, H., T. Opel, T. Laepple, A. Y. Dereviagin, K. Hoffmann, and M. Werner, Long-term winter warming trend in the Siberian Arctic during the mid- to late Holocene, *Nature Geoscience*, *8*(2), 122–125, https://doi.org/10.1038/ngeo2349, 2015.

Monin, A. S., and A. M. Obukhov, Basic laws of turbulent mixing in the surface layer of the atmosphere, *Tr. Akad. Nauk SSSR Geophiz. Inst*, *24*(151), 163–187, 1954.

Müller, W. A., et al., A Higher-resolution Version of the Max Planck Institute Earth System Model (MPI-ESM1.2-HR), *Journal of Advances in Modeling Earth Systems*, *10*, 1383–1413, https://doi.org/10.1029/2017MS001217, 2018.

Myneni, R., et al., Global products of vegetation leaf area and fraction absorbed PAR from year one of MODIS data, *Remote Sensing of Environment*, *83*, 214–231, https://doi.org/10.1016/S0034-4257(02)00074-3, 2002.

Narita, D., T. Gavrilyeva, and A. Isaev, Impacts and management of forest fires in the Republic of Sakha, Russia: A local perspective for a global problem, *Polar Science*, https://doi.org/10.1016/j.polar.2020.100573, 2020.

Nitzbon, J., M. Langer, S. Westermann, L. Martin, K. S. Aas, and J. Boike, Pathways of ice-wedge degradation in polygonal tundra under different hydrological conditions, *Cryosphere*, *13*(4), 1089–1123, https://doi.org/10.5194/tc-13-1089-2019, 2019.

Nitzbon, J., S. Westermann, M. Langer, L. C. P. Martin, J. Strauss, S. Laboor, and J. Boike, Fast response of cold ice-rich permafrost in northeast Siberia to a warming climate, *Nature Communications*, *11*, https://doi.org/10.1038/s41467-020-15725-8, 2020.

Ochsner, T. E., T. J. Sauer, and R. Horton, Field tests of the soil heat flux plate method and some alternatives, *Agronomy Journal*, *98*(4), 1005–1014, https://doi.org/10.2134/agronj2005.0249, 2006.

O'Donnell, J. A., J. W. Harden, A. D. McGuire, and V. E. Romanovsky, Exploring the sensitivity of soil carbon dynamics to climate change, fire disturbance and permafrost thaw in a black spruce ecosystem, *Biogeosciences*, *8*(5), 1367–1382, https://doi.org/10.5194/bg-8-1367-2011, 2011.

Ohta, T., T. Hiyama, H. Tanaka, T. Kuwada, T. C. Maximov, T. Ohata, and Y. Fukushima, Seasonal variation in the energy and water exchanges above and below a larch forest in eastern Siberia, *Hydrological Processes*, *15*(8), 1459–1476, https://doi.org/10.1002/hyp.219, 2001.

Oleson, K. W., et al., Technical description of version 4.5 of the Community Land Model (CLM) (No. NCAR/TN-503+STR), *Tech. rep.*, https://doi.org/10.5065/D6RR1W7M, 2013.

Oliver, S. A., H. R. Oliver, J. S. Wallace, and A. M. Roberts, Soil heat flux and temperature variation with vegetation, soil type and climate, *Agricultural and Forest Meteorology*, *39*(2-3), 257–269, https://doi.org/10.1016/0168-1923(87)90042-6, 1987.

Painter, S. L., and S. Karra, Constitutive Model for Unfrozen Water Content in Subfreezing Unsaturated Soils, *Vadose Zone Journal*, *13*(4), vzj2013.04.0071, https://doi.org/10.2136/vzj2013.04.0071, 2014.

Pearson, R. G., S. J. Phillips, M. M. Loranty, P. S. Beck, T. Damoulas, S. J. Knight, and S. J. Goetz, Shifts in Arctic vegetation and associated

feedbacks under climate change, *Nature Climate Change*, *3*(7), 673–677, https://doi.org/10.1038/nclimate1858, 2013.

Peng, X., T. Zhang, O. W. Frauenfeld, S. Wang, L. Qiao, R. Du, and C. Mu, Northern Hemisphere Greening in Association With Warming Permafrost, *Journal of Geophysical Research: Biogeosciences*, *125*(1), 1–20, https://doi.org/10.1029/2019JG005086, 2020.

Price, A. G., Prediction of Snowmelt Rates in a Deciduous Forest, *Journal of Hydrology*, *101*, 145–157, https://doi.org/10.1016/0022-1694(88)90032-7, 1988.

R Core Team, R: A Language and Environment for Statistical Computing, 2016.

Randerson, J. T., et al., The Impact of Boreal Forest Fire on Climate Warming, *Science*, *314*, https://doi.org/10.1126/science.1132075, 2006.

Rey, D. M., M. A. Walvoord, B. J. Minsley, B. A. Ebel, C. I. Voss, and K. Singha, Wildfire-Initiated Talik Development Exceeds Current Thaw Projections: Observations and Models From Alaska's Continuous Permafrost Zone, *Geophysical Research Letters*, *47*(15), https://doi.org/10.1029/2020GL087565, 2020.

Rogers, B. M., A. J. Soja, M. L. Goulden, and J. T. Randerson, Influence of tree species on continental differences in boreal fires and climate feedbacks, *Nature Geoscience*, *8*(3), 228–234, https://doi.org/10.1038/ngeo2352, 2015.

Romanovsky, V., et al., Terrestrial Permafrost in State of the Climate in 2016, *Bull Am Meteorol Soc*, *98*(8), 147–149, https://doi.org/10.1175/2017BAMSStateoftheClimate.1, 2017.

Ryder, J., et al., A multi-layer land surface energy budget model for implicit coupling with global atmospheric simulations, *Geoscientific Model Development*, *9*(1), 223–245, https://doi.org/10.5194/gmd-9-223-2016, 2016.

Sato, H., H. Kobayashi, and N. Delbart, Simulation study of the vegetation structure and function in eastern Siberian larch forests using the individual-based vegetation model SEIB-DGVM, *Forest Ecology and Management*, *259*(3), 301–311, https://doi.org/10.1016/j.foreco.2009.10.019, 2010.

Sato, H., H. Kobayashi, G. Iwahana, and T. Ohta, Endurance of larch forest ecosystems in eastern Siberia under warming trends, *Ecology and Evolution*, *6*(16), 5690–5704, https://doi.org/10.1002/ece3.2285, 2016.

Sawada, Y., Machine Learning Accelerates Parameter Optimization and Uncertainty Assessment of a Land Surface Model, *Journal of Geophysical Research: Atmospheres*, *125*(20), https://doi.org/10.1029/2020JD032688, 2020.

Schaphoff, S., C. P. Reyer, D. Schepaschenko, D. Gerten, and A. Shvidenko, Tamm Review: Observed and projected climate change impacts on Russia's forests and its carbon balance, *Forest Ecology and Management*, *361*, 432–444, https://doi.org/10.1016/J.FORECO.2015.11.043, 2016.

Scheffer, M., M. Hirota, M. Holmgren, E. H. Van Nes, and F. S. Chapin, Thresholds for boreal biome transitions, *Proceedings of the National Academy of Sciences of the United States of America*, *109*(52), 21,384–21,389, https://doi.org/10.1073/pnas.1219844110, 2012.

Schneider Von Deimling, T., M. Meinshausen, A. Levermann, V. Huber, K. Frieler, D. M. Lawrence, and V. Brovkin, Estimating the near-surface permafrost-carbon feedback on global warming, *Biogeosciences*, *9*(2), 649–665, https://doi.org/10.5194/bg-9-649-2012, 2012.

Schulze, E.-D., et al., Factors promoting larch dominance in central Siberia: fire versus growth performance and implications for carbon dynamics at the boundary of evergreen and deciduous conifers, *Biogeosciences*, *9*, 1405–1421, https://doi.org/10.5194/bg-9-1405-2012, 2012.

Schuur, E. A. G., and M. C. Mack, Ecological Response to Permafrost Thaw and Consequences for Local and Global Ecosystem Services, *Annual Review of Ecology, Evolution, and Systematics*, *49*, 279–301, https://doi.org/https://doi.org/10.1146/annurev-ecolsys-121415-032349, 2018.

Sellers, P., D. Randall, G. Collatz, J. Berry, C. Field, D. Dazlich, C. Zhang, G. Collelo, and L. Bounoua, A revised land surface parameterization (sib2) for atmospheric gcms. part i: Model formulation, *Journal of Climate*, *9*(4), 676 – 705, https://doi.org/10.1175/1520-0442(1996)009¡0676:ARLSPF¿2.0.CO;2, 1996.

Shuman, J. K., H. H. Shugart, and T. L. O'Halloran, Sensitivity of Siberian larch forests to climate change, *Global Change Biology*, *17*(7), 2370–2384, https://doi.org/10.1111/j.1365-2486.2011.02417.x, 2011.

Shuman, J. K., N. M. Tchebakova, E. I. Parfenova, A. J. Soja, H. H. Shugart, D. Ershov, and K. Holcomb, Forest forecasting with vegetation models across Russia, *Canadian Journal of Forest Research*, *45*(2), 175–184, https://doi.org/10.1139/cjfr-2014-0138, 2014.

Shvidenko, A. Z., and S. Nilsson, Extent, Distribution, and Ecological Role of Fire in Russian Forests, in *Fire, Climate Change, and Carbon Cycling in the Boreal Forest*, pp. 132–150, Springer, New York, NY, https://doi.org/10.1007/978-0-387-21629-4_8, 2000.

Sidorova, O. V., E. A. Vaganov, M. M. Naurzbaev, V. V. Shishov, and M. K. Hughes, Regional features of the radial growth of larch in north central Siberia according to millennial tree-ring chronologies, *Russian Journal of Ecology*, *38*(2), 90–93, https://doi.org/10.1134/S106741360702004X, 2007.

Simmons, A., S. Uppala, D. Dee, and S. Kobayashi, ERA-Interim: New ECMWF reanalysis 20 products from 1989 onwards, *Tech. rep.*, https://doi.org/10.21957/pocnex23c6, 2007.

Smith, B., D. Wårlind, A. Arneth, T. Hickler, P. Leadley, J. Siltberg, and S. Zaehle, Implications of incorporating N cycling and N limitations on primary production in an individual-based dynamic vegetation model, *Biogeosciences*, *11*, https://doi.org/10.5194/bg-11-2027-2014, 2014.

Soja, A. J., W. R. Cofer, H. H. Shugart, A. I. Sukhinin, P. W. Stackhouse, D. J. McRae, and S. G. Conard, Estimating fire emissions and disparities in boreal Siberia (1998-2002), *Journal of Geophysical Research D: Atmospheres*, *109*(14), https://doi.org/10.1029/2004JD004570, 2004.

Stuenzi, S. M., and G. Schaepman-Strub, Vegetation Trajectories and Shortwave Radiative Forcing following Boreal Forest Disturbance in Eastern Siberia, *Journal of Geophysical Research: Biogeosciences*, https://doi.org/10.1029/2019jg005395, 2020.

Stuenzi, S. M., J. Boike, A. Gädeke, U. Herzschuh, S. Kruse, L. A. Pestryakova, S. Westermann, and M. Langer, Sensitivity of ecosystem-protected permafrost under changing boreal forest structures, *Environmental Research Letters*, *16*(8), 084,045, https://doi.org/10.1088/1748-9326/AC153D, 2021a.

Stuenzi, S. M., et al., Automatic weather stations and stand-alone soil temperature sensors (Hobo logger) between August 2018 and August 2019 at two boreal forest sites in the region of Lake Ilirney and Lena-Viluy in Eastern Siberia, https://doi.org/10.1594/PANGAEA.919859, 2020.

Stuenzi, S. M., et al., Variability of the surface energy balance in permafrost-underlain boreal forest, *Biogeosciences*, *18*, 343–365, https://doi.org/10.5194/bg-18-343-2021, 2021b.

Sugimoto, A., N. Yanagisawa, D. Naito, N. Fujita, and T. C. Maximov, Importance of permafrost as a source of water for plants in east Siberian taiga, *Ecological Research*, *17*(4), 493–503, https://doi.org/10.1046/j.1440-1703.2002.00506.x, 2002.

Takahashi, K., Future perspective of forest management in a Siberian permafrost area, *Symptom of Environmental Change in Siberian Permafrost*, pp. 163–170, 2006.

Tanaka, H., T. Hiyama, N. Kobayashi, H. Yabuki, Y. Ishii, R. V. Desyatkin, T. C. Maximov, and T. Ohta, Energy balance and its closure over a young larch forest in eastern Siberia, *Agricultural and Forest Meteorology*, *148*(12), 1954–1967, https://doi.org/10.1016/j.agrformet.2008.05.006, 2008.

Tchebakova, N. M., E. Parfenova, and A. J. Soja, The effects of climate, permafrost and fire on vegetation change in Siberia in a changing climate, *Environmental Research Letters*, *4*(4), https://doi.org/10.1088/1748-9326/4/4/045013, 2009.

Thomas, G., and P. R. Rowntree, The Boreal Forests and Climate, *Quarterly Journal of the Royal Meteorological Society*, *118*(505), 469–497, https://doi.org/10.1002/qj.49711850505, 1992.

Thonicke, K., S. Venevsky, S. Sitch, and W. Cramer, The role of fire disturbance for global vegetation dynamics: Coupling fire into a dynamic global vegetation model, *Global Ecology and Biogeography*, *10*(6), 661–677, https://doi.org/10.1046/J.1466-822X.2001.00175.X, 2001.

Ulrich, M., H. Matthes, L. Schirrmeister, J. Schütze, H. Park, Y. Iijima, and A. N. Fedorov, Differences in behavior and distribution of permafrost-related lakes in Central Yakutia and their response to climatic drivers, *Water Resources Research*, *53*(2), 1167–1188, https://doi.org/10.1002/2016WR019267, 2017.

Van Everdingen, R. O., Multi-Language Glossary of Permafrost and Related Ground-Ice Terms, *Tech. rep.*, The Arctic Institute of North America The University of Calgary, 1998.

van Genuchten, M. T., A Closed-form Equation for Predicting the Hydraulic Conductivity of Unsaturated Soils, *Soil Science Society of America Journal*, *44*(5), 892–898, https://doi.org/10.2136/sssaj1980.03615995004400050002x, 1980.

Vionnet, V., E. Brun, S. Morin, A. Boone, S. Faroux, P. Le Moigne, E. Martin, and J.-M. Willemet, The detailed snowpack scheme Crocus and its implementation in SURFEX v7.2, *Geoscientific Model Development*, *5*, 773–791, https://doi.org/10.5194/gmd-5-773-2012, 2012.

Virkkala, A. M., et al., Statistical upscaling of ecosystem CO2 fluxes across the terrestrial tundra and boreal domain: Regional patterns and uncertainties, *Global Change Biology*, *27*(17), 4040–4059, https://doi.org/10.1111/GCB.15659, 2021.

Vitt, D. H., L. A. Halsey, I. E. Bauer, and C. Campbell, Spatial and temporal trends in carbon storage of peatlands of continental western Canada through the Holocene, *Canadian Journal of Earth Sciences*, *37*(5), 683–693, https://doi.org/10.1139/e99-097, 2000.

Westermann, S., T. V. Schuler, K. Gisnås, and B. Etzelmüller, Transient thermal modeling of permafrost conditions in Southern Norway, *The Cryosphere*, *7*(2), 719–739, https://doi.org/10.5194/tc-7-719-2013, 2013.

Westermann, S., M. Langer, J. Boike, M. Heikenfeld, M. Peter, B. Etzelmüller, and G. Krinner, Simulating the thermal regime and thaw processes of ice-rich permafrost ground with the land-surface model CryoGrid 3, *Geoscientific Model Development*, *9*(2), 523–546, https://doi.org/10.5194/gmd-9-523-2016, 2016.

Xiaodong, Y., and H. H. Shugart, FAREAST: a forest gap model to simulate dynamics and patterns of eastern Eurasian forests, *Journal of Biogeography*, *32*(9), 1641–1658, https://doi.org/10.1111/j.1365-2699.2005.01293.x, 2005.

Yershov, E., *General Geocryology*, 604 pp., Cambridge University Press, 2004.

Yershov, E., V. F. Kondrat'yeva, K. A., Loginov, and I. K. Sychev, *Geocryological map of Russia and neighbouring republics*, 1140 pp., Faculty of Geology, Chair of Geocryology, Lomonosov Moscow State University, 1991.

Yi, S., M.-k. Woo, and M. A. Arain, Impacts of peat and vegetation on permafrost degradation under climate warming, *Geophysical Research Letters*, *34*(16), https://doi.org/10.1029/2007GL030550, 2007.

Younes, S., and T. Muneer, Comparison between solar radiation models based on cloud information, *International Journal of Sustainable Energy*, *26*(3), 121–147, https://doi.org/10.1080/14786450701549824, 2007.

Zhang, N., H. H. Shugart, and X. Yan, Simulating the effects of climate changes on Eastern Eurasia forests, *Climatic Change*, *95*(3-4), 341–361, https://doi.org/10.1007/s10584-009-9568-4, 2009.

Zhang, N., T. Yasunari, and T. Ohta, Dynamics of the larch taiga-permafrost coupled system in Siberia under climate change, *Environmental Research Letters*, *6*(2), https://doi.org/10.1088/1748-9326/6/2/024003, 2011.

Zhang, Y., W. Chen, and J. Cihlar, A process-based model for quantifying the impact of climate change on permafrost thermal regimes, *Journal of Geophysical Research D: Atmospheres*, *108*(22), https://doi.org/10.1029/2002JD003354, 2003.

Zhang, Y., A. B. Sherstiukov, B. Qian, S. V. Kokelj, and T. C. Lantz, Impacts of snow on soil temperature observed across the circumpolar north, *Environmental Research Letters*, *13*(4), https://doi.org/10.1088/1748-9326/aab1e7, 2018.

Zhao, B., Q. Zhuang, N. Shurpali, K. Köster, F. Berninger, and J. Pumpanen, North American boreal forests are a large carbon source due to wildfires from 1986 to 2016, *Scientific Reports 2021 11:1*, *11*(1), 1–14, https://doi.org/10.1038/s41598-021-87343-3, 2021.

Zweigel, R. B., S. Westermann, J. Nitzbon, M. Langer, J. Boike, B. Etzelmüller, and T. V. Schuler, Simulating snow redistribution and its effect on ground surface temperature at a high-Arctic site on Svalbard, *Journal of Geophysical Research: Earth Surface*, *126*(3), https://doi.org/10.1029/2020jf005673, 2021.

# Publications

Articles published in peer-reviewed journals

1. Stuenzi, S. M., Boike, J., Cable, W., Herzschuh, U., Kruse, S., Pestryakova, L. A., Schneider von Deimling, T., Westermann, S., Zakharov, E. S., and Langer, M.: Variability of the surface energy balance in permafrost-underlain boreal forest, Biogeosciences, 18, 343–365, DOI: 10.5194/bg-18-343-2021, 2021.

2. Stuenzi, S. M., Boike, J., Gädecke, A. , Herzschuh, U., Kruse, S., Pestryakova, L. A., Westermann, S., and Langer, M.: Sensitivity of Ecosystem-Protected Permafrost Under Changing Boreal Forest Structures, Environmental Research Letters, 16, 084045, DOI: 10.1088/1748-9326/ac153d, 2021.

Articles submitted to peer-reviewed journals

1. Stuenzi, S. M., Boike, J., Herzschuh, U., Kruse, S., Oehme, A., Westermann, S., and Langer, M.: Thermohydrological impact of forest disturbances on ecosystem-protected permafrost, JGR: Biogeosciences, *in review, (9.9.2021)*.

2. Kruse, S., Stuenzi, S. M., Boike, J., Langer, M., Josias Gloy, and Herzschuh, U.: Novel coupled permafrost-forest model revealing the interplay between permafrost, vegetation and climate across eastern Siberia, Geoscientific Model Development, DOI: 10.5194/gmd-2021-304, *in review, (6.9.2021)*.

Articles not directly related to this dissertation published in peer-reviewed journals

1. Stuenzi, S. M., and Schaepman-Strub, G.: Vegetation trajectories and shortwave radiative forcing following boreal forest disturbance in eastern Siberia. Journal of Geophysical Research: Biogeosciences, 125, e2019JG005395, DOI: 10.1029/2019JG005395, 2020.

2. Boike, J., Chadburn, S., Martin, J., Zwieback, S. (lead authors), Stuenzi S. M. (contributor): Standardized monitoring of permafrost thaw: a user-friendly, multi-parameter protocol, Arctic Science, in Press, DOI: 10.1139/AS-2021-0007, 2021.

3. Shevtsova, I., Herzschuh, U., Heim, B., Schulte, L., Stünzi, S., Pestryakova, L. A., Zakharov, E. S., and Kruse, S.: Recent above-ground biomass changes in central Chukotka (Russian Far East) using field sampling and Landsat satellite data, Biogeosciences, 18, 3343-3366, DOI: 10.5194/bg-18-3343-2021, 2021.

Software code developed within this dissertation

1. Stuenzi, S. M., Boike, J., Cable, W., Herzschuh, U., Kruse, S., Pestryakova, L. A., Schneider von Deimling, T., Westermann, S., Zakharov, E. S., and Langer, M.: Coupled multilayer canopy-permafrost model (CryoGrid) for the use in permafrost underlain boreal forests, Zenodo, DOI: 10.5281/zenodo.4317107, 2020, December 11.

2. Stuenzi, S. M., Boike, J., Gädecke, A., Herzschuh, U., Kruse, S., Pestryakova, L. A., Westermann, S., and Langer, M.: Coupled multilayer canopy-permafrost model (CryoGrid) for the simulation of forest trajectories in permafrost underlain boreal forests, Zenodo, DOI: 10.5281/zenodo.4603668, 2021, March 14.

3. Stuenzi, S. M., Boike, J., Herzschuh, U., Kruse, S., Oehme, A., Westermann, S., and Langer, M.: Coupled multilayer canopy-permafrost model (CryoGrid) for the use with an individual-based larch vegetation simulator (LAVESI), Zenodo, DOI: 10.5281/zenodo.5119987, 2021, July 21.

Field data sets generated within this dissertation

1. Stuenzi, S. M., Cable, W., Kruse, S., Boike, J., Herzschuh, U., Langer, M., Schulte, L., Brieger, F., Vyse, S. A., Bernhard, N., Dietze, E., Pestryakova, L. A., Zakharov, E. S., Nikolajewitsch, A., Ushnizkaya, L., Levina, S.: Automatic weather stations and stand-alone soil temperature sensors (Hobo logger) between August 2018 and August 2019 at two boreal forest sites in the region of Lake Ilirney and Lena-Viluy in Eastern Siberia. PANGAEA, DOI: 10.1594/PANGAEA.919859, 2020.

2. Langer, M., Kaiser, S., Stuenzi, S. M., Schneider von Deimling, T., Oehme, A., Jacobi, S.: Soilsurface temperatures in 2 cm depth between summer 2018 and 2019 with iButton-sensors in the North Slope of Alaska (USA), around Churchill (Canada) and the region of Illirney and Lena-Viluy (Russia). PANGAEA, DOI: 10.1594/PANGAEA.914327, 2020.

3. Kruse, S., Herzschuh, U., Schulte, L., Stuenzi, S. M., Brieger, F., Zakharov, E. S., Pestryakova, L. A.: Forest inventories on circular plots on the expedition Chukotka 2018, NE Russia. PANGAEA, DOI: 10.1594/PANGAEA.923638, 2020.

Articles published in non-peer-reviewed journals

1. Kruse, S., Bolshiyanov, D., Grigoriev, M. N., Morgenstern, A., Pestryakova, L., Tsibizov, L. and Udke, A. (lead authors), Stuenzi, S. M. (contributor): Russian-German Cooperation: Expeditions to Siberia in 2018, Reports on polar and marine research, Bremerhaven, AWI, 734 , 257 p., 2019.

2. Fuchs, M., Bolshiyanov, D., Grigoriev, M., Morgenstern, A., Pestryakova, L., Tsibizov, L. and Dill, A. (lead authors), Stuenzi, S. M. (contributor): Russian-German Cooperation: Expeditions to Siberia in 2019, Reports on polar and marine research, Bremerhaven, AWI, 749, 272 p., 2021.

3. Biskaborn, B. K., Bolshiyanov, D., Grigoriev, M. N., Morgenstern, A., Pestryakova, L. A., Tsibizov, L. and Dill, A. (lead authors), Stuenzi, S. M. (contributor): Russian-German Cooperation: Expeditions to Siberia in 2020, Reports on polar and marine research, Bremerhaven, AWI, 756, 81 p., 2021.